CHARACTERIZATION OF ADSORPTION PROCESSES FOR THE REMOVAL OF METAL IONS FROM WASTE EFFLUENTS USING BIOSORBENTS ANDGRAPHENE-BASED SORBENTS. STUDIES IN BATCH AND IN FIXED-BED COLUMN

Marwa Ben Amar

Universitat de Girona

جامعة صفاقس
Université de Sfax

DOCTORAL THESIS

Characterization of adsorption processes for the removal of metal ions from waste effluents using biosorbents and graphene-based sorbents. Studies in Batch and in fixed-bed column

Marwa Ben Amar

2021

Universitat de Girona

DOCTORAL THESIS

Characterization of adsorption processes for the removal of metal ions from waste effluents using biosorbents and graphene-based sorbents. Studies in Batch and in fixed-bed column

Marwa Ben Amar

2021

Doctoral program in chemistry

Supervised by

Dr. Victòria Salvadó Martín (University of Girona)

Dr. Khaled Walha (University of Sfax)

Tutor

Dr. Monica Iglesias Junca (University of Girona)

Thesis submitted to the University of Girona for the degree of Doctor

Universitat de Girona

Dr. Victòria Salvadó Martín of University of Girona and Dr. Khaled Walha of University of Sfax

WE DECLARE:

That the thesis entitled: "Characterization of adsorption processes for the removal of metal ions from waste effluents using biosorbents and graphene-based sorbents. Studies in Batch and in fixed-bed column", presented by Marwa Ben Amar to obtain a doctoral degree, has been completed under our supervision and meets the requirements to opt for a Doctorate for the University of Girona and University of Sfax.

For all intents and purposes, we hereby sign this document.

Dr. Victòria Salvadó Martín

Dr. Khaled Walha

Girona, April 23rd

Universitat de Girona
Departament de Química

Química Analítica i Ambiental

This thesis was financed by the research projects CTM2016-78798-C2-2-P and PID2019-107033GB (AEI/FEDER/UE) of the "Agencia Española de Investigación". Marwa Ben Amar acknowledges the financial support of the Faculty of Science (University of Sfax, Tunisia) and of the Environmental and Analytical Chemistry Research Group of the Department of Chemistry (University of Girona, Spain). This research group forms part of the CASIMA, an interdisciplinary group, which has been recognized as consolidated research group by the Catalan Government (2017 SGR 1685).

Universitat de Girona

جامعة صفاقس
Université de Sfax

The research described in this thesis has result in the publication of two scientific articles published:

Amar M. B., Walha K., Salvadó V. (2020). Evaluation of Olive Stones for Cd(II), Cu(II), Pb(II) and Cr(VI) Biosorption from Aqueous Solution: Equilibrium and Kinetics. International Journal of Environmental Research, 14: 193-204. https://doi.org/10.1007/s41742-020-00246-5

Amar M. B., Walha K., Salvadó V. (2021). Valorisation of pine cone as an efficient biosorbent for the removal of Pb(II), Cd(II), Cu(II) and Cr(VI), Adsorption Science and Technology, Article ID 6678530, https://doi.org/10.1155/2021/6678530

Amar M. B., Walha K., Monclús H, Cabrera A, Salvadó V. (2021) Fixed-bed dynamic adsorption of Pb(II), Cu(II) and Cd(II) by pine cone. Application to the removal Cr(VI), Cu(II) and Ni(II) from electroplating solutions (to be submitted to Journal of Environmental Chemical Engineering).

Amar M. B., Walha K., Salvadó V. et al. (2021). Adsorption properties of Graphene Oxides: a tunable platform for removal of compounds of environmental interest.

Amar M. B., Walha K., Salvadó V. et al. (2021). Removal of As(III) and As (V) by Basolite® F300 and synthetic Nano-{Fe-BTC} MOF.

ACKNOWLEDGEMENTS

I would like to express my deep and sincere gratitude to my supervisor Victoria Salvadó for the continuous support in my ph.D study and immense research, for her patience, motivation, enthusiasm and immense knowledge, her guidance which help me in all the time of research and writing of this thesis. I am extremely grateful for what she has offered me. It was a great privilege and honor to work under her guidance. I would like to thank her for her friendship empathy and for helping me to meet very good persons Jordi Creus and Josefina Escandell that accept me in their house as a member of their family. Thanks to them.

I would like to extend my deepest gratitude to my friend Juli Creus for moral support in hard times, for giving me his opinions and listening to me. It was my pleasure to know a great person as him. Thank you for the wonderful times.

Moreover, I would like to acknowledge Professor Khaled Walha for his continuous support and suggestions and guidance keep me moving forward during these years of studies.

In the end, I would like to extend my thanks to my parents Habib and Fatma Mtibaa and my sisters. I really appreciate their help, support, encouragement and love.

LIST OF ABREVIATIONS

AAS	Atomic absorption spectrophotometry
AC	Activated carbon
CAN	Cantaloupe peel
CI	Covalent index
CNT	Carbon nanotube
DFT	Density functional theory
DMA	Dimethyl arsenate
DSC	Differential scanning calorimetry
DTA	Differential thermal analysis
ED	Electrodialysis
EDX	Energy-dispersive X-ray spectrometer
EDR	Electron spin resonance spectroscopy
EDX	Energy-dispersive X-ray spectrometer
FO	Forward osmosis
FTIR	Fourier-transform infrared spectroscopy
GO	Graphene oxide
ICP-AES	Inductively Coupled Plasma Optical Emission spectroscopy
IR	Infrared spectroscopy
ISE	Ion-selective electrodes
IUPAC	International Union of Pure and Applied Chemistry
LP	Litchi fruit peel
MTZ	Mass transfer zone
MF	MF: microfiltration
MOF	Metal organic framework
MWCNTs	Multi-wall carbon nanotubes
NF	Nanofiltration
NMR	Nuclear magnetic resonance
OS	Olive stone

PAMAM	Poly (amidoamine) dendrimer
PBI	Polybenzimidazole
PC	Pine cone
PES	Polyethersulfone
P-ASA	P-arsanilic acid
pH_{pzc}	Point of zero charge
PVP	Polyvinylpyrolidone
RO	Reverse osmosis
ROX	Roxarsone
R	Ionic radius
SEM	Scanning Electron Microscopy
SWCNTs	Single-wall carbon nanotubes
TGA	Thermogravimetric analysis
UF	Ultrafiltration
USEPA	United States Environmental Protection Agency
WHO	World Health Organization
ZIFs	Zeolite imidazolate framework
XRD	X-ray diffraction
XPS	X-ray photoelectron spectroscopy
SSA	Specific surface area, SSA and surface area SA
CSA	CSA is the cross-sectional area
MILs	MILs Materials Institute Lavoisier (MILs)

Contents

LIST OF FIGURES

LIST OF TABLES

Summary

Wastewater discharged from industrial and agricultural activities contains relatively large amounts of toxic metal ions, especially including Cd(II), Cu(II), Pb (II), and Cr(VI). The removal of these pollutants is of great interest from both health and environmental perspectives. Arsenic contamination, generally associated with the geochemical environment, is a global threat due to its acute toxicity and carcinogenicity. The oxidation of different mineral species due to the redox conditions causes arsenic to become soluble and enter into the surrounding environment through drainage water. Conventional technologies for wastewater treatment and water purification such as precipitation, coagulation-flocculation, membrane processes, electrodialysis and ion-exchange are of limited utility due to their high cost, inefficiency in removing low metal concentrations, and sometimes also because they can generate large volumes of sludge. Adsorption is an attractive alternative due to its simplicity, its ability to remove trace amounts of metal ions, low cost, short operation time, and for the capacity for the material to be reused. Sorption processes are based on physical adsorption, chemical adsorption and ion exchange mechanisms. Among the different sorbent materials, activated carbon is the most widely used despite its high initial cost together with its regeneration costs. In the search for highly efficient, eco-friendly and economic adsorbents, agricultural waste and by-products from forest industries, including tea waste, coffee, hulls and shells from different nuts, sawdust, barks, cellulosic and lignocellulosic waste, corncobs, rice hulls, olive cake, fruit peels, sugar beet pulp, palm fruit bunch, maize leaves, among others, have been evaluated as biosorbents. They all typically have a good capacity to adsorb metal ions due to their porous structure and the fact that they have having carboxyl, hydroxyl, and other functional groups on their surface. The type of functional groups and chemical components of lignocellulosic materials makes them a good alternative adsorbent to treat contaminated effluents. The costs of these treatments will be low if the most suitable locally available biosorbents are used. Hence, in our case, we have evaluated lignocellulosic agro-industrial waste that is available in the Mediterranean region, such as olive stones and pine cones, as efficient biosorbents for the removal of toxic metal ions such as Pb(II), Cu(II), Cd(II) and Cr(VI).

The physical and chemical characterization of these lignocellulosic materials were performed using different techniques such as infrared spectroscopy (FTIR), scanning electron microscopy (SEM), Energy-dispersive X-ray spectroscopy (EDX), Brunauer-Emmet-Teller (BET) and Thermogravimetric analysis (TGA). The results proved that these agricultural wastes were mainly composed of carbon (~53%) and oxygen (~45.5%), and those functional groups such as carboxylic and hydroxyl groups were present on their surfaces. Milled pine cone was found to have a greater surface area (0.2536 m^2 g^{-1}) than milled olive stone (0.1956 m^2 g^{-1}) whereas the latter had a smaller particle size at 30.67 µm than pine cone (50 µm).

Batch adsorption experiments were performed to evaluate the adsorption capacity for Cu(II), Cd (II), Pb(II) and Cr(VI) of milled olive stones and milled pine cone using single and multi-metal aqueous solutions. The different parameters affecting the metal adsorption efficiency, such as contact time, pH of the aqueous solution, amount of adsorbent and initial metal concentration, were evaluated. Adsorption isotherm models were then applied in order to characterize the adsorption process. In the case of olive stone, the experimental data was described well with the Langmuir isotherm with adsorption capacities at pH 6 of 0.557 mg g^{-1}, 0.3 mg g^{-1} and 0.581 mg g^{-1} for Cu(II), Cd(II) and Pb(II), respectively, whereas for Cr(VI), the Temkin model provided the best fit with a maximum capacity of 2.34 mg g^{-1} at pH 2. The kinetic data fitted well into the pseudo second-order model which allowed the adsorption rate constants to be calculated. Cd (II) proved to have the highest kinetic constant, followed by Cu(II), Cr(VI) and Pb(II). Multi-metal solutions containing equal concentrations of the three divalent metal ions were used to evaluate their competition for the olive stone sorption sites resulting in a decrease of 50% in the sorption capacity of Pb(II) when Cu(II) and Cd(II) were also present. In the case of these last two metals, the sorption capacities decreased by 30% and 15%, respectively, when the other metals were present. Since Cd(II) had the highest rate constant, this metal was the first to saturate the available surface sites, followed by Cu(II) and Pb(II).

The efficiency of milled pine cone to remove trace concentration levels of Pb(II), Cd(II) and Cu(II) has been demonstrated, resulting in capacities of 100.01 mg g^{-1}, 78.73 mg g^{-1} and 33.04 mg g^{-1} at pH 5.5, respectively. These capacities are higher than those reported for other biosorbents with similar characteristics. Moreover, an adsorption capacity of 57.36 mg g^{-1} was obtained for Cr(VI) at pH 2 and its maximum removal percentage (88.8%) was obtained at pH 2 with 10 g L^{-1}. The experimental adsorption data correlated well with the Langmuir model for

Cu(II) and Cr(VI) whereas for Pb(II) and Cd(II) the best correlations were obtained with the Langmuir-Freundlich model. In the case of the divalent ions (Pb(II), Cu(II), and Cd(II)), there was no competition between them towards the adsorbent sites at low metal concentration levels (1-10 mg L^{-1}), given that the presence of other metal ions did not reduce the removal efficiencies.

The results obtained using both olive stone and pine cone biosorbents show that pine cone has the highest adsorption capacities due to its greater surface area. The uptake of Pb(II), Cu(II) and Cd(II) for both biosorbents is explained by surface complexation with the carboxylic and hydroxyl functional groups of the adsorbent surface and the removal efficiencies were greater for Pb(II), which has greater electronegativity and ionic radius than for Cd(II) and Cu(II). In the case of Cr(VI), maximum adsorption percentages of 46% for olive stone and 88 % for pine cone were obtained at pH 2, showing that this toxic anion can be removed via an ion-exchange mechanism coupled to a reduction reaction of Cr(VI) to Cr(III). Moreover, in the case of multi-metal solutions of divalent metal ions there was no competition between them for the surface sites of pine cone, which performed better as a biosorbent than olive stone and other previously studied biosorbents such as custard apple, rice and maize husk, pine sandwust, and pine bark.

Batch experiments are used to obtain equilibrium sorption isotherms and to evaluate the sorption capacity of biosorbents. However, in the practical operation of full-scale biosorption processes, continuous-flow fixed bed columns and fluidized bed columns are often preferred to treat large volumes of effluent. In such systems, the concentration profiles in the liquid and sorbent phases vary in both space and time. Pine cone was selected as the biosorbent to evaluate the removal of toxic metal ions in dynamic conditions in a fixed bed column given its good performance and great affinity for Pb(II), Cu(II), Cd(II), and Cr(VI). The behaviour of the adsorbates in a fixed bed column is described in terms of the breakthrough curves and the effect of parameters such as the initial adsorbate concentration, bed height and flow rate on the profile of these curves and in the removal capacity for Pb(II) of pine cone in dynamic conditions were also studied.

The experimental data of Pb(II) adsorption into a lab-scale fixed bed column filled with pine cone was analyzed using Thomas, Adams-Bohart and Yoon-Nelson models. The results show that the experimental data of Pb(II) removal followed the Thomas model with a determination coefficient R^2>0.9 with the best results being obtained at the lowest flow rates and the highest bed heights. The sorption capacity for Pb(II) exhibited by pine cone was found to be 77.92 mg g^{-1} at a flow rate of 2.2 ml min^{-1}, a bed height 0.7 cm and an initial concentration of 50 mg L^{-1}. The separation

of Pb(II), Cu(II), and Cd(II) was evaluated by passing multi-metal aqueous solutions containing equal initial concentration of the three metal ions of 25 mg L^{-1}, 50 mg L^{-1}, and 100 mg L^{-1} through a bed height of 1 cm at a flow rate of 2.2 ml min^{-1}. The breakthrough and exhaustion times in the fixed bed system occurred earlier for Cd(II) followed by Cu(II) and Pb(II) allowing, in the case of the highest initial concentration (100 mg L^{-1}), the separation of Pb(II) from Cd(II) and Cu(II). The highest exhaustion time was for Pb(II) confirming the higher affinity of pine cone by this metal ion. Multi-metal solutions containing the three heavy metal ions at equal initial concentrations of 50 mg L^{-1} at pH 5.6 and soft divalent cations such as Ca(II) (100 mg L^{-1}) were passed through a fixed bed column with 1 cm bed height of pine cone at a flow rate of 2.2 mL $min^{-1}$and a to evaluate if Ca(II) competes with the other divalent metals for the surface sites of the adsorbent. The results obtained showed that Ca(II) was not adsorbed and its presence did not affect the adsorption of Pb(II), Cu(II) and Cd(II). Taking into account the affinity of milled pine cone for Cr(VI) and Cu(II) and that the presence of these metal ions in electroplating industry effluents can strongly affect the environment, the capacity of a fixed bed column filled with pine cone (bed height 2cm) to remove these metal ions was evaluated. An aqueous solution simulating an electroplating waste containing 20 mg L^{-1} of Cu(II), 100 mg L^{-1} of Ni(II) and 30 mg L^{-1} of Cr(VI) at pH 4.4 was prepared and passed through the system at a flow rate of 2.2 mL min^{-1}. At these experimental conditions, removal percentages of 97% for Cu(II), 94% for Ni(II) and 93% for Cr(VI) were obtained. Cr(VI) broke through the column faster than Cu(II) and Ni(II) as a result of its lower affinity for pine cone at pH >2. Ni(II) and Cu(II) broke through the column at 30 and 80 min, respectively. Desorption experiments were then performed using 1.0 M HCl solution, which resulted in desorption percentages of 90% for Cr(VI) and 94% for Cu(II) and Ni(II).

Conventional adsorbents and bioadsorbents have certain constraints such as low adsorption capacities, lack of functional tunability, and recyclability. To overcome such limitations, new sorbents in nano dimensions are being synthesized and adopted for water decontamination. The main advantages of engineered nano-adsorbents are their large specific surface area and availability of a large number of active groups for binding heavy metal ions that can be tailored to improve the selectivity of the adsorption process. Among engineered nano-adsorbents, graphene oxide (GO), which is obtained by the oxidation of graphene, is considered to be a promising adsorbent for the removal of heavy metal ions such as Cu(II), Cd(II), and Cr(VI). However, it is

important to remark that GO materials exhibited strong differences, depending on the oxidants, reaction conditions and graphite source used to prepare them. Within the framework of our collaboration with the Chemistry Department of Masaryk University (Brno, Czech Rep.), samples of four graphenoids, namely GO-I, GO-II, 97 D and 227 A, were characterized and evaluated for the removal of divalent metal ions such as Cu(II) and Cd(II) and chromate from aqueous solutions. The preparation of these GOs is not detailed here as they are under patent.

The characterization of the GOs was performed using different analytical techniques such aselemental analysis, X-ray photoelectron spectroscopy (XPS) and X-ray diffraction (XRD) analyses that were performed at Masaryk University whereas FTIR, SEM, EDX and TGA/DTA were done at the University of Girona. The results of XPS showed that the degree of functionalization was low and the percentage of C≈O groups ranged from 11.6 to 12.56%. Carbonyl/carboxyl and OH bands were identified by FTIR. All the graphene oxides presented the same XRD pattern and Raman spectrum, showing that the oxidation levels were relatively low. This low functionalization was confirmed by the surface composition determined by EDX which resulted in C percentages > 88%, and oxygen percentages between 4 and 9%. BET surface areas ranged from 14.2268 to 25.8041 $m^2\ g^{-1}$ which are lower than the areas reported for other graphene oxides. Pore volumes ranged from 0.063 to 0.070 $cm^3\ g^{-1}$.

The highest removal percentages of Cu(II) (> 90%) and Cd(II) (> 88%) with 227A, GO-I and GO-II were obtained at the lowest initial concentration (5 mg L^{-1}) at pH 6, an adsorbent concentration of 2 g L^{-1} and 1 hour of contact time. However, in the case of 97D, the adsorption efficiency was lower (< 80% for Cu(II) and < 60 % for Cd(II)) in all the experiments although a longer period of time (t=3 h) was required to achieve equilibrium. In the case of Cr(VI), the effect of the initial concentration on Cr(VI) adsorption was evaluated using GO-I and GO-II at pH 2 and 10 g L^{-1} of adsorbent resulting in a higher removal percentage (68%) for GO-I than for GO-II (45%).

The experimental data of the sorption systems studied fitted the Freundlich isotherm model well in the case of Cu(II) with 227A (K_F 2.68), 97D (K_F 2.61), GO-I (K_F 3.34) and GO-II (K_F 3.72). The Freundlich isotherm is also the best model to express the adsorption data of Cd(II) for 227A (K_F 2.32) and GO-II (K_F 2.71) whereas the Langmuir-Freundlich model provides the best fit for 97D and GO-I with adsorption capacities of 5.19 and 5.28 mg g^{-1}, respectively. The adsorption mechanism of Cu(II) and Cd(II) seems to take placedue to their interaction with the functional

groups (COO^-, or O^-) on the surface of GO to form a metal ion complex. For Cr(VI), Freundlich was considered the best model in the case of both GO-I (k_F 0.26) and GO-II (K_F 0.12). The adsorption mechanism of Cr(VI) occurred through an electrostatic interaction of $HCrO_4^-$ species with the protonated groups of the sorbent surface at low pHs (1-2).

In general, the adsorption capacities obtained for the target metal ions with these GOs were lower than those reported for other graphene oxides showing that the synthetic procedures led to a low degree of oxidation of the graphenes also affecting the physical properties (surface area, porosity and pore size) of the resulting graphene oxides.

Metal–organic frameworks (MOFs) are a class of adsorbent materials that have emerged within the past three decades. MOFs are constructed of secondary building units which are namely, metal ions or metal clusters, and organic ligands, which are connected into three-dimensional lattices. MOFs have numerous advantages as adsorbents due to their high surface area, typically ranging from 1000 to 10,000 $m^2 g^{-1}$, porosity, chemical stability, functionality and adsorption site accessibility by the diffusion of contaminants through the framework.

The presence of arsenic in water, especially groundwater, is a major problem in different areas of the world as it is a potent human carcinogen. The toxicity of inorganic arsenic is higher than that of organic arsenic and generally, arsenic exists in the dissolved inorganic forms of As(III), arsenite, and As(V), arsenate. While both these forms are toxic, As(III) is about 60 times more poisonous than As(V). Broad technologies for water purification such as chemical coagulation–precipitation, ion exchange, membrane separation, and adsorption, using conventional and engineered adsorbents, were proposed for removing arsenic from water. Advanced materials for arsenic removal include graphene oxides (GOs), carbon nanotubes (CNTs) and metal organic frameworks (MOFs) as well as many other porous materials. In the last ten years, MOFs and MOF-based composites have increasingly been applied in the removal of As(III) and As(V) from water, due to their excellent adsorption capacities.

Among them, iron-based MOFs such as MIL-53(Fe), MIL-88B, MIL-100(Fe), and MIL-101(Fe) exhibited a great affinity for As(V) due to the Lewis acid-base and electrostatic interactions between $H_2AsO_4^-$ and Fe^{3+}. Fe-BTC, a MOF containing iron nodes and 1,3,5-benzene tricarboxylic linkers, was the first used to remove As(V) species from water solutions. MIL-100(Fe) and Basolite F300 are commercial MOFs based on Fe-BTC.

In this study, Basolite F300 and a Nano-Fe-BTC MOF, synthesized within collaboration with the Department of Chemistry of the University of La Laguna, were characterized and evaluate as adsorbents for the removal of arsenite and arsenate from aqueous solutions. The elemental analysis of the adsorbent surface, performed by EDX, showed that Basolite F300 was found to contain lower iron percentage (2.97%) than Nano-{Fe-BTC} MOF (3.68%). The results of TGA show that both materials have similar behaviour in terms of stability. The infrared spectra of the commercial Basolite F300 and the synthesized nano-{Fe-BTC} MOF show similar bands, including in the 650-1800 cm^{-1} region, which is generally considered to be a fingerprint of MOFs. Moreover, the presence of mesopores with diameters between 2 nm and 50 nm were found on the surface of Nano-{Fe-BTC}. A series of cracks and asymmetric pores with open pores structure with particle size which generated a large internal surface area were observed in the SEM images of Nano-{Fe-BTC}. This nanomaterial has a higher pore volume (0.53 $cm^3\ g^{-1}$) than Basolite F300 (0.41 $cm^3\ g^{-1}$). However, Basolite F300 has a greater surface area (431.6 $m^2\ g^{-1}$) than Nano-{Fe-BTC} MOF (427.2 $m^2\ g^{-1}$).

The kinetics of the As(III) and As(V) adsorption were studied by varying the contact time from 2 min to 120 min using 0.1 g L^{-1} of Basolite F300 with an initial arsenic concentration of 10 mg L^{-1} at pH 5.6 for As(V) and the same concentration at pH 9.5 for As (III). The equilibrium was reached approximately after 1 hour. The experimental data of As(V) and As(III) fitted well the pseudo second-order model showing that chemisorption is the dominant mechanism for the adsorption of As(III) and As(V). The relatively linearity of the intraparticle diffusion kinetic model for As(III) and As(V) indicates that intraparticle diffusion can be the rate controlling process with a little contribution of boundary layer diffusion.

Arsenic adsorption occurred through coordination and electrostatic interaction and depends on the pH. In the case of As (V), $H_2AsO_4^-$ is the predominant species in the 3-8 pH range and $HAsO_4^{2-}$ species is the predominant one in the 8-11 pH range, both anions are Lewis base that can interact strongly with centred Fe^{3+}cations (Lewis acid). Additionally, electrostatic interaction between arsenate and the positive charge of the centred Fe^{3+} enhanced As (V) adsorption. The maximum uptake percentage (90 %) was obtained in the 5.6-9.6 pH range. In the case of As (III), adsorption occurred at pHs > 9 when $H_2AsO_3^-$ species, a soft Lewis base, can interact with the centred Fe^{3+}. At pH 9.5, the maximum removal percentage of As (III) (47%) at the experimental conditions, 5 mg L^{-1} and adsorbent concentration of 0.5 g L^{-1}, was achieved.

The FTIR analyses performed before and after adsorption with the two Fe-BTC materials seem to confirm that the adsorption of arsenic species over Fe-based materials is explained by Fe-O-As coordination.

The experimental data of As(V) onto Basolite F300 fitted well the Freundlich model (K_F=10 mg g^{-1}), indicating the high affinity of this MOF by As(V), whereas Langmuir was the best model to explain As(III) adsorption with a maximum adsorption capacity of 10 mg g^{-1}. This value is similar to that obtained from the kinetic data for As(III) while for As(V), the pseudo-second order kinetic model resulted in a maximum adsorption capacity of 32.67 mg g^{-1}.

The adsorption efficiency of Basolite F 300 was compared with nano Fe-BTC MOFs resulting in no differences between both adsorbents in the case of As(V) with removal percentages of 90% and 86.7% for Basolite F 300 and NanoFe-BTC, respectively. However, the removal percentage for As(III) by Basolite F300 (47%) was higher than for the synthetic Fe-BTC (36%).

The study of the presence of other anions with arsenic in the same solution is an important factor that can affect the efficiency of the adsorbent and its potential for applications. Therefore, the effect of PO_4^{3-} (10, 100 and 300 mg L^{-1}) on As(III) and As(V) removal was investigated maintaining an intial arsenic concentration of 10 mg L^{-1}. The results obtained show that the presence of phosphate reduces the removal percentage of As(III) and As(V) by 18.5% and 6%, respectively, when the solutions contained 10 mg L^{-1} of PO_4^{3-}. The increase of PO_4^{3-} concentration led to a decrease in the removal percentage of As(V) and As(III). The chemical similarity between these anions and the fact that As and P have similar electronegativity (2.18) explain that arsenic and phosphate anions compete for the adsorption active sites of the MOFs.

Resum

Les aigües residuals generades per activitats agrícoles i industrials diverses contenen quantitats relativament grans d'ions metàl·lics tòxics, entre els què s'inclouen els ions Cd(II), Cu(II), Pb(II) i Cr(VI). L'eliminació d'aquests contaminants té un gran interès tant des de la perspectiva de la salut com del medi ambient. La contaminació per arsènic, generalment associada a l'entorn geoquímic, és un problema mundial a causa de la seva aguda toxicitat i carcinogenicitat. L'oxidació de diferents espècies minerals a causa de les condicions redox del medi aquàtic fa que l'arsènic sigui soluble i entri al medi ambient a través de l'aigua de drenatge.

Les tecnologies convencionals per tractar les aigües residuals i depurar les aigües, com la precipitació, la coagulació-floculació, els processos de membrana, l'electrodiàlisi i l'intercanvi iònic, són d'utilitat limitada pel seu alt cost, la seva ineficiència en l'eliminació de baixes concentracions de metalls i, de vegades, també perquè poden generar grans volums de fangs.

L'adsorció és un tractament alternatiu d'interès atesa la seva simplicitat, la seva capacitat d'eliminar ions metàl·lics a nivell de traces, el seu baix cost, curt temps d'operació i la potencial reutilització dels adsorbents. L'adsorció es pot basar en processos d'adsorció física, adsorció química i d'intercanvi iònic. Entre els diferents materials absorbents, el carbó actiu és el més utilitzat malgrat el seu preu elevat i els costos de regeneració.

Com adsorbents alternatius, eficients i ecològics s'ha proposat l'ús de residus agrícoles i subproductes derivats de les indústries forestals, entre els que cal esmentar, entre d'altres, els residus de te i cafè, closques de diferents fruits secs, serradures, escorces, panotxes de blat de moro, pellofes d'arròs, pells de fruita, polpa de remolatxa sucrera, raïm de palma, fulles de blat de moro, i, en general, tot tipus de residus cel·lulòsics i lignocel·lulòsics. Molts d'aquests biosorbents han mostrat tenir una bona capacitat d'adsorció d'ions metàl·lics atesa la seva estructura porosa i la presència de grups funcionals carbonil, carboxil, hidroxil i d'altres tipus com amino o tiol en la superfície del biosorbent. .

El tipus de grups funcionals i composició química dels materials lignocel·lulòsics fa que siguin una bona alternativa a altres adsorbents pel tractament d'efluents contaminats. Els costos d'aquests tractaments serien baixos si s'utilitzen els biosorbents adients disponibles localment. Per tant, en el nostre cas, s'han seleccionat residus agro-industrials lignocel·lulòsics disponibles a la regió mediterrània, com els pinyols d'oliva i les pinyes (estròbils), i s'ha avaluat la seva eficiència en l'eliminació d'ions metàl·lics tòxics com Pb(II), Cu(II), Cd(II) i Cr(VI).

La caracterització física i química d'aquests materials lignocel·lulòsics es va realitzar utilitzant diferents tècniques com l'espectroscòpia d'infrarojos de transformada de Fourier (FTIR), la microscòpia electrònica de rastreig (SEM), el microanàlisi por dispersió d'energies de raigs-X (EDX), porosimetria i caracterització de l'àrea superficial pel mètode de Brunauer-Emmet-Teller (BET) i l'anàlisi termogravimètica (TGA). Els resultats van mostrar que la composició elemental superficial d'aquests residus agrícoles és carboni (~53%) i oxigen (~45,5%), i en la seva superfície es va identificar la presència de grups funcionals carbonil/carboxil i hidroxil. Es va comprovar que la pinya molta tenia una superfície superior (0,2536 m^2 g^{-1}) que el pinyol d'oliva molt (0,1956 m^2 g^{-1}), mentre que aquest últim tenia una mida de partícula menor (30,67 µm) que la pinya (50 µm).

Es van dur a terme experiments d'adsorció en discontinu per avaluar la capacitat d'adsorció dels dos biosorbents, pinyol d'oliva i pinya, d'ions metàl·lics com Cu(II), Cd(II), Pb(II) i Cr(VI) emprant solucions aquoses amb un únic ió metàl·lic i solucions multi-metàl·liques. També es va estudiar l'efecte dels diferents paràmetres com ara el temps de contacte, el pH de la solució aquosa, la quantitat d'adsorbent i la concentració inicial de metall, en la capacitat d'adsorció dels biosorbents. Seguidament, es van caracteritzar els processos d'adsorció aplicant els diferents models d'isotermes d'adsorció. Els resultats experimentals obtinguts emprant el pinyol d'oliva com a biosorbent s'ajusten al model de Langmuir amb capacitats d'adsorció màximes a pH 6 de 0,555 mg g^{-1} pel Cu(II), 0,3 mg g^{-1} pel Cd(II) i de 0,581 mg g^{-1} pel Pb(II), mentre que pel Cr(VI), les dades experimental s'ajusten millor al model Temkin amb una capacitat màxima de 2,34 mg g^{-1} a pH 2. Les dades cinètiques es corresponen al model de pseudo segon ordre i les constants de velocitat d'adsorció calculades amb aquest model segueixen l'ordre Cd(II) >Cu(II)> Cr(VI) >Pb(II).

Es van utilitzar solucions multi-metàl·liques que contenien concentracions iguals dels tres ions metàl·lics divalents per avaluar la seva competència pels llocs de sorció del pinyol d'oliva, obtenint com a resultat una reducció del 50% de la capacitat d'adsorció del Pb(II) quan Cu(II) i Cd(II) també hi eren presents. En el cas d'aquests dos darrers metalls, les capacitats d'adsorció del pinyol d'oliva per cada un d'aquests ions va disminuir un 30% i un 15%, respectivament, degut a la presència dels altres ions metàl·lics a la solució. Atès que la constant de velocitat més alta la té el Cd(II), aquest metall va ser el primer en ocupar fins la saturació els llocs disponibles a la superfície del biosorbent, seguit del Cu(II) i Pb(II).

S'ha demostrat l'eficiència de la pinya per adsorbir Pb(II), Cd(II) i Cu(II) a nivells traça, obtenint-se capacitats màximes de 100,01 mg g^{-1} 78,73 mg g^{-1} i 33,04 mg g^{-1} a pH 5,5, respectivament. Aquestes valors de capacitat són superiors als obtinguts per altres biosorbents de característiques similars. A més, es va obtenir una capacitat màxima d'adsorció de 57,36 mg g^{-1} per a Cr(VI) a pH 2 amb un percentatge màxim d'eliminació (88,8%) a pH 2 i emprant 10 g L^{-1} d'adsorbent.

Les dades experimentals d'adsorció es van correlacionar bé amb el model de Langmuir per a Cu(II) i Cr(VI), mentre que per a Pb(II) i Cd(II) es van obtenir les millors correlacions amb el model de Langmuir-Freundlich. En el cas dels ions divalents (Pb(II),Cu (II) i Cd(II)), no hi va haver competència entre ells pels llocs actius de l'adsorbent a baixes concentracions (1-10 mg L^{-1}), atès que la presència d'altres ions metàl·lics no va afectar l'eficiència en la seva eliminació.

Els resultats obtinguts amb els dos biosorbents avaluats, pinyol d'oliva i pinya, mostren que la pinya té capacitats d'adsorció més altes atesa la seva major àrea superficial. L'adsorció de Pb(II), Cu(II) i Cd(II) per aquests dos biosorbents es produeix mitjançant la complexació superficial dels ions metàl·lics amb els grups funcionals presents a la superfície de l'adsorbent que actuen com a lligands i les eficiències d'eliminació van ser majors per a Pb(II), que té una major electronegativitat i radi iònic que Cd(II) i Cu(II). En el cas de l'adsorció de Cr(VI), es van obtenir percentatges màxims d'eliminació del 46% amb el pinyol d'oliva i del 88% per la pinya a pH 2, el què suggereix que aquest anió tòxic es adsorbit mitjançant un mecanisme mixt d'intercanvi iònic i reducció de Cr(VI) a Cr(III).

A més, en el cas de les solucions multi-metàl·liques d'ions divalents, no hi va haver competència entre ells pels llocs superficials de la pinya molta, fet que avala el millor rendiment com a biosorbent de la pinya en comparació al pinyol d'oliva i també respecte altres biosorbents estudiats prèviament com les panolles de blat de moro, les pellofes d'arròs i l'escorça de pi.

Els experiments en discontinu permeten caracteritzar els processos d'adsorció en condicions d'equilibri i obtenir les isotermes d'adsorció i la capacitat màxima d'adsorció dels biosorbents. No obstant això, pel funcionament pràctic dels processos de biosorció a gran escala, on s'han de tractar grans volums d'efluents, es preferible dur a terme el tractament en condicions dinàmiques utilitzant columnes de llit fix de flux continu o columnes de llit fluïditzat. En aquests sistemes, els perfils de concentració en les fases líquida i adsorbent varien tant en funció de l'espai com del temps. Per avaluar l'eliminació d'ions metàl·lics tòxics en condicions dinàmiques en una

columna de llit fix es va seleccionar la pinya molta com a biosorbent degut al seu bon rendiment i gran afinitat per Pb(II), Cu(II), Cd(II) i Cr(VI).

El comportament dels adsorbats en una columna de llit fix es descriu per les corbes de trencament i l'efecte de paràmetres com la concentració inicial d'adsorbat, l'alçada del llit i el cabal en el perfil d'aquestes corbes es va investigar i també es va determinar la capacitat de la pinya molta en l'eliminació de Pb(II) en condicions dinàmiques.

Les dades experimentals d'adsorció de Pb(II) obtingudes en una columna de llit fix contenint pinya molta a escala de laboratori es van analitzar mitjançant els models de Thomas, Adams-Bohart i Yoon-Nelson. Les corbes de trencament experimentals s'ajusten al model de Thomas amb un coeficient de determinació $R^2 > 0,9$, obtenint-se els millors resultats a cabals més baixos i a alçades de llit més grans. La màxima capacitat d'adsorció de Pb(II) per la pinya molta va ser de 77,92 mg g^{-1} a un cabal de 2,2 mL min^{-1}, una alçada del llit de 0,7 cm i una concentració inicial de 50 mg L^{-1}.

La separació de Pb(II), Cu(II) i Cd(II) es va avaluar passant solucions aquoses multi-metàl·liques que contenien la mateixa concentració inicial dels tres ions metàl·lics (25 mg L^{-1}, 50 mg L^{-1} i 100 mg de L^{-1}) a través d'una alçada del llit d'1 cm a un cabal de 2,2 mL min^{-1}. Els temps necessaris per assolir la concentració de trencament i d'esgotament del llit fix van ser més curts pel Cd(II) seguit pels del Cu(II) i el Pb(II), el què va permetre la separació del Pb(II) de Cd(II) i Cu(II) a la concentració inicial més alta (100 mg L^{-1}) . El temps d'esgotament més alt va ser per Pb(II) confirmant la major afinitat de la pinya molta pel Pb (II). Solucions multi- metàl·liques de Pb(II), Cd(II) i Cu(II) a concentracions inicials iguals de 50 mg L^{-1} a pH 5,6 i Ca(II) (100 mg L^{-1}) es van passar per una columna de llit fix d'1 cm d'alçada del llit a un cabal de 2,2 mL min^{-1} amb l'objectiu d'avaluar si els ions Ca(II) competeixen amb els altres metalls divalents pels llocs d'adsorció superficial de l'adsorbent. Els resultats obtinguts van mostrar que el Ca(II) no s'adsorbia i que la seva presència no afectava l'adsorció de Pb(II), Cu(II) i Cd(II).

Tenint en compte l'afinitat de la pinya per Cr(VI) i Cu(II) i que la presència d'aquests ions metàl·lics en els efluents de la indústria de galvanitzats pot causar estralls en el medi ambient, es va avaluar la capacitat d'eliminació d'aquests ions metàl·lics d'una columna de llit fix amb una alçada de llit de 2 cm de pinya. Amb aquest objectiu, es va preparar una solució aquosa que simulava la composició d'un efluent d'aquesta indústria que contenia 20 mg L^{-1} de Cu(II), 100 mg L^{-1} de Ni(II) i 30 mg L^{-1} de Cr(VI) a pH 4,4 i es va fer passar pel sistema a un cabal de 2,2

mL min^{-1}. En aquestes condicions experimentals, els percentatges d'eliminació de Cu(II), Ni(II) i Cr(VI) van ser del 97%, 94% i 93%, respectivament. El Cr(VI) es l'ió que arriba més ràpidament a la concentració de trencament degut a la seva menor afinitat per la pinya a pH> 2 i seguidament assoleixen aquesta concentració el Cu(II) i el Ni(II) a 30 i 80 min., respectivament. Després es van realitzar experiments de desorció amb una solució de HCl 1,0 M, que va donar lloc a percentatges de desorció de 90% pel Cr (VI) i del 94% pel Cu (II) i el Ni (II).

Els adsorbents i bioadsorbents convencionals tenen certes limitacions, com baixes capacitats d'adsorció, manca d'adaptació funcional i reciclabilitat. Per superar aquestes limitacions, s'estan sintetitzant i utilitzant nous sorbents en dimensions nano per a la descontaminació de l'aigua. Els principals avantatges dels nano-adsorbents dissenyats són la seva gran àrea superficial específica i la seva funcionalització amb una gran diversitat de grups funcionals actius que només s'uneixen als ions metàl·lics que interessa eliminar, millorant la selectivitat del procés d'adsorció. Entre els nano-adsorbents dissenyats, l'òxid de grafè (GO), que s'obté per l'oxidació del grafè, es considera un adsorbent prometedor per a l'eliminació d'ions de metalls pesants com Cu(II), Cd(II) i Cr(VI). Tot i això, és important remarcar que les propietats com adsorbents dels òxids de grafè GO poden ser molt diferents ja que depenen del procés de preparació i, concretament, dels oxidants, condicions de reacció i grafit utilitzats en aquest procés. En el marc de la nostra col·laboració amb el Departament de Química de la Universitat Masaryk (Brno, República Txeca), es van caracteritzar quatre grafenoids, anomenats GO-I, GO-II, 97 D i 227 A, i també es va avaluar la seva eficiència en l'adsorció d'ions metàl·lics divalents com Cu(II) i Cd(II) i Cr(VI)de solucions aquoses. La preparació d'aquests GO no es detalla aquí, atès que el procés de síntesi està patentat.

La caracterització dels òxids de grafè es va dur a terme amb diferents tècniques analítiques com anàlisi elemental, anàlisi per XPS i XRD, realitzades a la Masaryk University, mentre que les anàlisis per FTIR, SEM, EDX i TGA / DTA es van fer a la Universitat de Girona. Els resultats de XPS van mostrar que el grau de funcionalització dels GOs era baix i el percentatge de grups C≈O variava entre l'11,6 i el 12,56%. Els espectres de FTIR van permetre identificar les bandes corresponents als grups funcionals carbonil/carboxil i hidroxil. Tots els òxids de grafè presentaven el mateix patró XRD i espectre Raman, mostrant que el grau d'oxidació dels grafens era relativament baix.

Aquesta baixa funcionalització es va confirmar amb la determinació de la composició superficial per EDX amb percentatges de C superiors o al voltant del 88% i percentatges d'oxigen entre el 4 i el 9%. Les àrees superficials dels GOs determinades per BET variaven entre 14.2268 i 25.8041 m^2 g^{-1}, valors inferiors als reportats per a altres òxids de grafè en altres estudis. Els màxims percentatges d'eliminació de Cu(II) > 90% i Cd(II) > 88% amb els òxids de grafè 227A, GO-I i GO-II es van obtenir a la concentració inicial més baixa (5 mg L^{-1}) a pH 6, una concentració adsorbent de 2 g de L^{-1} i 1 hora de temps de contacte.

No obstant, l'eficiència d'adsorció del 97D va ser menor (<80% per a Cu (II) i <60% per a Cd (II)) a la dels altres GOs en tots els experiments, tot i que va ser necessari més temps (t = 3 h) per arribar a l'equilibri. En el cas de Cr(VI), es va avaluar l'efecte de la concentració inicial en la seva adsorció per GO-I i GO-II obtenint-se percentatges d'eliminació del 68% per a GO-I i del 45% per a GO-II a pH 2 i amb una concentració de 10 g L^{-1} d'adsorbent.

Les dades experimentals d'adsorció de Cd(II) es van ajustar al model de Freundlich amb K_F 2,32 per 227A i K_F 2,71 per GO-II, mentre que pels òxids de grafè 97D i GO-I les dades es van ajustar al model de Langmuir-Freundlich amb capacitats màximes d'adsorció de 5,19 i 5,28 mg g^{-1}, respectivament. En el cas del Cu(II), les dades experimentals es van ajustar al model de Freundlich per a tots els GOs amb valors de K_F que variaven entre 2,61 (97D) i 3,72 (GO-II). L'adsorció de Cu (II) i Cd (II) s'explica per la seva interacció amb els grups funcionals (COO-, o O-) de la superfície dels GOs que actuen com a lligands en la formació de complexos amb els ions metàl·lics. En el cas de Cr(VI), les dades experimentals d'adsorció de GO-I i GO-II s'ajusten al model de Freundlich i l'adsorció es produeix per la interacció electrostàtica de $HCrO_4^-$ amb els grups funcionals protonats a pH baixos (1-2) de la superfície de l'adsorbent. En general, les capacitats d'adsorció obtingudes per als ions metàl·lics estudiats amb aquests GOs van ser inferiors a les reportades per a altres òxids de grafè fet que suggereix que els procediments utilitzats per produir els òxids de grafè no van ser efectius per obtenir un alt grau d'oxidació i de funcionalització dels grafens i que també van afectar les propietats físiques (superfície, porositat i mida de porus) dels òxids de grafè produïts.

Els Metall–organic frameworks (MOFs) són una classe de materials adsorbents que s'han desenvolupat en les darreres tres dècades. Els MOFs es construeixen amb unitats de construcció secundàries, que són ions metàl·lics o cúmuls metàl·lics i lligands orgànics, que es connecten formant gelosies tridimensionals. Els MOFs tenen nombrosos avantatges com a adsorbents a

causa de la seva elevada àrea superficial, que sol variar entre 1000 i 10.000 m^2 g^{-1}, porositat, estabilitat química, funcionalitat i accessibilitat al lloc d'adsorció per la difusió dels contaminants a través del MOF.

La presència d'arsènic a l'aigua, especialment aigües subterrànies, és un problema important a diferents zones del món atès que és un potent carcinogen. La toxicitat de l'arsènic inorgànic és superior a la dels organoarseniats, l'arsènic es troba generalment en el medi aquàtic en les seves formes inorgàniques dissoltes l'arsenit As(III) i l'arseniat As(V). Tot i que aquestes dues espècies són tòxiques, l'As(III) és aproximadament 60 vegades més verinós que l'As(V). Hi ha una amplia diversitat de tecnologies que permeten eliminar l'arsènic de les aigües, com ara la coagulació-precipitació, l'intercanvi iònic, la separació amb membranes, i l'adsorció, mitjançant adsorbents convencionals o adsorbents dissenyats específicament per eliminar l'arsènic.

Entre els materials avançats per eliminar l'arsènic cal esmentar els òxids de grafè (GOs), els nanotubs de carboni (CNT) i les estructures metàl·liques orgàniques (MOFs), així com molts altres materials porosos. En els darrers deu anys, els MOFs i els materials compostos basats en MOFs s'han utilitzat cada vegada més en l'eliminació d'As(III) i As(V) de l'aigua, ateses les seves excel·lents capacitats d'adsorció. Entre ells, els MOFs a base de ferro com MIL-53(Fe), MIL-88B, MIL-100(Fe) i MIL-101(Fe) han estat els més estudiats per la seva gran afinitat per As(V) ateses les interaccions àcid-base de Lewis i electrostàtiques que tenen lloc entre $H_2AsO_4^-$ i Fe^{3+}. El Fe-BTC, un MOF que conté nodes de ferro i l'àcid benzè-1,2,4-tricarboxílic com a lligant , va ser el primer que es va utilitzar per eliminar les espècies d'As(V) de les solucions aquoses. MIL-100(Fe) i Basolita F300 són dos MOFs comercials basats en Fe-BTC.

En aquest estudi, el MOF comercial Basolita F300 i un Nano-Fe-BTC MOF, sintetitzat en col·laboració amb el Departament de Química de la Universitat de La Laguna, s'han caracteritzat i avaluat com a adsorbents en l'eliminació de l'arsenit i l'arseniat de solucions aquoses. L'anàlisi elemental de la superfície de l'adsorbent, realitzada per EDX, va mostrar que la Basolita F300 contenia un percentatge de ferro inferior (2,97%) al Nano- {Fe-BTC} MOF (3,68%).

Els espectres d'infrarojos de la Basolita F300 i el MOF sintetitzat, nano- {Fe-BTC}, mostren bandes similars, incloent les de la regió 650-1800 cm^{-1}, que t corresponen al perfil característic dels MOFs. Pel que fa a la àrea superficial i al volum de porus, el material sintetitzat té un volum de porus més gran que Basolita F300, mentre que l'àrea superficial és més gran en la Basolita F300. Els resultats de BET també mostren que el nano-{Fe-BTC} MOF presenta meso porus amb

un diàmetre de mida superior (entre 2 nm i 50 nm) als de la Basolite F300. A les imatges SEM de nano-{Fe-BTC}, es van observar una sèrie d'esquerdes i porus asimètrics amb una estructura de porus oberts amb mida de partícula.

Es va estudiar la cinètica de l'adsorció d'As(III) i As(V) variant el temps de contacte de 2 min a 120 min utilitzant 0,1 g L^{-1} de Basolita F300 amb una concentració inicial d'arsènic de 10 mg L^{-1} a pH 5.6 per l'As(V) i a pH 9.6 per l'As(III). L'equilibri es va assolir aproximadament després d'una hora de contacte. Les dades experimentals d'As(V) i As(III) es van ajustar al model de pseudo segon ordre, el què suggereix que l'adsorció d'As(III) i As(V) per la Basolita F300 és basa en la quimisorció. La relativa linealitat del model cinètic de difusió intra-particula per a As(III) i As(V) indica que la difusió intra-particula pot ser el pas que determina la velocitat del procés amb una contribució baixa de la difusió a través de la capa límit.

L'adsorció d'arsènic es dona mitjançant la coordinació i la interacció electrostàtica i depèn del pH. En el cas d'As(V), $H_2AsO_4^-$ és l'espècie predominant en el rang de pH de 3-8 i l'espècie $HAsO_4^{2-}$ és la predominant en el rang de pH 8-11, ambdós anions són base de Lewis que poden interactuar fortament amb el centre de Fe^{3+} (àcid de Lewis) del MOF. A més, la interacció electrostàtica entre l'arseniat i el Fe^{3+} incentiva l'adsorció de l'As(V). El percentatge màxim d'adsorció (90%) es va obtenir en l'interval de pH de 5.6-9.5. En el cas d'As(III), l'adsorció es va produir a pH> 9 quan l'espècie $H_2AsO_3^-$, una base de Lewis tova, pot interactuar amb el Fe^{3+}. A pH 9.5, es va aconseguir el percentatge màxim d'eliminació d'As(III) (47%) en les condicions experimentals utilitzades, concentració inicial d'As(III) de 5 mg L^{-1} i concentració d'adsorbent de 0,5 g L^{-1}.

Les anàlisis FTIR realitzades abans i després de l'adsorció amb els dos materials de Fe-BTC semblen confirmar que l'adsorció de les espècies d'arsènic sobre MOFs basats en Fe s'explica per la coordinació Fe-O-As. Les dades experimentals d'adsorció d'As(V) per la Basolita F300 s'ajusten al model de Freundlich (K_F = 10), indicant l'alta afinitat d'aquest MOF per l'As(V), mentre que el model de Langmuir permet explicar l'adsorció d'As(III) amb una màxima capacitat d'adsorció de 10 mg g^{-1}. Aquest valor és similar a l'obtingut a partir de les dades cinètiques per a As(III) mentre que per a As(V), a partir del model cinètic de pseudo-segon ordre es va calcular una màxima capacitat d'adsorció de 32,67 mg g^{-1}.

L'eficiència d'adsorció de Basolita F 300 es va comparar amb la del nano Fe-BTC MOF, i no van trobar-se grans diferències entre els dos adsorbents en el cas d'As(V) amb percentatges

d'eliminació del 90% i 86,7%, respectivament, mentre que en el cas de l'adsorció d'As(III) les diferències van ser més grans, amb un percentatge del 47% per Basolita F300 i d'un 36% pel Fe-BTC sintetitzat . La presència d'altres anions amb l'arsenit i l'arseniat en la mateixa solució pot afectar l'eficiència de l'adsorbent i les seves potencials aplicacions. Per tant, es va investigar l'efecte del PO_4^{3-} (10, 100 i 300 mg L^{-1}) sobre l'eliminació d'As(III) i As(V) quan la concentració d'arsènic és de 10 mg L^{-1}. Els resultats obtinguts mostren que la presència de fosfat redueix el percentatge d'adsorció d'As(III) i As(V) en un 18,5% i un 6%, respectivament, quan les solucions contenien 10 mg L^{-1} de PO_4^{3-}. L'augment de la concentració de PO_4^{3-} va provocar una disminució encara més gran en el percentatge d'adsorció d'As(V) i As(III). La similitud química entre aquests anions i el fet que As i P tinguin una electronegativitat similar (2.18) expliquen que els anions arsenit, arseniat i fosfat competeixen pels llocs actius d'adsorció dels MOFs.

Resumen

Las aguas residuales de actividades industriales y agrícolas contienen cantidades relativamente grandes de iones metálicos tóxicos, especialmente Cd(II), Cu(II), Pb(II) y Cr(VI). La eliminación de estos contaminantes es de gran interés tanto desde el punto de vista de la salud como del medio ambiente. La contaminación por arsénico, generalmente asociada con el entorno geoquímico, es una amenaza mundial debido a la toxicidad aguda y carcinogenicidad del arsénico. La oxidación de diferentes especies minerales debido a las condiciones redox hace que el arsénico se solubilicé y entre en el medio acuático a través del agua de drenaje.

Las tecnologías convencionales para el tratamiento de aguas residuales y purificación de las aguas, como la precipitación, la coagulación-floculación, los procesos de membrana, la electrodiálisis y el intercambio iónico, son de utilidad limitada debido a su alto costo, su ineficiencia en la eliminación de bajas concentraciones de metales, y a veces también porque pueden generar grandes volúmenes de lodos.

La adsorción es una alternativa atractiva debido a su simplicidad, su capacidad para eliminar trazas de iones metálicos, bajo costo, tiempo de operación corto, y por la potencial reutilización de los adsorbentes. Los mecanismos en los procesos de sorción se basan en la adsorción física, la adsorción química y el intercambio iónico. Entre los diferentes materiales absorbentes, el carbón activado es el más utilizado a pesar de su alto coste inicial y los costess de regeneración.

En la búsqueda de adsorbentes alternativos que sean altamente eficientes, ecológicos y económicos, los desechos agrícolas y subproductos de las industrias forestales, entre los que se incluyen los residuos de té y café, cáscaras de diferentes frutos secos, serrín, cortezas, mazorcas de maíz, cáscaras de arroz, pieles de fruta, pulpa de remolacha azucarera, manojo de palma, hojas de maíz y residuos celulósicos y lignocelulósicos, entre otros, han sido evaluados como biosorbentes.

Todos ellos suelen tener una buena capacidad para adsorber iones metálicos debido a su estructura porosa y a la presencia en su superficie de grupos funcionales como el carbonilo, carboxilo, hidroxilo, amino y tiol, entre otros. El tipo de grupos funcionales y componentes químicos de los materiales lignocelulósicos los hace particularmente interesantes para su uso como adsorbentes alternativo para el tratamiento de efluentes contaminados. Los costes de estos tratamientos serán bajos si se utilizan los biosorbentes más adecuados que sean localmente

disponibles. Por lo tanto, en nuestro caso, hemos evaluado la utilización de residuos agroindustriales lignocelulósicos disponibles en la región mediterránea, como los huesos de aceitunas y las piñas, como biosorbentes eficientes para la eliminación de iones metálicos tóxicos como Pb(II), Cu(II), Cd(II) y Cr(VI).

La caracterización física y química de estos materiales lignocelulósicos se realizó utilizando diferentes técnicas como la espectroscopia infrarroja con transformada de Fourier (FTIR), microscopía electrónica de barrido (SEM), microanálisis por espectroscopia de rayos X por dispersión de energía (EDX), el análisis de la superficie por el método de Brunauer-Emmet-Teller (BET) y análisis termogravimétrico (TGA).

Los resultados mostraron que estos residuos agrícolas estaban compuestos principalmente de carbono (~53%) y oxígeno (~45,5%), y en la superficie de los adsorbentes se identificaron las bandas de grupos funcionales como los grupos carbonilo, carboxílicos e hidroxilos. Se encontró que la piña molida tenía una superficie mayor (0,2536 m^2 g^{-1}) que el hueso de aceituna molido (0,1956 m^2 g^{-1}), mientras que el tamaño de partícula era menor (30,67 µm) en el hueso de aceituna que en la piña (50 µm).

Se realizaron experimentos de adsorción en discontinuo para evaluar la capacidad de adsorción de Cu(II), Cd(II), Pb(II) y Cr(VI) de ambos biosorbentes utilizando disoluciones acuosas monometálicas y multimetálicas. Se evaluaron los diferentes parámetros que afectan a la eficiencia de adsorción del metal, como el tiempo de contacto, el pH de la solución acuosa, la cantidad de adsorbente y la concentración inicial de metal.

A continuación se caracterizó el proceso de adsorción mediante los modelos de isotermas de adsorción. Los datos experimentales del biosorbente de hueso de aceituna se ajustaron al modelo de isoterma de Langmuir con capacidades de adsorción máximas a pH 6 de 0,557 mg g^{-1}, 0,3 mg g^{-1} y 0,581 mg g^{-1} para Cu(II), Cd(II) y Pb(II), respectivamente, mientras que para Cr(VI), el modelo Temkin proporcionó el mejor ajuste con una capacidad máxima de 2,34 mg g^{-1} a pH 2.

Los datos cinéticos se ajustaron al modelo cinético de pseudosegundo orden con el que se calcularon las constantes de velocidad de adsorción. Obteniéndose el valor más alto para el Cd(II) seguido de Cu(II), Cr(VI) y Pb(II). Se utilizaron soluciones multa-metálicas que contenían concentraciones iguales de los tres iones metálicos divalentes para evaluar la competitividad por los sitios de sorción del biosorbente, lo que resultó en una disminución del 50% en la capacidad de sorción de Pb(II) en presencia de concentraciones iguales deCu(II) y Cd(II).

En el caso de estos dos últimos metales, las capacidades de sorción disminuyeron un 30% y un 15%, respectivamente, cuando estaban presentes los otros metales. Dado que Cd(II) tenía la constante de velocidad más alta, este metal fue el primero en saturar los sitios activos disponibles den la superficie del biosorbente, seguido por Cu(II) y Pb(II).

Se ha demostrado la eficiencia de la piña molida para eliminar de Pb(II), Cd(II) y Cu(II) a los niveles traza, obteniéndose capacidades máximas de adsorción de 100,01 mg g^{-1}, 78,73 mg g^{-1} y 33,04 mg g^{-1} a pH 5,5, respectivamente. Estas capacidades son superiores a las publicadas para otros biosorbentes de características similares. Además, se obtuvo una capacidad máxima de adsorción de 57,36 mg g^{-1} para Cr(VI) a pH 2 y su un porcentaje máximo de eliminación (88,8%) a pH 2 con 10 g L^{-1} de adsorbente.

Los datos experimentales de adsorción se correlacionaron bien con el modelo de Langmuir para Cu(II) y Cr(VI), mientras que para Pb(II) y Cd(II) se obtuvieron las mejores correlaciones con el modelo de Langmuir-Freundlich. En el caso de los iones divalentes (Pb(II), Cu(II) y Cd(II)), no hubo competencia entre ellos por el adsorbente a niveles bajos de concentración de metal (1-10 mg L^{-1}), dado que la presencia de otros iones metálicos no redujo las eficiencias de eliminación.

Los resultados obtenidos con los dos biosorbentes, hueso de aceituna y piña, muestran que la piña presenta mayores capacidades de adsorción debido a su mayor área superficial. La adsorción de Pb(II), Cu(II) y Cd(II) para ambos biosorbentes se explica por la formación de complejos entre los grupos funcionales presentes en la superficie del adsorbente y los iones metálicos de la solución. Las eficiencias en la eliminación fueron mayores para Pb(II), que tiene mayor electronegatividad y radio iónico, que para Cd(II) y Cu(II).

En el caso de la adsorción de Cr(VI), se obtuvieron porcentajes máximos de eliminación de 46% para el hueso de aceituna y 88% para la piña a pH 2, lo que demuestra que este anión tóxico es adsorbido mediante un mecanismo mixto de intercambio iónico acoplado a una reacción de reducción de Cr(VI) a Cr(III).

Además, en el caso de las soluciones multimetálicas de iones metálicos divalentes no se ha encontrado competencia entre ellos por las superficie de la piña, indicando que esté biosorbente es más efectivo que el hueso de aceituna y que otros biosorbentes previamente estudiados, como las como las mazorcas de maíz, las cascarillas de arroz y la corteza de pino.

Los experimentos en discontinuo permiten caracterizar los procesos de adsorción en condiciones de equilibrio y obtener las isotermas de adsorción y la capacidad máxima de adsorción de los

biosorbentes. Sin embargo, para el funcionamiento práctico de los procesos de biosorción a gran escala, donde se han de tratar grandes volúmenes de efluentes, es preferible llevar a cabo el tratamiento en condiciones dinámicas utilizando columnas de lecho fijo de flujo continuo o columnas de lecho fluidizado. En estos sistemas, los perfiles de concentración en las fases líquida y adsorbente varían tanto en función del espacio como del tiempo. Para evaluar la eliminación de iones metálicos tóxicos en condiciones dinámicas en una columna de lecho fijo se seleccionó la piña como biosorbente debido a su buen rendimiento y gran afinidad por Pb(II), Cu(II), Cd(II) y Cr(VI).

Los datos experimentales de adsorción de Pb(II) obtenidos en una columna de lecho fijo conteniendo piña a escala de laboratorio se analizaron mediante los modelos de Thomas, Adams-Bohart y Yoon-Nelson. Las curvas de ruptura experimentales se ajustan al modelo de Thomas con un coeficiente de determinación R2> 0,9, obteniéndose los mejores resultados a caudales más bajos y con las alturas de lecho más grandes. La máxima capacidad de adsorción de Pb(II) con la piña fue de 77,92 mg g^{-1} a un caudal de 2,2 mL min-1, una altura de lecho de 0,7 cm y una concentración inicial de 50 mg L^{-1}.

La separación de Pb(II), Cu(II) y Cd(II) se evaluó pasando soluciones acuosas multi-metálicas que contenían la misma concentración inicial de los tres iones metálicos (25 mg L^{-1}, 50 mg L^{-1} y 100 mg de L^{-1}) a través de un lecho de 1 cm de altura a un caudal de 2,2 mL min-1. Los tiempos necesarios para alcanzar la concentración de ruptura y de agotamiento del lecho fijo fueron más cortos para el Cd(II), seguido por los del Cu(II) y el Pb(II), lo qué facilito la separación del Pb(II) de Cd(II) y Cu(II) a la concentración inicial más alta (100 mg L^{-1}). El tiempo de agotamiento más alto se obtuvo para Pb(II) confirmando la mayor afinidad de la piña para esté ion metálico. Soluciones multimetálicas de Pb(II), Cd(II) y Cu(II) con concentraciones iniciales iguales de 50 mg L^{-1} a pH 5,6 y Ca(II) (100 mg L^{-1}) se pasaron por una columna de lecho fijo de 1 cm de altura a un caudal de 2,2 mL min^{-1} con el objetivo de evaluar si los iones Ca(II) compiten con los otros metales divalentes por los puestos de adsorción superficial del adsorbente. Los resultados obtenidos mostraron que el Ca(II) no se adsorbía y que su presencia no afectaba la eficiencia de adsorción de Pb(II), Cu(II) y Cd(II).

Teniendo en cuenta la afinidad de la piña para Cr(VI) y Cu(II) y que la presencia de estos iones metálicos en los efluentes de la industria de galvanizados puede causar estragos en el medio ambiente, se evaluó la capacidad de eliminación de estos iones metálicos de una columna de

lecho fijo con una altura de lecho de 2 cm de piña. Con este objetivo, se preparó una solución acuosa que simulaba la composición de un efluente de esta industria y que contenía 20 mg L^{-1} de Cu(II), 100 mg L^{-1} de Ni(II) y 30 mg L^{-1} de Cr(VI) a pH 4,4 y se hizo pasar por el sistema a un caudal de 2,2 mL min-1. En estas condiciones experimentales, los porcentajes de eliminación de Cu(II), Ni(II) y Cr(VI) fueron del 97%, 94% y 93%, respectivamente. El Cr(VI) es el ion que llega más rápidamente a la concentración de ruptura debido a su menor afinidad por la piña a pH> 2 y seguidamente logran alcanzar las respectivas concentraciones de ruptura el Cu(II) a 30 min, y el Ni(II) a 80 min. Después se realizaron experimentos de desorción con una solución de HCl 1,0 M, que dio lugar a porcentajes de desorción de 90% para el Cr(VI) y del 94% para el Cu(II) y el Ni(II).

Los adsorbentes y biosorbentes convencionales tienen ciertas limitaciones, como bajas capacidades de adsorción, falta de adaptación funcional y reciclabilidad. Para superar estas limitaciones, se están sintetizando y utilizando nuevos sorbentes en dimensiones nano para la descontaminación del agua. Las principales ventajas de los nano-adsorbentes diseñados son su gran área superficial específica y su funcionalización con una gran diversidad de grupos funcionales activos que sólo se unen a los iones metálicos que interesa eliminar, mejorando la selectividad del proceso de adsorción. Entre los nano-adsorbentes diseñados, el óxido de grafeno (GO), que se obtiene por la oxidación del grafeno, se considera un adsorbente prometedor para la eliminación de iones de metales pesados como Cu(II), Cd(II) y Cr(VI). Sin embargo, es importante destacar que las propiedades como adsorbentes de los óxidos de grafeno GO pueden ser muy diferentes ya que dependen del proceso de preparación y, concretamente, de los oxidantes, condiciones de reacción y grafito utilizados en este proceso. En el marco de nuestra colaboración con el Departamento de Química de la Universidad Masaryk (Brno, República Checa), se caracterizaron cuatro grafenoides, GO-I, GO-II, 97 D y 227 A, y también se evaluó su eficiencia en la adsorción de iones metálicos divalentes como Cu(II) y Cd(II) y Cr(VI) de soluciones acuosas. La preparación de estos GOs no se detalla aquí, dado que el proceso de síntesis está patentado.

La caracterización de los óxidos de grafeno se llevó a cabo con diferentes técnicas analíticas como análisis elemental, análisis por XPS y XRD, realizados en la Masaryk University, mientras que los análisis por FTIR, SEM, EDX y TGA / DTA se hicieron en la Universidad de Girona. Los resultados de XPS mostraron que el grado de funcionalización de los perro era bajo y el

porcentaje de grupos C≈O variaba entre el 11,6 y el 12,56%. Los espectros de FTIR permitieron identificar las bandas correspondientes a los grupos funcionales carbonilo / carboxilo e hidroxilo. Todos los óxidos de grafeno presentaban el mismo patrón XRD y espectro Raman, mostrando que el grado de oxidación de los grafeno era relativamente bajo.

Esta baja funcionalización se confirmó con la determinación de la composición superficial por EDX con porcentajes de C superiores o alrededor del 88% y porcentajes de oxígeno entre el 4 y el 9%. Las áreas superficiales de los GOs determinadas por BET variaban entre 14.2268 y 25.8041 m^2 g^{-1}, valores inferiores a los reportados para otros óxidos de grafeno en otros estudios. Los máximos porcentajes de eliminación de Cu(II)> 90% y Cd(II)> 88% con los óxidos de grafeno 227A, GO-I y GO-II se obtuvieron con una concentración inicial baja (5 mg L^{-1}) a pH 6, una concentración adsorbente de 2 g de L^{-1} y 1 hora de tiempo de contacto.

Sin embargo, la eficiencia de adsorción del 97D fue menor (<80% para Cu(II) y <60% para Cd(II)) a la de los demás MOFs en todos los experimentos, aunque fue necesario más tiempo (t = 3 h) para alcanzar el equilibrio. En el caso de Cr(VI), se evaluó el efecto de la concentración inicial en su adsorción por GO-I y GO-II obteniéndose porcentajes de eliminación del 68% para GO-I y del 45% para GO-II a pH 2 y con una concentración de 10 g L^{-1} de adsorbente.

Los datos experimentales de adsorción de Cd(II) se ajustaron al modelo de Freundlich con K_F 2,32 por 227A y K_F 2,71 por GO-II, mientras que para los óxidos de grafeno 97D y GO-I los datos se ajustaron al modelo de Langmuir-Freundlich con capacidades máximas de adsorción de 5,19 y 5,28 mg g-1, respectivamente. En el caso del Cu (II), los datos experimentales se ajustaron al modelo de Freundlich para todos los MOFs con valores de K_F que varían entre 2,61 (97D) y 3,72 (GO-II). La adsorción de Cu(II) y Cd(II) se explica por su interacción con los grupos funcionales (COO^-, o O-) de la superficie de los MOFs que actúan como ligandos en la formación de complejos con los iones metálicos. En el caso de Cr(VI), los datos experimentales de adsorción de GO-I y GO-II se ajustan al modelo de Freundlich y la adsorción se produce por la interacción electrostática de $HCrO_4^-$ con los grupos funcionales protonados a pH bajos (1-2) de la superficie del adsorbente. En general, las capacidades de adsorción obtenidas para los iones metálicos estudiados con este MOFs fueron inferiores a las reportadas para otros óxidos de grafeno que sugiere que los procedimientos utilizados para producir los óxidos de grafeno no fueron efectivos para obtener un alto grado de oxidación y de funcionalización de los grafeno y

que también afectaron las propiedades físicas (superficie, porosidad y tamaño de poro) de los óxidos de grafeno producidos.

Los metal-organic frameworks (MOFs) son una clase de materiales adsorbentes que se han desarrollado en las últimas tres décadas. Los MOFs se construyen con unidades de construcción secundarias, que son iones metálicos o cúmulos metálicos y ligandos orgánicos, que se conectan formando celosías tridimensionales. Los MOFs tienen numerosas ventajas como adsorbentes debido a su elevada área superficial, que suele variar entre 1000 y 10.000 m^2 g^{-1}, porosidad, estabilidad química, funcionalidad y accesibilidad al lugar de adsorción para la difusión de los contaminantes a través del MOF.

La presencia de arsénico en el agua, especialmente aguas subterráneas, es un problema importante en diferentes zonas del mundo dado que es un potente carcinógeno. La toxicidad del arsénico inorgánico es superior a la de los organoarseniatos, el arsénico se encuentra generalmente en el medio acuático en sus formas inorgánicas disueltas el arsenito As(III) y el arseniato As(V). Aunque estas dos especies son tóxicas, el As(III) es aproximadamente 60 veces más venenoso que el As(V). Hay una amplia diversidad de tecnologías que permiten eliminar el arsénico de las aguas, como la coagulación-precipitación, el intercambio iónico, la separación con membranas, y la adsorción, está última mediante adsorbentes convencionales o adsorbentes diseñados específicamente para eliminar el arsénico.

Entre los materiales avanzados para eliminar el arsénico cabe mencionar los óxidos de grafeno (MOFs), los nanotubos de carbono (CNT) y las estructuras metálicas orgánicas (MOFs), así como muchos otros materiales porosos. En los últimos diez años, los MOFs y los materiales compuestos basados en MOFs han utilizado cada vez más en la eliminación de As(III) y As(V) del agua, debido a sus excelentes capacidades de adsorción. Entre ellos, los MOFs a base de hierro como MIL-53(Fe), MIL-88B, MIL-100(Fe) y MIL-101(Fe) han sido los más estudiados por su gran afinidad por As(V) debido a las interacciones ácido-base de Lewis y electrostáticas que tienen lugar entre $H_2AsO_4^-$ y Fe^{3+}. El Fe-BTC, un MOF que contiene nodos de hierro y el ácido benceno-1,2,4-tricarboxílico como ligando, fue el primero que se utilizó para eliminar las especies de As(V) de las soluciones acuosas. MIL-100(Fe) y Basolita F300 son dos MOFs comerciales basados en Fe-BTC.

En este estudio, el MOF comercial Basolita F300 y un Nano-Fe-BTC MOF, sintetizado en colaboración con el Departamento de Química de la Universidad de La Laguna, se han caracterizado y evaluado como adsorbentes en la eliminación de la arsenito y arseniato de soluciones acuosas. El análisis elemental de la superficie del adsorbente, realizada por EDX, mostró que la Basolita F300 contenía un porcentaje de hierro inferior (2,97%) en el Nano-{Fe-BTC} MOF (3,68%).

Los espectros de infrarrojos de la Basolita F300 y el MOF sintetizado, nano-{Fe-BTC}, muestran bandas similares, incluyendo las de la región 650 a 1800 cm^{-1}, que corresponden al perfil característico de los MOFs. Con respecto al área superficial y al volumen de poro, el material sintetizado tiene un volumen de poro mayor que Basolita F300, mientras que el área superficial es mayor en la Basolita F300. Los resultados de BET también muestran que el nano- {Fe-BTC} MOF presenta mesoporos con un diámetro de tamaño superior (entre 2 nm y 50 nm) a los de la Basolita F300. En las imágenes SEM de nano-{Fe-BTC}, se observaron una serie de grietas y poros asimétricos con una estructura de poros abiertos con tamaño de partícula.

Se estudió la cinética de la adsorción de As(III) y As(V) variando el tiempo de contacto de 2 min a 120 min utilizando 0,1 g L^{-1} de Basolita F300 con una concentración inicial de arsénico de 10 mg L^{-1} a pH 5.6 por el As (V) ya pH 9.6 por el As(III). El equilibrio se alcanzó aproximadamente después de una hora de contacto. Los datos experimentales de As(V) y As(III) se ajustaron al modelo de pseudo-segundo orden, lo que sugiere que la adsorción de As(III) y As(V) por la Basolita F300 se basa en la quimisorción. La relativa linealidad del modelo cinético de difusión intrapartícula para As(III) y As(V) indica que la difusión intrapartícula puede ser el paso que determina la velocidad del proceso con una contribución baja de la difusión a través de la capa límite.

La adsorción de arsénico se da mediante la coordinación y la interacción electrostática y depende del pH. En el caso de As(V), $H_2AsO_4^-$ es la especie predominante en el rango de pH de 3-8 y la especie $HAsO_4^{2-}$ es la predominante en el rango de pH de 8-11, ambos aniones son base de Lewis que pueden interactuar fuertemente con el centro de Fe^{3+} (ácido de Lewis) del MOF. Además, la interacción electrostática entre el arseniato y el Fe^{3+} incentiva la adsorción del As(V). El porcentaje máximo de adsorción (90%) se obtuvo en el intervalo de pH de 5.6-9.5. En el caso de As(III), la adsorción se produjo a pH> 9 cuando la especie $H_2AsO_3^-$, una base de Lewis blanda, puede interactuar con el Fe^{3+}. A pH 9.5, se alcanzó el porcentaje máximo de eliminación de

As(III) (47%) en las condiciones experimentales utilizadas, concentración inicial de As(III) de 5 mg L^{-1} y concentración de adsorbente de 0,5 g L^{-1}.

Los análisis FTIR realizadas antes y después de la adsorción con los dos materiales de Fe-BTC parecen confirmar que la adsorción de las especies de arsénico sobre MOFs basados en Fe se explica por la coordinación Fe-O-As. Los datos experimentales de adsorción de As(V) por la Basolita F300 ajustan al modelo de Freundlich (K_F = 10), indicando la alta afinidad de este MOF por el As(V), mientras que el modelo de Langmuir permite explicar la adsorción de As (III) con una máxima capacidad de adsorción de 10 mg g^{-1}. Este valor es similar al obtenido a partir de los datos cinéticos para As(III) mientras que para As(V), a partir del modelo cinético de pseudo-segundo orden se calculó una máxima capacidad de adsorción de 32,67 mg g^{-1}.

La eficiencia de adsorción de Basolita F 300 se comparó con la del nano Fe-BTC MOF, y no se encontraron grandes diferencias entre los dos adsorbentes en el caso de As(V) con porcentajes de eliminación del 90 % y 86,7%, respectivamente, mientras que en el caso de la adsorción de As(III) las diferencias fueron mayores, con un porcentaje del 47% para Basolita F300 y de un 36% por Fe-BTC sintetizado. La presencia de otros aniones con el arsenito y el arseniato en la misma solución puede afectar la eficiencia del adsorbente y sus potenciales aplicaciones. Por tanto, se investigó el efecto del PO_4^{3-} (10, 100 y 300 mg L^{-1}) sobre la eliminación de As(III) y As(V) cuando la concentración de arsénico es de 10 mg L^{-1}. Los resultados obtenidos muestran que la presencia de fosfato reduce el porcentaje de adsorción de As(III) y As(V) en un 18,5% y un 6%, respectivamente, cuando las soluciones contenían 10 mg L^{-1} de PO_4^{3-}. El aumento de la concentración de PO_4^{3-} provocó una disminución aún mayor en el porcentaje de adsorción de As(V) y As(III). La similitud química entre estos aniones y el hecho de que As y P tengan una electronegatividad similar (2,18) explican que los aniones arsenito, arseniato y fosfato compiten por los sitios activos de adsorción de los MOFs.

Résumé

Les eaux usées rejetées par les activités industrielles et agricoles contiennent des quantités relativement importantes d'ions métalliques toxiques, notamment le Cd(II), le Cu(II), le Pb(II) et le Cr(VI). L'élimination de ces polluants présente un grand intérêt du point de vue de la santé et de l'environnement. La contamination à l'arsenic, généralement associée à l'environnement géochimique, constitue une menace mondiale en raison de sa toxicité aigüe et de sa cancérogénicité. L'oxydation de différentes espèces minérales en raison des conditions de redox fait que l'arsenic devient soluble et pénètre dans le milieu environnant par l'eau de drainage. Les technologies classiques de traitement et d'épuration des eaux usées, telles que la précipitation, la coagulation-floculation, les procédés membranaires, l'électrodialyse et l'échange d'ions, sont d'une utilité limitée en raison de leur coût élevé et de leur inefficacité dans l'élimination des faibles concentrations de métaux, et parfois aussi parce qu'ils peuvent générer de grands volumes de boues.

L'adsorption est une alternative intéressante en raison de sa simplicité, de sa capacité à éliminer des quantités infimes d'ions métalliques, de son faible coût, de sa courte durée de fonctionnement et de la capacité de réutilisation du matériau. Les processus de sorption sont basés sur l'adsorption physique, l'adsorption chimique et les mécanismes d'échange d'ions. Parmi les différents matériaux absorbants, le carbone activé est le plus utilisé malgré son coût initial élevé et ses coûts de régénération.

Dans la recherche d'adsorbants économiques, écologiques et hautement efficaces, de déchets agricoles et de sous-produits issus des industries forestières, y compris les déchets de thé, le café, les coques et les coquilles de différentes noix, la sciure, les écorces, les déchets cellulosiques et lignocellulosiques, les épis de maïs, les coques de riz, gâteau aux olives, pelures de fruits, pulpe de betterave à sucre, grappe de palmiers, feuilles de maïs, entre autres, ont été évalués comme des biosorbents. Ils ont tous une bonne capacité d'adsorber les ions métalliques en raison de leur structure poreuse et du fait qu'ils ont de carboxyle, de l'hydroxyle et d'autres groupes fonctionnels à leur surface.

Le type de groupes fonctionnels et les composants chimiques des matériaux lignocellulosiques en font une bonne alternative d'adsorbant pour traiter les effluents contaminés. Les coûts de ces traitements seront faibles si les biosorbents disponibles localement les plus adaptés sont utilisés.

Ainsi, dans notre cas, nous avons évalué les déchets agro-industriels lignocellulosiques disponibles dans la région méditerranéenne, tels que les noyaux d'olive et les cônes de pin, comme biosorbants efficaces pour l'élimination des ions métalliques toxiques tels que Pb(II), Cu(II), Cd(II) et Cr(VI).

La caractérisation physique et chimique de ces matériaux lignocellulosiques a été réalisée à l'aide de différentes techniques telles que la spectroscopie infrarouge (FTIR), la microscopie électronique à balayage (SEM), la spectroscopie à rayons X à dispersion d'énergie (EDX), Brunauer-Emmet-Teller (BET) et analyse thermogravimétrique (TGA). Les résultats ont montré que ces déchets agricoles étaient principalement composés de carbone (53%) et d'oxygène (45.5%) et que des groupes fonctionnels tels que les carboxyliques et hydroxyles étaient présents sur leurs surfaces. On a constaté que la surface de la pomme de pin moulue était plus grande (0,2536 m^2 g^{-1}) que celle de la pierre d'olive moulue (0,1956 m^2 g^{-1}), alors que cette dernière avait une taille de particules plus petite à 30,67 µm que celle de la pomme de pin (50 µm). Des expériences d'adsorption par lots ont été effectuées pour évaluer la capacité d'adsorption de Cu(II), de Cd(II), de Pb(II) et de Cr(VI) de grignons d'olive moulues (30.67 µm) et de cône de pin moulu (50 µm) à l'aide de solutions aqueuses simples et multi-métalliques. Les différents paramètres affectant l'efficacité d'adsorption des métaux, tels que le temps de contact, le pH de la solution aqueuse, la quantité d'adsorbant et la concentration initiale des métaux, ont été évalués.

Des modèles isothermes d'adsorption ont ensuite été appliqués afin de caractériser le processus d'adsorption. Dans le cas de la pierre d'olive, les données expérimentales ont été bien décrites avec l'isotherme Langmuir avec des capacités d'adsorption à pH 6 de 0,557 mg g^{-1}, 0,3 mg g^{-1} et 0,581 mg g^{-1} pour Cu(II), Cd(II) et Pb(II), respectivement, alors que pour Cr(VI), le modèle Temkin a fourni le meilleur ajustement avec une capacité maximale de 2,34 mg g^{-1} à pH 2.

Les données cinétiques s'insèrent bien dans le modèle du pseudo second ordre qui permet de calculer les constantes du taux d'adsorption. Cd(II) s'est avéré avoir la constante cinétique la plus élevée, suivie de Cu(II), Cr(VI) et Pb(II). Des solutions multi-métalliques contenant des concentrations égales des trois ions métalliques divalents ont été utilisées pour évaluer leur concurrence pour les sites de sorption de la pierre d'olive, entraînant une diminution de 50 % de la capacité de sorption de Pb(II) lorsque Cu(II) et Cd(II) étaient également présents.

Dans le cas de ces deux derniers métaux, les capacités de sorption ont diminué de 30% et 15%, respectivement, lorsque les autres métaux étaient présents. Comme le Cd avait la constante de

taux la plus élevée, ce métal a été le premier à saturer les sites de surface disponibles, suivi de Cu et Pb. L'efficacité du cône de pin moulu pour éliminer les traces de concentration de Pb(II), Cd(II) et Cu(II) a été démontrée, ce qui donne des capacités de 100,01 mg g^{-1}, 78,73 mg g^{-1} et 33,04 mg g^{-1} à pH de 5,5, respectivement. Ces capacités sont supérieures à celles signalées pour d'autres biosorbents ayant des caractéristiques semblables. De plus, une capacité d'adsorptionde 57,36 mg g^{-1} a été obtenue pour le Cr(VI) à pH 2 et son pourcentage maximal d'élimination (88,8 %) a été obtenu à pH 2 avec 10 g L^{-1}.

Les données expérimentales d'adsorption ont bien corrélé avec le modèle de Langmuir pour Cu(II) et Cr(VI), tandis que pour Pb(II) et Cd(II) les meilleures corrélations ont été obtenues avec le modèle de Langmuir-Freundlich. Dans le cas des ions divalents (Pb(II), Cu(II) et Cd(II)), il n'y avait aucune concurrence entre eux à l'égard des sites adsorbants à de faibles concentrations de métaux (1-10 mg L^{-1}), étant donné que la présence d'autres ions métalliques ne réduisait pas l'efficacité de l'élimination. Les résultats obtenus à l'aide de biosorbants de grignon d'olive et cône de pin montrent que le cône de pin a les capacités d'adsorption les plus élevées en raison de sa plus grande surface. L'adsorption de Pb(II), de Cu(II) et de Cd(II) pour les deux biosorbants est expliquée par la complexation de surface avec les groupes fonctionnels de la surface adsorbante et l'efficacité d'élimination était plus grande pour Pb(II), qui a la plus grande électronégativité et le rayon ionique, que pour Cd(II) et Cu(II).

Dans le cas de l'adsorption du Cr(VI), des pourcentages maximaux d'élimination de 46 % pour la pierre d'olive et de 88 % pour la pomme de pin ont été obtenus à pH 2, ce qui montre que cet anion toxique peut être éliminé par un mécanisme d'échange d'ions couplé à une réaction de réduction du Cr(VI) au Cr(III).

En outre, dans le cas de solutions multi-métalliques d'ions métalliques divalents, il n'y avait aucune concurrence entre elles pour les sites de surface de cône de pin, qui fonctionnaient mieux en tant que biosorbant que la pierre d'olive et d'autres biosorbants précédemment étudiés tels que la pomme crème anglaise, le riz et l'enveloppe de maïs. Des expériences par lots sont utilisées pour obtenir des isothermes de sorption d'équilibre et pour évaluer la capacité de sorption des biosorbants.

Cependant, dans le fonctionnement pratique des processus de biosorption à grande échelle, les colonnes à lit fixe à débit continu et les colonnes à lit fluidisé sont souvent préférées pour traiter de grands volumes d'effluents.

Dans de tels systèmes, les profils de concentration dans les phases liquide et sorbant varient à la fois dans l'espace et dans le temps. Le cône de pin a été choisi comme biosorbant pour évaluer l'élimination des ions métalliques toxiques dans des conditions dynamiques dans une colonne à lit fixe en raison de sa bonne performance et de sa grande affinité pour Pb(II), Cu(II), Cd(II) et Cr(VI). Le comportement des adsorbants dans une colonne à lit fixe est décrit en termes de courbes de percée et d'effet de paramètres tels que la concentration initiale d'adsorbant, la hauteur du lit et le débit sur le profil de ces courbes et la capacité de retrait de Pb(II) On a également étudié la présence de cônes de pin dans des conditions dynamiques.

Les données expérimentales de l'adsorption de Pb(II) dans une colonne à lit fixe à l'échelle du laboratoire remplie de cône de pin ont été analysées à l'aide de modèles Thomas, Adams-Bohart et Yoon-Nelson. Les résultats montrent que les données expérimentales de l'élimination de Pb(II) ont suivi le modèle Thomas avec un coefficient de détermination R2>0,9, les meilleurs résultats étant obtenus aux débits les plus faibles et aux hauteurs de lit les plus élevées. La capacité de sorption de Pb(II) de la pomme de pin était de 77,92 mg g^{-1} à un débit de 2,2 mL min^{-1}, à une hauteur de lit de 0,7 cm et à une concentration initiale de 50 mg L^{-1}.

La séparation du Pb(II), du Cu(II) et du Cd(II) a été évaluée en faisant passer des solutions aqueuses multi-métalliques contenant une concentration initiale égale des trois ions métalliques de 25 mg L^{-1}, 50 mg L^{-1} et 100 mg L^{-1} à une hauteur de lit de 1 cm à un débit de 2,2 mL min^{-1}.

La percée et l'épuisement du lit fixe se sont produits plus tôt pour le Cd, suivis du Cu et du Pb, ce qui a permis, dans le cas de la concentration initiale la plus élevée (100 mg L^{-1}), de séparer le Pb(II) du Cd(II) et le Cu(II).

Le temps d'épuisement le plus élevé a été pour Pb(II) suivi de Cu(II) et Cd(II) confirmant l'affinité plus élevée de la pomme de pin par Pb(II). De plus, l'adsorption des trois ions métaux lourds à des concentrations initiales égales de 50 mg de L^{-1} à un pH de 4,4 en présence de cations divalents mous (100 mg de L^{-1} de Ca(II)) a été évaluée en utilisant une hauteur de lit de 1 cm de cône de pin et un débit de 2,2 mL min^{-1}.

Les résultats obtenus ont montré que Ca(II) n'était pas adsorbé et que sa présence n'affectait pas l'adsorption de Pb(II), Cu(II) et Cd(II). Compte tenu de l'affinité des cônes de pin moulus pour Cr(VI) et Cu(II) et du fait que la présence de ces ions métalliques dans les effluents de l'industrie de la galvanoplastie peut fortement affecter l'environnement, la capacité d'une colonne à lit fixe remplie de cônes de pin (hauteur du lit 2 cm) pour éliminer ces ions métalliques a été évalué à un débit de 2,2 mL min^{-1}. À cette fin, une solution aqueuse simulant un déchet de galvanoplastie contenant 20 mg L^{-1} de Cu(II), 100 mg L^{-1} de Ni(II) et 30 mg L^{-1} de Cr(VI) à pH 4,4 a été préparée. Dans ces conditions expérimentales, les pourcentages d'élimination de Cu(II), Ni(II) et Cr(VI) étaient respectivement de 97 %, 94 % et 93 %. Cr(VI) a traversé la colonne plus rapidement que Cu(II) et Ni(II) de son affinité plus faible pour les cônes de pin à pH>2. Ni(II) et Cu(II) ont traversé la colonne à 30 et 80 minutes respectivement.

Des expériences de désorption ont ensuite été effectuées à l'aide d'une solution de HCl de 1,0 M, ce qui a donné des pourcentages de désorption de 90 % pour Cr(VI), et 94 % pour Cu(II) et Ni(II).

Pour surmonter ces limites, de nouveaux sorbants de dimensions nanométriques sont synthétisés et adoptés pour la décontamination de l'eau. Les principaux avantages des nano-adsorbants d'ingénierie sont leur grande surface spécifique et la disponibilité d'un grand nombre de groupes actifs pour la liaison des ions de métaux lourds qui peuvent être adaptés pour améliorer la sélectivité du processus d'adsorption. Parmi les nano-adsorbants fabriqués, l'oxyde de graphène (GO), obtenu par oxydation du graphène, est considéré comme un adsorbant prometteur pour l'élimination des ions de métaux lourds tels que Cu(II), Cd(II) et Cr(VI).

Cependant, il est important de noter que les matériaux GO présentaient de fortes différences, selon les oxydants, les conditions de réaction et la source de graphite utilisée pour les préparer. Dans le cadre de notre collaboration avec le département de chimie de l'université Masaryk (Brno, République tchèque), des échantillons de quatre graphénoides, à savoir GO-I, GO-II, 97D et 227A, ont été caractérisés et évalués pour l'élimination des ions métalliques divalents tels que Cu(II) et Cd(II) et chromate à partir de solutions aqueuses. La préparation de ces OGM n'est pas détaillée ici car ils sont sous brevet.

La caractérisation des organismes génétiquement modifiés a été effectuée à l'aide de différentes techniques d'analyse, comme l'analyse élémentaire, les analyses XPS et XRD qui ont été

effectuées à l'Université Masaryk, tandis que les analyses FTIR, SEM, EDX et TGA/DTA ont été effectuées à l'Université de Gérone. Les résultats de XPS ont montré que le degré de fonctionnalisation était faible et que le pourcentage de groupes C=O variait de 11,6 à 12,56 %. Les bandes carbonyl/carboxyl et OH ont été identifiées par FTIR.

Tous les oxydes de graphène présentaient le même schéma XRD et le même spectre Raman, montrant que les niveaux d'oxydation étaient relativement faibles. Cette faible fonctionnalisation a été confirmée par la composition de surface déterminée par EDX qui a donné des pourcentages de C plus élevés ou autour de 88%, et des pourcentages d'oxygène entre 4 et 9%. Les surfaces de BET variaient de 14,2268 à 25,8041 $m^2\ g^{-1}$, celles-ci étant inférieures à celles déclarées pour les autres oxydes de graphène.

Les pourcentages d'élimination les plus élevés pour Cu(II) (> 90 %) et Cd(II) (> 88 %) avec les oxydes de graphène 227A, GO-I et GO-II ont été obtenus à la plus faible concentration initiale (5 mg L^{-1}) à pH 6, une concentration adsorbante de 2 g L^{-1} et une heure de temps de contact. Toutefois, dans le cas de 97D, l'efficacité d'adsorption était inférieure (80 % pour Cu(II) et 60 % pour Cd(II)) dans toutes les expériences, bien qu'une période plus longue (t=3 h) ait été nécessaire pour atteindre l'équilibre.

Dans le cas du Cr(VI), l'effet de la concentration initiale sur l'adsorption du Cr(VI) a été évalué à l'aide de GO-I et de GO-II à un pH de 2 et de 10 g de L^{-1} d'adsorbant, ce qui a donné lieu à un pourcentage d'élimination plus élevé (68 %) pour le GO-I que pour le GO-II (45 %). Les données expérimentales d'adsorption de Cd(II) correspondaient bien au modèle isotherme de Freundlich avec K_F 2.32 pour 227A et K_F 2.71 pour GO-II alors que Langmuir-Freundlich était le meilleur modèle pour 97D et GO-I avec des capacités d'adsorption de 5,19 et 5,28 mg g^{-1}, respectivement.

Les données expérimentales de Cu(II) convenaient bien au modèle de Freundlich pour tous les OG avec des valeurs de K_F allant de 2,61 (97D) à 3,72 (GO-II). L'adsorption de Cu(II) et de Cd(II) semble se faire par son interaction avec les groupes fonctionnels (COO-, ou O-) à la surface de GO pour former un complexe d'ions métalliques.

Dans le cas du Cr(VI), le meilleur ajustement des données expérimentales était avec le modèle de Freundlich pour GO-I et GO-II et l'interaction électrostatique du $HCrO_4^-$ avec les groupes protonés de la surface sorbante à des pHs faibles (1-2) peut expliquer l'absorption du Cr(VI).

En général, les capacités d'adsorption obtenues pour les ions métalliques cibles avec ces OGM étaient inférieures à celles rapportées pour d'autres oxydes de graphène, ce qui montre que les procédés synthétiques ont conduit à un faible degré d'oxydation des graphènes affectant également les propriétés physiques (surface, porosité et taille des pores) des oxydes de graphène résultants.

Les cadres métalliques et organiques sont une classe de matériaux adsorbants qui ont émergé au cours des trois dernières décennies. Les MOF sont construits à partir d'unités de construction secondaires, à savoir des ions métalliques ou des amas métalliques, et des ligands organiques, qui sont reliés en treillis tridimensionnels.

Les MOF présentent de nombreux avantages en tant qu'adsorbants en raison de leur surface élevée, généralement comprise entre 1000 et 10000 m^2 g^{-1}, de leur porosité, de leur stabilité chimique, de leur fonctionnalité et de l'accessibilité du site d'adsorption par la diffusion de contaminants dans le cadre.

La présence d'arsenic dans l'eau, en particulier dans les eaux souterraines, est un problème majeur dans différentes régions du monde, car elle est un puissant cancérogène pour l'homme. La toxicité de l'arsenic inorganique est plus élevée que celle de l'arsenic organique et, en général, l'arsenic existe dans les formes inorganiques dissoutes de l'arsenic As(III), de l'arsenite et de l'arsenate As(V).

Bien que ces deux formes soient toxiques, As(III) est environ 60 fois plus toxique qu'As(V). On a proposé de vastes technologies pour la purification de l'eau, comme la coagulation chimique, la précipitation, l'échange d'ions, la séparation membranaire et l'adsorption, à l'aide d'adsorbants conventionnels et artificiels, pour éliminer l'arsenic de l'eau.

Les matériaux avancés pour l'élimination de l'arsenic comprennent les oxydes de graphène (OGM), les nanotubes de carbone (CNT) et les cadres organiques métalliques (MOF) ainsi que de nombreux autres matériaux poreux. Au cours des dix dernières années, les MOF et les composites à base de MOF ont été de plus en plus utilisés pour éliminer As(III) et As(V) de l'eau, en raison de leurs excellentes capacités d'adsorption.

Parmi eux, les MOF à base de fer tels que MIL-53(Fe), MIL-88B, MIL-100(Fe), et MIL-101(Fe) ont montré une grande affinité pour As(V) en raison de la base acide de Lewis et des interactions électrostatiques entre $H_2AsO_4^-$ et Fe^{3+}. Le Fe-BTC, un MOF contenant des nœuds de fer et des

liants tricarboxyliques au 1, 3, 5-benzène, a été le premier à être utilisé pour éliminer les espèces d'As(V) des solutions aqueuses. MIL-100(Fe) et Basolite F300 sont des MOF commerciaux basés sur Fe-BTC.

Dans cette étude, le Basolite F300 et un MOF Nano-Fe-BTC, synthétisés en collaboration avec le Département de chimie de l'Université de La Laguna, ont été caractérisés et évalués comme adsorbants pour l'élimination de l'arsenite et de l'arsenate des solutions aqueuses. L'analyse élémentaire de la surface adsorbante, effectuée par EDX, a montré que le Basolite F300 contenait un pourcentage de fer inférieur (2,97 %) à celui du Nano-{Fe-BTC} MOF (3,68 %).

Les spectres infrarouges du Basolite F300 commercial et du MOF nano-{Fe-BTC} synthétisé montrent des bandes similaires, y compris dans la région 650-1800 cm^{-1}, qui est généralement considérée comme une empreinte de MOF. En ce qui concerne la surface et le volume des pores, la matière synthétisée a un plus grand volume de pores que la Basolite F300 alors que la Basolite commerciale a une plus grande surface. BET results also show that mesopores with a diameter in the upper size range (between 2 nm and 50 nm) were present in nano-{Fe-BTC} MOF. In the SEM images of Nano-{Fe-BTC}, a series of cracks and asymmetric pores with an open pores structure with particle size were observed.

La cinétique de l'adsorption As(III) et As(V) a été étudiée en faisant varier le temps de contact de 2 min à 120 min en utilisant 0,1 g L^{-1} de basolite F300 avec une concentration initiale d'arsenic de 10 mg L^{-1} à pH 5.6 pour As(V) et la même concentration à pH 9.5 pour As(III). L'équilibre a été atteint environ après 1 heure.

Les données expérimentales d'As(V) et d'As(III) ont bien adapté le modèle du pseudo-second ordre montrant que la chimisorption est le mécanisme dominant pour l'adsorption d'As(III) et d'As(V). La relative linéarité du modèle cinétique de diffusion intraparticule pour As(III) et As(V) indique que la diffusion intraparticule peut être le processus de contrôle du débit avec une faible contribution de la diffusion de la couche limite.

L'adsorption de l'arsenic s'est produite par coordination et interaction électrostatique et dépend du pH. Dans le cas d'As(V), le $H_2AsO_4^-$ est l'espèce prédominante dans la plage de pH 3-8 et l'$HAsO_4^{2-}$ est l'espèce prédominante dans la plage de pH 8-11, les deux anions sont la base de Lewis qui peut interagir fortement avec les cations Fe^{3+} centrés (acide Lewis).

De plus, l'interaction électrostatique entre l'arsenate et la charge positive de l'adsorption Fe^{3+} centrée a augmenté As(V). Le pourcentage d'absorption maximal (90 %) a été obtenu à pH. Dans le cas d'As(III), l'adsorption s'est produite à des pHs > 9 lorsque les espèces H_2AsO_3, une base molle de Lewis, peuvent interagir avec le Fe3+ centré. À un pH de 9.5, le pourcentage maximal d'élimination d'As(III) (47 %) dans les conditions expérimentales, 5 mg de L^{-1} et la concentration adsorbante de 0,5 g de L^{-1}, ont été atteints.

Les analyses FTIR effectuées avant et après adsorption avec les deux matériaux Fe-BTC semblent confirmer que l'adsorption des espèces d'arsenic sur les matériaux à base de Fe est expliquée par la coordination Fe-O-As.

Les données expérimentales d'As(V) sur Basolite F300 ont bien ajusté le modèle de Freundlich (K_F=10 mg g^{-1}), indiquant l'affinité élevée de ce MOF par As(V), alors que Langmuir était le meilleur modèle pour expliquer l'adsorption d'As(III) avec une capacité d'adsorption maximale de 10 mg g^{-1}. Cette valeur est similaire à celle obtenue à partir des données cinétiques pour As (III), tandis que pour As (V), le modèle cinétique du pseudo-second ordre a donné une capacité d'adsorption maximale de 32,67 mg g^{-1}. L'éfficacité d'adsorption de Basolite F300 a été comparée aux MOF nano Fe-BTC, ce qui n'a pas montré de différences entre les deux adsorbants dans le cas de As(V) avec des pourcentages d'élimination de 90 % et 86,7 % pour Basolite F300 et Nano Fe-BTC, respectivement.

Cependant, le pourcentage d'élimination d'As(III) par Basolite F300 (47 %) était plus élevé que pour le Fe-BTC synthétique (36 %).
L'étude de la présence d'autres anions avec de l'arsenic dans la même solution est un facteur important qui peut affecter l'efficacité de l'adsorbant et son potentiel pour les applications. Par conséquent, l'effet du PO_4^{3-} (10, 100 et 300 mg L^{-1}) sur l'élimination d'As(III) et As(V) a été étudié en maintenant une concentration constante d'arsenic de 10 mg L^{-1}.
Les résultats obtenus montrent que la présence de phosphate réduit le pourcentage d'élimination d'As(III) et d'As(V) de 18,5% et de 6%, respectivement, lorsque les solutions contenaient 10 mg de L^{-1} de PO_4^{3-}. L'augmentation de la concentration de PO_4^{3-} a entraîné une diminution du pourcentage d'élimination d'As(V) et As(III). La similitude chimique entre ces anions et le fait que As et P ont une électronégativité similaire (2.18) expliquent que les anions arsenic et phosphate sont en concurrence pour les sites actifs d'adsorption des MOFs.

1. INTRODUCTION

1.1. Environmental pollution

Pollution is one of the main environmental problems in the world nowadays through different factors such as the increase of population and the rapid development of industrialization, which can result in the destruction and the damaging of the ecosystem causing health problems. Pollution can affect air, water, biota and soil. For this reason, the objective of the United Nations (the UN) is to achieve up to 16 sustainable development goals (United Nations, 2015). Although all the goals are important, goal number 6 "Clear water and sanitation" is fundamental for the other goals to be achieved. This need is explained by two main facts: i) Proper sanitation is not available for all populations yet since about 2500 million people still do not have access to satisfactory sanitation (UN-Water, 2014); ii) About 40% of the global population is affected by water shortages, and this is expected to increase in the future due to population growth and climate change. Water is essential for human health as it represents 75% of the human body and it plays several functions such as a lubricant in the body, temperature regulation etc. It has been reported that each person requires 20 to 50 liters of clean water for daily needs such as drinking, cooking, hygiene etc. (Khalifa and Bidaisee, 2018). To reach the targets required for assuring worldwide clean water and sanitation, there is a need to develop technologies that can improve both wastewater treatment and water reuse at low capital and operational costs. Wastewater is classified into domestic wastewater, storm water/run-off and industrial wastewater. Wastewater from industrial processes is the major source of water pollution that contains different concentrations of organic pollutants like dyes, pesticides, oils, etc., and inorganic pollutants such as heavy metals which are discharged into rivers and can cause health problem as most of them are non-biodegradable. Nowadays, metal pollution through industrial effluents discharge from pigment mining, electroplating, tanning, textile industries is one of the main environmental problems because they can affect human health through food, water, air or absorption through the skin and accumulate in the body causing different kinds of diseases (Masindi and Muedi, 2018). Effluents are the main contributor to metal pollution even where the legally required pretreatment of these effluents has been performed (Abdel Salam et al., 2011). The growing water demand in urban, rural and industrial sites poses serious ecological and economic concerns in water

management linked to resource depletion and waste disposal. Several industrial processes use large water volumes, thus producing high quantities of wastewater containing contaminants and valuable components such as metals or nutrients. The recovery of these components and the reuse of water require the design and implementation of advanced treatment methods. In this sense, the zero liquid discharge concept aims to develop strategies to close the material loop and minimizing the liquid waste (Muhammad Yaqub and Lee, 2019).

1.2. Metal pollutants

Heavy metals are natural elements having characteristics of higher density, malleability and toxicity even at low concentrations. Heavy metals are the group of metals and metalloids, which are defined as the elements having atomic weights between 63.5 and 200.6 and with a density greater than 5 g cm^3 (Aeisyah et al., 2014). They occur naturally as ions, compounds and complexes (Malik et al., 2016). Some of the examples of heavy metals include copper, cadmium, zinc, chromium, arsenic, lead, cobalt, nickel, mercury, etc. Heavy metals like copper, zinc, nickel, boron, iron, molybdenum are basic needs for the growth of the plants but they are harmful when their concentrations go beyond the permissible limits. A few other heavy metals such as lead, mercury, and cadmium as well as metalloids like arsenic have harmful effects on human health, fauna and flora, even at low concentrations (Edelstein and Ben-Hur, 2018). The high toxicity and non-biodegradability of heavy metals make them a serious environmental concern as their accumulation results in damage to both ecosystems and human health (Galvez and Lefrançois, 2016; Johnson et al., 2008). It is increasingly difficult to obtain access to clean water due to the highly contaminating effect of certain industries being compounded by ever more frequent conditions of drought and so the removal of heavy metals and metalloids such as Cd(II), Cu(II), Cr(VI), As(III),As(V) and Pb(II) from industrial wastewater is a major concern for society (Ofomaja et al., 2010). The World Health Organization (WHO) set the maximum allowed limit of Pb(II), Ni(II) and Cu(II) in drinking water at 0.01, 0.07 and 2 mg L^{-1}, respectively (World Health Organization, 2017). Moreover, soil becomes polluted with heavy metals because of the entry of industrial wastewater, sewage sludge, fertilizers, utilization of treated wastewater in land application and weathering of soil minerals (Liu et al., 2018). The main physico-chemical properties and toxicity of these metals are described below.

1.2.1. Chromium

Chromium is one of the most available metals, the seventh, in the earth and it is present as an ore composed of ferric chromite ($FeCr_2O_4$), crocoite ($PbCrO_4$), and chrome ochre (Cr_2O_3). The major industrial source of chromium waste is from leather industries, tanning industries, electroplating industries, textile industries, etc. These industries develop a waste product in which hexavalent form of Cr(VI) and trivalent form of Cr(III) are present. Cr(VI) is more harmful than Cr(III) for plants, animals, and organisms (Ali et al., 2013). These two forms are utilized in industries like steel production, chrome plating, wood conservation, glass industry, pigment fabrication, plating and electroplating industries and as leather tanning agents. Chromium causes skin inflammation, liver and kidney damage, pulmonary congestion, vomiting and the creation of ulcers (Miretzky and Cirelli, 2010). Because of these effects, the chromium must be removed from the wastewater before it gets released into the environment, or the chromium metal needs to be modified into less toxic forms, which is also necessary for human nutrition (Kumar et al., 2012).

1.2.2. Copper

As commented above, copper is an essential element for humans as it is important in enzyme synthesis, bone development and in tissues. The different forms of copper are Cu(0), Cu(I), and Cu(II) which is the most toxic cupric ion and the most present in the environment (Awual et al., 2014). The major contributors of copper in wastewater are mining and electroplating industries, chemical manufacturing (i.e. paints, fertilizers, etc.), metallurgy, steel industries, and circuit printing. The effects of copper are hair loss, anemia, kidney damage and headache, and this metal accumulates in the liver, brain or pancreas and leads to death (Zhou et al., 2009). Hence, an adequate technological treatment to remove copper from the wastewater is needed.

1.2.3. Cadmium

Cadmium (Cd) is one of the most toxic heavy metals and is considered non-essential for living organisms. Cadmium, which is widely used and extremely toxic in relatively low dosages, is one of the principal heavy metals responsible for causing kidney damage, renal disorder and destruction of red blood cells. Cd(II) has been considered as a priority pollutant by the Environmental Protection Agency (USEPA) due to its toxicity and bioaccumulation, The main anthropogenic pathway through which Cd(II) enters the water bodies is via waste and wastewater

from industrial processes such as electroplating, plastic manufacturing, metallurgical processes and industries of pigments and Cd/Ni batteries. In view of its persistence as a cumulative poison and the low tolerance of the human body towards cadmium, it is of interest to develop schemes for its removal (Carolin et al., 2017).

1.2.4. Nickel

This is an element with atomic number 28, and its main oxidation state is +2. The main source of nickel in the environment is in the discharge of wastewater from electroplating industries, silver refineries, and battery manufacturing industries. Nickel causes breathing problems, nausea, diarrhea, skin eruption, and pulmonary fibrosis in human beings (Malamis and Katsou, 2013).

1.2.5. Lead

Lead is a harmful metal that readily accumulates in the human body. It exists in the form of sulfide, cerussite ($PbCl_2$) and galena and it may be present in several oxidation states: 0, +1, +2 and +4. The (+2) form is the most stable ionic species in natural environments. Wastewater from electroplating industries, electrical industries, steel industries, explosive manufacturers, and paint and automotive industries can contain lead and other heavy metals (Cechinel et al., 2014). Lead causes damage to the central nervous system, produces anemia and cancer, and affects liver, kidney and gastrointestinal system (Carolin et al., 2017).

1.2.6. Arsenic

Arsenic (As) is a well-known toxic and carcinogenic element that naturally exists in environmental systems, especially in water and soil. The presence of arsenic in natural water is generally associated with the geochemical environment. The redox conditions and the mineral composition in the subsurface environment play an important role in the mobility of arsenic. The oxidation of different mineral species causes arsenic to become soluble and enter into the surrounding environment through drainage water. Any phenomena that affect the redox conditions such as pumping rate and the land use pattern can result in an excess of arsenic content in groundwater. Moreover, anthropogenic activities such as smelting of metal ores, use of arsenical pesticides and wood preservative agents may also release arsenic directly into the environment (Nicomel et al., 2015). Inorganic forms of As(III) are: H_3AsO_3, $H_3AsO_3^{2-}$, and of As

(V): H_3AsO_4, $HAsO_4^-$, $HAsO_4^{2-}$, and organic arsenic compounds are, methylated or aromatic organoarsenicals that can also be found in aquatic environments (Jain and Ali, 2000). The toxicities of the different arsenic species vary a lot, being the toxicity of inorganic species several times higher than the organic ones. Among inorganic species, As (III) is more toxic than As(V) given that it can combine with thiol(-SH) groups of the biomolecules in the human body. It is difficult to remove As(III) due to its solubility and stability in comparison with As(V) (Pholosi et al., 2019a).

Arsenic is an element used in different fields such as medicine, electronics, agricultural application, and metallurgy (Shafique et al., 2012). It causes a variety of serious problems: dermal changes, respiratory and cardiovascular problems, lung cancer, or genetic disorders.

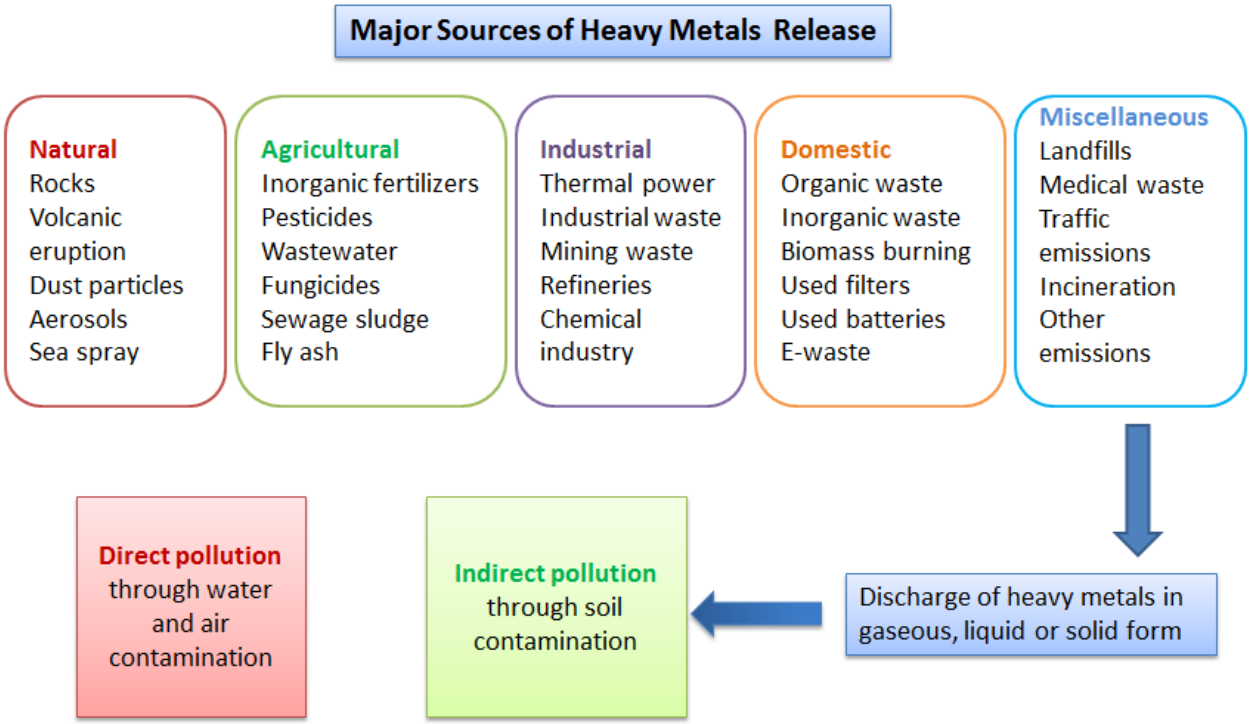

Figure 1.1. Major sources of heavy metals release. Adapted from (Rizvi et al., 2020).

1.3. Legislation

Various regulatory bodies from different countries have set the maximum prescribed limits for the discharge of toxic heavy metals in aquatic systems. However, metal ions are being added to

the water stream, through industrial activities, at a much higher concentration than the prescribed limits, thus leading to health hazards and environmental degradation. Wastewater from factories contains a large amount of heavy metals that may contaminate the soils and the water. The metal concentration present in the effluent discharge depends on the industries and the countries. Table 1.1 shows the limits of heavy metals in industrial wastewater recommended by Spanish legislation. The standard limits of metals in drinking water change from country to country; the limit of Cd (II) is 0.03 mg L^{-1} in the case of China and 0.01 mg L^{-1} for Kenya. Therefore, both concentrations are higher than the standard limit of WHO, which is 0.003 mg L^{-1} (Kinuthia et al., 2020). Table 1.1 shows the WHO guidelines for the metals in drinking water and their limits in wastewater in Spanish regulations.

Table 1.1. Limits of heavy metals in industrial effluents to be discharged by Catalan government regulations (Decret 130/2003, Generalitat de Catalunya) and in drinking water (World Health Organization, 2017).

Metals	**Recommended limits in wastewater (Catalan government regulations) (mg L^{-1})**	**Recommended limits in drinking water (WHO) (mg L^{-1})**
Arsenic	1	0.01
Cadmium	0.5	0.003
Copper	3	2
Total chromium	3	0.05
Hexavalent chromium	0.5	-
Tin	-	-
Iron	10	-
Manganese	2	-
Mercury	0.1	0.006
Nickel	5	0.07
Silver	-	-
Lead	1	0.01
Selenium	0.5	0.04
Zinc	10	-

1.4. Conventional methods to remove heavy metals

Due to the toxicity and non-biodegradability of metals and their presence in wastewaters, especially in those generated from industrial activities, different treatment techniques have been developed to efficiently remove these pollutants from wastewater. Moreover, the development and implementation of these techniques has become an important research area. Techniques for wastewater treatment can be broadly classified into three sections: physical, chemical and biological (Fig. 1.2).

Among all these techniques I will focus on the main techniques for the removal of metals by summarizing their principles in the next sections as well as their advantages and disadvantages that are listed in Table 1.2.

1.4.1. Precipitation

This process uses chemical agents to convert metal ions into insoluble precipitates of hydroxide, sulphide, carbonate and phosphate. The solid precipitate is later separated by a filtration process. Chemical reagents such as lime and limestone can be employed due to their availability and low cost to produce a basic media pH (9-11) in which the metal ions can precipitate as hydroxide (Wang, 2018). This precipitate is obtained as a result of the formation of a low soluble chemical compound by the interaction of the precipitation agent and the metal ions. The pH is an important parameter that needs to be controlled in this method. The precipitation process is represented by the equation:

$$M^{n+} + n(OH)^{-} \longrightarrow M(OH)_n$$

Where M^{n+} is the dissolved metal ion, OH^- is the precipitant agent and $M(OH)_n$ is the insoluble metal hydroxide.

This technique was employed to remove heavy metal such as Cr (III) from wastewater using magnesium hydroxy carbonate as the precipitating agent to obtain Cr_2O_3 (Zhang and Duan, 2020).

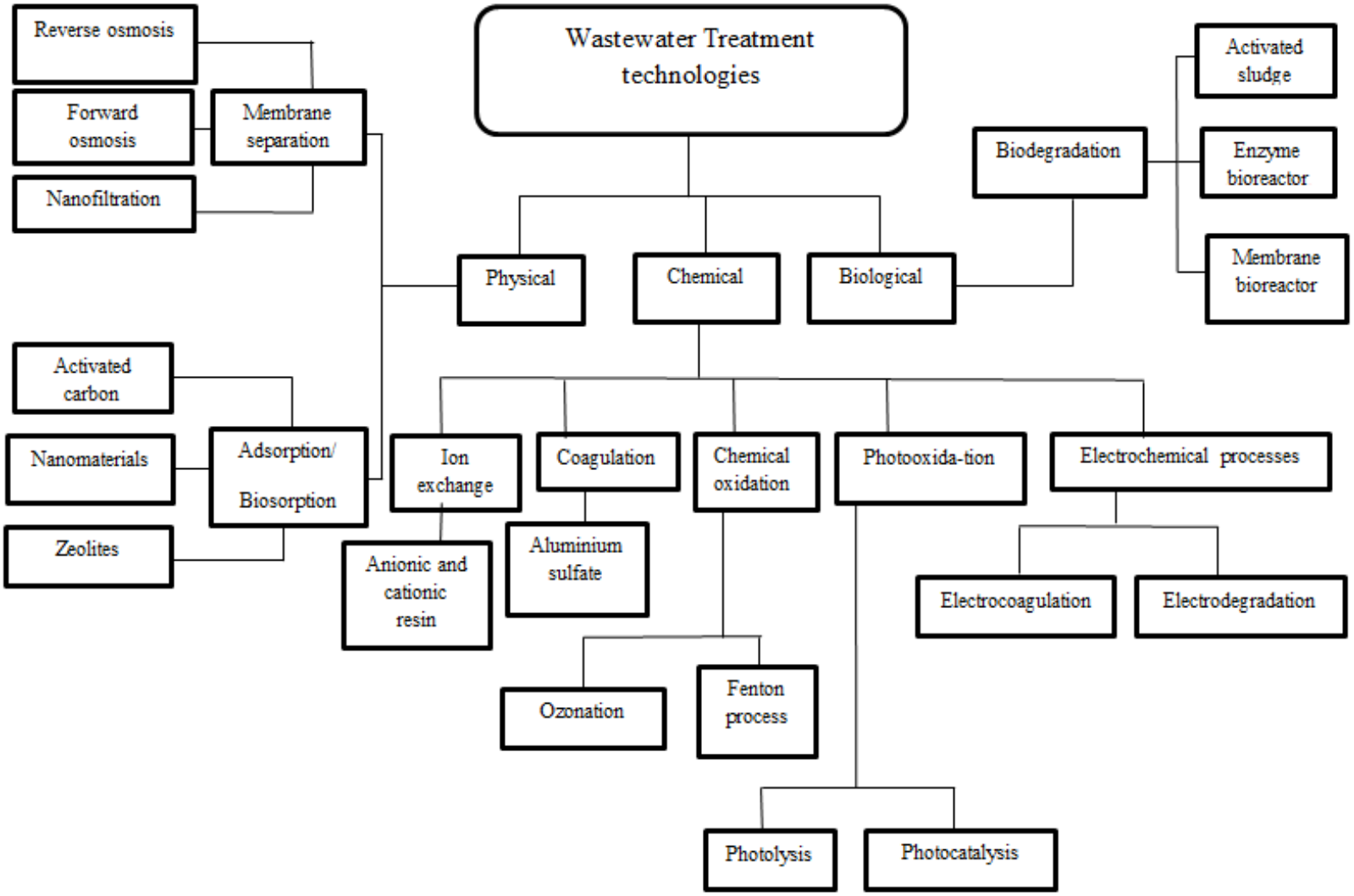

Figure 1.2. Classification of wastewater treatment techniques.

1.4.2. Coagulation/ flocculation

In this process, a positively charged coagulant is introduced to reduce the surface negative charge of particles and allow them to aggregate. Anionic flocculent is then added to react with the positively charged aggregates, binding them to form a larger group that can be separated by the filtration process. The effectiveness of coagulation depends upon the types of the coagulant used, the dosage of coagulant, pH, temperature, alkalinity, and mixing conditions. Chemical reagents like $Al_2(SO_4)_3$ (alum), $Fe_2(SO_4)_3$ and $FeCl_3$, and derivatives of these materials such as poly aluminum chloride and poly ferric chloride were used as coagulants. A maximum of 99% removal of lead was obtained using alum at an optimum pH of 6.2-7.8 (Pang et al., 2011), Poly diallyldimethylammonium chloride or polyethyleneimine was used as a cationic polymer and sodium dodecyl sulphate as an anionic surfactant in the removal of chromium, zinc and copper by polymer surfactant complexation and flocculation. A maximum of 99% removal was obtained at an optimum pH of 6 pH (Shen et al., 2015).

1.4.3. Membrane processes

In principle, a membrane acts as a barrier that inhibits the passage of certain constituents while allowing other constituents to pass through. The treated and collected streams are called permeate while the rejected constituent is referred to as retentate. The performance of a membrane is usually determined by its selectivity and flux rate. Flux is defined as the volumetric flow of liquid through a membrane per unit area per unit time. On the other hand, selectivity is referred to as the part of a substance in a feed stream that a membrane must maintain. The membrane acts as a physical barrier, the size exclusion mechanism is thus the most important mechanism involved in membrane separation process. Different types of porous and thin-film composite membranes can be used for water/wastewater treatment.

These include low pressure-driven membrane processes (microfiltration (MF), ultrafiltration (UF), distillation), high pressure-driven membrane processes (nanofiltration (NF) and reverse osmosis (RO)), osmotic pressure-driven membrane process (forward osmosis (FO) and others (electrodialysis (ED), etc.) (Abdullah et al., 2019). NF, RO, and FO are effective in removing heavy metal ions owing to the presence of a dense skin layer on top of their structure. However, MF or UF membranes having pore sizes of approximately 0.1 µm and 0.01 µm, respectively, are

ineffective in removing metal ions from feed solutions. In the case of UF membranes, it is possible to remove metal ions by adding complexing or micelle agents during the separation process. The combination of a UF membrane with metal adsorption by extracellular polymeric substances over the membrane allowed 94.8% of Pb (II) to be removed from wastewater (Cao et al., 2020).

1.4.3.1. Nanofiltration

NF membranes have pore sizes in the range of 0.01–0.001 µm, which are pore sizes between UF and RO membranes. Their loose selective thin film structure and small pore sizes make them excellent membranes for separating metallic ions. Commercial NF membranes are made of aliphatic amine monomers and, normally, present a negatively charged surface due to the presence of sulfonic and carboxylic groups. Besides commercial membranes, other modified NF membranes with different surface charge properties have been developed. A hollow fiber nanofiltration (NF) membrane modified by grafting poly (amidoamine) dendrimer (PAMAM) on the interfacially polymerized layer of a polyethersulfone (PES) membrane was able to reject over 99% of heavy metals like Pb^{2+}, Cu^{2+}, Ni^{2+}, Cd^{2+}, Zn^{2+} and As^{5+} (Zhu et al., 2015). (Zhu et al., 2014) has fabricated a membrane by simultaneous co-extrusion of polybenzimidazole (PBI) and polyethersulfone (PES)/polyvinylpyrrolidone (PVP) dopes through a triple orifice spinneret with the help of dry jet wet phase inversion process. It proved its efficiency on the removal of Cd(II), Cr(VI) and Pb(II) with 95%, 98% and 93%, respectively.

1.4.3.2. Reverse osmosis

Reverse osmosis (RO) membranes are denser than NF and do not have definite pores. Based on the theoretical principle of osmosis, the net movement of water goes from the region of low solute concentration to a region of high solute concentration. RO works in the opposite direction where pressure is exerted to force water molecules to move against the concentration gradient. Heavy metal removal using the RO process was used for treating electroplating wastewater containing low concentrations (>10 mg L^{-1}) of various heavy metals (Cu(II), Cr(VI), and Ni(II)) resulting in more than 98.75% rejection (Ozaki et al., 2002). This technique is used for the desalination of seawater in order to obtain ultra-pure water (Gunatilake, 2015). RO was also

evaluated in combination with a membrane bioreactor to treat low concentrations of heavy metals (Pb(II), Ni(II), Cu(II), and Cr(VI)) resulting in almost 100% removal of Pb(II) and Ni(II), while removal of Cr(VI) (89%) and Cu(II) (49%) were lower (Dialynas and Diamadopoulos, 2009). Abdullah et al., (2019) reported the removal of 100% of Pb(II) and Ni(II), and 89% of Cu (II) and 49% of Cr(VI) using RO membranes.

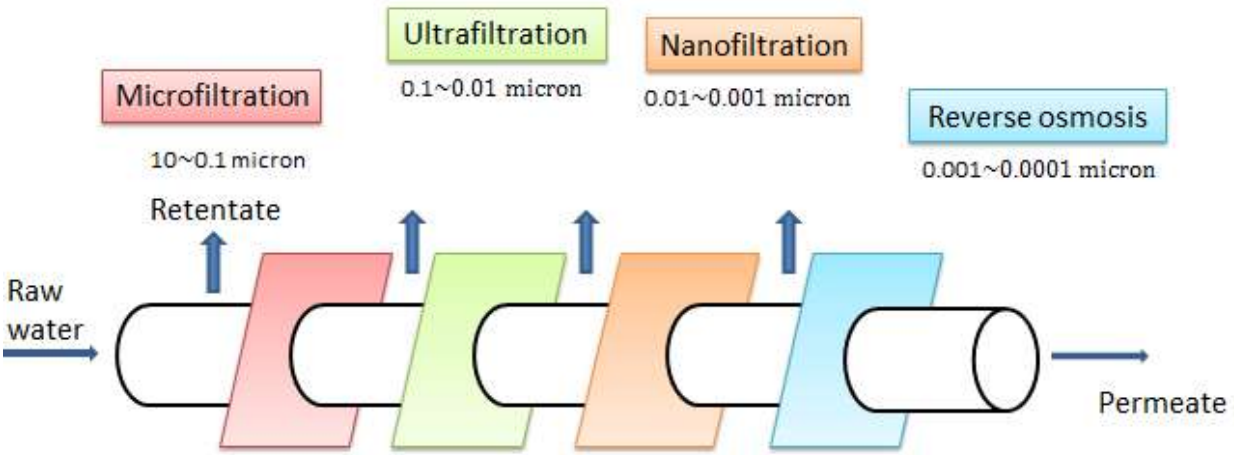

Figure 1.3. Classification of membrane separation processes. Adapted from (Selatile et al., 2018).

1.4.3.3. Electrodialysis

Electrodialysis (ED) is a membrane separation process that uses an electrical potential difference as a driving force for separating metal ions through a selective semi-permeable membrane. This separation is due to charge rather than size differences. The membranes are cation or anion-selective, which basically means that either positive ions or negative ions will flow through. Cation-selective membranes are polyelectrolytes with negatively charged matter, which rejects negatively charged ions and allows positively charged ions to flow through (Gurreri et al., 2020). Electrodialytic methods have been tested for industrial effluents from several processes (metal

finishing, leather industry, etc.) aiming at reuse. For instance, ED can recuperate water and metals from spent baths or rinse waters of plating processes (Scarazzato et al., 2017). Clogging is one of the major drawbacks of electrodialysis membranes as well as scaling up of the membrane.

1.4.3.4. Ion exchange

Ion exchange is another method used to separate and remove heavy metals from effluent wastewater that has been extensively used due to its great removal rates, the high capacity to treat great volumes and rapid kinetics (Lalmi et al., 2018). This method is based on the exchange of metal ions from the effluent by other ions that are interacting with the adsorbent, normally a resin, due to electrostatic forces. The resins are classified into two types; synthetic and natural resins. Synthetic resins are made up of a cross-linked polymer matrix in which the functional groups are attached through covalent bonding in the resin structures, and spaces in the structures allow the ions to transfer appropriately. Cationic exchanger resins consisting of strongly acidic functional groups such as sulfonic acid or in carboxylic acid groups are the most widely used in adsorbing metal cations.

Zeolites, consisting of Al and silicates connected through oxygen bridges are natural cation exchangers which exchange Na^{+}, K^{+}, Ca^{2+}, and Mg^{2+}, which are electrostatically bound to Al, by the metal ions present in the effluent. Different factors such as pH, temperature, and initial metal concentration can affect the efficiency of the metal removal by ion-exchangers. The cation exchanger DOWEXHCR S/S has been applied to remove Ni(II) and Zn(II) resulting in a removal percentage of 98% at pH 4, whereas Ambersep132 anion exchanger has shown an adsorption capacity of 92.1 mg g^{-1} for Cr(VI) (Azimi et al., 2017).

Table 1.2. Advantages and disadvantages of conventional methods (Crini and Lichtfouse, 2019).

Method	Advantages	Disadvantages
Ion exchange	-Simple technology and rapid -High regeneration of resin -Efficient method to remove metals -Produce high quality treated water	-High-maintenance cost, not all ion-exchange resins are suitable for metal removal. -Rapid saturation and clogging of the resins
Membrane processes (Reverse osmosis, ultrafiltration, nanofiltration)	-Small space required high separation selectivity. -Efficient at high concentration level, Rapid and simple	-Limited flow rates, high initial capital cost, high maintenance and operation costs -High energy requirement
Electrodialysis	-No chemical required (depending on the system) -Production of highly treated water, Removal of all types of dyes, salts, minerals	-Clogging and scaling of the membrane -Inefficient in low solute feed concentration -High cost of the equipment
Precipitation	-Simple process, low investment -High degree of selectivity -Precipitants are relatively inexpensive	-Inefficient in the removal of metal ions at low concentration -Excessive sludge production -Slow metal precipitation -Aggregation of metal precipitates
Coagulation/flocculation	Simple process	-Increases heavy metal concentration in wastewater -Large volume of sludge

1.5. Adsorption

Adsorption is an effective physicochemical treatment process that can be applied to remove organic and inorganic contaminants from wastewater as well as other contaminants (Jibesh and Umesh, 2015). The adsorption process implies the enrichment of chemical species from an aqueous phase onto a solid surface. The solid material that provides the surface for adsorption is called adsorbent; the species that will be adsorbed are named adsorbate. It is a surface phenomenon in which the adsorbate molecule accumulates on the sites available on the surface of the adsorbent through different mechanisms depending on the nature of the adsorbent such as ion exchange, complexation and precipitation.

The attraction of atoms, ions or molecules by the adsorbent sites is explained by the formation of interaction forces of physical and chemical nature (Afroze and Sen, 2018). The interaction between adsorbate and adsorbent depends on their physical and chemical properties and, in the case of the adsorbent, is mainly related to its surface area and structure. The adsorbents used in industrial applications are typically highly porous materials with surface areas in the range between 102 and 103 m^2 g^{-1}.

It is a simple process, easy operation, wide applicability etc. The bonding between adsorbate and adsorbent depends on the nature of the adsorbate (Sadegh et al., 2017). The adsorption is classified into physisorption when the interaction between the adsorbate species and the surface sites takes place through Van der Waals forces, and chemisorption when there is a chemical reaction, consisting in a covalent binding or an electrostatic interaction, between the molecules of the adsorbate and the active sites of the adsorbent (Sadegh et al., 2017). In the case of chemisorption, different mechanisms such as complexation, redox reaction, ion exchange and precipitation can take place depending on the nature of the adsorbate. The main characteristics of these adsorption mechanisms are described in the next paragraphs.

The physical adsorption corresponds to the accumulation of metals on the surface of the adsorbent by physical forces such as Van der Waals-type bonds, hydrogen bonds, polarity, dipole-dipole and π-π interaction (Afroze and Sen, 2018). It is a reversible phenomenon that occurs at low temperatures with the development of a multilayer of metal on the adsorbent. It has a low enthalpy of adsorption (ΔH=20 to 40 KJ mol^{-1}) (Mathew et al., 2016) whereas, the chemical adsorption corresponds to the formation of a chemical bond between the adsorbate and

the adsorbent. It is an irreversible reaction that generates a monomolecular layer which results in a modification of the adsorbed molecules. This process is favored at high temperature and involves a higher enthalpy (200 to 400 KJ mol^{-1}).

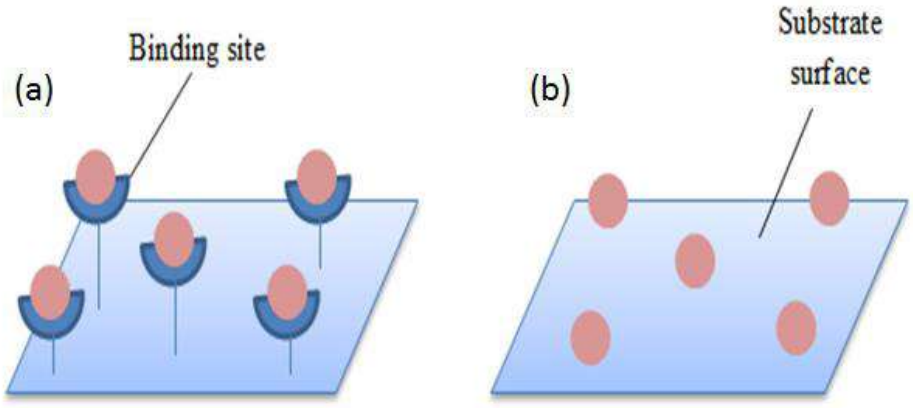

Figure 1.4. (a) Chemisorption and (b) physisorption process.

1.5.1. Adsorbent characterization

Several key characteristics control the adsorption ability of adsorbents, among them, physicochemical characteristics. Specific surface area, pore volume, particle sizes, pH, charge/polarity and surface functional groups are the most important.

1.5.1.1. Specific surface area

The Specific surface area, SSA, is the most meaningful morphological characteristic of solid substances in applications related to porous structures, such as adsorbents, catalysts, etc. Specific area means the surface area available for the adsorption of 1 gram of adsorbent. The amount of adsorption depends on the surface area of the solid. The greater the surface area, the greater the adsorption. Specific surface area is defined as the pore size distribution (nm^2) divided by the mass unit (g). A large specific surface area is preferable for providing large adsorption capacity, but the creation of a large internal surface area in a limited volume inevitably gives rise to large numbers of small-sized pores between adsorption surfaces.

The average thickness of the adsorbate is often expressed with the names mono- and multilayer adsorption. In monolayer adsorption, all the adsorbed molecules are in contact with the surface of the adsorbent. In multilayer adsorption, the adsorption space accommodates more than one layer of molecules so that not all adsorbed molecules are in direct contact with the molecules of the adsorbent (Tóth et al., 2000).

1.5.1.2. Pore volume

According to the definition of the International Union of Pure and Applied Chemistry (IUPAC), three types of pores can be distinguished: macropores, mesopores, and micropores. Pores with a diameter (d_{pore}) <2 nm are classified as micropores, while mesopores lie between 2 to 50 nm, and macropores exceed 50 nm in diameter. The macropores and the mesopores are primarily relevant for the mass transfer into the interior of the adsorbent particles, whereas the micropore volume mainly determines the size of the internal surface and therefore the adsorbent capacity. As a rule, the internal surface area increases with increasing micropore volume. In principle, the higher the micropore volume, the larger the amount of adsorbate that can be adsorbed. However, it has to be considered that in the case of very fine pores and large adsorbate molecules, there may be a limitation of the extent of adsorption by size exclusion.

Pore volume distributions can be determined by either gas adsorption porosimetry (typically N_2, Ar or CO_2) or mercury intrusion porosimetry. Gas porosimetry measures pores from 3.5 Å to about 4000 Å in diameter. Mercury porosimetry is applicable to pores from 30 Å up to 900 μm in diameter. The physical characteristics, i.e., micropore area and pore volume distribution, may have a greater effect on the adsorption capacity of adsorbents.

1.5.1.3. Particle size

The surface area of a particle is a function of the particle's size. An increase in particle size decreases metal adsorption while an increase in pore size increases the metal adsorption. This may be due to the availability of more surface area for adsorption in the case of small size particles (Kumar et al., 2010). The removal efficiency and sorption capacity increases with the decrease of the particle size. This indicates that the smaller the sorbent particle size, then for a

given mass, more surface area is made available and therefore the number of sites increases (De Gisi et al., 2016).

1.5.1.4. pH

The value of the pH necessary to obtain a net zero charge on a solid surface in the absence of specific sorption is called the point of zero charge (pH_{PZC}). Adsorption capacities of adsorbents are strongly dependent on initial solution pH. Initial solution pH affects the magnitude of negative charge on adsorbent surface and the adsorption capacities (Abdel-Ghani and Elchaghaby, 2007). The adsorption capacity of an adsorbent increases with increases in solution pH. Low adsorption capacities observed for metal ions in an acidic medium may be due to hydrogen ions strongly competing with adsorbate for negatively charged sites on the adsorbent. As solution pH increases, the hydrogen ion concentration of the solution is reduced thereby reducing the competition for binding sites by hydrogen ions. It is also known that at a specific pH range, functional groups such as carboxylic acids with pKa value around 3.5 (Abate and Masini, 2005; Abdel-Ghani and Elchaghaby, 2007) will be in the ionized form, increasing the magnitude of negative charge on the adsorbent surface.

1.5.1.5. Surface functional groups

In the case of chemisorption processes, the functional groups present in the adsorbent surface play an important role in explaining the adsorption mechanism. There are several functional groups in the adsorbents which are surface-oxygenated groups or non-oxygenated. Carbonyl, phenolic and lactone were the major surface-oxygen functional groups for adsorbents of biological origin. Depending on the chemical composition of the adsorbent as well as the chemical properties of the metal ions, the metal ion binding mechanism during adsorption processes involves ion exchange, complexation, electrostatic attraction and microprecipitation processes (Majumder et al., 2016).

The FTIR (Fourier transform infrared spectroscopy) technique is used to examine the surface groups of the adsorbent and to identify those groups responsible for adsorption. Adsorption in the

IR region takes place because of rotational and vibrational movements of the molecular groups and the chemical bandof a molecule.

Adsorbents can be of natural origin or the result of industrial production. In general, the natural adsorbents have a smaller surface area than synthetic adsorbents but their low cost makes them important adsorbents to use. In contrast, the synthetic materials provide higher surface area and higher porosity which lead to a greater internal surface area.

In water treatment, the selection of the adsorbent depends on the properties of the substances to be removed (organic or inorganic contaminants). The removal process consists of the mass transfer of the contaminants from the bulk solution to the adsorbent surface and their adsorption on the adsorbent surface. Generally, the process can be performed in reversible mode and the adsorbents may be regenerated by desorption.

Some commercial adsorbents such as inorganic materials (e.g. clay materials and zeolites) and activated carbon have been extensively explored for water pollution control.

1.5.2. Adsorption with inorganic materials

Inorganic materials such as clay minerals and zeolites are natural materials that are used in the water treatment domain to remove metals and treat water. Clay minerals have the typical characteristics, high specific surface area, high ion exchange capacity, chemical and mechanical stability and layered structure, which make them good adsorbents (Atkovska et al., 2018). They are widely used to adsorb various kinds of pollutants from large volumes of aqueous solutions. Clays are those aluminosilicate minerals that make up the colloid fraction (< 2 μm) of soils and act as natural scavengers for heavy metal ions. Their tetrahedral and octahedral layers are seen to incorporate different ions which develop a range of properties with different responses to experimental conditions such as contact time, temperature, pH, adsorbent dosage, concentration of adsorbate etc. Heavy metal adsorption studies using clay materials show the impact of pH on the adsorption efficiency, obtaining the best removal efficiencies for Zn(II) and Pb(II) at pH 5 (Atkovska et al., 2018). Bentonite, a typical layered silicate structure consisting of two silica tetrahedral sheets with a central alumina octahedral sheet, has also been applied to remove divalent metal ions such as Cu(II) and Pb(II).

Zeolites are microporous aluminosilicate minerals with different cavity structures consisting of a three dimensional framework and a negatively charged lattice. The negative charge is balanced by cations like Na^+, K^+, Ca^{2+}, and Mg^{2+} that can be easily exchanged by heavy metal cations present in the solutions. High ion-exchange capacity, high specific surface areas and their relatively low cost make zeolites attractive adsorbents for the removal of heavy metal ions from aqueous systems. Clinoptilolite, a natural zeolite, adsorbed Cd(II) (32 %), Cu(II) (75 %), Ni(II) (28 %), Pb(II) (99 %), and Zn(II) (59 %) (Shaheen et al., 2012).

Moreover, the surface activation by chemical or thermal treatment of clay materials and zeolites resulted in an improvement of their adsorption capacity (Atkovska et al., 2018).
Zeolite membranes have been intensively investigated in a wide range of applications including the removal of heavy metal ions from aqueous solutions due to their uniform pore structure and high thermal stability. In these membranes, adsorption and the filtration processes are coupled by impregnating a polysulfone membrane with zeolite nanoparticles for the removal of Ni (II) and Pb (II) (Yurekli, 2016).

1.5.3. Adsorption with activated carbon

Activated carbon (AC) is a porous carbonaceous material with a high specific surface area, high degree of porosity and excellent sorption properties obtained from materials rich in carbon. The most common sources of activated carbon on a commercial scale are wood, anthracite and bitumen charcoal, lignite, peat shells and coconut. Alternative sources such as olive and almond shells are also used. The carbon content of these materials ranges from 40 to 90% (wt.), with a density of 0.4-1.45 g m^3. Activated carbon can also be produced from agricultural residues (Fig.1.5 a, b) such as olive corn, biomass, rice rolls, corn stalks, bagasse, fruit stones (cherry and apricot stones, grape seeds), hard shells (pistachio, pine cone, almond and pecan shell), fruit pulp, bones and coffee beans, due to their low cost, their abundance and these wastes contain different types of functional groups as carboxylate, hydroxyl, amide, amine, phosphate (Dai et al., 2018). The unique adsorption properties depend on the existence of functional groups on the activated carbon, which are derived mainly from activation processes, precursors and thermal purification.

AC is an effective adsorbent due to its special characteristics such as richness in micropores <2 nm and mesopores (2-50 nm) and high internal pore structure which provides high surface area,

ranging from 600 to 2000 m^2 g^{-1}. Moreover, uniform pore size and a higher degree of surface reactivity, degree of ionization and the type of functional groups present on the surface increase their capacity to attract the pollutants (Singh et al., 2019). The adsorption capacity of AC is higher for organic compounds than for metal ions due to its hydrophobic surface. The adsorption of metal ions by AC is related to its weak acidic ion-exchange character. Hence, the introduction of acidic functional groups such as carboxyl, lactone, phenolic, hydroxyl on the AC surface improves the adsorption capacity for metal ions. The oxidation of AC with H_2SO_4 /HNO_3 allowed the removal of Pb(II) by ion exchange (Aguilar et al., 2016) and this mechanism also allowed the removal of Zn(II), Ni(II) and Pb(II). Activated carbon prepared from olive stones has been applied to remove Cd(II), Pb(II) and Cu(II) (Bohli et al., 2015), and AC from olive branches was used to remove Zn(II), Pb(II), Cu(II), and Cd(II) (Alkherraz et al., 2020).

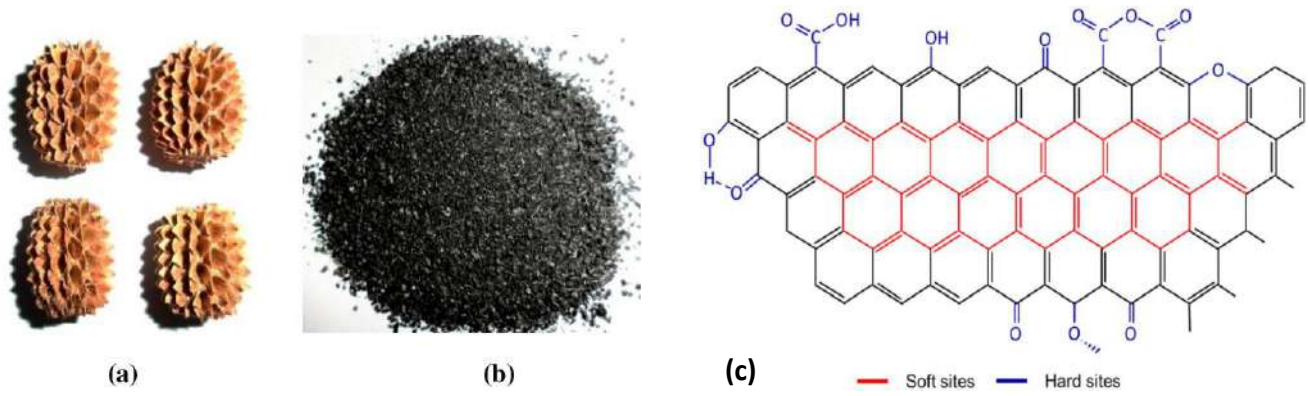

Figure 1.5. Activated carbon production from Australian pine-cones (a), activated carbon (b) (Muslim, 2017) and (c) hard sites and soft sites in graphene (Kuroki et al., 2019).

The adsorption of divalent metal ions by AC is strongly dependent on solution pH (Joseph et al., 2019). When the pH of the solution exceeds the isoelectric point of the adsorbents, cations such as Pb(II), Cu(II), Co(II), and Zn(II) are likely to adsorb because the surface is negatively charged due to dissociation of acidic functional groups (Kuroki et al., 2019). Following the HSAB theory, class A metal ions tend to adsorb to the surface functional groups classified as hard bases, and class B ions tend to adsorb on graphite surfaces classified as soft bases (Fig. 1.5 c). Borderline class ions behave as hard ions or soft ions, depending on the solution pH.

Moreover, metal ion adsorption capacity on AC prepared from the same raw materials increases as the surface area and the pore volume increase (Guezguez et al., 2016), as the adsorption mechanism is controlled by the diffusion of the metal ion in the pore. Hence, adsorption of heavy metal ions by AC depends on the chemical (e.g. surface charge and functional groups) and physical (e.g. surface area and pore size) properties of the adsorbent as well as the metal ion properties (Aldawsari et al., 2017).

In order to enhance the capacity of the adsorbent, surface modification by introducing a functional group on the AC surface has been performed by treating the surface of activated carbon from chickpea husks with KOH, which resulted in an improvement of Pb(II), Cu(II), and Cr(VI) removals (Özsin et al., 2019).

Pinecone biomass-based biochar was chemically activated with H_2SO_4 and H_3PO_4 to increase the presence of functional groups in order to allow the removal of Pb(II) metal from aqueous solutions (Biswas et al., 2019). Activated carbon from olive stones was chemically activated with a phosphoric acid solution (50% by weight) at 110 °C to improve their efficiency to remove Ni(II), Cu(II) and Cd(II) (Bohli et al., 2017).

In the case of anions such as Cr(VI), this can be adsorbed onto the AC surface by electrostatic interaction at low pHs (~ 2). The favorable effect at low pH is explained by the excess of hydrogen ions that can protonate the functional groups of the AC surface, the surface protonation of activated carbon leads to the formation of positively charged sites that electrostatically interact with hydrogen chromate ion ($HCrO_4^-$), which is the predominant Cr(VI) species between pH 1 and 4.0, favoring Cr(VI) adsorption. At a pH higher than the isoelectric point of the adsorbent, the oxygenated functional groups such as lactone or hydroxyl groups are negatively charged and the adsorption of Cr(VI) decreases (Labied et al., 2018). However, at very acidic pHs (~ 1), more protons are available which can promote the reduction of Cr(VI) to Cr (III) which results in a decrease of Cr(VI) adsorption (Liu et al., 2014). AC obtained from sugar beet bagasse was employed to adsorb Cr(VI) (Yunus et al., 2020).

Despite the relative abundance and productive use of activated carbons, there have been some restrictions on its applicability due to its high cost, which are related to its production even when it is produced from agricultural waste, their losses during operation and to its regeneration. Therefore, researchers are on the lookout for cheap and abundant forms of adsorbent that can be applied to pollution control. Attention has now been diverted to the development and production

of cheap alternative adsorbents using various raw materials that are abundant, possess high carbon content and less difficult to activate. However, despite the excellent performance of commercial inorganic materials and activated carbon, these systems are expensive to use and cannot be thought of as a truly viable option in many parts of the world.

Because of this, attention has turned to the adsorptive properties of other non-conventional solid materials proposed as low-cost, efficient and green adsorbents for pollutant removal (Crini et al., 2019).

1.6. Biosorption

Biosorption is a biological method based on the use of biomass to accumulate target pollutants through different mechanisms, such as complexation, chelation, ion exchange, inorganic micro precipitation, and hydrolysis of metal ions. The adsorption mechanism depends on the nature of the pollutant and the functional groups present on the biosorbent surface. The term biosorbent includes the usage of dead biomass such as fibers, peat, rice hulls, forest by-products, chitosan and agro-food wastes as well as living plants, fungi, algae (unicellular microalgae, cyanobacteria, multicellular macroalgae) and bacteria. Biosorbents represent cheap filter materials often with high affinity, capacity and selectivity, they are abundant in nature or as by-product or waste materials from industry, and available in most places (Gupta et al., 2015). Generally, biosorption processes can significantly reduce capital costs, operational costs and total treatment costs compared with the conventional systems (Abdolali et al., 2014).

Agricultural waste and by-products from forest industries including tea waste, coffee, hazelnut shells, peanut hulls, sawdust, barks, palm kernel husks, coconut husks, peanut skins, cellulosic and lignocellulosic waste, hemp-based products, cotton and modified cotton, corncobs, rice hulls, apple waste, wool fibers, olive cake, almond shells, cactus leaves, banana and orange peels, sugar beet pulp, palm fruit bunch, maize leaves and other different by-products have been evaluated as biosorbents (Oyewole et al., 2018). They have a good capacity to adsorb metal ions due to their porous structure and the different functional groups such as carboxyl, hydroxyl, and other reactive groups on their surface that are able to bind the metal ions. Table 1.3 presents some examples of the application of biosorbents for the removal of metal ions.

Table 1.3. Maximum adsorption capacity of different agricultural wastes on the removal of heavy metals.

Adsorbents	**Adsorbate**	**q_{max} (mg g^{-1})**	**References**
Coconut-shell biochar	Cd	3.5	(Paranavithana et al., 2016)
Sugar cane bagasse	Cd	0.96	(Moubarik and Grimi, 2015)
Grapefruit peel	Cd	42.1	(Torab-Mostaedi et al., 2013)
Orange peel	Pb	27.9	(Abdelhafez and Li, 2016)
Peanut shells	Pb	39	(Taşar et al., 2014)
Sugar cane bagasse	Pb	87	(Abdelhafez and Li, 2016)
Rice straw	Cu	18.4	(Singha and Das, 2013)
Banana peel	Cu	7.4	(DeMessie et al., 2015)
A. Hypogea (peanut) shells	Cr(VI)	4.3	(Ahmad et al., 2017)
Hazelnut shells	Cd Pb	1.6 6.2	(Cataldo et al., 2028)
Almond shells	Cd Pb	2.7 4.2	(Cataldo et al., 2018)

1.6.1. Agricultural and household wastes

The basic components of the agricultural waste are hemicelluloses, lignin, lipids, proteins, simple sugars, water, hydrocarbons and starch, containing a variety of functional groups with a potential sorption capacity for various pollutants including dyes and metal ions (Bhatnagar et al., 2015). Agricultural waste products are used in natural and modified form. In the natural form, the product is washed, ground and sieved until reaches the desired particle size and subsequently

used in adsorption tests. While, in the modified form, the product is pre-treated by means of well-known modification techniques in order to enhance and reinforce the functional group potential and, consequently, increase the number of active sites. Modification techniques include the production of activated carbon from these wastes as has been explained in section 1.5.3.
Several review articles have already been published reporting the high efficiency of lignocellulosic, agricultural, agroforestry and agroindustry waste in the removal of metallic ions (Afroze and Sen, 2018; Kyzas and Kostoglou, 2014).

Studies on the use of lignocellulosic adsorbents to remove toxic metal ions from aqueous systems have increased exponentially in the last 20 years given that these materials have demonstrated to have several advantages over commercial adsorbents. Around 300 articles have been published in the last 10 years (2010-2020) and 35% of them are dedicated to the adsorption of metal ions. Most of these studies were performed in aqueous systems containing Cd(II) ions (41 articles), Pb(II) ions (36 articles) and Cr(III)/Cr(VI) ions (30 articles), which are highly toxic metal ions (Neris et al., 2019).
The adsorption capacity of lignocellulosic materials is related to a relatively high surface area per unit mass and to the presence of different functional groups, such as carboxylic, sulphates, phosphates and amino groups with ion exchange, electrostatic interaction and complexation as the principal adsorption mechanisms (Fig. 1.6). Moreover, pH, temperature and initial concentration, among other factors, influence the adsorption processes (Dai et al., 2018). As in the case of the other adsorbents, chemically modified agricultural residues result in a higher metal ion adsorption capacity compared to unmodified materials (Acharya et al., 2018).

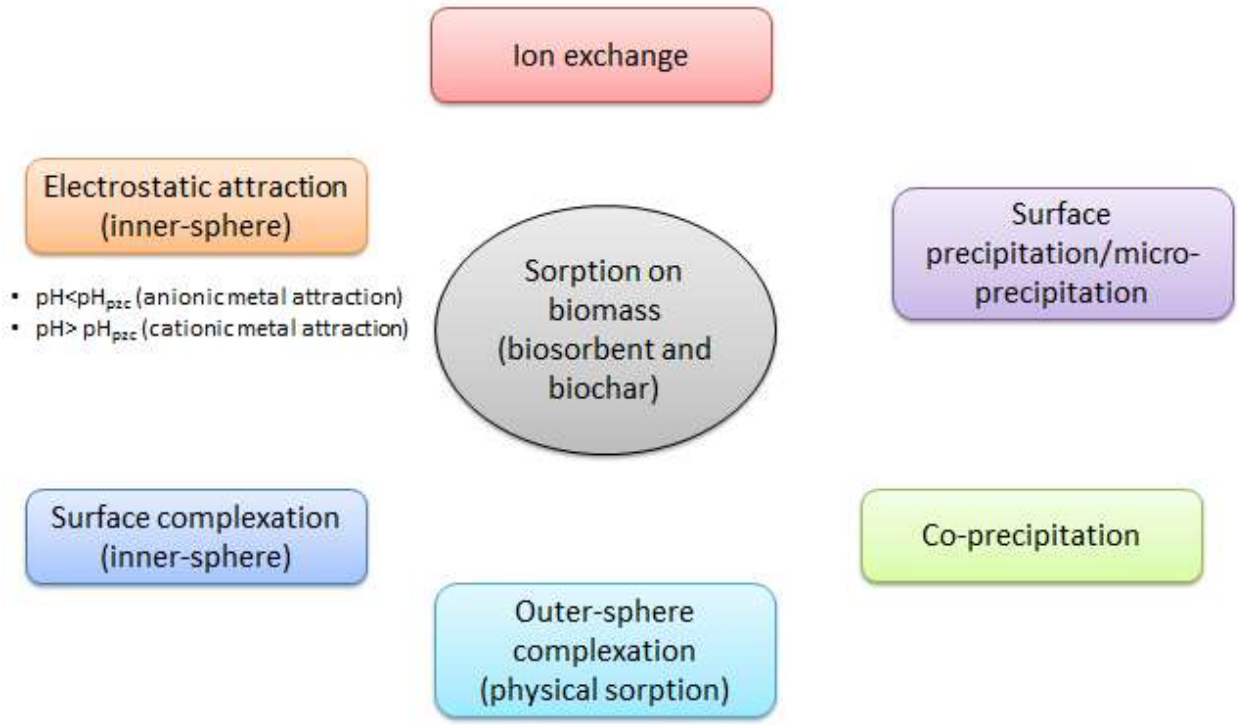

Figure 1.6. Adsorption mechanisms involved in the removal of heavy metals by agricultural waste.

Lignocellulosic adsorbents are structurally comprised of cellulose, hemicellulose, and lignin and are also called biopolymers. Cellulose is the most important component of lignocellulosic materials (30–50%), consisting of a linear polymer of β–D–glucopyranose sugar units whose average chain has a degree of polymerization of about 9000–10,000 units. Approximately 65% of the cellulose is highly oriented and crystalline with no accessibility to water and other solvents, while the rest is composed of less oriented chains that have an association with hemicellulose (20–40%) and lignin (15–25%). The chemical reactivity of cellulose is a function of the high donor reactivity of the OH groups. With a lower degree of polymerization than cellulose, hemicellulose includes a group of polysaccharide polymers that contain a number of sugars including xylose, mannose, galactose, arabinose and glucuronic acids. These are generally insoluble in water, but some hemicelluloses containing acids are water-soluble. The

hemicelluloses vary in structure and polymer composition depending on the source (Neris et al., 2019).

Lignin is a highly branched polymer consisting of phenol units which include trans-coniferyl, trans-sinapyl and trans-p-coumaryl, although its structure and chemical composition are a function of their source. The materials with high lignin contents are cereal material husks, other shells, leaves, barks, grasses and fruit seeds (Gupta et al., 2015). Extractives in lignocellulosic sources are a large number of both lipophilic and hydrophilic constituents such as water, ash, cyclic hydrocarbons, inorganic and organic materials (resin, fats, alcohols, turpentine, tannins, fatty acids, waxes and flavonoids).

The biopolymers generally contain a large amount of hydroxyl, phenolic, and carbonyl groups. The type of functional groups and chemical components in lignocellulosic materials are similar, but in different amounts. The main mechanisms known for metal and dye adsorption on cellulosic biosorbents are chelating, ion exchanging and making complexion with functional groups and releasing protons into aqueous solution. Many studies confirmed that an ion-exchange mechanism could be included in the biosorption process rather than complexation with functional groups on the biosorbent surface. They also showed the role of sodium, potassium, calcium and magnesium present in the adsorbent during ion exchange (Ding et al., 2012).

Most of the lignocellulosic materials have a low adsorption capacity in raw form and to enhance and reinforce their potential capacity by increasing the number of active sites and their hydrophilicity, some chemical and thermal pre-treatment methods can be applied by treating the materials. Reagents such as organic and mineral acids, bases and basic solutions, oxidizing agents and other chemical compounds were applied in the chemical treatment (Abdolali et al., 2014). The adsorption capacities to remove Pb(II), Cd(II) and Cu(II) of lignocellulosic materials such as cantaloupe peel, pine cone, litchi fruit peel, and annona squamosal were evaluated before and after chemical treatment with acrylic acid, demonstrating that the chemical modification enhanced the efficiency of the adsorption processes (Tran and Chao, 2018). Two more examples are the chemical treatment applied to modify lemon peel, resulting in an improved capacity to remove Ni(II) (Villen-Guzman et al., 2019) and the thermal treatment of pea peels at 600 °C to adsorb Pb(II) (Novoseltseva et al., 2020). In the development of reed-based beads both chemical and thermal treatments were used to produce an adsorbent for simultaneously removing Oxytetracycline and Cd(II) with a maximum sorption capacity of 23.95 mg of Cd(II) g^{-1} (Karoui

et al., 2020). Chemically modified almond shell-based adsorbents, such as bleached almond shell, lyophilized-bleached almond shell, and oxidized cellulose nanofibers were investigated for Cu(II) adsorption (Maaloul et al., 2017). A great improvement of the adsorption capacity for Cu(II) of almond shell derivates, up to 141.44 mg g^{-1}, was obtained when new adsorbent beds were prepared by chemical crosslinking bleached almond shell with sodium trimetaphosphate (Maaloul et al., 2020). A similar sorption capacity, 131.16 mg of Cu(II) g^{-1}, has recently been reported for a biopolymer composite produced from cellulose nanocrystals of almond shell as adsorbent (Maalul et al., 2021). These almond-shell derivates can be regenerated using diluted HCl solutions (Maaloul et al., 2020; Maaloul et al.,2021).

Despite the benefits in terms of increase of the adsorption capacities obtained after performing these chemical treatments, they require the use of energy and chemical reagents, which increase the cost and the complexity of the process.

Biosorbents can be used to generate important, low-cost technologies for contaminated water treatment systems if these costs are related to their availability, involving only transport costs and few raw material process costs (Gadd, 2009). There are several lignocellulosic agro-industrial waste and by-products that are available in the Mediterranean region such as cork, olive stones and pinecones that have been evaluated as potential biosorbents for the removal of organic and inorganic pollutants.

Cork comes from the outer bark of the cork oak tree, known botanically as Quercus suber L. Its harvest and subsequent transformation supports one of the most important industries in the Mediterranean region. The traditional use of cork has been on stoppers for wine bottling, however, other applications and uses are possible (de Aguiar et al., 2019). Cork is mainly composed of two hydrophobic biopolymers, suberin and lignin, and hydrophilic polysaccharides cellulose and hemicellulose. Although highly variable with tree maturity and geographical area, the typical chemical composition of cork is approximately 40% of suberin, 22% lignin, 18% polysaccharides and 15% extractives. The content of suberin is the chemical fingerprint of cork and it is directly related to most of its typical properties (Pereira, 2015).

Cork has been used as a biosorbent for pollutants, such as phenolic compounds and pharmaceutical and personal care products (Mallek et al., 2018). Moreover, several studies focused on the removal of heavy metals using powdered or granulated cork as biosorbent (Pintor et al., 2012). Cork biomass was applied for the removal of Pb(II) and Cd(II) from aqueous

solutions showing that the adsorption process is pH dependent and that in a mixture of the two metals, the active sites of cork presented a higher affinity for Pb(II) than for Cd(II) (López-Mesas et al., 2011). Efficiencies of 97% were achieved in the adsorption of Cr(VI) by powdered cork at pHs of around 2.5-3 (Sfaksi et al., 2014).

1.6.1.1. Olive stones

The cultivation of olive trees (*Olea europaea L.*), the production and use of olive oil have been a well-known and established practice in Mediterranean countries for more than 7,000 years. The area where this crop is most concentrated is in Spain, followed by Italy, Greece and Tunisia (International Oil Council) (Fig. 1.7). With the high production of olive oil in the world (1300 million tons per year), there has been a rise in the volume of olive mill waste production, which is composed of the olive stones and pulp residual fraction. Olive oil can generate up to 30-40% of solid waste depending on moisture and the olive fraction content in the fruit as well as extraction processes, resulting in solid waste production of about 1300 million tons per year (Ouazzane et al., 2017). Spain, the world's leading olive oil producer and exporter, generates an estimated 360,000 tons of olive stones per year that are considered as an environmental problem because olive stone remains are a waste product with no use, so it is incinerated or dumped without control. However, olive milled solid wastes can be valorised as biofuel, soil amendment and livestock feeding (Martín-Lara et al., 2013).

The chemical composition of olive stone waste mainly consists of lignin, cellulose, and hemicelluloses. The active functional groups of olive stone waste are the carbonyl and hydroxyl groups of the lignocellulosic material which can interact with metal ions. The use of different types of olive mill solid waste as biosorbent in the removal of heavy metals from water was reviewed (Bhatnagar et al., 2014). Several studies using olive waste as biosorbents were performed by the Department of Chemical Engineering, University of Granada, (Spain) (Blázquez et al., 2010; Calero et al., 2009; Martín-Lara et al., 2017). In these articles, the kinetic and biosorption capacities of olive stones for divalent metals such as Cd(II), Cu(II) and Pb(II) and of Cr(VI) and Cr(III) were investigated in batch and dynamic conditions using a fixed-bed column. A new process, based on olive stones as adsorbent material in a fixed-bed column, for the remediation of electroplating industry effluents was proposed (Martín-Lara et al., 2014).

The results obtained showed that the removal of Cr(VI) took place by two parallel mechanisms: adsorption of Cr(VI) and reduction of Cr(VI) to Cr(III) and that it was not possible to eliminate all the chromium of the solution (Martín-Lara et al., 2017). The adsorption of Fe(III) by olive stones (Nieto et al., 2010) and the removal of Ni(II) were also reported (Corral Bobadilla et al., 2020). The interaction of olive stones with Cu(II), Ni(II) and Cd(II) was characterized by performing potentiometric and carbon-13 nuclear magnetic resonance (NMR) analyses suggesting a specific complexation between metal ions and hydroxyl groups on guaiacyl and syringyl moieties of the phenylpropanoid residues of lignin (Nurchi et al., 2007).

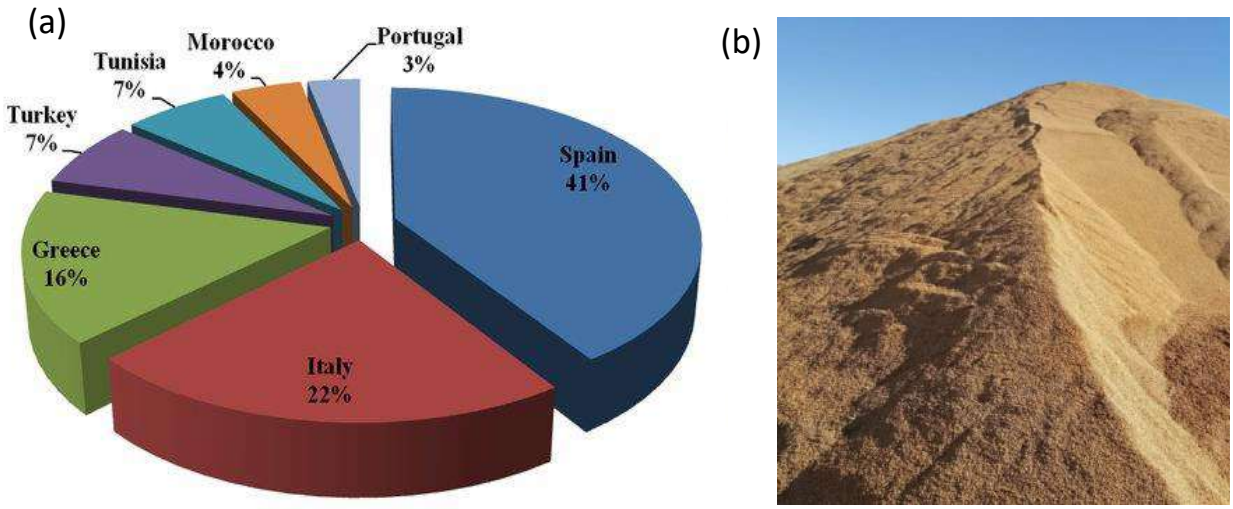

Figure 1.7. (a) Olive oil production worldwide and (b) Milled Olive stones (data from International Olive Oil Council, IOOC 2014).

In order to enhance the adsorption efficiency of olive stones, chemical treatments using different kinds of modifying agents (such as base solutions, mineral and organic acid solutions, organic compounds, oxidizing agents, etc.) have been performed in different studies (Bohli and Ouederni, 2016; Martín-Lara et al., 2013). The modification of olive stones with nitric acid (HNO_3), and sulfuric acid (H_2SO_4), resulted in a higher adsorption capacity for Pb(II) than when they were untreated. The better performance by chemically modified olive stones is explained by the changes in the surface area that led to the conversion of macropores to micropores, a higher number of active binding sites, better ion-exchange properties, and the formation of new

functional groups that favors lead uptake (Martín-Lara et al., 2013). Carbonization of the biomass is one approach that generates a high specific surface area, leading to a good adsorption capacity, a review about carbonized olive stone-based adsorbent has been recently published (Saleem et al., 2019). The influence of several treatments on surface proprieties of olive mill solid wastes and olives stones was reviewed by Ouazzane et al., (2017).

Chemical modification of lignocellulosic olive stones was also performed by grafting with succinate or maleate spacers, which contributed to the chelation of the metal ions enhancing the removal capacity of cadmium and lead ions (Belalia et al., 2018). The coating of olive stones with zerovalent iron and magnetite nanoparticles was investigated and applied to the removal of Cr(VI). The coated biomass adsorption capacity significantly increased (2.54 and 4.11 mg Cr g^{-1}) when compared to the uncoated one (1.48 mg Cr g^{-1}) (Vilardi et al., 2018). Delignification of olive stone powder with sodium chlorite ($NaClO_2$) resulted in the introduction of carboxylic groups, an increase of specific surface area, and a decrease in the particle size. The adsorption capacities have been improved and are 7.76 mg g^{-1} for Fe(III), 21.1 mg g^{-1} for Cu(II), and 16.62 mg g^{-1} for Zn (II) (Gao et al., 2021).

1.6.1.2. Pine cones

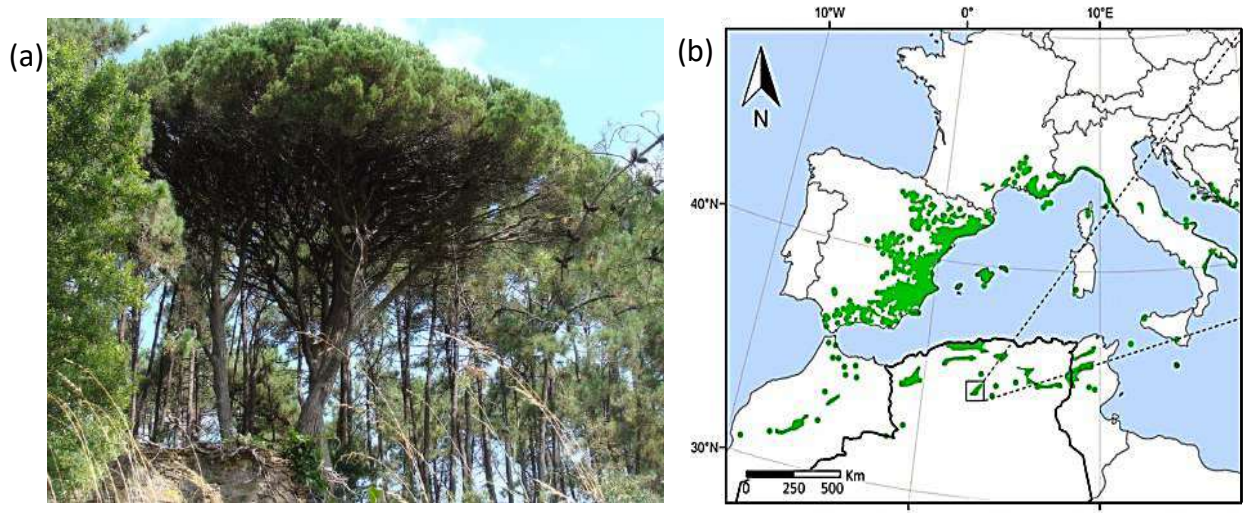

Figure 1.8. a) Pine tree forest and b) map of the pine tree distribution in the Mediterranean Rim.

Pine cones are produced in large quantities annually all over the world. In the Western Mediterranean, Spain has a pine-cultivated area of 460,000 hectares, whereas in the Southern

Mediterranean 320,000 hectares of the forest cover in Tunisia is made up of *Pinus halepensis* and *Pinus pinea* (Fig. 1.8). Forests of Mediterranean Stone pine (*P. pinea*) yield from 200 to 600 kg of cones per hectare annually, these pine cones contain pine nuts, a fruit that has a high economic value. After collecting the nuts, cones are usually discarded or burned for energy (Almendros et al., 2015). Generally, cones and pine bark are some of the most readily available biomasses but are treated as residue. A number of alternative uses for this large biomass have been examined, such as wood panels and biosorbents (Neis et al., 2019). The lignocellulosic natures of the pine cone shell make this material an efficient biosorbent to remove metal ions from wastewater. The biosorption capacity of untreated pine cone shells for Cu(II) was determined to be 6.81 mg g^{-1}. and a surface complexation model was proposed to explain the Cu(II) adsorption (Blázquez et al., 2012). Pb(II) adsorption by pine cone biomass was investigated in several studies (Almendros et al., 2015; Awad and Erkurt, 2014; Martín-Lara et al., 2016). The adsorption capacity of the pine cone for Pb(II) was shown to be higher than for Cu(II), even in binary solutions containing both metal ions the affinity order was Pb(II) > Cu(II). These metal ions can be desorbed with a 0.3 M HCl solution (Martín-Lara et al., 2016). The kinetic studies showed that the equilibrium is reached in less than two hours and the adsorption of Cu(II) and Pb(II) followed a pseudo-second-order kinetic model (Awad and Erkurt, 2014). Hence, a great advantage of the use of pine cone powder as a biosorbent is the fact that a large number of metal ions from the solution can be removed in a relatively short time.

Pine cones were also used to remove Cr(VI) from aqueous solutions resulting in a maximum adsorption capacity of 37.59 mg g^{-1} at pH 1.0 (Najim and Yasin, 2013). Cone biomass of *Pinus sylvestris L*. exhibited the highest Cr(VI) uptake capacity (238.10 mg g^{-1}) at 45 ◦C. (Ucun et al., 2009). The biosorption capacity of the pine cone was improved through chemical activation of the surface, increasing the number of functional groups, using $Ca(OH)_2$, KOH and NaOH (Ofomaja and Naidoo, 2010) or phosphoric acid (Huong et al., 2016). An ion exchanger from pine cones was prepared by a cross-linking treatment with citric acid allowing the use of this modified pine cone for the reduction of the hardness of the water and the adsorption of Pb(II) (Altundoğan et al., 2016).

Chemical modification of pine bark with sulfuric acid improved the adsorbent characteristics for the removal of Cd(II), Pb(II) and Cr(VI) (Schwantes et al., 2018). Carboxylate-modified pine

cones were synthesized via esterification of pine cones with isopropylidene malonate for eliminating lead ions from aqueous media. This modification led to a maximum adsorption capacity for Pb(II) of 400.0 mg g^{-1} being obtained (Bagherian et al., 2021). Modification of pine cones with magnetite nanoparticles which were co-precipitated on NaOH treated pine cones enhanced both the adsorption efficiency and kinetics of As(III) biosorption (Pholosi et al., 2019). The magnetic pine cone was synthesised using different masses of pine cone until obtaining the highest adsorption capacity for Cr(VI) (Pholosi et al., 2020).

Activated carbon prepared from the cones of the European Black pine was used as an adsorbent for the removal of Pb(II) ions from aqueous solutions with a maximum adsorption capacity of 27.53 mg g^{-1}. Activated carbon derived from cones of *Pinus roxburghii* (Himalayan Pine) was used as an adsorbent for the removal of copper, nickel and chromium ions from waste water with a maximum adsorption capacity of 14.2, 31.4 and 29.6 mg g^{-1} for Cu(II), Ni(II) and Cr(VI), respectively (Saif et al., 2015).

1.7. Engineered adsorbents

Conventional adsorbents and bio-adsorbents have certain constraints such as low adsorption capacities, lack of functional tunability, reusability and recyclability. To overcome such limitations, new sorbents in nano dimensions are being synthesized and adopted for water decontamination. Nano-adsorbents, due to their high specific surface area, short intraparticle diffusion distance, and tunable pore sizes and unique surface chemistry, offer significant advantages over conventional adsorbents. The main advantages of engineered nano-adsorbents are their large specific surface area and availability of a large number of active groups for binding of heavy metal ions that can be tailored to improve the selectivity of the adsorption process. Furthermore, nanostructured adsorbents can be reused and recycled repeatedly which makes them cost-effective and highly attractive for the treatment of wastewater (Sarma et al., 2019).

1.7.1. Adsorption with nanomaterials

Nanomaterials are materials that have external dimensions (1 nm–100 nm) or those that have a nanoscale internal structure/surface. Moreover, they exhibit special properties, such as a surface effect, small size effect, quantum effect, and macro quantum tunnel effect. These properties show their extraordinary adsorption capacity and reactivity, which make them an adsorbent favorable for the removal of heavy metal ions. Nowadays, nanomaterials have a wide range of applications in technology and the environment as medicine, catalysis, water treatment. In comparison with conventional methods, nanomaterial has attracted attention because of their higher capacity; they are environmentally friendly and low cost. Among them, we can cite graphene oxide, carbon nanotube, and nanoparticles (Tan et al., 2015).

1.7.1.1. Graphene Oxides

Graphene is a two-dimensional carbon nanomaterial, a fundamental building black for graphitic materials with a single layer of sp^2. They attract the interest of scientists on account of their exceptional properties: their structure, large surface area with a value of 2630 m^2 g^{-1}, and electrical, thermal, mechanical properties, high transparency, high strength and abundant functional groups (Deng et al., 2013). Due to these properties and their planar structure, graphene-based materials have been used in various fields such as electronics, energy storage, sensors, batteries, solar cells etc. (Wang and Chen, 2015). The hexagonal array of carbon in graphene sheets are ideal for strong interactions with other molecules, however, it is insoluble and hard to disperse in all solvents due to strong Van der Waals that can hamper the sorption of organic compounds or metal ions (Wadhawan et al., 2020). Graphene can also be functionalized in order to enhance its specificity, loading capacity, solubility, biocompatibility, etc. The oxidation of graphene using potassium permanganate concentrated sulfuric acid produces graphene oxide (GO) (Fig. 1.9).

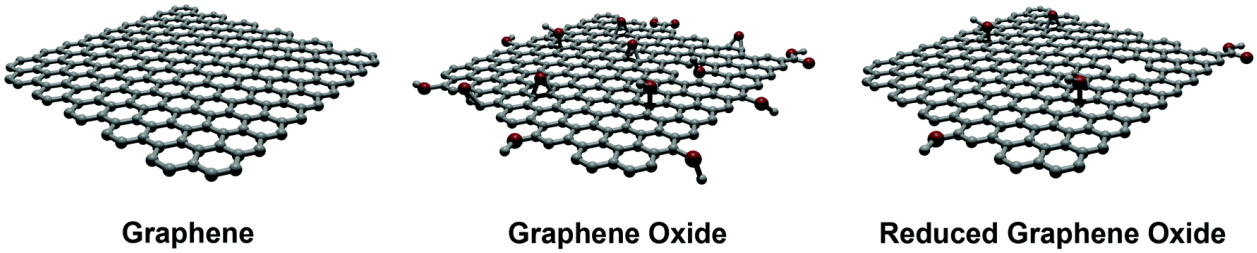

Figure 1.9. Graphene-based materials (Reina et al., 2017).

Monolayer graphene oxide (GO) contains a range of reactive oxygen functional groups, epoxides, hydroxyl, ketones and carboxyl groups (Liu et al., 2019). Monolayer GO can be obtained by exfoliating graphene oxide through sonication or mechanical stirring. The thickness of this monolayer GO, 0.7-1.2 nm is greater than graphene, 0.335 nm, due to the existence of epoxy, carboxyl, and hydroxyl groups on both sides of GO sheets (Ali et al., 2019), resulting in a negatively charged surface. The electrostatic interaction between metal ions and the negatively charged surface of GO can explain the adsorption of metal ions by this adsorbent. The metal ion adsorption by GO can be explained by an ion-exchange mechanism involving the exchange of the protons of COOH and OH functional groups located in the GO surface by the metal ions present in the aqueous solution. The release of protons to the solution results in a pH decrease (Chawla et al., 2015). Another possible mechanism is surface complexation of the metal ions by oxygenated functional groups located at the edge of graphene oxide sheets (Peng et al., 2017) (Fig. 1.10).

Graphene oxide can adsorb metals due to the presence of the oxygen group, its large theoretical specific surface area, surface hydrophobic π-π interaction, high negative charge density, high adsorption for cations and basic compounds. The affinity of GO for metal ions is strong and follows the order Pb(II) > Cu(II) ≫ Cd(II) > Zn(II) in agreement with the metal electronegativity and the first stability constant of the associated metal hydroxide (Dastgheib and Rockstraw, 2002).

Pb(II) was removed by graphene oxide in the study of Wang et al., (2015). The elimination of metals from wastewater was investigated by different researchers. Fu and Huang, (2018) studied the removal of Cu(II), Wang et al., (2018) the removal of Co(II), Pakulski et al., (2018) the

removal of Cd(II), and the efficiency of graphene oxide on the removal of anions as Cr(VI) was also proved (Zhang et al., 2013). Table 1.4 summarizes some applications of GOs.

The adsorption capacity of GO can be increased by functionalizing GO by using various reagents such as ethylene diamine tetraacetic acid, ethylenediamine, sulfanilic acid, sodium sulphide, and triethylenetetramine to introduce heteroatoms (N, S), which have a high affinity for heavy metals (Ahmad et al., 2020), or modifying its surface with manganese oxide, FeOOH, and ion nanoparticles, among others. This functionalization will also improve the selectivity of the metal adsorption as well as the separation of GO after adsorption (Peng et al., 2017). A critical problem of the use of nanomaterials as graphene oxides is their tendency to aggregate in order to reduce the energy associated with the high ratio of surface area to volume. To overcome this problem, new composite materials can be synthesised by combining GO with other adsorbents (Luo et al., 2012). The composite graphene oxide/almond shell (GO@AS) allowed maximum sorption capacities 121.95 mg g^{-1} for Cd (II) and 69.93 mg g^{1} for Ni(II) to be reached (Moghaddam et al., 2019).

Table 1.4. GO adsorption of heavy metal ions (Ali et al., 2019).

Adsorbent	Adsorbate	Concentration (mg L^{-1})	pH	Temperature (K)	Contact time (h)	Adsorption capacity (mg g^{-1})	Reference
GO	Pb (II)	5-300	6.8	298 ± 2	24	367	(Madadrang et al., 2012)
GO	Zn (II)	-	5.6	-	-	30.1 ± 2.5	(Lee and Yang, 2012)
GO	Cd (II)	-	5.6	-	-	14.9 ± 1.5	(Lee and Yang, 2012)
GO	Pb (II)	-	5.6	-	-	35.6 ± 1.3	(Lee and Yang, 2012)
GO	Cu (II)	25–250	5.3		2.5	117.5	(Wu et al., 2012)
GO	Pb (II)	5-300	7.0 ± 0.5	298 ± 5	24	692.66	(Musico et al., 2013)
GO	Cu (II)	-	5	298± 2	-	294	(Sitko et al., 2013)
GO	Zn (II)	-	5	298± 2	-	345	(Musico et al., 2013)
GO	Cd (II)	-	5	298± 2	-	530	(Musico et al., 2013)
GO	Pb (II)	-	5	298± 2	-	1119	(Musico et al., 2013)
GO	Zn (II)	10–100	7.0 ± 0.1	293	-	246	(Wang et al., 2013)
GO	Zn (II)	-		318	-	225	(Wang et al., 2013)
GO	Zn (II)	-		303	-	236	(Wang et al., 2013)

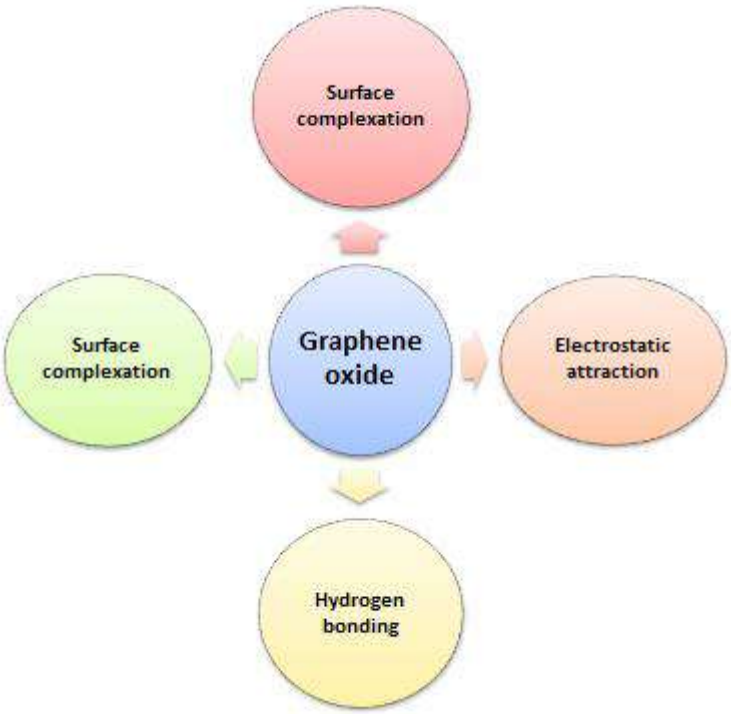

Figure 1.10. Types of mechanisms on the adsorption of metal ions by Graphene Oxide.

1.7.1.2. Carbon nanotube

The carbon nanotube (CNT) can be synthesized by electric arc discharge, pulse laser vapour and catalytic decomposition of gaseous hydrocarbons CNT. It is considered as a sheet of graphite that has been rolled into a tube with single, double or multiple walls. CNT have a diameter in the range 0.1-10 nm and a length of up to centimetres. CNT surfaces have a strong interaction with other molecules (Kumar et al., 2015). The carbon nanotube has a hollow cylindrical structure, large surface area, high length to radius ratio, hydrophobic interaction π-π, hydrogen bonds, and electrostatic interactions which are important to remove metals (Wang et al., 2019).

There are two types of carbon nanotube: multi-wall carbon nanotubes (MWCNTs) contain more than one graphene sheet, while single-wall carbon nanotubes (SWCNTs) contain only one sheet (Fig. 1.11 a, b). In order to enhance the adsorption capacity and efficiency of CNT for the removal of heavy metal ions, the incorporation of oxygen-containing functional groups on the surface of CNTs by chemical oxidation with oxidizing reagents such as HNO_3, H_2O_2 and $KMnO_4$

is required. Oxidized CNT sheets allowed the removal of various divalent heavy metal ions (Cu^{2+}, Zn^{2+}, Pb^{2+}, Cd^{2+}, Co^{2+}) from water (Tofighy and Mohammadi, 2011). As in the case of GO, the surface of MWCNTs can be modified with chitosan or with ethylene diamine in order to improve their adsorption capacity for Cd(II), Cu(II), Zn(II), and Ni(II) (Lu and Astruc, 2018).

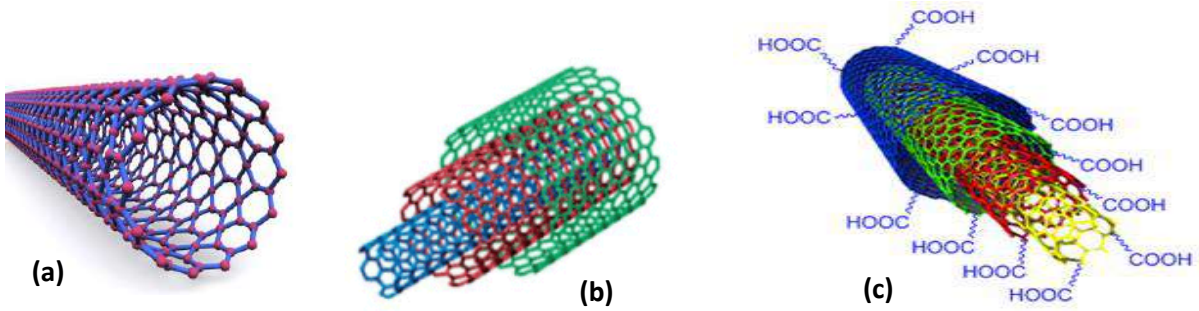

Figure 1.11. (a) Simple walled carbon nanotube (CNT), b) multi walled MWCNT and (c) oxidized MWCNT (Khalaf and Awad., 2016).

Double-oxidized MWCNTs have been applied to remove copper, manganese, and zinc from acid mine drainage wastewater showing increments of 79%, 78%, and 48%, respectively, in comparison with oxidized MWCNTs (Fig. 1.11 c). The metal adsorption process is pH-dependent increasing the adsorption capacity when the pH increases (Rodríguez and Leiva, 2020). The point of zero charge (pH_{PZC}) indicates the pH at which the sum of positive charges equals the sum of negative charges. CNTs have shown a good performance at low pH values for the adsorption of heavy metals, since they may have a pH_{PZC} of less than 5.

1.7.2. Adsorption with metal-organic framework (MOF)

Metal–organic frameworks (MOFs) are a class of adsorbent materials that have emerged within the past three decades. MOFs are constructed of secondary building units which are namely, metal ions or metal clusters, and organic ligands, which are connected into three-dimensional lattices (Martínez et al., 2018) (Fig. 1.12). Ag(I), Cu(II), Mg(II), Zn(II), Co(II), Fe(III), Al(III), Ln(III), Zr(IV) are the most used metals for the construction of MOFs, which can adopt various coordination geometries such as trigonal bipyramidal, pyramidal, square, tetrahedral and

octahedral. Organic linkers such as amines, carboxylates, sulfonates and phosphates are also key components for MOF synthesis. The attractive properties of MOFs such as large surface areas, permanent porosity, multi-functionalization, changeable structures and open metal sites are beneficial to a wide range of applications, including gas storage, separation, catalysis, sensing, drug delivery, bioimaging, and chemical adsorption. MOFs have numerous advantages as adsorbents due to their high surface area, typically ranging from 1000 to 10,000 $m^2 g^{-1}$, exceeding those of traditional porous materials like activated carbon and zeolites, porosity, chemical stability, functionality and adsorption site accessibility by the diffusion of contaminants through the framework (Chen et al., 2020). Owing to their crystalline structure, MOF pores are highly ordered and the size of the pores, as well as their shape, can be adjusted by choosing the linkers used as well as the connectivity of the metal ions. MOFs can be synthesized at an ambient temperature of up to 220°C, at atmospheric pressure and in a pH range of 1-10 by various methods such as solvo(hydro) thermal, mechanochemical, sonochemical, electrochemical layer by layer growth and microwave. Recently, some review articles have been published on the removal of heavy metal pollutants from water by MOFs (Feng et al., 2018; Kobielska et al., 2018; Wen et al., 2018). The adsorption mechanisms of metal ions by MOFs are summarized in Figure 1.13.

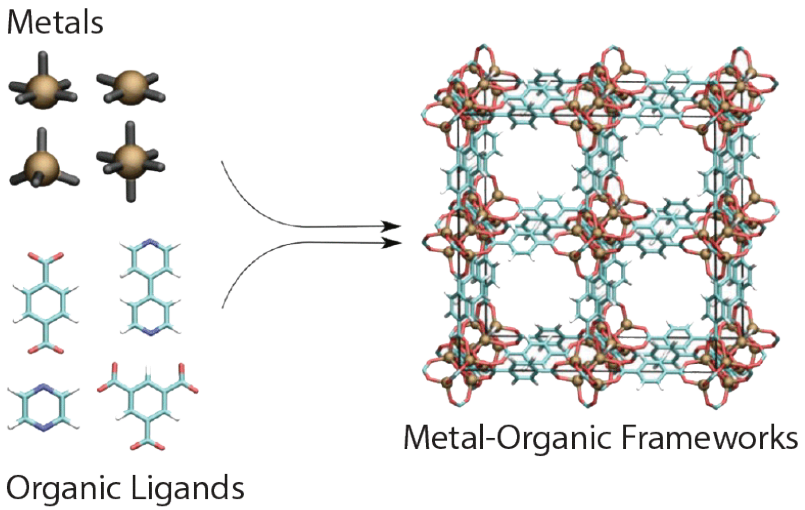

Figure 1.12. Metal-organic frameworks (MOFs) (Xia et al., 2019).

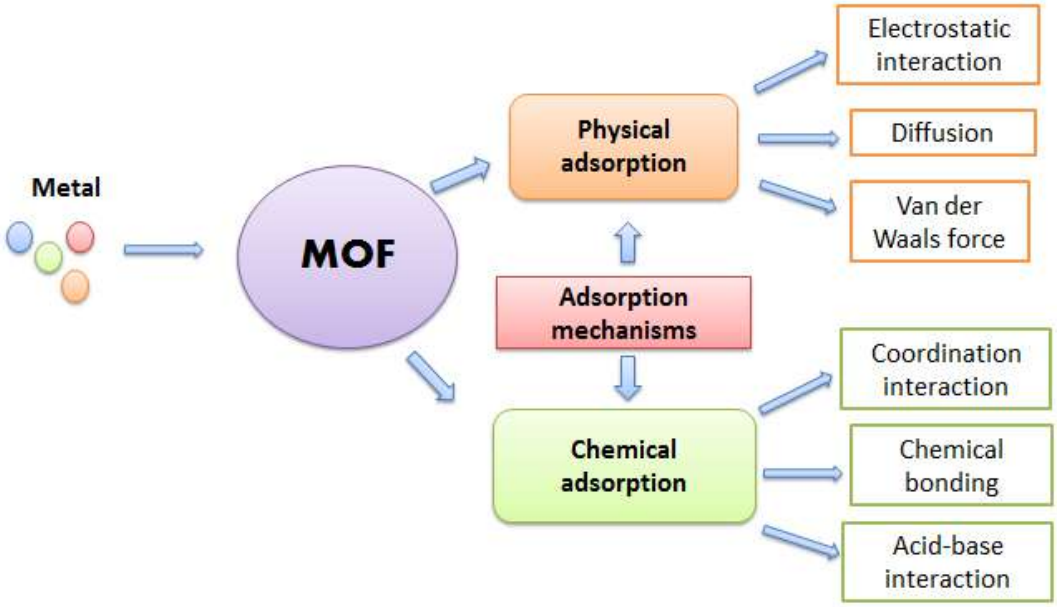

Figure 1.13. Adsorption mechanisms of metals by MOF (Manousi et al., 2019).

MOFs-based materials including unmodified MOFs, modified MOFs and magnetic MOFs composites have been prepared and used for removing toxic metal ions owing to the tunable property of MOFs. A review has been published regarding this application (Rani et al., 2020). Some examples of unmodified MOFs to remove Pb(II), Cd(II), Cr(VI) and As(III) and As(V) are given. A Zr-MOF produced via a microwave-promoted synthesis was applied to remove Pb (II) with an adsorption capacity of 135 mg g $^{-1}$, which is higher than GO (125 mg g^{-1}) (Yin et al., 2016). Cu-based MOFs also show an excellent adsorption capacity for the removal of Pb(II) ion in comparison with other engineered adsorbents (Rahimi and Mohaghegh, 2016). An NH_2-functionalized Zr-MOF shows excellent adsorption capacity for Cd(II) removal and the maximum adsorption capacity is 177.35 mg g^{-1}. The mechanisms followed for Cd(II) removal is based on the coordination interaction between Cd(II) and $–NH_2$ (amino group) that also can interact with Pb(II) (Wang et al., 2017). For Cr(VI) removal, which was attained by ion exchange, cationic MOFs such as MOFs FIR- 53 and FIR-54 were prepared through a nanoscale route (Zhang et al., 2015).

As previously explained, arsenic is a highly hazardous contaminant that is toxic to living organisms. The toxicity of inorganic arsenic is higher than that of organic arsenic and generally,

arsenic exists in the dissolved inorganic forms of As(III), arsenite, and As(V), arsenate. While both these forms are toxic, As(III) is about 60 times more poisonous than As(V). MOFs and MOF-based composites have increasingly been applied in the removal of As(III) and As(V) from water, due to their excellent adsorption capacities. Among them, the materials from the Lavoissier Institute (MIL) such as MIL 53(Fe) showed excellent adsorption properties for As(V) and fast kinetics due to the Lewis acid-base and electrostatic interactions between $H_2AsO_4^-$ and Fe^{3+} at pH 5 (Vu et al., 2014). MIL-53(Al) also exhibited a relatively high adsorption capacity for As(V) over a solution with a pH range of 6–9, reaching a maximum of 105.6 mg g^{-1} at pH 8.0. The effect of several coexistent anions such as sulfate, chloride, nitrate and phosphate in the adsorption of As(V) showing that only PO_4^{3-} competes with AsO_4^{3-} for the binding sites of MIL-53(Al) (Li et al., 2014).

The synthesized MIL-88 bears microporous channels and cages, which made it a good adsorbent for As (V). It has been found that the arsenic adsorption ratio declines with an increase in initial As (V) concentration, thus, MIL-88A could act as a good adsorbent for a low-concentration arsenic solution (Wu et al., 2018). The capacity of 110 mg g^{-1} exhibited by MIL-100(Fe) for arsenate is higher than those presented for other materials and has also good reusability and excellent selectivity in the presence of other anions. In this case, the adsorption of the arsenate implies strong Fe–O–As(V) interactions that destroyed the long-range order of uniform mesoporous channels in the framework, which is recovered immediately after As(V) desorption (Cai et al., 2016).

The adsorption capacity MIL-101(Fe), a typical Fe-based MOF comprised of octahedral chains of Fe (III) as secondary building units and 1,4-benzene dicarboxylic acid linkers, was investigated for the removal of arsenate (As(V)) and its organic forms such as roxarsone (ROX), p-arsanilic acid (p-ASA) and dimethyl arsenate (DMA) from aqueous solutions. The formed Fe-O-As inner-sphere coordination between arsenic species and the incomplete-coordinated cationic Fe in the MIL-101(Fe) cluster is found to be the primary adsorption mechanism, which resulted in maximum adsorption capacities of 232.98, 507.97, 379.65 and 158.94 mg g^{-1} for As (V), ROX, p-ASA and DMA, respectively (Li et al., 2019).

Fe-BTC, a MOF containing iron nodes and 1, 3, 5-benzene tricarboxylic linkers, was the first used to remove As(V) species from water solutions. It can be used in a pH range of 2-10, although the highest adsorption capacity (12.3 mg g^{-1}) was obtained at pH 4 (Zhu et al., 2012).

In the case of As(III) adsorption, zeolitic imidazolate frameworks (ZIFs) - a subclass of MOFs structured with Zn(II) or Co(II) ions and imidazolate and its derivatives, showed great adsorption capabilities for As(III) species, with a maximum adsorption value of 122.6, 108.1, 117.5 mg g^{-1} for cubic ZIFs, leaf-shaped ZIFs and dodecahedral ZIFs, respectively. FTIR and XPS results evidenced that As(III) adsorption occurred through surface complexation by substitution of zinc hydroxyl (Liu et al., 2015). ZIF-8 showed moderate capacities for both As(V) and As(III)- 60 mg g^{-1} and 49 mg g^{-1}, respectively, at neutral pH due to the presence of both hydroxyl and amine groups although kinetics were not favourable (Jian et al., 2015). UIO-66 is a porous crystalline material containing zirconium. It is constructed with $Zr_6O_4(OH)_4$ clusters and terephthalate (1.4-benzene dicarboxylate, BDC) linkers. As(V) can be removed through the formation of Zr-O-As coordination bonds (Wang et al., 2015).

A review about the use of MOFs and modified and composite MOFs for arsenic adsorption has been published (Wang et al., 2019). Moreover, in some reviews devoted to the adsorption of toxic/heavy metal ions by MOFs, sections about arsenic removal by MOFs were included (Kobielska et al., 2018; Shayegan et al., 2020; Wen et al., 2018).

1.8. Characterization of the adsorption process

Adsorption technology has been widely applied to remove pollutants such as toxic metal ions from water and wastewater. The characterization of the adsorption processes is essential in order to design efficient adsorption systems. This characterization includes the knowledge of the adsorption mechanisms and the kinetics of the adsorption process as well as the physical and chemical characterization of the adsorbent as has been explained in section 1.5.1. Chemical adsorption corresponding to the formation of chemical bonds, physical adsorption related to the Van der Waals force, and ion exchange are the main adsorption mechanisms. These mechanisms can be investigated by the modelling of the adsorption equilibrium data, the characterization of adsorbent before and after adsorption, the study of molecular dynamics, and the density functional theory (DFT) calculation (Wang and Guo, 2020). Among them, modelling of adsorption data by isotherm models is the most convenient and widely used method that also allows the calculation of the maximum adsorption capacity.

The characterization of adsorbent/biosorbent and sorbate require the use of a number of analytical techniques that are summarized in Figure 1.14. Atomic absorption spectrophotometry (AAS), ion-selective electrodes (ISE), UV–Vis spectrophotometry, and inductively coupled plasma atomic emission spectroscopy (ICP-OES) can be used to determine metal ions. Potentiometric titration, scanning or transmission electron microscopy coupled with energy-dispersive X-ray spectroscopy (SEM/TEM–EDX), infrared spectroscopy or Fourier-transform infrared spectroscopy (IR or FTIR), X-ray absorption spectroscopy (XAS), X-ray diffraction (XRD) analysis, electron spin resonance spectroscopy (ESR), nuclear magnetic resonance (NMR), X-ray photoelectron spectroscopy (XPS), thermogravimetric analysis (TGA), and differential scanning calorimetry (DSC) are techniques used for the characterization of the adsorbent as well as for giving insights into the mechanisms of adsorption.

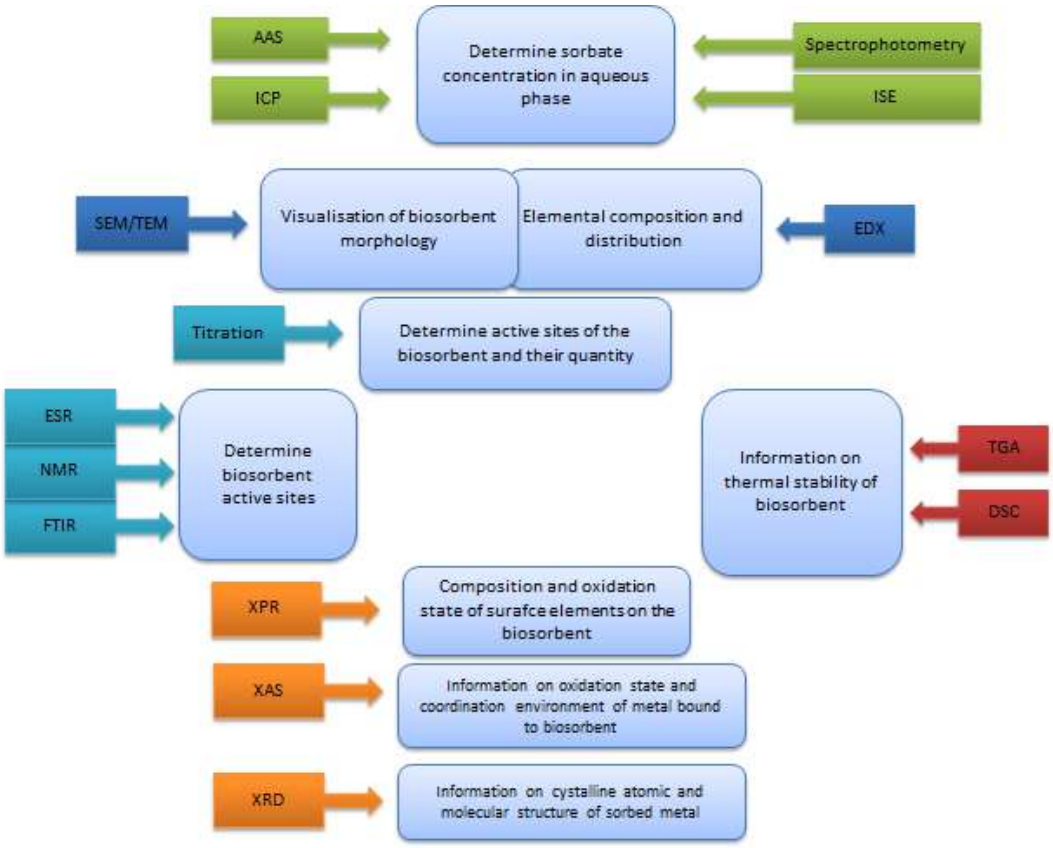

Figure 1.14. Analytical techniques in the characterization of biosorption/adsorption processes. Adapted from (Fomina and Gadd, 2014).

1.8.1. Adsorption kinetics

The mass transfer from the solution to the adsorption sites within the adsorbent particles is limited by mass transfer resistances determining the time required to reach the state of equilibrium. The time progress of the adsorption process is referred to as adsorption kinetics. The rate of adsorption is usually limited by diffusion processes toward the external adsorbent surface and within the porous adsorbent particles. The study of the adsorption kinetics is required in order to understand the rate-limiting mass transfer mechanisms and to evaluate the characteristic mass transfer parameters. The adsorption kinetics include three steps: the first step is the external diffusion from the bulk of the solution to the surface of the adsorbent, the second step is the internal diffusion of the adsorbate in the pores of the adsorbent, and the third step is the adsorption of the adsorbate in the active sites of the adsorbent. Adsorption kinetic models, such as the pseudo-first-order model, the pseudo-second-order model and the intraparticle diffusion model have been widely applied for the analysis of adsorption kinetics.

1.8.1.1. Kinetic models

- **Pseudo-first order**

The first model assumes that the rate of occupation of sorption sites is proportional to the number of unoccupied sites, expressed by the equation:

$$\frac{dq_t}{dt} = K_1(q_e - q_t) \qquad (1.1)$$

Where q_e and q_t are the adsorption capacity at equilibrium and at time *t*, respectively (mg g^{-1}) and k_1 is the pseudo-first-order adsorption rate constant (min^{-1}).

- **Pseudo-second order**

The pseudo-second-order kinetic model is based on the assumption that the rate-limiting step is the chemical sorption and is expressed by the equation:

$$\frac{dq_t}{dt} = K_2(q_e - q_t)^2 \qquad (1.2)$$

where K_2 (g mg^{-1} min^{-1}) is a second-order adsorption rate constant.

- **Intraparticle diffusion model**

The diffusion processes involved in the adsorption process are (i) diffusion of metal ions from the bulk solution to the liquid film on the adsorbent surface, (ii) diffusion of metal ions across the liquid film on the adsorbent surface, (iii) adsorption of metal ions on the active sites on the surface, the strength of the bonding depending on whether the process is physical or chemical and (iv) diffusion of metal ions through pores of different sizes in the adsorbent particles. The diffusion of adsorbate in the liquid film around the adsorbent and the adsorption onto the active sites are instantaneous while the diffusion of adsorbate within the pores of the adsorbent is the slowest step. Hence, intraparticle diffusion is the limiting rate in the adsorption process if a plot of metal ions adsorbed against the square root of the contact time yields a straight line. The most widely applied intraparticle diffusion equation for adsorption system is given by:

$$q_t=K_p t^{0.5}+C \qquad (1.3)$$

where K_P is the intraparticle diffusion rate constant (g mg^{-1} min^{-1}) and the intercept of the plot, C reflects the boundary layer effect or surface adsorption. It was observed that the larger the intercept, the greater the contribution of the surface adsorption in the rate-limiting step.

1.8.2. Factors affecting adsorption

Apart from the type and chemical form of the sorbate, a number of physico-chemical factors determine overall adsorption performance. These factors are: the pH of the solution, the ionic strength, the initial metal ion concentration, the amount of adsorbent and the presence of other ions that can compete with the adsorbate for the binding sites or interfere with the adsorption process.

The effect of these parameters should be investigated in each adsorbate-adsorbent system.

The pH of the solution is an important parameter affecting the solution chemistry of the adsorbate themselves, the activity of functional groups in the adsorbents and competition with coexisting ions in solution. Increasing pH enhances the removal of cationic metals, but reduces that of

anionic metals. In the case of the ionic strength of solution (I), the presence of other ions in the solution reduces the adsorption of the metal ions when I is increased due to the competition of these ions with the adsorbate for binding sites on the adsorbent. This effect is enhanced when the adsorption mechanism is ion-exchange. The effect of other chemical species including competition for binding sites and interferences generally reduces the adsorption efficiency. Anionic effects on metal adsorption depend on metal speciation, co-existing metals and the adsorbent nature. For example, the inhibition of Cr(VI) adsorption by the presence of anions such as nitrate, chloride or sulphate, the formation of insoluble metal precipitates or the formation of metal chloride complexes with Cd(II).

1.8.3. Adsorption isotherm

An adsorption isotherm is a curve, q= f(C), relating the equilibrium concentration of a solute on the surface of an adsorbent, q_e, to the concentration of the solute in the liquid, C_e, with which it is in contact. The adsorption isotherm is also an equation relating the amount of solute adsorbed onto the solid and the equilibrium concentration of the solute in solution at a given temperature. The number of metal ions adsorbed at equilibrium per mass unit of adsorbent is determined by applying the equation:

$$q_e = \frac{(C_i - C_e).v}{m} \qquad (1.4)$$

where C_i is the initial concentration (mg L^{-1}), C_e is the equilibrium concentration (mg L^{-1}), V is the volume of the solution (L) and m is the mass of the adsorbent (g).

According to the classification of Giles (Gauden et al., 2008), the adsorption isotherms are categorized into four types based on their initial slopes and shapes, High affinity (H), Langmuir (L), constant partition (C), and sigmoidal-shaped (S) (Fig. 1.15).

- Type H: this is a particular case of the ‘‘L’’ isotherm, where the initial slope is very high. This isotherm is indicative of a strong adsorbate-adsorbent interaction such as inner-sphere complexes.
- Type L: corresponds to a decrease of site availability as the solution concentration increases. This behavior can be explained by the high affinity of the adsorbent at a low

concentration which decreases as the concentration increases providing the saturation of the adsorbent.

- Type C: this isotherm is indicative of a partitioning mechanism whereby adsorptive ions are distributed or partitioned between the interfacial phase and the bulk solution phase without any specific bonding between the adsorbent and adsorbate. If the solid has a limited quantity of adsorption sites, the isotherm could be nonlinear because of a possible saturation plateau.
- Type S: the curve has a point of inflexion. This type of isotherm implies that adsorption becomes easier as the concentration in the liquid phase increases and decreases as the vacant adsorbent sites are filled. This indicates that at low concentration, the surface has a low affinity for the adsorptive. For a given molecule, this character may depend on both the nature of the adsorbent surface and the nature of the solvent. The point of inflexion illustrates the concentration for which the adsorption overcomes the complexation.

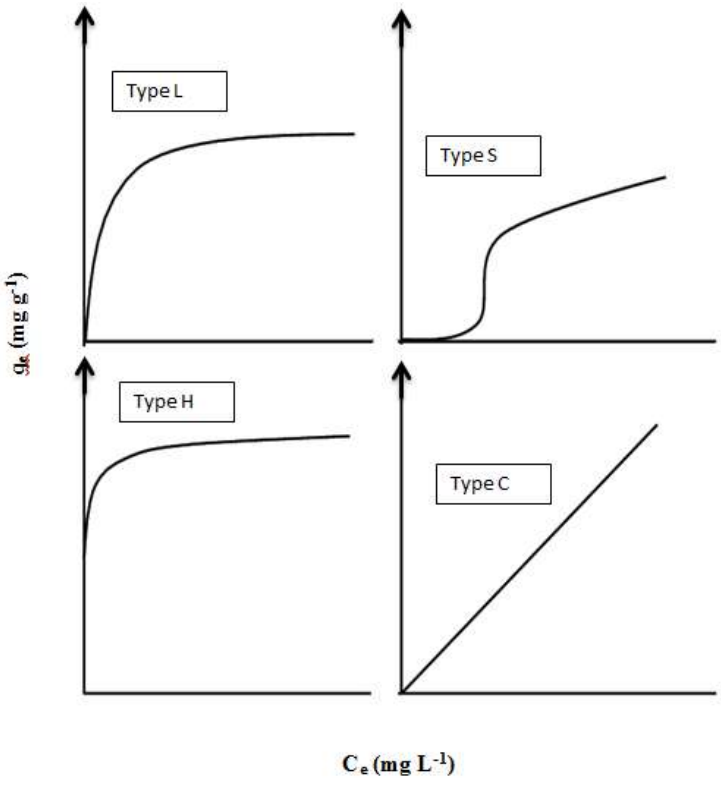

Figure 1.15. Types of adsorption isotherms (Mahmoud et al., 2012).

1.8.3.1. Adsorption isotherm models

- **Langmuir model**

The Langmuir adsorption isotherm assumes the formation of a monolayer of adsorbate on the outer surface of the adsorbent, and after this is completed no further adsorption takes place. The Langmuir isotherm is valid for monolayer adsorption onto a surface containing a finite number of identical sites. The linear Langmuir model is presented by Eq. 1.5:

$$\frac{C_e}{q_e} = \frac{1}{q_{max}.b} + \frac{1}{q_{max}} C_e \qquad (1.5)$$

Where q_{max} is the maximum adsorption capacity (mg g^{-1}) and *b* is the Langmuir constant (L mg^{-1}) The essential characteristic of the Langmuir isotherm can be explained by the equilibrium separation factor (R_L), defined as follows:

$$R_L = \frac{1}{1+C_i b} \qquad (1.6)$$

$R_L = 0$: irreversible adsorption, $0 < R_L < 1$: favorable adsorption and $R_L = 1$: linear adsorption, so the R_L at all the concentrations was between 0 and 1, showing that the adsorption is favorable for all the metals. R_L decreases with increasing initial metal concentration, which indicates that in higher concentration the sites available decrease indicating its saturation.

- **Freundlich model**

The Freundlich isotherm model assumes that the metal ion adsorption takes place on a heterogeneous surface with multilayer adsorption. The linear Freundlich model is expressed by Eq. 1.7:

$$\ln q_e = \ln K_F + \frac{1}{n} \ln C_e \qquad (1.7)$$

where q_e is the amount of metal adsorbed at equilibrium (mg g^{-1}), C_e is the equilibrium concentration (mg L^{-1}) and K_F is the Freundlich constant. The constant K_F is an indicator of adsorption capacity, while 1/n is the strength of adsorption in the adsorption process.

- **Temkin model**

Temkin isotherm model takes into account the effects of indirect adsorbate–adsorbate interactions on the adsorption process; it is also assumed that the heat of adsorption of all molecules in the layer decreases linearly as a result of increased surface coverage. It is expressed by the following Eq. 1.8:

$$q_e = B\ lnA + B\ lnC_e \qquad (1.8)$$

where A is the Temkin constant (L mg^{-1}) and B is the Temkin constant related to heat adsorption (J mol^{-1}).

- **Langmuir-Freundlich model**

Langmuir-Freundlich isotherm includes the knowledge of adsorption heterogeneous surfaces. It describes the distribution of adsorption energy onto the heterogeneous surface of the adsorbent. At low adsorbate concentration, this model becomes the Freundlich isotherm model, while at high adsorbate concentration it becomes the Langmuir isotherm. Langmuir-Freundlich isotherm can be expressed by Eq. 1.9:

$$q_e = \frac{q_{MLF}(K_{LF}C_e)^{M_{LF}}}{1+(K_{LF}C_e)^{M_{LF}}} \qquad (1.9)$$

where q_{MLF} is Langmuir-Freundlich maximum adsorption capacity (mg g^{-1}), K_{LF} is the equilibrium constant for a heterogeneous solid, and M_{LF} is the heterogeneous parameter and it lies between 0 and 1. These parameters can be obtained by using nonlinear regression analysis.

1.9. Fixed-bed column

Batch adsorption can be easily applied in the laboratory for the treatment of small volumes of effluents. However, it is not convenient for application on an industrial scale where large volumes of wastewater are continuously generated. Industrial applications of adsorption require continuous operation by using fixed-bed columns. The equilibrium and kinetic data obtained during batch adsorption represent inaccurate data for the proper design and optimization of fixed-bed columns. Thus, continuous experiments are required to obtain practical information under flow conditions in terms of breakthrough curves. The analysis of these data is useful for calculating the design parameters and identifying the best-operating conditions in a fixed-bed column as cyclic adsorption-desorption processes take place.

Furthermore, the adsorbent can be regenerated and used again. The fixed bed is packed with adsorbent, there is a continuous passage of liquid to be treated through the inlet column with a constant flow rate until the outlet concentration becomes equivalent to the inlet concentration. The pollutant is removed by transfer of the fluid phase into the porous solid. The portion between the exhaustion point and breakthrough point where the transfer material is held is called mass transfer zone (MTZ) or adsorption front (Patel, 2019).

As a function of time, this zone moves in the adsorbent to reach the exit from the bed at the end of the column until the concentration of the exit C is equal to that of the entry C_0 and the bed can no longer adsorb. The dynamic response of the adsorption column was determined by the breakthrough time and the shape of the breakthrough curve. The breakthrough time (t_b) is the time taken when the outlet concentration reaches a specific concentration (50% of the initial concentration) (Radhakrishnan et al., 2016). The breakthrough curve is plotted as the concentration of pollutant (C_t/C_0) as a function of time. These characteristics describe the dynamic response and the efficiency of the adsorbent to bind metals (Thuong et al., 2019).

During the initial stage, the adsorbate inserted through the inlet of the column is adsorbed rapidly by the upper layer of the adsorbent. This is due to the availability of sites and the smaller levels of the adsorbate. The adsorbate continues its escape to the lower strata of the bed. In this case, the concentration of the outlet of the column is 0 and the ratio of $C/C_0=0$ ($t=t_p$). The upper layer of

the adsorbent is gradually saturated, after some time ($C_{s)}$, the column is completely saturated or exhausted, at this point $C/C_0=1$ ($t=t_s$) (Davila-Guzman et al., 2016).

A breakthrough curve indicates the temporal change of the outlet liquid concentration when the adsorption zone passes through the farthest point in the bed. Therefore, if the adsorption zone length does not change with time, the slope of the curve keeps constant even though the bed height increases. Generally, the shorter the adsorption zone length is, the steeper the slope of the break-through curve becomes.

1.9.1. Mass Transfer Zone

During the adsorption process, a large number of metal ions are concentrated on the surface of the adsorbent material, respectively at the interface between the two phases. The adsorption of the metal ions on the adsorbent is realized with maximum efficiency when: (i) the transport of the metal ions to the surface of the adsorbent can be realized by diffusion or dispersion; (ii) the metal ion transfer occurs at the level of the adsorbent interface; (iii) intraparticle diffusion takes place by moving the solution ions into the adsorbent pores. The performances of the adsorption process in the fixed-bed column are highlighted by the study of the breakthrough curves (Fig. 1.16), which means following the evolution of the ratio between the residual concentration of metal and its initial concentration (C/C_0) according to the time (Negrea et al., 2020).

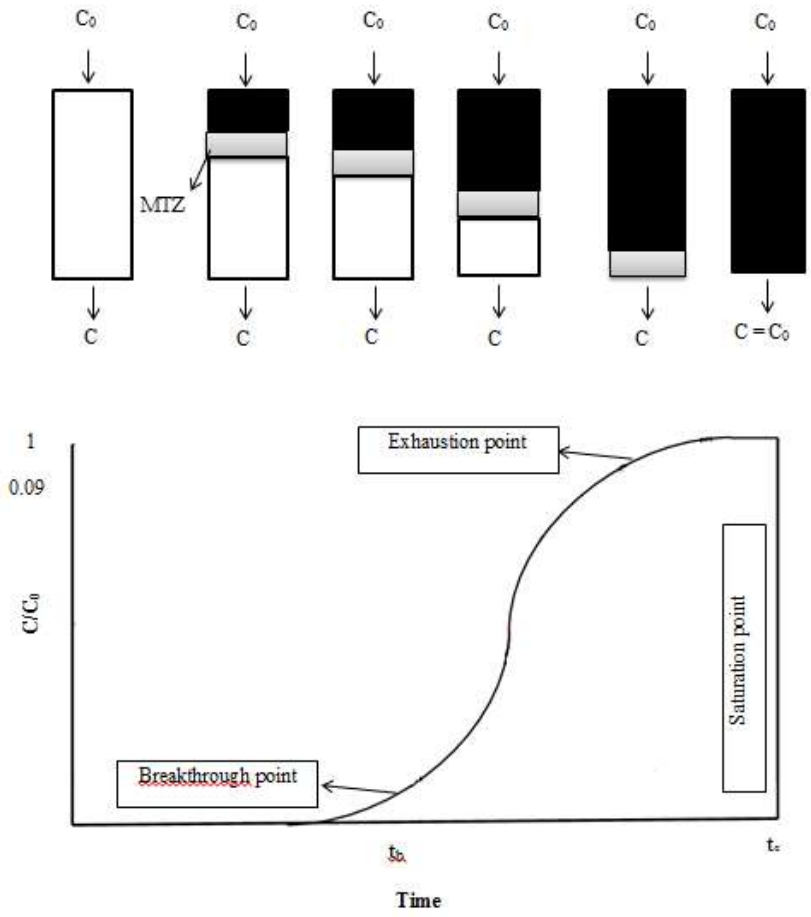

Figure 1.16. Scheme of a typical breakthrough curve in a fixed-bed adsorption process (Chowdhury et al., 2014).

1.9.2. Application of fixed-bed column on the removal of heavy metals

Due to higher industrialization development, industrial wastewater plays a deteriorating role on the environment through the discharge of heavy metals. Electroplating or metal finishing industries are the main activities responsible for the presence of heavy metals which cause various diseases. Furthermore, they consume and discharge large volumes of wastewater. These effluents contain Ni(II), Cu(II), Cr(VI), Zn(II), Pb(II), Ag(I), cyanide, hydrogen sulfides, ammonia, oil and grease, and suspended solids (Singh et al., 2016).

Researchers have investigated agricultural residues as an effective adsorbent to remove heavy metals from wastewater due to the presence of hydroxyl and carboxyl groups on their surface. As an example, (Kaur et al., 2013) focused on the filtration of the effluents discharged from the electroplating industries containing Ni, Cu and Cr using *Syzygium cumini* and *Populus deltoides* leaf powder as an adsorbent packed on a fixed-bed column.

Moreover, Martín-Lara et al., (2014) studied the capacity of olive stones as an adsorbent packed in a fixed-bed column, on the elimination of Cu, Cr and Ni from electroplating effluents. The performance of a fixed-bed column packed with encapsulation of *moringa oleifera* beads was studied by Radhakrishnan et al., (2016) in order to remove Zn(II), Cu(II), Mn(II), Co(II), and Ni(II) from electroplating wastewater.

1.9.3. Dynamic column models

In order to predict breakthrough curves and subsequently determine the parameters model, the experimental adsorption data obtained from the fixed-bed column was fitted with some known models (Thomas model, Adams-Bohart model and Yoon and Nelson model), which were used to analyze the column performance (Abbas et al., 2018).

1.9.3.1. Adams-Bohart model

This assumes that the adsorption rate is proportional to both the residual capacity of the adsorbent and the concentration of the adsorbing species. This model may be able to describe the initial part of the breakthrough curve by Eq. 1.10:

$$\ln(\frac{C_i}{C_t}) = K_{AB}C_0 t - K_{AB}N_0 \frac{Z}{F} \qquad (1.10)$$

C_i and C_t are the metal ion concentrations of influent and effluent respectively (mg L^{-1}), K_{AB} is the kinetic constant (L mg^{-1} min^{-1}), N_0 is the maximum volumetric sorption capacity of bed (mg L^{-1}), Z is the bed depth (cm), F is the linear velocity (cm min^{-1}).

1.9.3.2. Thomas model

This model determines the maximum adsorption capacity of the solute onto the adsorbent and the constant rate which is required in the column in the design of the fixed-bed column. The main assumptions of this model are; the kinetics of the adsorption-desorption follows Langmuir isotherm, the rate of driving force obeys second-order reversible reaction kinetics and the axial and radial dispersion in fixed-bed column are negligible (Abbas et al., 2018).

The Thomas model is given by the following equation (Eq. 1.11):

$$\ln(\frac{C_i}{C_t} - 1) = \frac{K_{Th} q_0 m}{F} - K_{Th} C_i t \qquad (1.11)$$

K_{Th} Thomas model constant (ml min^{-1} mg^{-1}), q_0 is the adsorption capacity (mg L^{-1}), m is the amount of adsorbent (g). q_0 and K_{Th} were determined by fitting the experimental data into linear regression analysis.

1.9.3.3. Yoon-Nelson model

This model assumes that the probability of the adsorption of metals decrease is related to both the probability of both adsorbate adsorption and adsorbate breakthrough on the adsorbent (Eq. 1.12). It applies to describe the practical industrial adsorption process.

$$\frac{C_t}{C_0} = \frac{1}{1+e^{(\tau - t).K_{YN}}} \qquad (1.12)$$

Where t is operating time (min), K_{YN} is the constant of proportionality of the Yoon-Nelson model (min^{-1}), τ is the time required to retain 50% of the initial adsorbate (min).

2. OBJECTIVES

Heavy metal pollution is a serious environmental problem and the toxicity and persistence of metal ions in water and soils makes their removal a particularly pressing concern. The main source of this pollution is the discharge of wastewaters from industries such as metal plating facilities, mining operations, fertilizer industries, and tanneries. Adsorption is widely used to remove heavy metal ions from industrial effluents due to its low cost, simplicity, short operation time, and for the capacity for the material to be reused. In the case of biosorption, additional advantages are the availability of these adsorbents and their eco-friendly nature. The toxic metals and metalloids of most concern include lead (Pb), copper (Cu), cadmium (Cd), chromium (Cr), nickel (Ni), and arsenic (As). This last can also be present in the environment as a result of geochemical processes. The main objective of this thesis is to evaluate the efficiency of different biosorbents and nanosorbents in removing Pb(II), Cu(II), Cd(II), Cr(VI), As(III), and As(V) from aqueous solutions by characterizing their corresponding adsorption processes. The adsorbents that will be evaluated are milled olive stones and pine cones, which are biosorbents that are widely available as agricultural waste in the Mediterranean region, and engineered adsorbents such as graphene-oxide and iron-trimesate metal organic frameworks, a nanomaterial that will be used for the adsorption of As(III) and As(V).

The specific objectives of this thesis are:

1) To characterize the physical and chemical properties of the different adsorbents that are evaluated and especially those affecting their performance in the adsorption process. Characterization includes the determination of the morphology, elemental composition of the adsorbent surface, point of zero charge, adsorbent stability, porosity, pore size, and surface area, and the identifcation of the functional groups.

2) To characterize the adsorption process of Pb (II), Cu (II), Cd (II) and Cr (VI) by olive stone and pine cone using single and multi-metal (Cd (II), Cu (II) and Pb (II)) aqueous solutions. Adsorption kinetics and isotherms will be investigated as well as the effect of pH, initial metal concentration, and the amount of sorbent on the adsorption efficiency of each biosorbent.

3) To evaluate the removal efficiency of toxic metal ions in dynamic conditions using a lab-scale fixed-bed column packed with the biosorbent that presented the best performance in batch experiments. First of all, the system will be applied to Pb(II) removal and the parameters affecting removal efficiency, such as inlet metal concentration, bed height and flow, will be studied. Thomas, Adams-Bohart and Yoon-Nelson models will be applied to characterize the system. Performance will also be evaluated with multi-metal solutions containing Pb(II), Cu(II), Cd(II)) and solutions simulating the composition of electroplating industry effluents composed of Cu(II), Ni(II) and Cr(VI) at pH 4.4.

4) To investigate the performance of four synthesized graphene-oxides on the adsorption of Cu(II), Cd(II) and Cr(VI) from aqueous solutions and the effect of the pH, amount of adsorbent and initial metal concentration on their adsorption capacity, study the adsorption isotherms, and compare the results obtained with the physico-chemical characteristics of each graphene oxide.

5) To evaluate the efficiency of two iron-trimesate metal organic frameworks, commercial Basolite F300 and synthesized Nano{Fe-BTC}, for As(III) and As(V) uptake from aqueous solutions. Adsorption kinetics and isotherms for arsenate and arsenite will be investigated as well as the effect of the pH, initial arsenic concentration, amount of Basolite F300, and the presence of other anions such as PO_4^{3-}.

3. METHODOLOGY

This chapter presents the materials and the methods used in the experimental studies carried out during the thesis whose main objective is to characterize the adsorption of toxic metal ions (Cu(II), Cd(II), Pb(II) and Cr(VI)) and metalloids (As(V) and As(III)) from aqueous effluents using biosorbents (olive stone, pine cone) and engineered adsorbents (graphene oxides and metal-organic framework materials: Basolite F®300) and Nano-{Fe-BTC} MOF).

3.1. Standards and Reagents

All the reagents used were of analytical grade. Stock individual solutions of 1000 $mg.L^{-1}$ of Cu(II), Cd(II), Pb(II), Cr(VI), As(V) and As(III) were prepared by adding appropriate amounts of $Cu(NO_3)_2 \cdot 3H_2O$, $Cd(NO_3)_2 \cdot 4H_2O$, $Pb(NO_3)_2$, K_2CrO_4, $Ni(NO_3)_2.6H_2O$, $NaAsO_2$ and $Na_2HAsO_4.7H_2O$ (Panreac, Barcelona, Spain) in doubly deionized water (MilliQ) obtained from a Millipore water purification system (18.2 $M\Omega\ cm^{-1}$, Millipore, Bedford, MA, USA). Intermediate and working metal solutions were prepared by dilution of the stock solutions with doubly deionized water (MilliQ). A COBOS precision ATX-224 balance was employed to weigh the amounts of the reagents as well as of the adsorbents.

Calibration solutions of different concentrations were prepared by dilution of a 1000 $mg\ L^{-1}$ standard solution (SPEX CertiPrep, United Kingdom and Merck Mollet del Vallès, Spain) of each individual metal. The pH of the working solutions was adjusted to the desired value by adding HNO_3 0.1 M and NaOH 0.1M (Panreac, Barcelona, Spain). NaOH (98%, Panreac, Barcelona, Spain) and 65% HNO_3 (Darmstadt, Germany) were used to prepare the solutions. The pH of the solutions was measured using a pH-meter Basic 20^+ (Crison Instruments, S.A., Allela, Barcelona, Spain). Before using this instrument, the pH-meter should be calibrated with two buffer solutions. The pH-meter was calibrated with standard buffer solution of pH 7.0 and pH 4.0.

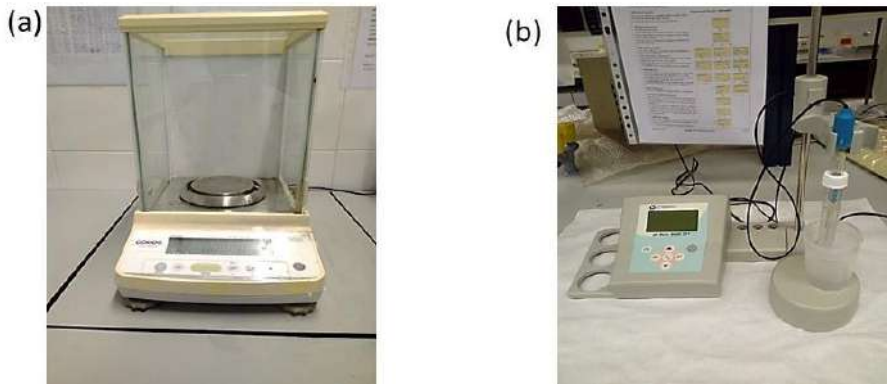

Figure 3.1. (a) Analytical balance COBOS precision ATX-224 and (b) pH-meter CRISON.

3.2. Adsorbents

3.2.1. Olive stone

The biomass used in this study consisted of milled olive stone which passed through a 1 mm sieve.

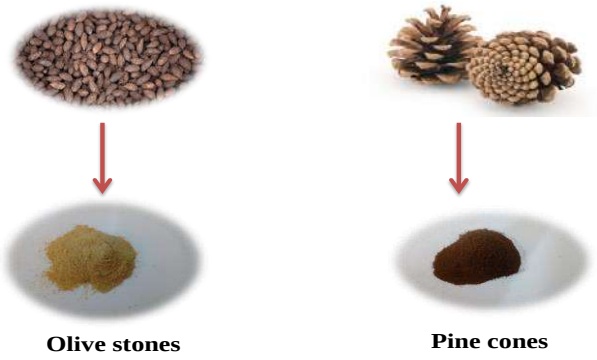

Figure 3.2. Biosorbents: milled olive stone and milled pine cone.

3.2.2. Pine cone

Pine cones were collected from a forest in Tunisia and were washed several times with distilled water and sun-dried for two days. The dried samples were then crushed using an electrical grinding machine to a powder and passed through a 1 mm sieve.

3.2.3. Graphene oxide

The graphene oxides studied in this project were provided by the Department of Chemistry of Masaryk University (Brno, Czech Republic). Four different graphene oxides were received and taken into study. Their references were 227A, 97D, GO-I and GO-II. The last two are of different types, type I is C_8O and type II is $C_{16}O$. The other two graphene oxides, 227 A and 97 D, were prepared by modification of GO-I and GO-II, respectively.

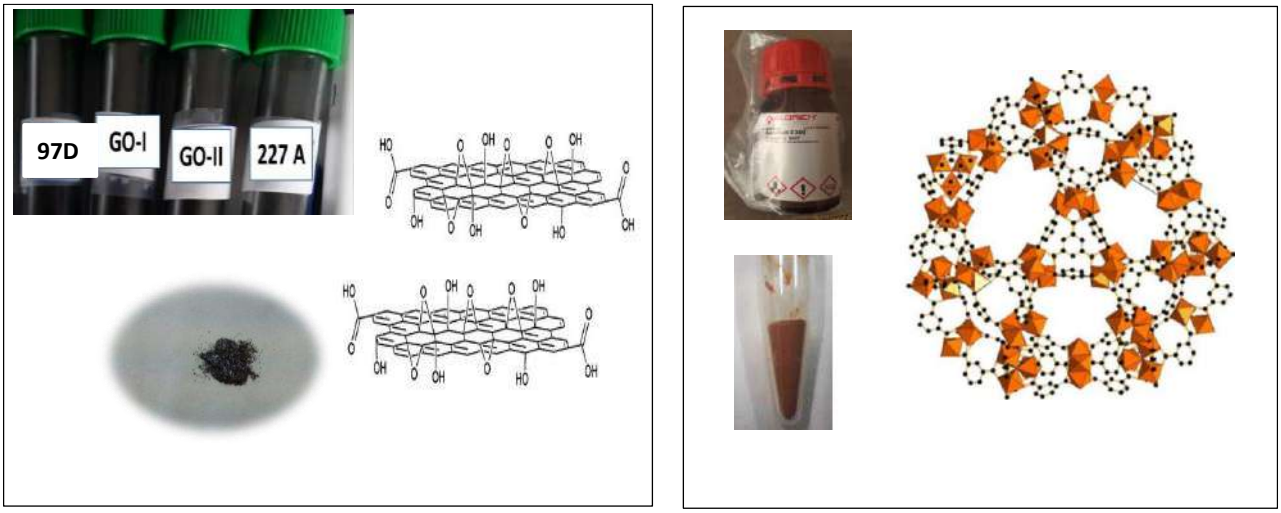

a) Graphene Oxides

b) Basolite F®300 and Fe-(1,3,5-tricarboxylic acid)

Figure 3.3. (a) Graphene oxides used in this study and structure of graphene oxide adapted from (Kharisov et al., 2016) and (b) Basolite F®300, Nano-{Fe-BTC} and structure adapted from (Dhakshinamoorthy et al., 2012).

3.2.4. Metal-organic frameworks: Basolite F300 and Fe-(1, 3, 5-tricarboxylic acid)

Basolite®F300 (Sigma-Aldrich Chemie GmbH, Steinheim, Germany) is a crystalline material composed of metal ions or clusters connected by organic linkers. It is a nanoporous metal-organic framework (MOF), that has a hybrid super tetrahedral build-up from oxo-centered trimmers of iron(III) octahedron that are connected by trimesate anions (Dhakshinamoorthy et al., 2012). Nano-{Fe-BTC} MOF material (BTC: 1,3,5-benzenetricarboxylate) was synthesized in the

Department of Chemistry of the University of La Laguna (Tenerife, Canary Islands, Spain). They had synthesized and characterized the Nano-{Fe-BTC} MOF (Conde-González et al., 2021).

3.3. Characterization of the adsorbents

The adsorbents were first characterized using a number of techniques including Fourier transform infrared spectroscopy (FTIR), scanning electron microscopy (SEM), Energy-dispersive X-ray spectroscopy (EDX), Brunauer-Emmet-Teller (BET) and Thermogravimetric analysis (TGA). The pH of the point of zero charge (pH_{pzc}) of each adsorbent was also determined.

3.3.1. Fourier transform infrared spectroscopy (FTIR)

The adsorbents are characterized for the reactive functional groups containing O, N, S, and P donor atoms and are capable of coordinating different metal ions. FTIR spectroscopy can be used to characterize the functional groups of adsorbents and to assess the interaction of these functional groups with the metal ions. FTIR analysis was performed using a Perkin-Elmer Paragon 2000 FTIR spectrometer, USA.

3.3.2. SEM

Scanning electron microscopy (SEM) images of the different adsorbents were obtained for the purpose of visualizing the topography of the adsorbent surfaces. A scanning electron microscope (Model ZEISS DSM- 960A) operating at 30 kV equipped with an energy-dispersive X-ray spectrometer Bruker Nano XFlash Detector 5010 (Fig. 3.4 (a)) was employed at the Technical Services of the University of Girona. The images were taken at different magnifications depending on the adsorbent and the EDX spectra allowed the determination of the elemental composition of the adsorbent surface.

3.3.3. BET surface area

The Brunauer–Emmett–Teller (BET) method uses a measurement of the physisorption of a gas to derive a value of “surface area” for a sample. The gas molecules can pass between particles and

into all pores, cracks, and surface roughness, so that the measurement probes the full microscopic surface area of the sample. The BET equation (Eq 3.1) describes the relationship between the number of gas molecules adsorbed (X) at a given relative pressure (P/P_0), where C is a second parameter related to the heat of adsorption. The BET equation strictly describes a linear plot of $1/[X(P_0/P)-1]$ vs. P/P_0 which for most solids, using nitrogen as the adsorbate, is restricted to a limited region of the adsorption isotherm, usually in the P/P_0 range of 0.05 to 0.35. The surface area, SA, is calculated from the slope and intercept of the line by using the BET equation surface area and porosimetry of the adsorbents. An ASAP 2020 (Micromeritics France S.A., Mérignac, France) instrument was employed to perform the measurements. The sample of GO-II was analysed by Dr. Rafel Prohens from the Polymorphism and Calorimetry Unit (Scientific and Technological Centers, University of Barcelona). Milled olive stone and milled pine cone were analyzed by J.Abderraouf from the Faculty of Sciences of Gafsa, University of Gafsa (Tunisia).

$$\frac{1}{X[(\frac{P_0}{P})-1]} = \frac{1}{X_m C} + \frac{C-1}{X_m C}\ (\frac{P}{P_0}) \qquad (3.1)$$

$$SA = \frac{1}{\text{Slope+intercept}} . CSA \qquad (3.2)$$

Where CSA is the cross-sectional area of the adsorbate (Thommes et al., 2015), X is the specific amount adsorbed at the relative pressure p/p_0 and X_m is the specific monolayer capacity.

3.3.4. Thermogravimetric analysis (TGA)

TGA measures the absolute amount and rate of change in weight of a sample as either functions of time or temperature in a controlled environment. TGA has a wide range of properties that can be measured such as thermal stability, oxidative stability, the effect of different atmospheres, moisture and volatile content, and sometimes the composition of multi-component systems. TGA determines if and how different components within a material are bonded differently. When TGA is coupled with DSC or differential thermal analysis (DTA), the mode of analysis is called simultaneous DSC-TGA (or DTA) (SDT). SDT measures the amount and rate of change in

weight, but also measures the heat flow of the sample as a conventional DSC does. Thermogravimetric analysis was performed to characterize the thermal stability of the adsorbents as well as moisture and volatile content. A METTLER TOLEDO TGA/DSC 1 from the Technical Services of the University of Girona was used to perform TGA and DTA analyses of the adsorbents (Fig. 3.4 (b)).

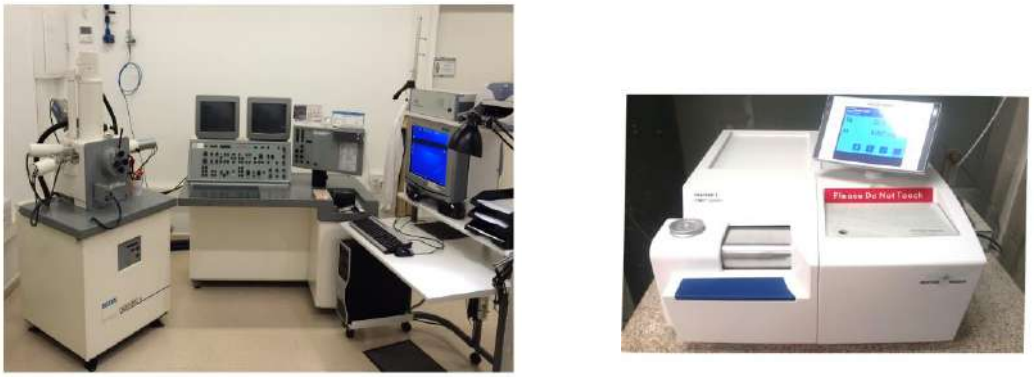

a) Scanning electron microscope b) TGA and DTA instrument

Figure 3.4. (a) Scanning electron microscope ZEISS DSM- 960A and (b) METTLER TOLEDO TGA/DSC instrument.

3.3.5. pH of the point of zero charge (pH_{pzc})

The point of zero charge is the pH at which the surface of one adsorbent is globally neutral, i.e., contains as many positively charged as negatively charged functional groups in the adsorbent surface. Below this value, the surface is positively charged; beyond this value, it is negatively charged. Normally, it is easier to adsorb a cation on a negatively charged surface, and an anion on a positively charged surface. The adsorption mechanism is not always an electrostatic interaction between the adsorbate and the adsorbent; we use the pH of zero point charge (pH_{pzc}) to explain whether the adsorption mechanism is electrostatic or follows another mechanism. This is also an important parameter that helps understand the effect of pH on the adsorption process. There are several methods to determine the pH_{pzc}: (1) the pH drifts method, measuring pH where the adsorbent behaves as neutral species; (2) potentiometric titration, measuring the adsorption of H^+ and OH^- on surfaces in solutions of varying ionic strengths; and (3) direct assessment of the surface charge via nonspecific ion adsorption as a function of pH (Khan and Sarwar, 2007). We

selected the pH drift method, adding 1 g of the biosorbent to 100 mL of distilled water and varying the pH from 3 to 11, stirring for 2 hours. The initial pH was adjusted by adding either HCl (0.1M) or NaOH (0.1M). The final pH of the solution was measured and the $\Delta pH = pH_f - pH_i$ plotted against the pH of the initial solution (Fig. 3.5).

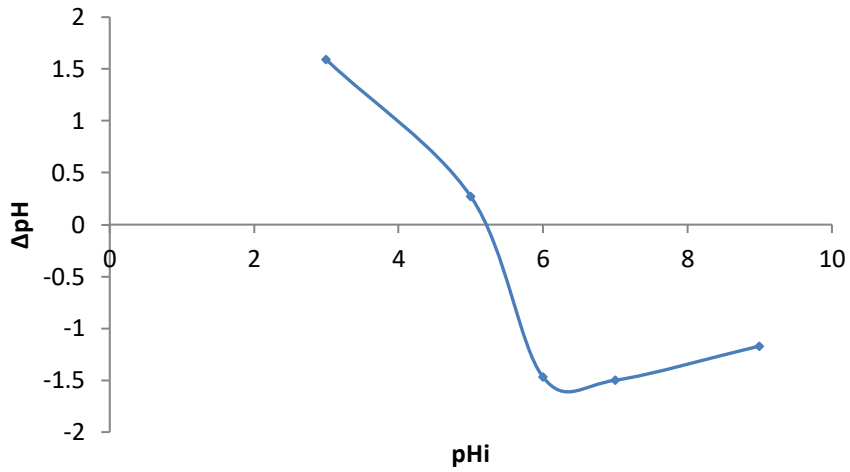

Figure 3.5. Determination of pH_{pzc} of olive stone.

3.4. Experimental procedures

3.4.1. Batch adsorption experiments

Batch experiments were performed with each sorbent and metal ion in order to characterize the adsorption process under controlled conditions and varying the contact time, the amount of adsorbent, the pH of the solution and the initial metal concentration. Adsorption experiments using multi-metal solutions were also performed to study metal competitively towards the adsorbent. The experiments were carried out at a constant room temperature of 22±1ºC. In all sets of experiments, amounts of the selected adsorbent were accurately weighted in 25 mL glass extraction tubes, and 20 mL of the corresponding metal solution was added.

The system was shaken on a rotary mixer (DINKO Instruments Barcelona) at 50 rpm until equilibrium was achieved. After that, the two phases were separated by decantation followed by

filtration. The metal concentration in the remaining aqueous solutions was determined by ICP-AES.

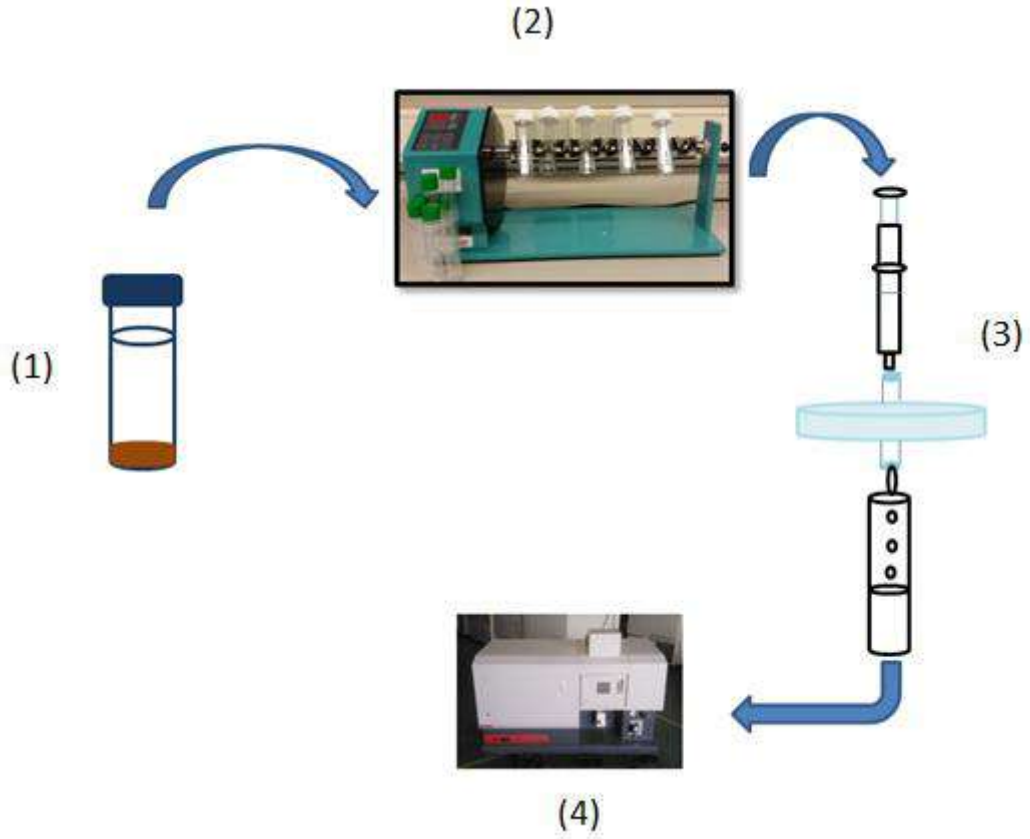

Figure 3.6. Schematic operational process of batch adsorption experiments. 1) Weigthed adsorbent and aqueous solution, 2) Agitation in a rotatory mixer, 3) Filtration and 4) analysis by ICP-AES.

The sorption efficiency in each experiment was calculated as the removal percentage of metal ions by using the following equation:

$$\%= \frac{C_i - C_{eq}}{C_i} * 100 \qquad (3.3)$$

where C_i and C_{eq} (mg L^{-1}) are the liquid-phase concentrations of the target at the initial and equilibrium times, respectively.

The amount of adsorbed compound at the equilibrium, q_e (mg g^{-1}), was calculated by:

$$qe = \frac{(Ci - Ceq) \cdot V}{W} \qquad (3.4)$$

Where V (L) is the volume of the solution, and W (g) is the mass of dry adsorbent used.

3.4.2. Inductively coupled plasma emission spectrometry (ICP-AES)

ICP-AES is an elemental analysis technique that uses the emission spectra of a sample to identify and quantify the elements present. Samples are introduced into the plasma in a process that desolvates, ionizes, and excites them. The constituent elements can be identified by their characteristic emission lines and quantified by the intensity of the same lines. Two ICP-AES instruments a Varian, Liberty series, Australia and an Agilent 4200 MP-AES, USA were used for the quantitation of the metals and metalloid in the aqueous solutions. The initial metal concentrations and the remaining metal concentrations in liquid solution after equilibrium was attained were determined by ICP-AES. Calibration curves were built by analyzing six individual metal standard solutions prepared in the same pH and matrix media of the experimental solutions by dilution of 1000 mg L^{-1} standard solutions of each metal.

Figure 3.7. ICP-AES instrument (Agilent 4200 MP-AES).

Table 3.1. Conditions of ICP-AES analyses.

Nebulizer flow (L min^{-1})	0.7
Plasma flow (L min^{-1})	12
Aux flow(L min^{-1})	1

The wavelengths used to analyze the different metals are shown in the table below:

Table 3.2. Analytical wavelengths, detection and quantification limits, correlation coefficients and correlation equations of the calibration curves for the determination of metals.

Metal	**Wavelength (nm)**	**Detection limit (mg L^{-1})**	**Quantification limit**	**Correlation coefficient**	**Calibration curve**
Cr	428	0.047	0.14	0.999	y=12707x+ 5150.6
Cu	324	0.037	0.113	0.999	y=1133.9x+ 70.11
Cd	228	0.018	0.057	0.999	y=5708.1x+ 125
Pb	217	0.095	0.288	0.999	y=38.248x+ 8.623
Ni	305	0.067	0.205	0.999	y=311.74x+ 261.57
As	188	0.055	0.167	0.999	y=43.347x+ 0.947
Ca	393	0.043	0.117	0.999	y=2896.3x+ 1286

3.4.3. Biosorption of heavy metals by milled olive stone

The equilibrium time was studied by adding 100 mg of olive stone per 20 mL of metal solution with an initial concentration of 5 mg L^{-1} at pH 6. In order to determine the optimum pH of metal solution, 100 mg of adsorbent was added to a 5 mg L^{-1} solution at different pHs (2, 3 and 6).

Different adsorbent quantities (40, 80, 100, 120, 150, 200, 250 and 300 mg) were tested by adding each amount to 20 mL of a 5 mg L^{-1} metal solution at pH 6 and shaking them for 1 hour in the case of Cd(II), Cu(II) and Pb(II), and for 2 hours for Cr(VI) at pH 2.

Separate tests with initial Cd(II), Cu(II) and Pb(II) concentrations of 1, 2, 5 and 10 mg L^{-1} were performed by adding 80 mg of adsorbent to 20 mL of each solution for 1 hour. In the case of Cr(VI), 200 mg was used and the period of time was 2 hours. Competition experiments were then performed using 100 mg of adsorbent and 20 mL of metal solution containing 5 mg L^{-1} of each metal (Cu, Cd and Pb) at pH 6 for 1 hour.

3.4.4. Biosorption of heavy metals by pine cone

The equilibrium time was studied by adding 40 mg of milled pine cone to 20 mL of metal solution with an initial metal concentration of 5 mg L^{-1} at pH 5.4.

The effect of the amount of adsorbent was studied by using different concentrations ranging from 1 g L^{-1} to 10 g L^{-1} with an initial metal concentration of 5 mg L^{-1} at pH 5.5 for Pb(II), Cu(II) and Cd(II), except for Cr(VI), which was at pH 2.

Separate tests with initial Cd(II), Cu(II), Cr(VI) and Pb(II) concentrations ranging from 1 to 500 mg L^{-1} were performed by adding 40 mg of adsorbent to 20 mL of each solution for 2 hours.

The effect of pH on the metal adsorption was evaluated by adding 40 mg of adsorbent to 20 mL of a 5 mg L^{-1} solution at different pHs (2, 5.5 and 9), adjusted by adding HNO_3 0.1M and NaOH 0.1M (Panreac, Barcelona, Spain). The pH of the solution was measured before and after adsorption.

Competition experiments between Cd(II), Cu(II) and Pb(II) were then performed using 40 mg of adsorbent and 20 mL of metal solution containing 5 mg L^{-1} of each metal at pH 5.5 for 2 hours. All experiments were performed in triplicate at room temperature.

3.4.5. Adsorption of heavy metals by Graphene Oxide materials

The equilibrium time was determined by adding 40 mg of adsorbent 97D per 20 mL of the solution of Cu(II) and Cd(II). In the case of Cr(VI), the amount of adsorbent GO-I was 200 mg for 20 mL of solution. In all the cases, the initial concentration of metal was 5 mg L^{-1}.

To determine the optimum pH of metal solution, experiments were carried out in solutions of different pH (2, 4 and 6). In the case of Cu(II) and Cd(II), the graphene oxide used was 97D, while for Cr(VI) the adsorbent used was GO-I.

Different amounts of adsorbent (1, 2 and 3 g L^{-1}) were studied by adding an appropriate quantity (97D) to be tested to 20 mL of a metal solution of 5 mg L^{-1} of Cu(II) and Cd(II) at pH 6, in the case of Cr(VI), GO-I was used as the adsorbent.
Separate tests at different initial metal concentrations (5, 7.5 and 10 mg L^{-1}) were performed by adding 40 mg of graphene 97D to 20 mL of single-metal solutions of Cu(II) and Cd(II), and 200 mg of graphene GO-I to Cr(VI) solutions of the same concentrations.
Competitive experiments were only performed for ions Cu(II) and Cd(II) using 40 mg of the adsorbent (97D) and 20 mL of metal solution containing 5 mg L^{-1} of each metal at pH 6.

3.4.6. Adsorption of As(III) and As(V) by Basolite F300 and synthesized Fe-(1, 3, 5-tricarboxylic acid) metal-organic framework

The kinetics of the adsorption was evaluated to determine the time needed to reach the equilibrium. The time effect was studied by varying the contact time from 2 min to 120 min using 0.1 g L^{-1} of adsorbent in solution with concentration 10 mg L^{-1} at pH 7 for As(V) and pH 11 for As(III).
The pH effect on the adsorption of these metals was studied by adjusting the pH from 2 to 11 and maintaining the other parameters constant (C_i=5 mg L^{-1}, 0.5 g L^{-1} and t=1h). The amount of adsorbent effect was also studied to determine the quantity needed to adsorb these metals from aqueous solutions using 5 mg L^{-1} at pH 7 for As(V) and pH 11 for As(III) agitating in 1 hour of contact time.

The isotherm adsorption was investigated by changing the initial concentration from 0.5 to 10 mg L^{-1} to study the effect of the concentration on the removal of arsenic. The amount of adsorbent used was 0.1 g L^{-1} for As(III) at pH 11 and 0.5 g L^{-1} for As(V) at pH 7 in 1 hour. Competitive adsorption was investigated to study the effect of PO_4^{3-} on the removal of arsenite and arsenate, experiments were carried out at pH 7 for As(V), pH 11 for As(III) using 0.1 g L^{-1} of

adsorbent in initial concentration of arsenic of 10 mg L^{-1} and various concentrations of PO_4^{3-} (10, 100 and 300 mg L^{-1}).

Adsorption experiments of As(III) and As(V) were evaluated to study the efficiency of Fe-(1, 3, 5-tricarboxylic acid) in comparison with Basolite F300, at pH 11 and pH 7 respectively, using 0.5 g L^{-1} of adsorbent in initial concentration 5 mg L^{-1}.

3.5. Fixed-bed column experiments

Adsorption experiments were also performed in a fixed-bed column in order to evaluate the efficiency of pine cone in the separation and removal of Cd(II), Cu(II), and Pb(II) in dynamic conditions. The applicability of pine cone in the treatment of industrial effluents was assessed using an aqueous solution simulating electroplating industry effluent. A lab-scale glass column (12 mm diameter and 200 mm length) with a fritted glass at the bottom was packed with pine cone up to a pre-established height corresponding to a known amount of adsorbent that was accurately weighed. The metal solutions at pH 5.6 were passed through the column at a constant flow controlled and impulsed by a peristaltic pump (Minipuls 3, Gilson Incorporated, Middleton, WI, USA). Samples of metal solution were collected at prefixed times until the concentration of the exit C_t is equal to that of the entry C_i and the bed can no longer adsorb (saturation). The initial metal concentration and metal concentrations in the collected samples were determined by ICP-AES (Agilent 4200 MP-AES). The amounts of metal adsorbed at the different prefixed times were calculated by the difference between the initial concentration of the metal and the concentration in the sample collected at the same prefixed time. The dynamic response of the adsorption column is determined by the breakthrough time (t_b), corresponding to the moment at which the metal concentration of adsorbate reaches 10% of the feed concentration (C_t/C_i=0.1), and the shape of the breakthrough curve. Whereas, the time at which the saturation occurs is called the exhaustion time (t_s), which is set when the effluent concentration exceeds a value between 90% and 95% of the initial concentration (Vera et al., 2019).

Different initial metal concentrations (20, 50, 75, 100 mg L^{-1}) and bed heights (0.5, 0.7, 1 cm) were used at a flow of 2.2 mL min^{-1}. The effect of the flow rate in the adsorption process was studied at different flow rates: 1.4, 2.2, and 3.1 mL min^{-1}.

The competitive adsorption between Cd(II), Cu(II) and Pb(II) was studied by filling the column with 330 mg of milled pine cone, corresponding to a bed height of 1 cm. Solutions of these three metals having different initial concentrations of each individual metal (25 mg L^{-1}, 50 mg L^{-1} and 100 mg L^{-1}) were passed through the column at a flow rate of 2.2 mL min^{-1}.

The multi-metal samples were collected at regular time intervals from the outlet of the column and the metal concentrations of the effluent were determined by ICP-AES.

A synthetic electroplating wastewater was prepared using Cu(II), Ni(II) and Cr(VI) with an initial metal concentration of 20 mg L^{-1}, 30 mg L^{-1} and 100 mg L^{-1} respectively. The multi-metal solution passed through the column, which was filled to 2 cm, corresponding to 650 mg of adsorbent (milled pine cone) and 2.2 mL min^{-1} of inlet flow rate.

In order to recover metals, column desorption experiments were performed to desorb Cu(II), Cr(VI) and Ni(II) retained onto the adsorbent using 0.5M HCl as an eluting agent.

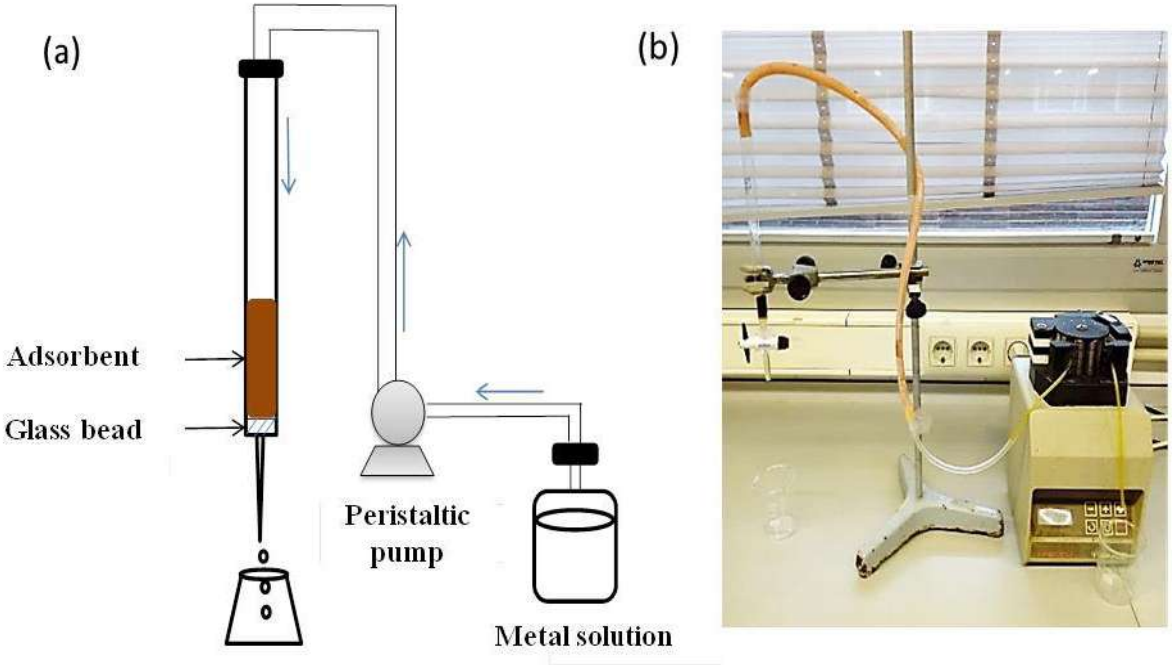

Figure 3.8. Fixed-bed column set-up (a) scheme and (b) picture of the experimental set-up.

4. RESULTS AND DISCUSSION

The capacity of different adsorbents to remove heavy metals has been investigated in this thesis. Lignocellulosic materials such as milled olive stone and milled pine cone, containing hydroxyl and carboxyl functional groups, have been evaluated as biosorbents as well as engineered adsorbents such as graphene oxides and metal organic frameworks such as Basolite F300. This last adsorbent was investigated for its capacity to adsorb As(V) and As(III).

The adsorption processes have been investigated by performing batch experiments in order to characterize adsorption equilibrium and in dynamic conditions. A fixed bed column filled with a biosorbent was tested to study the separation of different metals ions from a solution simulating the effluent of an electroplating industry at laboratory-scale. The characterization of the separation process in the fixed-bed column will allow this method to be applied at large scale wastewater treatment. This chapter is divided into five sections; each of them is dedicated to evaluate one of the adsorbents for metal removal.

The first section presents the removal of Cd(II), Cu(II), Pb(II) and Cr(VI) by milled olive stone. The second section deals with the removal of the same metals by milled pine cone. The third section is focused on separation of trivalent cations such as Cd(II), Cu(II), and Pb(II) in a lab-scale fixed-bed column filled with milled pine cone. The last two sections are dedicated to characterize and evaluate the adsorption capacities of engineered adsorbents such as graphene oxides and a metal organic framework. In the fourth section, four graphene oxides have been investigated for the adsorption of Cd(II), Cu(II), Pb(II), and Cr(VI) and the fifth and final section describes the capacity of Basolite F300 and Nano-{Fe-BTC} MOF to adsorb arsenite and arsenate anions and the effect of different parameters, such as pH, amount of adsorbent, initial adsorbate concentration and contact time, on their removal.

4.1. Adsorption of Cd(II), Pb(II), Cu(II) and Cr(VI) by milled olive stone

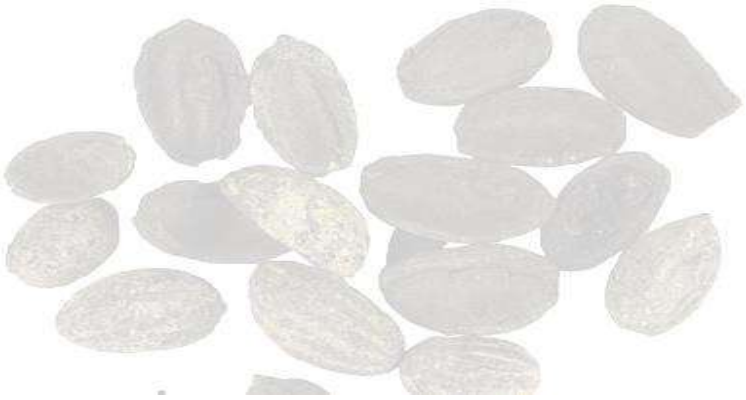

Biosorption is a physico-chemical adsorption process based on the use of dead biomass to accumulate target pollutants through different mechanisms, such as complexation, chelation, ion exchange, inorganic micro precipitation, and hydrolysis of metal ions (Pintor et al., 2012). In the search for highly efficient, eco-friendly and economic adsorbents, agricultural residues such as fava beans (Etorki et al., 2014), bark (Şen et al., 2015), maize stalk (El-Sayed et al., 2011), date stones (Abudaia et al., 2013), bone charcoal (Ghrab et al., 2017), rice straw (Brahmaiah et al., 2015), cork (Sfaksi et al., 2014), olive stones (Martín-Lara et al., 2016), pomegranate seeds (Ghaneian et al., 2017), coffee waste (Kyzas et al., 2013), and saxaul tree ash (Sanchooli Moghaddam et al., 2016) have been evaluated as biosorbents to efficiently eliminate heavy metals. Agricultural and forest waste adsorbents have been used to remove Pb(II) ions in wastewater treatments (Saka et al., 2012). 98% removals of lead were achieved using apple pomace with a maximum uptake of 16.14 mg g^{-1} (Chand and Pakade 2013), and 99% removals of chromium (VI) at pH 2 and an initial concentration of 250 mg L^{-1} were obtained with eucalyptus bark with maximum uptake of 45 mg g^{-1} (Sarin and Pant, 2006). Coconut shell was able to remove 4.72 mg g^{-1} of Pb(II), 2.92 mg $g^{-1}$of Cu(II), 4.57 mg g^{-1} of Cd(II), and 2.02 mg g^{-1} of As(V) from a 5 mg L^{-1} aqueous solution (Okafor et al., 2012). Furthermore, other researchers have studied the removal of some heavy metals by milled olive stone. The maximum uptake of Pb(II) by milled olive stone was 6.57 mg g^{-1} at pH 6 and 10 mg L^{-1} (Hernáinz et al., 2008) and 43.46% of Cu(II) of an initial concentration of 10 mg L^{-1} at pH 5 was eliminated by the same sorbent (maximum uptake of 1.96 mg g^{-1}) (Blázquez et al., 2011). Olive-stone in packed-bed columns has been successfully applied in the removal of heavy metals from electroplating wastewaters containing Cr(VI), Cu(II) and Ni(II) (Martín-Lara et al., 2014). In the case of Cr(VI), the biosorption process is greatly pH-dependent and in the sorption process two phenomena (biosorption and reduction) should be considered (Martín-Lara et al., 2016).

In this study, milled olive stone, which can be easily produced from abundant and inexpensive agricultural waste in many Mediterranean countries, are evaluated as potential biosorbents due to their high adsorption capacity, which is related to the different functional groups on their surface, including carboxylate, hydroxyl, amine, amide and phosphate (Budinova et al., 2006).

The aim of this study is to investigate the capacity of milled olive stones to remove heavy metal from aqueous solution, to study the kinetics of the adsorption processes for Cd(II), Pb(II), Cu(II) and Cr (VI) and to characterize these processes by applying isotherm adsorption models. Moreover, the effect of the pH, the competition between metals, and the amount of adsorbent on the removal process were also studied.

4.1.1. Milled olive stone characterization

The characterization of the biosorbent is important to understand, explain its behavior during the sorption process and the mechanism of the metal removal. Among these characterizations FTIR, SEM, elemental analysis, BET surface area and pH_{pzc}.

Fourier transform infrared spectroscopy (FTIR) spectra were recorded in the range of 600 cm^{-1} to 4000 cm^{-1} to identify the chemical groups present in the milled olive stones. Moreover, FTIR spectra were also recorded after performing metal biosorption. As can be seen in Figure 4.1, the broad band that appeared at 3364 cm^{-1} is characteristic of the stretching vibration of the hydroxyl group, which is due to hydrogen bonding O–H to a carboxyl, phenol or alcohol group. The peak observed at 1727 cm^{-1} may correspond to the stretching vibration of the carbonyl C–O or the aromatic C–C. The peaks around 1239 cm^{-1} and 1031 cm^{-1} show stretching vibrations of the C–O group in the carboxylic and alcoholic groups. Other bands observed at 899 cm^{-1} are attributed to inorganic groups or stretching vibrations of C–C. These peaks and bands proved the presence of the hydroxyl group and the carboxylic groups of the lignin, cellulose and hemicellulose in the biosorbent, which are responsible for the metal adsorption. The results are similar to those obtained by other researchers (Ronda et al., 2014). The results of the adsorbent before and after biosorption were compared, as can be seen there are significant changes in some bands, 3364 cm^{-1}, 2907 cm^{-1} and 1727 cm^{-1} and 1031 cm^{-1}. These bands shifts indicated that the hydroxyl group and carboxyl group are involved in the adsorption of the metals.

The SEM images (Fig. 4.2) show irregularly shaped milled olive stone particles with an average diameter of 30.67 μm (Fig. 4.2 1000 ×), which favor the biosorption of heavy metals ions. The BET surface area, which is related to the adsorption capacity of adsorbent, is 0.1956 $m^2\ g^{-1}$, whereas the Langmuir surface area is 0.2341 $m^2\ g^{-1}$. These values are similar than those reported by other authors (Martín-Lara et al., 2016). The pH at the point of the zero charge (pH_{pzc}) of

milled olive stone is 5.3. Above this pH, the surface charge becomes negative facilitating the interaction with the metal cations.

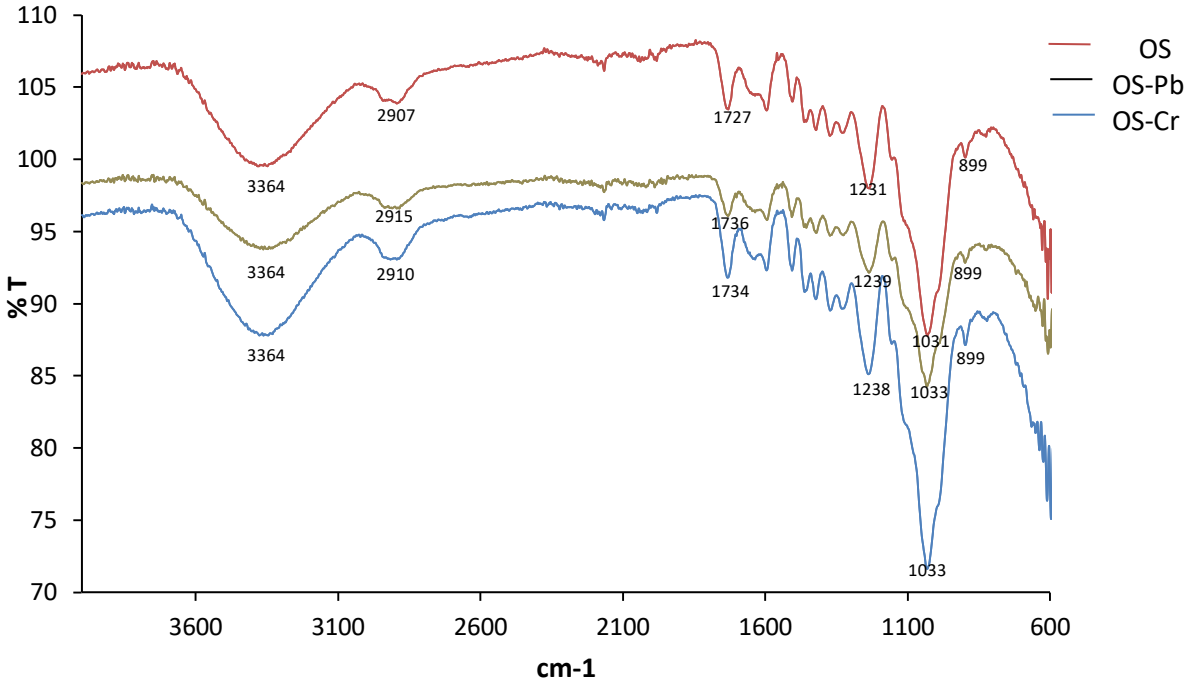

Figure 4.1. FTIR spectra of milled olive stone (OS), OS after lead biosorption (OS-Pb) and OS after chromium biosorption (OS-Cr).

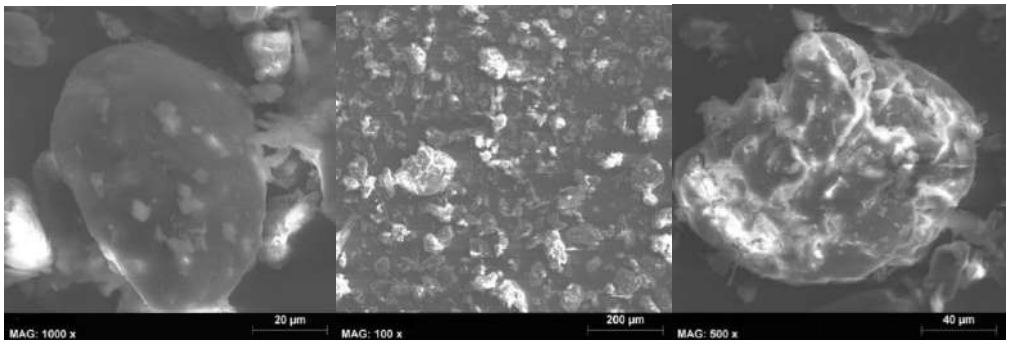

Figure 4.2. SEM images of milled olive stone at different magnifications (100, 500, and 1,000×).

4.1.2. Batch adsorption

4.1.2.1. Equilibrium Time

The percentage of copper, cadmium, lead and chromium adsorbed over time is shown in Figure 4.3. Maximum removal percentages for Cd(II), Cu(II), and Pb(II) of 22.6%, 40%, and 75.2%, respectively, are achieved in just 1 hour in the experimental conditions tested (C_i= 5 mg L^{-1}) at pH 6 and 5 g L^{-1} of adsorbent. This good performance is explained by the high number of sites that are initially available to receive metal ions. In the case of Cr(VI), equilibrium is reached after 2 hours and the maximum sorption percentage is 39% at pH 2.

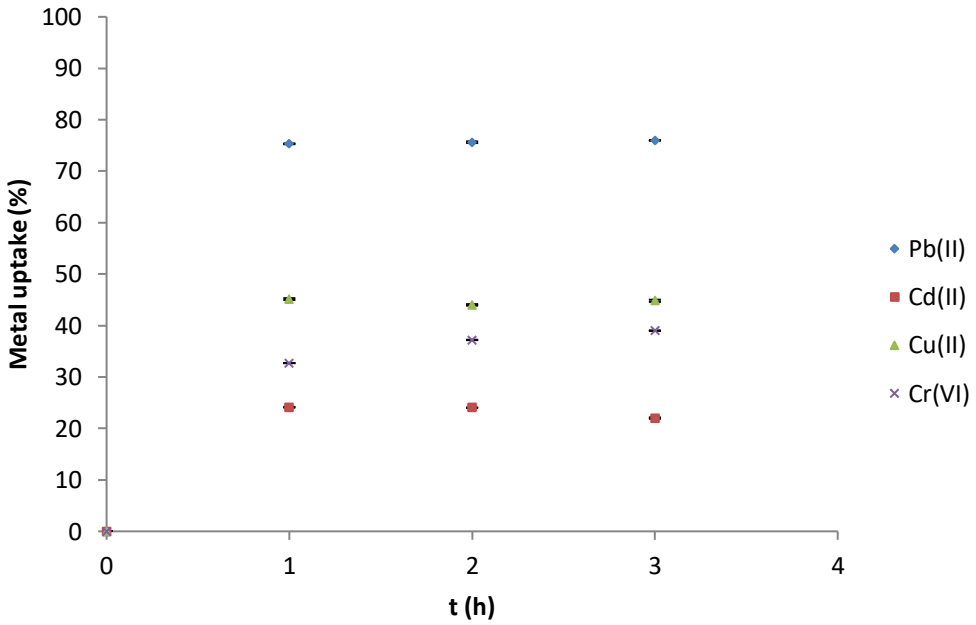

Figure 4.3. Effect of the contact time on the removal of Pb (II), Cd (II), Cu (II) and Cr (VI). $[C]_i$= 5 mg L^{-1} at pH= 6, except for Cr (VI) (pH 2), adsorbent concentration of 5 g L^{-1} (n=3).

4.1.2.2. Effect of pH

The pH is an important parameter that influences the removal of heavy metal by milled olive stone since it affects metal speciation and the charge of the adsorbent surface, given that the

functional groups can be protonated depending on the pH of the solution. As can be seen in Figure 4.4, the percentages of sorption increased for the three divalent metals when the pH increased from 2 to 6. These results can be explained by the decrease in the number of H^+ in the

media, which resulted in less competition with the metal ions for the available sites on the sorbent surface. Hence, at pH < pH_{pzc}= 5.3 the competition of H^+ for the sorbent sites is high. However,

at pH > pH_{pzc} metal sorption is more favorable given that the surface becomes negatively charged and the metals ions are retained better.

In the case of chromium, the sorption percentage decreases from 37 to 18% as the pH is increased from 2 to 6. These results can be explained by the fact that at low pH, $HCrO_4^-$ is the predominant species and the sorbent surface is protonated. The increase in the pH led to a reduction in the surface protonation and, at pH > 5.3, the surface is negatively charged, causing a decrease in the interaction between negatively charged species as CrO_4^{2-} and the adsorbent (Blázquez et al., 2009). Several authors (Martín-Lara et al., 2016; Mishra et al., 2015) have reported a reduction of Cr(VI) to Cr(III) at acidic pHs when biosorbents such as milled olive stone and rice straw were used at acidic conditions. According to Nakano et al., (2001), a large amount of protons are consumed in the reduction of Cr(VI) by the carbon present in the biosorbent, resulting in an increase of the pH of the metal solution. To verify this fact, the pH of 5 mg L^{-1} Cr(VI) solution, that was in contact with 10 g L^{-1} of milled olive stone, was measured after 2 hours (equilibrium time) resulting in a decrease of 0.23 units of the pH after metal adsorption showing that in our experimental conditions Cr(VI) was not reduced to Cr(III). In the case of the other metal ions, Pb(II), Cd(II) and Cu(II), the pH variation before and after biosorption was of 0.1 units when initial metal concentrations of 5 mg L^{-1} at pH 6 were used. At this pH > 5.3, we assumed that most of the functional groups of the biosorbent are negatively charged and that biosorption is taking place through electrostatic interactions rather than by the exchange of the H^+ of the functional groups by the metal ions.

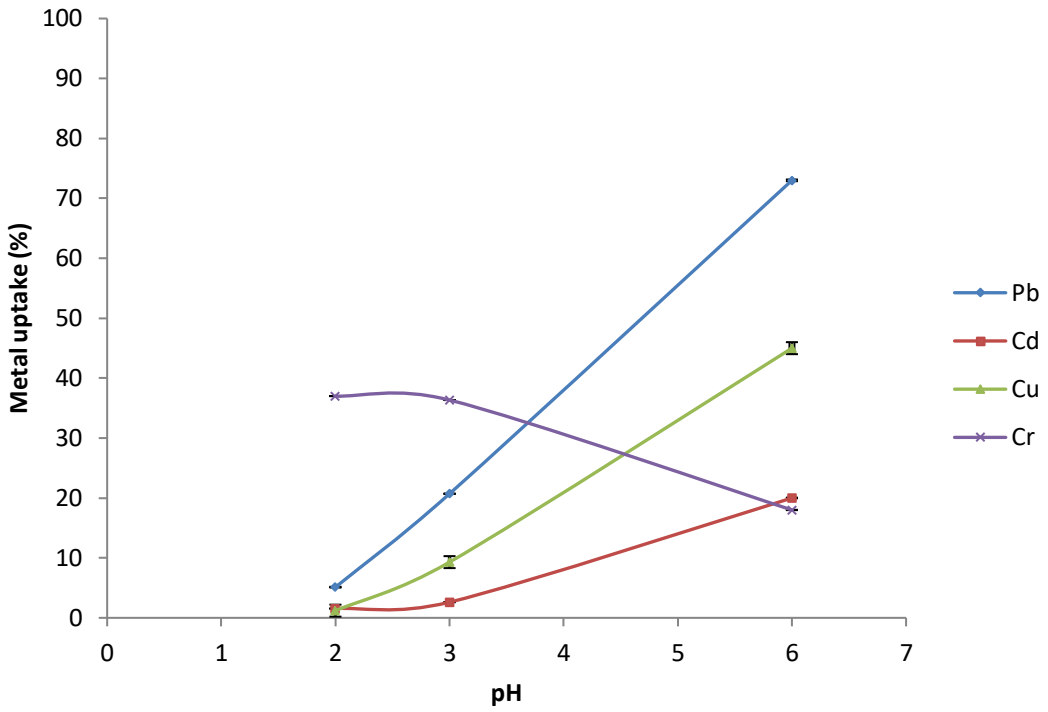

Figure 4.4. Effect of the pH on the removal of Pb(II), Cd(II), Cu(II) and Cr(VI). $[C]_i$= 5 mg L^{-1}, adsorbent concentration of 5 g L^{-1}, 1 h of contact time, except for Cr(VI) (2 h) (n=3).

4.1.2.3. The Effect of the Adsorbent Concentration

The percentage of metal ions adsorbed by milled olive stone depends on the amount of sorbent as well as the initial metal concentration and the pH of the solution.

The removal percentages of cadmium, copper and lead increased to 22.4%, 45.8% and 74.5%, respectively, as the amount of adsorbent was raised from 2 to 6 g L^{-1}, before rapidly falling off on further increasing the amount of sorbent (Fig. 4.5). This fact is explained by the aggregation of the biosorbent particles, avoiding the interaction of the metals with the surface sites, when more than 6 g L^{-1} of adsorbent solution was used. As can be seen in Figure 4.5, the sorption percentage for the three metals was the same with 7.5 g L^{-1} at pH 6, showing that at these conditions, there are fewer available sites and that metal sorption at these conditions occurred through unspecific interactions. However, in the case of Cr(VI), the removal percentage increased significantly up to 4 g L^{-1} before continuing with a much slower but constant rise up to 15 g L^{-1}, finally reaching 46.84%. (Martín-Lara et al., 2016) obtained higher removal rates of 96.38% for Cr(VI) using 10

g L^{-1} of adsorbent and an initial concentration of 10 mg L^{-1} of Cr(VI) at pH 2. Moreover, they found that Cr(VI) was reduced to Cr(III) by the adsorbent at low pHs and the removal process of Cr(VI) was reported to involve two processes: biosorption and reduction. Taking into account that in this study the sorption of Cr(VI) decreased until 18% when the pH increased from 2 to 6, we consider that Cr(VI) biosorption occurred only through an ion-exchange mechanism.

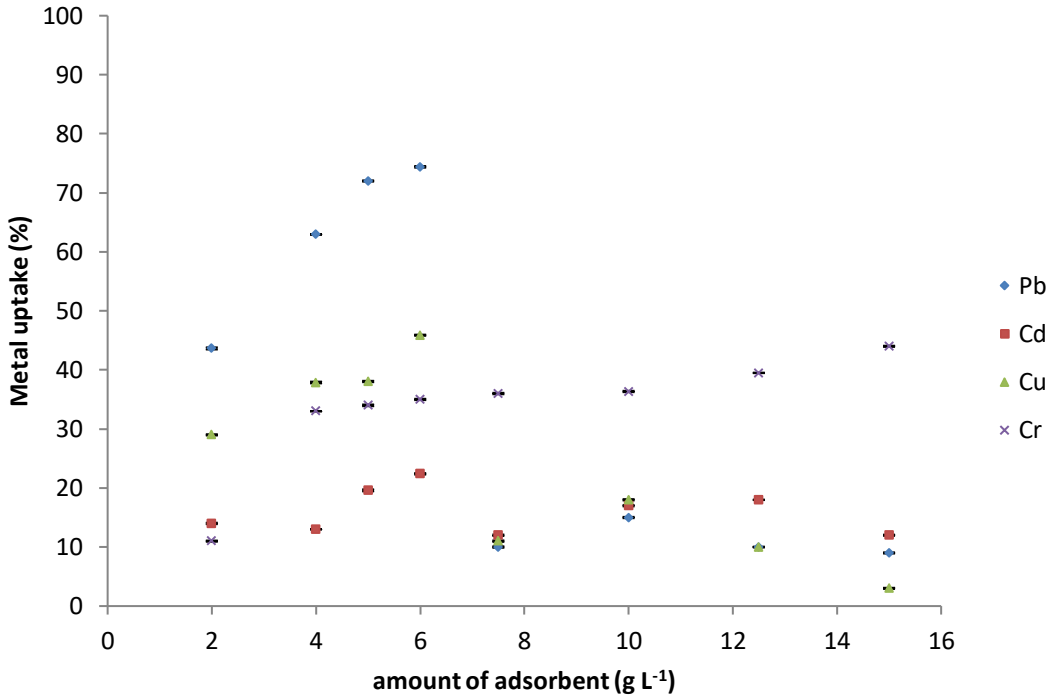

Figure 4.5. Effect of the adsorbent concentration on the removal of Pb(II), Cd(II), Cu(II), and Cr(VI). $[C]_i$= 5 mg L^{-1} at pH 6, 1h of contact time, except for Cr(VI) (pH 2, 2h) (n=3).

4.1.2.4. The Effect of the Initial Metal Concentration

The results given in Figure 4.6 show that the percentage of biosorption decreased as the initial concentration increased in the case of Cu(II), Pb(II) and Cd(II), due to the lack of availability of sites on the surface of the sorbent at a sorbent concentration of 5 g L^{-1}. As can be seen in this figure, at an initial metal concentration of 2 mg L^{-1} the highest removal percentage was achieved with Pb(II) (84.4%), followed by Cu(II) (60.9%), and Cd(II) (47.9%). When the initial metal concentration was increased to 5 mg L^{-1}, the removal efficiency decreased to 60%, 37%, and 18.29% for Pb(II), Cu(II) and Cd(II), respectively. In the case of Cr(VI), the removal rate

decreased from 46 to 35% when the initial concentration increased from 2 to 5 mg L^{-1} at pH 2 and a solution containing 10 g L^{-1} of biosorbent was used.

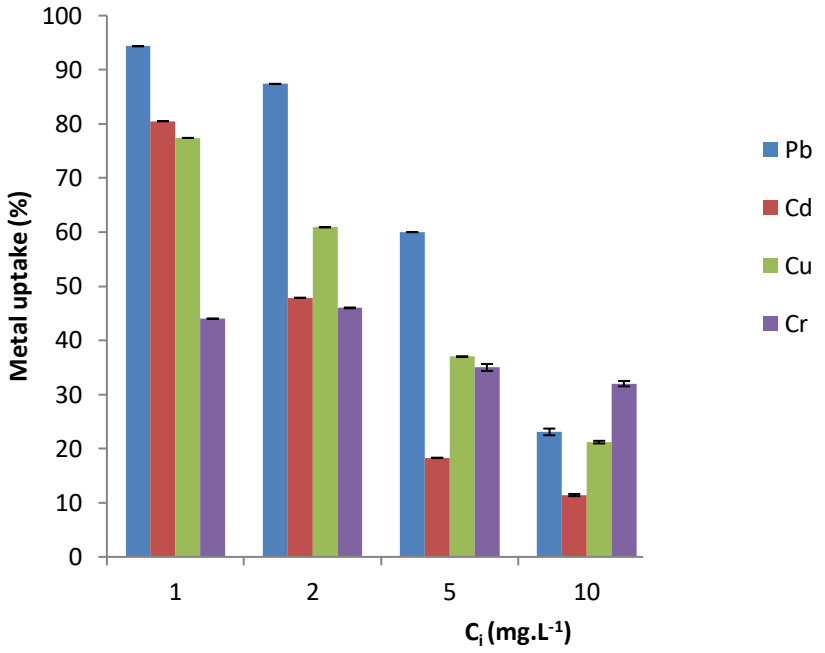

Figure 4.6. Effect of initial concentration on the removal of Pb(II), Cd(II), Cu(II), and Cr(VI). Adsorbent concentration of 4 g L^{-1} at pH 6, 1 h of contact time except for Cr(VI) (10 g L^{-1} at pH 2, contact time of 2 h) (n=3).

4.1.2.5. Adsorption isotherm

The Langmuir, Freundlich and Temkin isotherm constants and their determination coefficients (R^2) are listed in Table 4.1. As can be observed, the Cu data fitted well with the Langmuir, Freundlich and Temkin models with a determination coefficient > 0.92 and a maximum adsorption capacity of 0.557 mg g^{-1}. In the case of Pb, the adsorption isotherm followed the Langmuir model and the corresponding adsorption constant is higher (80 L mg^{-1}) than those obtained for copper and cadmium, 2.32 and 2.80, respectively, showing the great affinity of this metal for milled olive stone. Cd correlated with both the Langmuir and Temkin models with a maximum adsorption capacity of 0.3 mg g^{-1}. Similar results were obtained by other authors (Blázquez et al., 2011) and (Hernáinz et al., 2008). They showed that Cu(II), Cd(II) and Pb(II) adsorbed by milled olive stone fitted the Langmuir model with maximum adsorption capacities of

1.97 mg g^{-1}, 4.897 mg g^{-1} and 6.57 mg g^{-1} at pH 5. As can be seen in Table 4.1, the q_m values obtained in this study are lower given that the BET surface area is approximately the half than those reported by these researchers (Blázquez et al., 2011).

In the case of the Cr(VI), the best fit of the data was with the Temkin isotherm, with a correlation of 0.92 and a Temkin constant of 1.005 L mg^{-1}. However, it is important to remark that the Temkin isotherm is valid only for an intermediate range concentration. In comparison, the experimental data for the adsorption of Cr(VI) by rice straw at pH 2 fitted well with the Langmuir model with a q_m of 3.15 mg g^{-1} (Gao et al., 2008).

Table 4.1. Results obtained by applying the Langmuir, Freundlich and Temkin models to the experimental data.

Isotherm model	**Isotherm parameters**	**Cu**	**Cd**	**Pb**	**Cr**
Langmuir	q_m (mg g^{-1})	0.557	0.3	0.581	2.345
	K_L (L mg^{-1})	2.318	2.801	80.64	0.026
	R^2	**0.99**	**0.98**	**0.99**	0.03
Freundlich	n	3.285	1.375	5.649	0.889
	K_F (mg g^{-1})	0.61	0.537	0.739	0.299
	R^2	0.92	0.718	0.73	0.84
Temkin	A (L mg^{-1})	4.125	102.51	20.65	1.005
	B (J mol^{-1})	0.245	0.0531	0.174	0.437
	R^2	0.92	0.97	0.71	**0.92**

As can be seen in Table 4.2, the R_L at all the concentrations was between 0 and 1, showing that the adsorption is favorable for all the metals. R_L decreases with increasing the initial metal concentration indicate that in higher concentration the sites available decrease indicating its saturation. In the case of Cr(VI), R_L values are close to 1 (linear adsorption) for the lowest concentrations (1 and 2 mg L^{-1}) in agreement with the results obtained in Figure 4.7.

Table 4.2. Values of the separation factor **(**R_L) obtained for the adsorption of Cu(II), Cd(II), Pb(II) and Cr(VI) by milled olive stone.

Metal	**C_i (mg L^{-1})**	**R_L**
Cu	1	0.301
	2	0.177
	5	0.079
	10	0.043
Cd	1	0.263
	2	0.151
	5	0.066
	10	0.034
Pb	1	0.012
	2	0.0061
	5	0.0024
	10	0.0012
Cr	1	0.97
	2	0.94
	5	0.88
	10	0.79

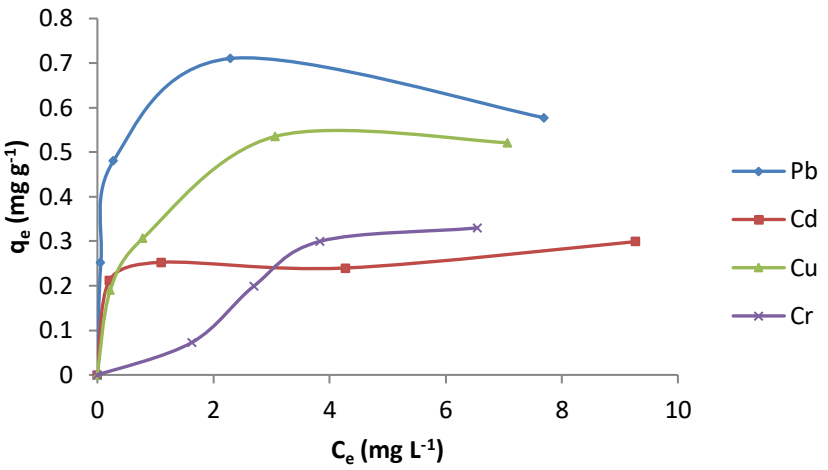

Figure 4.7. Adsorption isotherms on milled olive stone of Pb (II), Cd (II), Cu (II) at pH 6, and Cr (VI) at pH 2.

4.1.2.6. Kinetic adsorption

The parameters calculated for both kinetic models are collected in Table 4.3. Good correlation (R^2 > 0.99) is obtained between the experimental data and the pseudo-second-order model indicating that the adsorption of Cu(II), Cd(II), Pb(II), and Cr(VI) was controlled by a chemical process. The results obtained show that Cd(II) presented the highest K_2 and that the maximum sorption capacity q_e was found for Pb(II), however, this metal ion presented the lowest kinetic rate constant.

Table 4.3. Kinetic parameters of metal ion adsorption by milled olive stone.

	Pseudo first order			**Pseudo second order**		
Metal	**q_e (mg g^{-1})**	**K_1 (min^{-1})**	**R^2**	**q_e (mg g^{-1})**	**K_2 (g mg^{-1} min^{-1})**	**R^2**
Cd	0.021	0.0088	0.436	0.252	1.086	0.999
Cu	0.240	0.0038	0.207	0.474	0.251	0.998
Pb	0.444	0.0031	0.635	0.856	0.124	0.993
Cr	0.383	0.0035	0.800	0.392	0.188	0.998

4.1.2.7. Competitive Adsorption of Cd, Cu and Pb

We then investigated the effect on the sorption capacity of milled olive stones when a mixture of Cu(II), Cd(II), and Pb(II) was employed. Figure 4.8 shows a decrease in the percentage of the metals removed when there was competition. In single metal experiments with milled olive stone, for 1 h at pH 6, lead was the most adsorbed metal (75%). This value decreased to 37.8% (50% of reduction) in the case of multiple metal experiments, when Cu and Cd were also present at the same concentration. In the case of Cu(II) and Cd(II), the sorption capacities decreased to 6.8% (30% reduction), and 9.8% (15% reduction), respectively. Since Cd(II) has the highest rate constant, this metal was the first to saturate the available surface sites, followed by Cu(II) and Pb(II). The highest reduction on the sorption capacity in multiple metal experiments was obtained for Pb(II), which has the lowest kinetic rate constant although this metal ion showed the maximum sorption capacity (Table 4.3). These results demonstrated that the kinetic parameters can significantly affect the sorption process in the case of multi-metal biosorption. Ronda et al., (2014) reported that the greater affinity of the functional groups of the biosorbent to one metal ion is related to the ionic characteristics of this metal, which are measured by parameters including the ionic radius (r), the electronegativity (X_m) or covalent index: $CI = X_m^2 \ (r + 0.85)$. The sorption capacity is higher for metals with a higher covalent index than the other metals: lead has a covalent index of 11.1 whereas copper and cadmium have covalent indexes of 5.56 and 5.14, respectively.

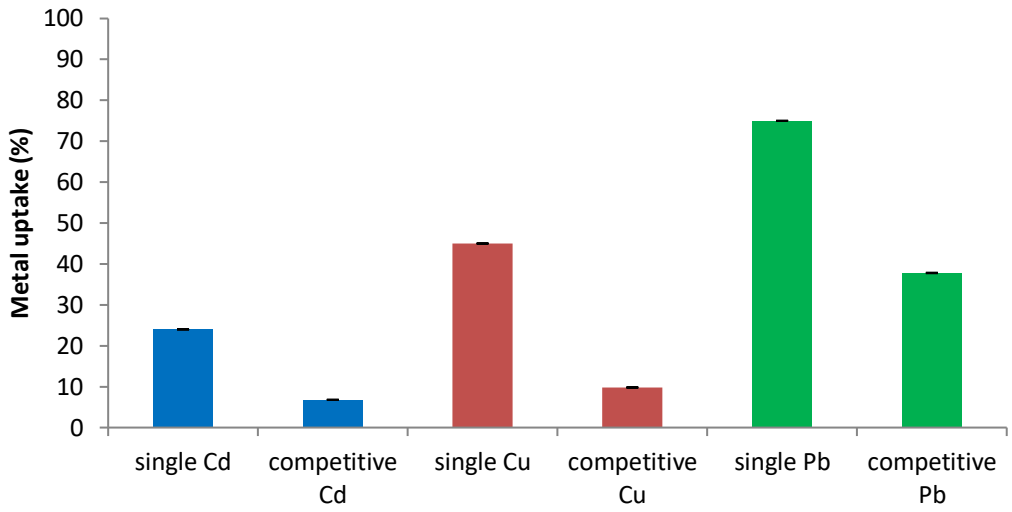

Figure 4.8. Comparison of the removal in multi-metal competitive (Cu(II), Cd(II) and Pb(II)) adsorption by milled olive stone with the removal of a single metal solution. $[C]_i$= 5 mg L^{-1}, adsorbent concentration of 5 g L^{-1} and 1 h of contact time (n=3).

This study has proved the efficiency of milled olive stones, which contains carboxylic and hydroxyl groups, in removing Cu(II), Cd(II), Pb(II) and Cr(VI) as a biosorbent. The maximum removal percentage for individual metal solutions containing 1 mg L^{-1} of Cd(II), Cu(II), and Pb(II) was 77.4%, 80.5%, and 94.5%, respectively, at pH 6 with 5 g L^{-1} of sorbent. In the case of Cr(VI), a removal percentage of 46% was obtained in 2 h at pH 2 using a larger amount of sorbent (10 g L^{-1}) and an initial concentration of 2 mg L^{-1}.

The Langmuir isotherm correlated well with the experimental data in single-ion solutions, resulting in maximum adsorption capacities at pH 6 of 0.581, 0.557 and 0.3 mg g^{-1}, for Pb(II), Cu(II) and Cd(II), respectively, whereas the data for Cr(VI) correlated well with the Temkin isotherm model, with a maximum capacity of 2.345 mg g^{-1} at pH 2. The good correlation found for all the metals with the pseudo-second-order kinetic model indicates a chemical sorption process.

4.2. Adsorption of Pb(II), Cd(II), Cu(II) and Cr (VI) by milled pine cone

A wide variety of agricultural residues have been evaluated as biosorbents taking advantage of the local availability of different vegetable matter around the world and their low cost as most of them are considered to be waste products. These include, among others, potato and banana peels (Pooja D, 2016), waste tea leaves (Cheraghi et al., 2015), plantain peels (Nkechi and Chizaram, 2018), rice husk (Jabbar et al., 2016), and sweetsop (Isaac and Sivakumar, 2013), pistachio shells (Hamidpour et al., 2018), date palm leaves (Shafiq et al., 2018), mahogany leaves (Ibrahim and Mohammed, 2017), lemon grass (Adesola et al., 2016), coconut shell (Aravind et al., 2017), and almond green hull (Nasseh et al., 2017). One drawback of using biosorbents is their low sorption capacity in comparison with other sorbents. Although this limitation can be overcome by modifying their surface through physical and chemical treatments that improve their capacity to bind to metal ions, these treatments require the use of energy and chemical reagents, which increase the cost. Two examples are the chemical treatment applied to modify lemon peel, resulting in an improved capacity to remove Ni(II) (Villen-Guzman et al., 2019) and the thermal treatment of pea peels at 600 °C to adsorb Pb(II) (Novoseltseva et al., 2020). Besides the use of lignocellulose-rich biomass for bioethanol production, this biomass has been shown to be more efficient than other biosorbents to remove metal ions. The different types of plant parts such as stems, stalks, leaves, husk, shells, roots, and barks and many others as raw material or as agricultural residues can be used to reduce environmental pollution.

Pine cones are produced in large quantities annually all over the world. In the Western Mediterranean, Spain has a pine-cultivated area of 460,000 hectares (Almendros et al., 2015), whereas in the Southern Mediterranean 320,000 hectares of the forest cover in Tunisia is made up of Pinus halepensis and Pinus pinea (Nasri et al., 2004). After the separation of the pine nuts, the remaining material is typically released into the environment as waste (Khouja et al., 1997). Pine cones are mainly composed of cellulose, hemicellulose and lignin, which have functional groups such as carbonyl (ketone), carboxyl, sulfhydryl (thiol), sulfonate, thioether, amine, alcohols, and esters that can bind heavy metals. Moreover, the cones have excellent physicochemical properties, including water retention, swelling capacity, and mechanical strength, that make them particularly suitable for use as an adsorbent (Altundoğan et al., 2016). Pine cones have been used in previous studies to adsorb different metal ions including Cr(VI) (Altundoğan et al., 2016), Cu(II) and Cd(II) (Değirmen et al., 2012), Cu(II) (Blázquez et al., 2012), Pb(II) (Ucun et al.,

2003), and binary solutions of Cu(II) and Pb(II) (Martín-Lara et al., 2016). Moreover, pine cones have also been applied to the removal of textile dyes from coloured wastewater (Mahmoodi et al., 2011). A chemical treatment using KOH was successfully applied to improve the surface properties of pine cone to adsorb Pb(II) and Cu(II) (Ofomaja and Naidoo, 2010). Pine cone was also used as a precursor of organic carbon and then directly applied to the removal of Pb(II), Cu(II), Ni(II), and Cr(VI) (Momčilović et al., 2011), and to produce a porous carbon low-cost photocatalyst support for environmental remediation (Sanni et al., 2020).

However, milled pine cone is used in this study without performing any previous biosorbent treatment in order to reduce costs and the complexity of the biosorbent process. Hence, the aims of the present study are to characterize milled pine cone and to valorise it as a biosorbent for the removal of heavy metals such as Pb(II), Cd(II), Cu(II) and Cr(VI) from water solutions.

4.2.1. Characterization of pine cone

Pine cone was characterized by performing FTIR, SEM, elemental analysis, and measuring the BET surface area and pH_{pzc} in order to study the efficiency of this adsorbent to remove metal ions. The FTIR spectrum of milled pine cone is presented in Figure 4.9. Five bands corresponding to the different functional groups can be seen in this figure. The broad band at 3379 cm^{-1} proved the presence of hydroxyl groups (O-H stretching vibration), indicating strong hydrogen bonding. The peak at 2935 cm^{-1} indicates the presence of aliphatic C-H group stretching. The peak observed at 1635 cm^{-1} denotes the stretching vibration of C=O of carboxylic groups, the peak at 1386 cm^{-1} can be assigned to COO, and the peak at 1033cm^{-1} shows the stretching vibrations of the alcoholic C-O group. As can be seen in Figure 4.9, there are changes in the bands at 3352 cm^{-1}, 2929 $cm^{-1,}$ 1610 cm^{-1}, 1378 cm^{-1}, and 1027 cm^{-1} after metal biosorption. These band shifts indicate that the hydroxyl and the carboxylic groups are involved in the adsorption of the metals as have been reported for lignocellulosic substrates in which two acid site - a low-pH (carboxylic) site and a high-pH (phenolic) site - are present (Ravat et al., 2000). Moreover, there is a decrease in the intensity after metal biosorption indicating an ion exchange or surface complexation process as the interaction with the metal ions prevents, in most of the cases, the vibration of the bonds (Ho, 2003). Martin-Lara et al., (2016) also reported that the carboxylic group is the main active site of pine cone and this finding is supported by the slightly acidic value of pH_{pzc} 5.62. However, in our study we found a pH_{pzc} of 6.2.

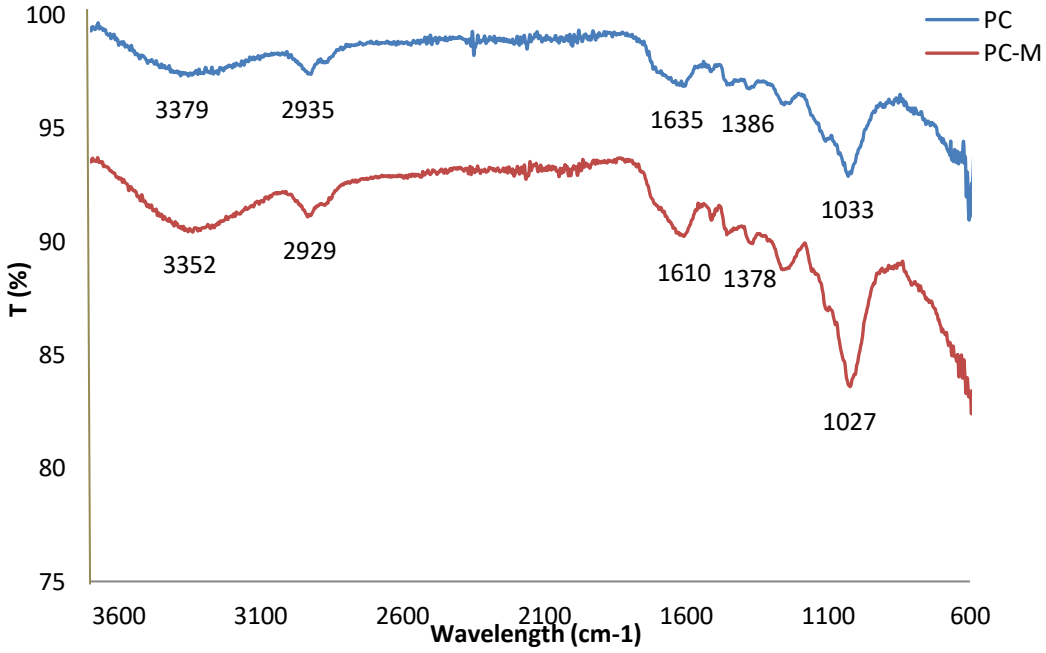

Figure 4.9. FTIR Spectra of pine cone before adsorption (PC) and after metal adsorption (PC-M).

The SEM images before and after adsorption (Figure 4.10) show some modifications, an accumulation of the metals on the cracks of the adsorbent surface. The study of the chemical composition of the biosorbent is important to explain its behaviour during the sorption process. Pine cone is a lignocellulosic material with hemicelluloses, lignin, celluloses and extractive materials (Pholosi et al., 2013). The surface elemental analysis of milled pine cone performed by EDX analysis showed a composition of 53.48% of C and 44.77% of O and 0.17% of S which is similar to the findings of other studies (Almendros et al., 2015; Martín-Lara et al., 2016). The characterization by EDX after adsorption, which was performed by putting milled pine cone into contact with a solution containing the three divalent metal ions, confirms the presence of Cd(II), Cu(II) and Pb(II) in the material with weight percentages of 0.3, 4.61 and 12.41%, respectively. Lead has the highest percentage, indicating the greater affinity of the biosorbent for this metal ion, followed by copper and cadmium. This result is in agreement with the strength of binding by the carboxylic and hydroxyl functional groups that follow the sequence Pb(II) >Cu(II) > Cd(II) (Ravat et al., 2000). The BET surface area, which is related to the capacity of the adsorbent, is

0.2536 m^2 g^{-1}, whereas the Langmuir surface area is 0.3108 m^2 g^{-1}. These values are smaller than those reported for pine cone and other agricultural waste ($0.5 > S_{BET} > 5$ m^2 g^{-1}) (Martín-Lara et al., 2016).

The results obtained for the particle size distribution show that 70% of the particles of the 5,271 particles analysed have a diameter of 50 µm, 15.8% of 100 µm, 7% of 150 µm with the rest being >150 µm.

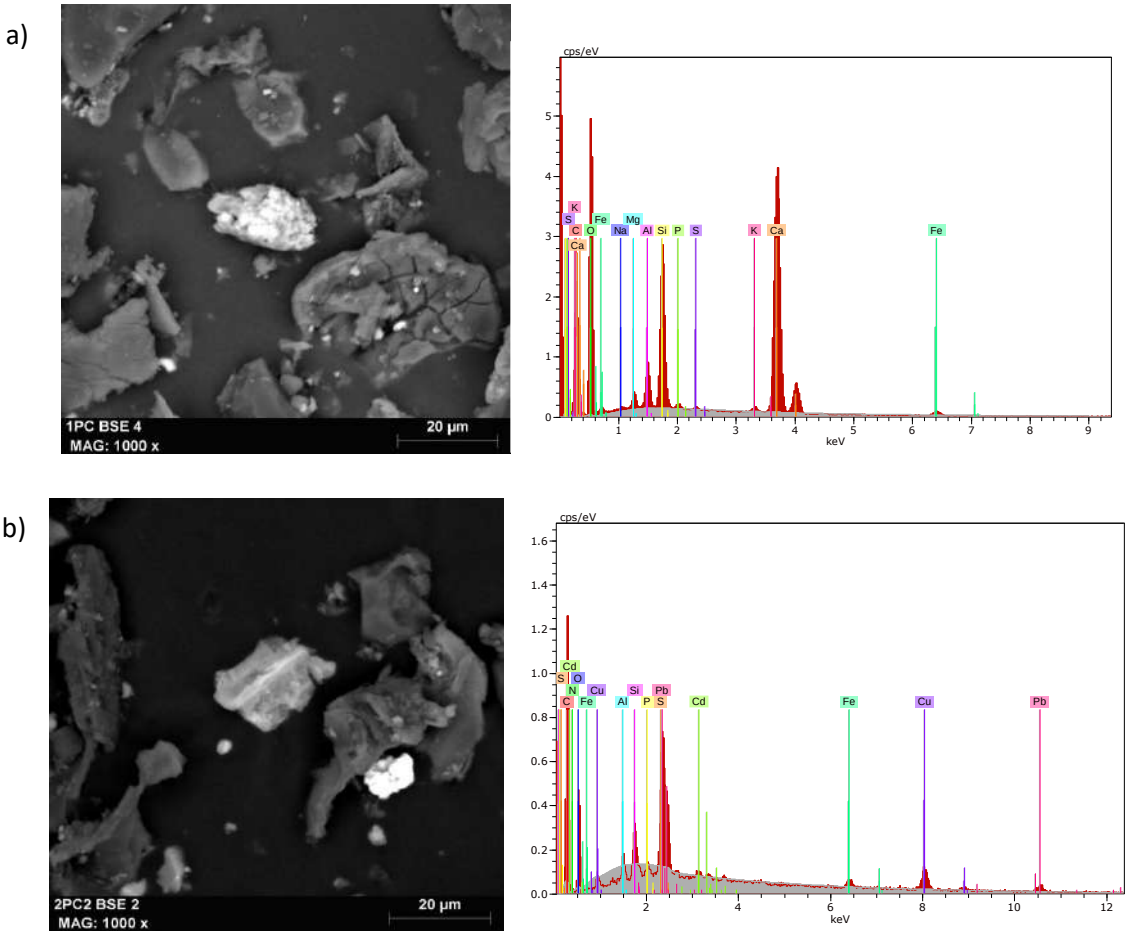

Figure 4.10. (a) SEM micrograph and EDX spectrum of pine cone, (b) SEM micrograph and EDX spectrum of pine cone after adsorbing Cu(II), Cd(II) and Pb(II).

4.2.2. Batch experiments with milled pine cone

4.2.2.1. Contact time effect on biosorption

The effect of contact time on the adsorption of metals onto pine cone was studied. All four metals achieved equilibrium in 2 hours with removal percentages of 82.24% for Cd(II), 93.71% for Cu(II), 94.67% for Pb(II), and 75.43% for Cr(VI) (Figure 4.11).

The high adsorption percentage of Cu(II) and Pb(II) is explained by their greater affinity to the carboxylic, ketonic and aldehyde functional groups (Najim and Yasin, 2013).

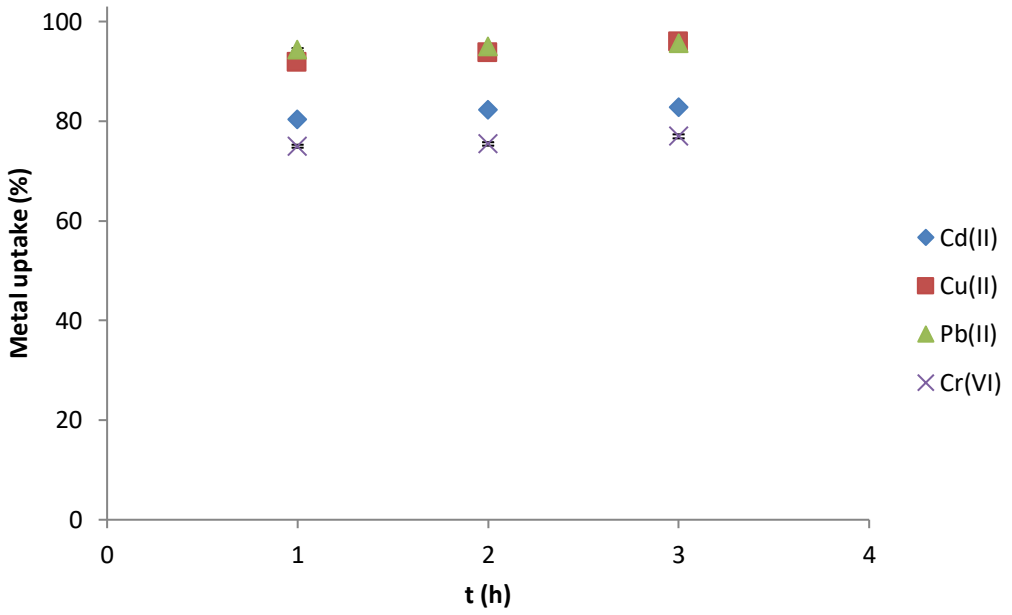

Figure 4.11. Effect of the contact time on the adsorption of Cd(II), Cu(II), Pb(II) and Cr(VI) (pH=2), C_i=5 mg L^{-1}, pH=5.4, adsorbent concentration=2 g L^{-1}, (n=3).

4.2.2.2. Effect of pH

The influence of the pH solution is an important parameter as it affects both the protonation of the functional groups on the adsorbent surface and the metal speciation. Figure 4.12 shows the percentage removal of Cd(II), Cu(II), Pb(II) and Cr(VI) at different pHs.

At pH 2, low percentages of metals were removed. This percentage was higher when the pH was increased, reaching a maximum at pH 5.5 with percentages of 82.24%, 93.17%, and 94.67% for Cd(II), Cu(II) and Pb(II), respectively. This result is explained by the competition between protons and metal ions for the available sites of the functional groups on the adsorbent surface. At acidic pH, the presence of protons H^+ increased in the solution, protonating the functional groups present on the adsorbent surface. At higher pHs, the percentage of H^+ decreased in the solution resulting in the binding of a greater number of metal ions to the functional groups. This tendency continued until pH 8.8 only in the case of Cd(II) as precipitation of Cu(II) and Pb(II) hydroxides starts at pH > 6.7 in accordance with the fraction diagrams calculated with Medusa software (Puigdomenech, 2016). The fraction diagrams (Fig. 4.13) were calculated at 5 mg L^{-1} showing that Cu^{2+} and Pb^{2+} ions are the predominant species until pH 6 while Cd^{2+} is predominant until pH 9. Moreover, the adsorbent surface becomes deprotonated at pH > pH_{PZC}, facilitating the electrostatic interaction between Cd(II) and the negatively charged groups (OH^- and COO^-) of the adsorbent, explaining the increase in the percentage of metal removal from 82.24 % at pH 5.5 to 94.12% at pH 8.8.

In the case of chromium, the lower the pH, the greater the adsorption percentage, with values of 76% at pH 2, 70% at pH 5.5, and 5.8% at pH 9. The pH of the aqueous solution influences chromium speciation and the acid-base properties of active functional groups (–OH, –COOH) of the lignocellulosic material, which are protonated at low pHs. Negatively charged $HCrO_4^-$ and CrO_4^{2-} species predominate in the aqueous solution at pH values between 2.0 and 6.0 for concentrations less than 500 mg L^{-1}. These negatively charged species can interact with the protonated functional groups at the adsorbent surface. At pH > 6, the competition of the anionic CrO_4^{2-} with the OH^- for the active sites of the adsorbent and the fact that at pHs > pH_{PZC} most of these active sites are negatively charged led to a dramatic reduction of the Cr(VI) adsorption (Ucun et al., 2003). Similar results were reported in other studies (Blázquez et al., 2011; Javaid et al., 2011; Najim and Yasin, 2013), which found the maximum Cr(VI) removal at low pH. Nowadays, the adsorption-coupled reduction reaction is the most accepted mechanism to explain Cr(VI) biosorption by natural materials (Martín-Lara et al., 2016; Miretzky and Cirelli, 2010; Park et al., 2007). In this mechanism, the removal of Cr(VI) involved two processes: biosorption and reduction to Cr(III) (Blázquez et al., 2009). Different biomaterials, including pine cone, were used to demonstrate this coupled mechanism by verifying the oxidation state of chromium by X-

ray photoelectron spectroscopy and measuring the pH variation during the adsorption process at low pHs. Protons and electrons, supplied by electron-donor groups of the biomaterial such as carboxylic groups, are required for the reduction of Cr(VI) to Cr(III), resulting in an increase in the pH of the metal solution (Park et al., 2007). In our study, an increase of 0.3 units of pH of the solution after the adsorption of chromium proved the reduction of one part of Cr(VI) to Cr(III), showing that adsorption of Cr(VI) may take place through this coupled mechanism.

In the case of the divalent metals, Pb(II), Cu(II), and Cd(II), the removal was through surface complexation by their association with carboxylic or OH groups as is indicated by the band shifts of these functional groups in the FTIR spectra after the adsorption of the metal ions (Fig. 4.9). As the pH of the solution is increased, the presence of ligands and the deprotonation of functional groups such as hydroxyl (-OH) and carboxyl (-COOH) on the surface of the biosorbent facilitate the formation of complexes with the metal ions, leading to further adsorption.

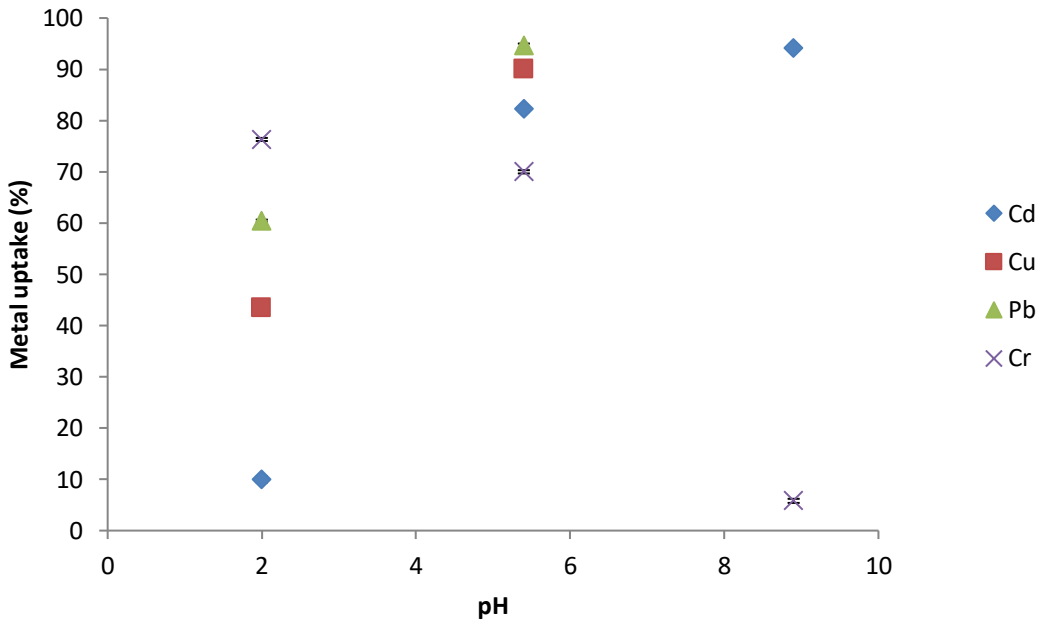

Figure 4.12. Effect of the pH on the adsorption of Cd(II), Cu(II), Pb(II) and Cr(VI), C_i=5 mg L^{-1}, adsorbent concentration=2 g L^{-1}, t=2 h (n=3).

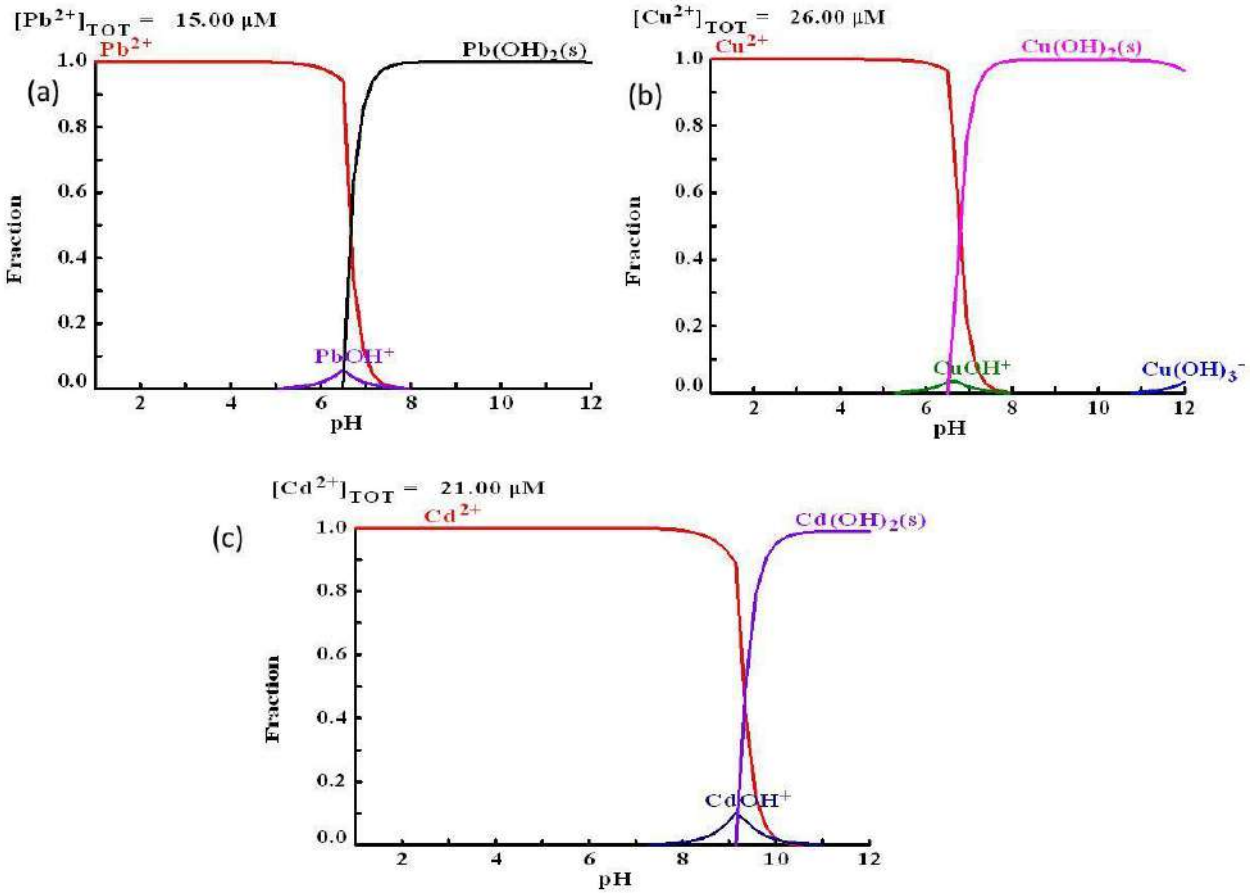

Figure 4.13. Fraction diagrams of Pb(II), Cd(II) and Cu(II) at a metal concentration of 5 mg L^{-1}.

4.2.2.3. Effect of the adsorbent concentration

Figure 4.14 shows that a higher removal percentage of Cd(II) and Cr(VI) were obtained on increasing the amount of biosorbent, while for Pb(II) and Cu(II) the removal percentages did not change when the amount was increased. As can be deduced from this Figure, 2 g L^{-1} is the optimum dosage of milled pine cone at pH 5.5 to remove Cu(II) and Pb(II) with percentages of 93.71% and 94.97%, respectively. In the case of Cd (II), the best results (89%) were obtained with a dose of 5 g L^{-1} at pH 5.5 whereas for Cr(VI) this percentage was achieved with a dose of 10 g L^{-1} at pH 2.

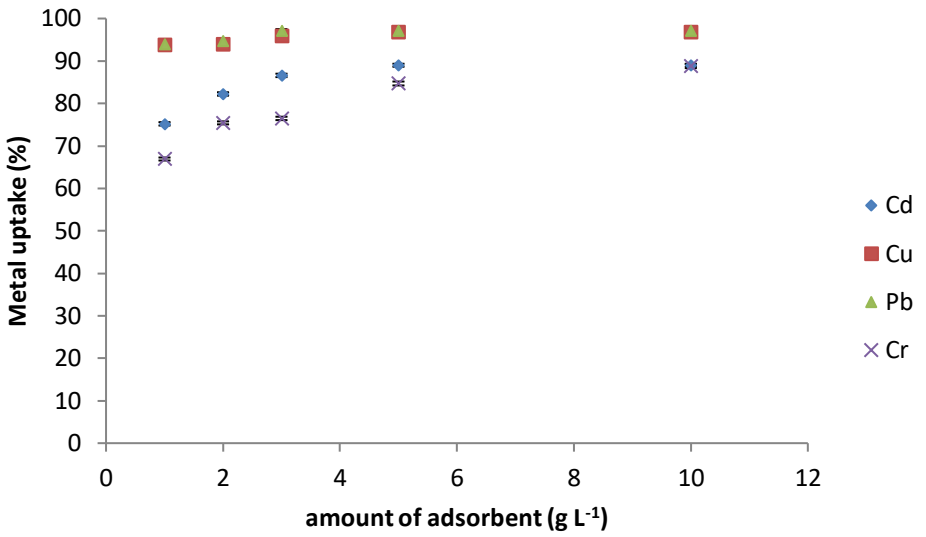

Figure 4.14. Effect of the adsorbent concentration on the removal of Pb(II), Cu(II), Cd(II) and Cr(VI) (pH=2), C_i=5 mg L^{-1}, pH 5.4, t=2 h (n=3).

4.2.2.4. Effect of the initial metal concentration

The initial metal concentration is an important parameter that affects the efficiency of biosorption. It was studied at different values ranging from 1 to 500 mg L^{-1}. Figure 4.15 shows the removal percentage of metals as a function of the initial metal concentration. As can be seen, the removal efficiency of milled pine cone decreases as the initial metal concentration increases. However, this effect is higher for Cu(II), Cd(II), and Cr(VI) than for Pb(II), more than 60% of which is removed for 300 mg L^{-1}. This decrease is explained by the fact that at higher concentrations the saturation of the adsorbent surface is faster given the competition for the available binding sites resulting in more ions without there being more sites to attach to. However, in the case of Pb(II), the adsorption capacity increases when the initial concentration was increased from 1 to 20 mg L^{-1} indicating that the presence of more metal ions generates a driving force that overcomes the mass transfer resistance between the aqueous and the solid phases. The biosorption capacity for Pb(II) remains practically constant from 20 to 100 mg L^{-1}, showing that there were available binding sites on the pine cone surface. The greater affinity of milled pine cone to Pb(II) can be explained by its longer ionic radius (119 pm) in comparison with Cd(II) (95 pm) and Cu(II) (73 pm) as well as by the fact that it has the lowest hydration ion

radius and the highest covalent index (Martín-Lara et al., 2016). The covalent index is a function of the ionic radius (r) and the electronegativity (X_m) and is defined by: CI =X_m^2 (r+0.85). The greater the covalent index of the metal ion, the greater the potential of this metal ion to form covalent bonds with the functional groups of the biosorbent. Lead has a covalent index of 11.1 whereas copper and cadmium have covalent indexes of 5.56 and 5.14, respectively (Amar et al., 2020). Moreover, the metal removal efficiencies at low concentrations such as 1 and 3 mg L^{-1} are greater for Cu (II) than for the other metals, whereas at concentrations ranging from 5 to 30 mg L^{-1} removal rates of more than 90% were obtained for Cu(II) and Pb(II). At higher concentrations, the removal percentages of Cu(II), Cd(II) and Cr(VI) fell. The removal efficiencies for the divalent metals follow the order Pb(II)>Cu(II)>Cd(II), which corresponds to the order of their affinity towards OH from phenolic groups (Ravat et al., 2000).

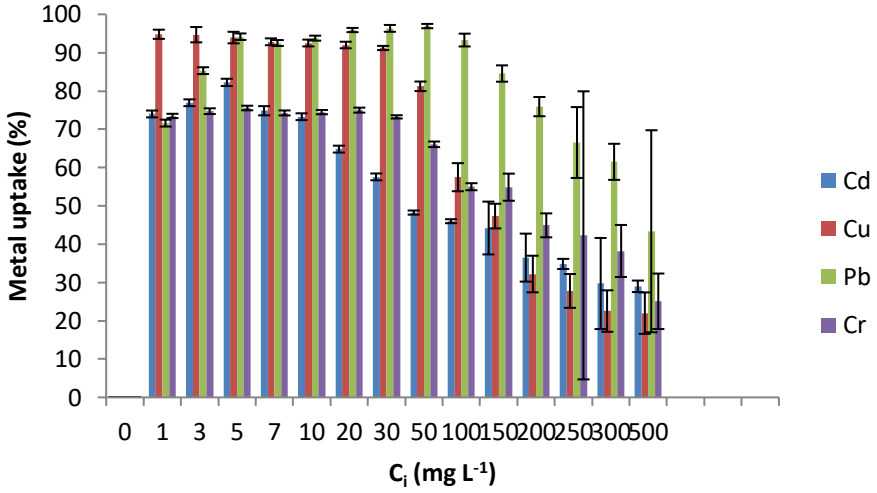

Figure 4.15. Effect of the initial metal concentration on the removal of Cd (II), Cu (II), Pb (II), and Cr (VI) (pH=2), adsorbent concentration=2 g L^{-1}, t=2 h, pH=5.4 (n=3).

4.2.2.5. Adsorption isotherms

In the adsorption isotherm graphs, the amount of adsorbate per mass unit of adsorbent is represented as a function of the equilibrium concentration in the solution at a constant temperature. The shape of the line depends on the adsorbent and adsorbate characteristics and on the type of interaction between them. This shape is used to classify the adsorption isotherms in different types following the Giles classification (Gauden et al., 2008). As can be seen in Figure

4.16, the sorption isotherms for Pb(II), Cu(II) and Cr(VI) are Type I (convex shape), corresponding to an L type isotherm where the slopes remain constant at a maximum sorption value. The L type is associated to a monolayer adsorption of non-porous or microporous adsorbent, which is the type of adsorption isotherm most typically found in the case of agricultural wastes. The sorption isotherm of Cd(II) is type IV, which is characterized by the presence of two plateaus separated by an inflection due to the change from the first plateau to a concave shape until the second plateau is reached. The Langmuir, Freundlich and Langmuir-Freundlich models (Table 4.4) can be used to characterize experimental data of the metal adsorption isotherm.

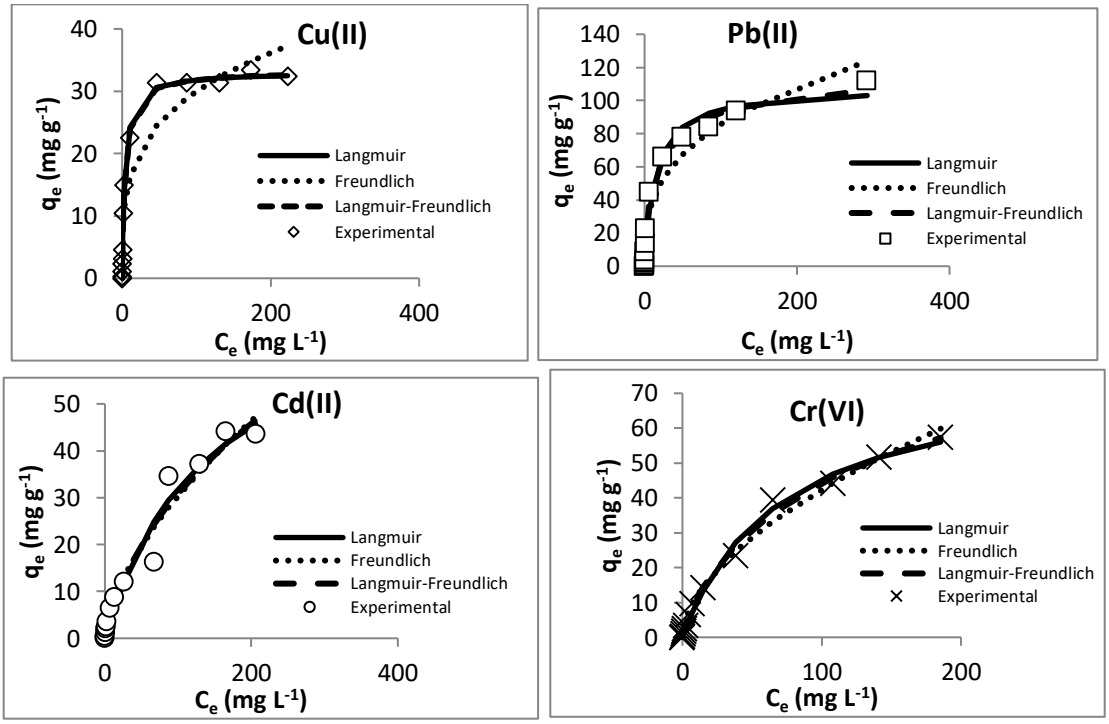

Figure 4.16. Adsorption isotherms of Cd(II), Cu(II), Pb(II) and Cr(VI) (pH=2) at pH=5.4, adsorbent concentration=2 g L^{-1}, t=2 h.

The Langmuir isotherm is characterized by the separation factor R_L, which can measure the facility for adsorption. R_L = 0, it means that an irreversible adsorption process is taking place, whereas if R_L = 1, the adsorption is linear, and if 0 <R_L<1, it is considered that the adsorption is favoured. The R_L values obtained, which varied between 0 and 1, indicate that biosorption onto milled pine cone was favoured. When the initial metal concentration was increased, the

separation factor R_L decreased at a constant rate for all the metals, indicating the high affinity of these metals to the biosorbent even with high metal concentrations. In the case of the lowest initial metal concentration, 1 mg L^{-1}, the R_L values were close to 1 (linear adsorption) for Cd(II), Pb(II), Cu(II) and Cr(VI), whereas in the case of the highest initial concentration, 300 mg L^{-1}, R_L values were lower and varied between 0.02-0.13. Moreover, Cu(II) and Pb(II) had the lowest separation factor R_L values at an initial concentration of 20 mg L^{-1} (0.25 and 0.56, respectively) indicating the greater affinity of both metal ions to the biosorbent.

The fit of the experimental data to Langmuir, Freundlich, and Langmuir-Freundlich isotherm models was determined by using both non-linearized and linearized equations. In the case of the non-linearized equations, both the experimental points and the calculated models are depicted in Figure 4.16. As can be seen in this figure, there is good agreement between the experimental points in the case of Cu(II) and Pb(II) and the curves corresponding to the Langmuir and the Langmuir-Freundlich isotherm models, while in the case of Cd(II) and Cr(VI) the curves of the three models agree with the experimental points. In order to find out the best adsorption isotherm model, we employed linearized equations, as have most published papers (Wang and Guo, 2020), despite the inherent bias created by linearization. The results obtained by applying the linearized Langmuir, Freundlich, and Langmuir-Freundlich equations are recorded in Table 1. The degree of agreement was assessed by comparing the determination coefficient (R^2) of each model and by applying Akaike's criterion (AIC) and the F test as R^2 is insufficient to perform the comparison of the models.

In the case of the Akaike criterion, the model for which corrected AIC (AICc) has the lowest value is selected as the best model (Akpa and Unuabonah, 2011). The F test, based on traditional statistical hypothesis testing, compares the least-square regression fits of the linearized Langmuir or Freundlich equations with those of the linearized Langmuir-Freundlich model. As can be seen in Table 1, when the F test was used to compare Freundlich and Langmuir-Freundlich, the latter was the best model for all the metal ions, however, in comparing Langmuir and Langmuir-Freundlich models, Langmuir was the selected model for Cr(VI) and Cu(II) and Langmuir-Freundlich model for Pb(II) and Cd(II). These results are in agreement with those obtained by applying the Akaike criterion (Table 4.4).

The experimental data of Cu(II) fitted the Langmuir model with a maximum adsorption capacity of 33.04 mg g^{-1}. Consequently, this metal ion was adsorbed onto the surface of the pine cone, forming a monolayer, which provides a single site to attach each metal ion. A similar result was obtained by Blázquez et al. (2012), who proposed a surface complexation model for the adsorption of Cu(II) by pine cone shell. The Langmuir model was also the best suited to describe the experimental data for Cr(VI) adsorption with a maximum adsorption capacity of 57.36 mg g^{-1}. In the case of Pb(II) and Cd(II), the best model is the Langmuir-Freundlich isotherm with maximum adsorption capacities of 100.01 and 78.73 mg g^{-1}, respectively. This model is suitable for predicting adsorption on heterogeneous surfaces, thereby avoiding the limitation of increased adsorbate concentrations associated with the Freundlich model but at a high concentration of adsorbate, it predicts the Langmuir model (monolayer adsorption), hence, the Langmuir-Freundlich isotherm is a concentration-dependent model. The differences between the adsorption isotherm models for Cu(II) and Pb(II) can explain the differences in the metal removal percentages when the initial metal concentration was varied from 1 to 5 mg L^{-1}. As has been discussed earlier in the case of Cu(II), at these low initial concentrations the metal uptake percentage remained constant (~94%) whereas for Pb(II) it increased from 73.5 to 94%.

As can be in Table 4.4, the values of the maximum adsorption capacities calculated from the Langmuir and the Langmuir-Freundlich models are similar in the case of Cd(II) and Pb(II) and the same, considering the standard deviation, in the case of Cr(VI) and Cu(II). With regards to R^2, the highest values correspond to the Langmuir model for Cu(II) and Cr(VI), and to the Langmuir-Freundlich model for Cd(II) and Pb(II). This statistic is in agreement with the results of the application of Akaike and F tests to compare the different models for each metal ion.

Table 4.4. Results obtained from the linearized Langmuir, Freundlich and Langmuir-Freundlich isotherms.

	Langmuir (L) $q_e = \frac{q_{max} b C_e}{1 + b C_e}$			**Freundlich (F)** $q_e = K_F C_e^{1/n}$			**Langmuir-Freundlich (L-F)** $q_e = \frac{q_{LF}(K_{LF}C_e)^{M_{LF}}}{1 + (K_{LF}C_e)^{M_{LF}}}$				**Akaike* Criterion**	**F test* L and L-F**	**F test* F and L-F**
Metal	**q_{max} (mg g^{-1})**	**b (L mg^{-1})**	**R^2**	**K_F**	**1/n**	**R^2**	**q_{LF} (mg g^{-1})**	**K_{LF}**	**M_{LF}**	**R^2**	**AICc**	**P <0.05**	**P <0.05**
Cu(II)	33.04±0.75	0.26±0.01	0.99	8.67±0.05	0.27±0.15	0.86	33.21±0.08	0.25±0.03	0.97±0.04	0.90	50.69(F)>16.34 (L-F)>**10.92(L)**	F=0.12 P=0.735 **L**	F=186.32 P<0.0001 L-F
Cd(II)	77.12±0.41	0.007±0.01	0.90	1.81±0.75	0.61±0.007	0.98	78.73±0.06	0.009±0.005	0.72±0.07	0.94	48.27(F)>44.02(L) >**14.98(L-F)**	F=104.22 P<0.0001 **L-F**	F=144.72 P<0.0001 **L-F**
Cr(VI)	57.36±0.70	0.014±0.004	0.96	3.21±0.90	0.55±0.10	0.80	56.31±0.05	0.018±0.007	0.79±0.10	0.90	32.86(F)>29.14 (L-F)>**28.53(L)**	F=4.19 P=0.0709 **L**	F=133.19 P<0.0001 L-F
Pb(II)	108.05±0.77	0.07±0.02	0.8	17.75±0.02	0.34±0.09	0.75	100.01±0.04	0.05±0.03	0.71±0.02	0.90	72.04(F)>63.58 (L)> **58.31(L-F)**	F=10.92 P=0.008 **L-F**	F=104.48 P<0.0001 **L-F**

*AICc: the lowest value corresponds to the best model.

*F test: the null hypothesis is that the simpler model (Langmuir or Freundlich) is correct, alternative model L-F is better than L or F when P < 0.05.

Table 4.5 summarizes the comparison of the adsorption capacity of milled pine cone for Cu(II), Cd(II), Pb(II) and Cr(VI) with other biosorbents. It is seen in these results that milled pine cone has the highest adsorption capacity for all the metals. Pine cone was a more effective biosorbent for Pb(II) than custard apple (Isaac and Sivakumar, 2013), sea lettuce (El-Sikaily et al., 2007), and milled olive stone (Amar et al., 2020). Moreover, milled pine cone presents a higher adsorption capacity for Cd(II) and Cr(VI) than those obtained by rice husk (Al-Baidhani and Al-Salihy, 2016) and olive stones (Amar et al., 2020)**.** In the case of Cu(II)**,** pine cone is also more efficient than maize husk (Duru et al., 2019) and olive stones (Amar et al., 2020; Blázquez et al., 2011). Therefore, milled pine cone has been demonstrated to be more efficient than milled olive stones in the removal of Pb(II), Cu(II), Cd(II) and Cr(VI). However, the maximum adsorption capacities for these ions differ depending on the experimental conditions used (initial metal concentrations, particle size, dosage of adsorbent and pH and the type of pine biomass: pine bark or pine cone, pinus halepensis or pinus resinosa). Almond shell and hazelnut shell were used to adsorb Cd(II) and Pb(II) at pH 5 resulting in maximum adsorption capacities ranging from 1.6 to 6.2 mg g^{-1} (Cataldo et al., 2018) which are lower than those found by pine cone.

Table 4.5. Comparison of the adsorption capacity of milled pine cone for Pb(II), Cu(II), Cd(II) and Cr(VI) with the other biosorbents.

Biosorbents	Metals	Particle size	pH	Concentration (mg L^{-1})	Dose (g L^{-1})	q_m (mg g^{-1})	References
Custard apple	Cd(II)	-	5	50-200	1.5	71	Isaac and Sivakumar 2013
	Pb(II)		5	5-200	1.5	90.93	
Ulva lactuca	Cr(VI)	≤0.063mm	1	5-50	2	10.61	El-Sikaily et al., 2007
Olive stone	Cu(II)	<0.250-1mm	5	10-300	10	1.97	Blázquez et al., 2011
Pine bark	Cu(II)	-	5	10-300	10	11.94	
Maize husk	Cu(II)	1.8mm	6	-	-	1.21	Duru et al., 2019
Pine sawdust	Pb(II)	0.6-1.2mm	5	1-50	10	13.48	Semerjian, 2018
	Cu(II)		7	1-50	10	9.59	
Rice husk	Cd(II)	<0.125mm	-	-	-	5.54	Jabbar et al., 2016
Pine cone	Cd(II)	-	7	20-200	2	14.7	Isanloo and Nasseri, 2005
Pine cone	Cr(VI)	-	1	10-120	2	65.36	Najim and Yasin, 2013
Pine cone	Cu(II)	-	5	50-250	3	18.69	Değirmen et al., 2012
	Pb(II)		7	50-250	3	23.2	
Pine cone	Cu(II)	4-8mm	5	5-100	10	6.52	Martín-Lara et al., 2016
	Pb(II)		5	5-100	10	17.41	
Pine cone (*p. resinosa*)	Cu(II)	<0.15mm	5	10-300	10	9.68	Award and Erkurt, 2014
	Pb(II)		5	10-300	10	17.24	
Olive stone	Pb(II)	-	6	1-10	5	0.581	Amar et al., 2020
	Cu(II)		6	1-10	5	0.557	
	Cd(II)		6	1-10	5	0.3	
	Cr(VI)		2	1-10	10	2.345	

Hazelnut shell	Cd(II)	0.40-1.8mm	5	30	5	1.6	Cataldo et al., 2018
	Pb(II)		5	30	5	6.2	
Almond shell	Cd(II)	0.40-1.8mm	5	30	5	2.7	Cataldo et al., 2018
	Pb(II)		5	30	5	4.2	
Pine cone	Pb(II)		5.4	1-500	2	95	Present study
	Cu(II)		5.4	1-500	2	33.55	
	Cd(II)		5.4	1-500	2	50	
	Cr(VI)		2	1-500	2	68.03	

4.2.2.6. Competition between Cu(II), Pb(II) and Cd(II)

The competition of the different metals to occupy the binding sites of the adsorbent was investigated using three multi-metal solutions containing Pb(II), Cd(II) and Cu(II) at different initial concentrations of 1 mg L^{-1}, 5 mg L^{-1} and 10 mg L^{-1} at pH 5.4 using 2 g L^{-1} of adsorbent for 2 h. Figure 4.17 compares the adsorption efficiency of milled pine cone towards a solution containing a single metal ion and the three metal ions. In the case of Pb(II), the removal percentage increases from 71.6 % to 94% when the initial concentration was increased from 1 to 5 mg L^{-1} and the same results were obtained when Cu(II) and Cd(II) were present at the same concentration levels, showing that the presence of these metal ions did not affect Pb (II) removal. A similar trend was observed in the case of Cd(II), whose removal percentages were the same for both the single and multi-metal solutions except in the case of the highest concentration (10 mg L^{-1}). Cu(II) was the only metal ion affected by the competition with the other ones and its removal percentage decreased by around 10% in the presence of Pb(II) and Cd(II) at all the concentrations tested, confirming the higher affinity of pine cone by Pb(II). The biosorption of the binary Cu(II)–Pb(II) system by pine cone was investigated in a batch reactor and in a fixed-bed column. The results obtained in both operational modes confirmed a slightly suppression of copper biosorption due to the presence of lead when both metal ions are present in solution (Martín-Lara et al., 2016). Recently, a review on the dominance of Pb(II) during competitive biosorption from multi-metal systems has concluded that most biosorbents can effectively remove Pb(II) even in the presence of other heavy metals but the adsorption of Cu(II), Cd(II), Zn(II), Ni(II) and Cr(III) decreases significantly due to the presence of Pb(II) (Mahamadi, 2019).

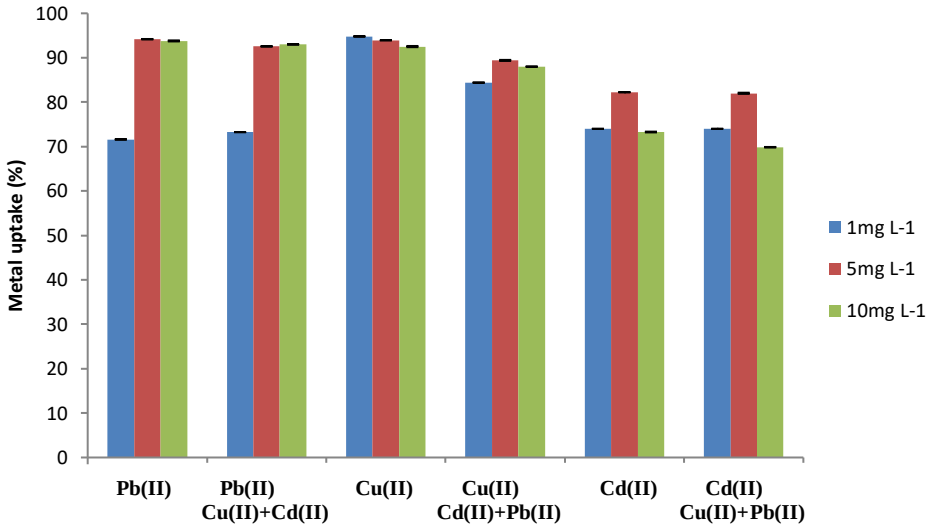

Figure 4.17. Comparison of the removal of Pb(II), Cu(II) and Cd(II) by pine cone between a single metal and multi-metal solutions at different initial concentrations: pH=5.4, adsorbent concentration=2g L^{-1}, t=2 h (n=3).

Milled pine cone, a resource that is widely available and relatively cheap, is seen to be an effective biosorbent for the removal of divalent metal ions due to the high affinity of these ions for the carboxylic and hydroxyl groups, which are present on the adsorbent surface. The efficiency of milled pine cone to remove trace concentration levels of Pb(II), Cd(II) and Cu(II) has been demonstrated, resulting in capacities of 100.01 mg g^{-1}, 78.73 mg g^{-1} and 33.04 mg g^{-1} at pH 5.5, respectively. These capacities are higher than those reported for other biosorbents with similar characteristics. Moreover, an adsorption capacity of 57.36 mg g^{-1} was obtained for Cr (VI) at pH 2 and its maximum removal percentage (88.8%) was obtained at pH 2 with 10 g L^{-1}. The experimental adsorption data correlated well with the Langmuir model for Cu(II) and Cr(VI) whereas for Pb(II) and Cd(II) the best correlations were obtained with the Langmuir-Freundlich model. In the case of the divalent ions (Pb(II), Cu(II), and Cd(II)), there is no competition between them towards the adsorbent sites at low metal concentration levels (1-10 mg L^{-1}), given that the presence of other metal ions did not reduce the removal efficiencies.

4.3. Removal of heavy metals using a fixed-bed column containing milled pine cone

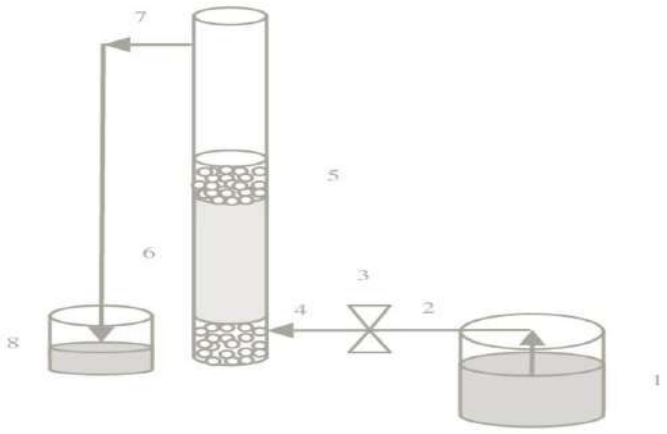

Batch experiments are used to obtain equilibrium sorption isotherms and to evaluate the sorption capacity of biosorbents (see section 4.1 for milled olive stones and 4.2 for milled pine cone). However, in the practical operation of full-scale biosorption processes, continuous-flow fixed-bed columns and fluidized bed columns are often preferred to treat large volumes of effluent. In such systems, the concentration profiles in the liquid and sorbent phases vary in both space and time. As a result, it is difficult to carry out a priori design and optimization of fixed-bed columns without a quantitative approach. From the perspective of process modeling, the dynamic behavior of a fixed-bed column is described in terms of the breakthrough curves. Several studies have been performed to investigate metal adsorption using fixed bed columns, which have the advantage of being continuously in contact with the solution. This configuration allows the treatment of high volumes of wastewater due to the large surface area per unit of volume that can be achieved, which results in a high mass transfer (Nassar et al., 2003). Moreover, the efficiency of dynamic adsorption has been proved in the case of electroplating industries. Tsai et al., (2016) have investigated the use of chitosan-coated bentonite to remove Pb(II), Cu(II) and Ni(II), obtaining adsorption capacities of 13.49 mg g^{-1}, 12.14 mg g^{-1} and 10.29 mg g^{-1}, respectively. An adsorption capacity of 130.12 mg g^{-1} for Cr(VI) was obtained using xanthated chitosan as the biosorbent in a fixed bed column (Chauhan and Sankararamakrishnan, 2011). Other agricultural residues tested as biosorbents are watermelon rind and spent coffee grains, which have been reported to be efficient in reducing heavy metal concentrations in aqueous solution containing these pollutants (Lakshmipathy and Sarada, 2015; Davila-Guzman et al., 2016). Encapsulated moringa oleifera has been applied in the removal of Zn(II), Cu(II), Mn(II), Co(II) and Ni(II) from electroplating wastewater using a fixed bed column (Radhakrishnan et al., 2016). Almond shell, containing hydroxyl, carboxyl and aliphatic functional groups that can bind metals, was investigated as an efficient biosorbent operating in a column mode for the simultaneous removal of Cu(II) and Cr(VI) from tannery wastewater resulting in adsorption capacities of 2.39 and 21.92 mg g^{-1}, respectively (Yahya et al., 2020). Grape stalk waste was applied to remove Pb(II) and Cd(II) in column experiments with adsorption capacities of 56.11 and 33.12 mg g^{-1} (Miralles et al., 2010). Furthermore, simultaneous removal of Cu(II) and Ni(II) from synthetic solution and electroplating effluents using brown algae was studied, obtaining capacities of 1.656 mmol L^{-1}

and 1.404 mmol L^{-1}, respectively (Barquilha et al., 2019). Moreover, the efficiency of pine cone in the removal of methylene blue and acid dyes onto a fixed bed column has also been studied (Yagub et al., 2015; Hadi et al., 2011)

The aim of the present study was to investigate the ability of milled pine cone to remove Cu(II), Cd(II), Pb(II), Ni(II) and Cr(VI) in a fixed bed column and the capacity of this biosorbent to separate the metals from the same solution. The effect of parameters such as the initial adsorbate concentration, bed height and flow on the removal capacity of pine cone in dynamic conditions has also been studied.

4.3.1. Operating Parameters of the column

The efficiency of fixed bed column is described by the breakthrough curve which is the result from plotting the concentration C_t/C_i versus time (C_i and C_t are initial concentration and the effluent concentration at the column outlet (mg L^{-1}). The dynamic response of the adsorption column is determined by the breakthrough time (t_b), corresponding to the moment at which the metal concentration of adsorbate reaches 10% of the feed concentration (C_t/C_i=0.1), and the shape of the breakthrough curve. Whereas, the time at which the saturation occurs is called the exhaustion time (t_s), which is set when the effluent concentration exceeds a value between 90% and 95% of the initial concentration.

To evaluate the column performance, several parameters has to be defined. The mass transfer zone (MTZ) is the zone where the ion transfer between the adsorbent and the adsorbate takes place. It is assumed to have a constant length or depth, $\mathcal{Z}$. The total time taken (t_x) (min) for the MTZ to be established, to move down the length of the fixed bed of the adsorbent then out of the bed is defined as:

$$t_x = \frac{V_e}{Q} \qquad (4.1)$$

Where V_e is throughput volume (mL), Q is the volumetric flow rate, mL min^{-1}. The time ($t_{\mathcal{Z}}$) (min) required for the movement of the MTZ downward in the column is defined as:

$$t_{\mathcal{Z}} = \frac{V_e - V_b}{Q} \qquad (4.2)$$

where V_b is the throughput volume at breakthrough (mL).

Accordingly, it is possible to calculate the time required for the initial formation of MTZ (t_f) (min) from the equation:

$$t_f = \frac{V_b}{Q} \qquad (4.3)$$

The fixed-bed height can, thus, be equated with the time ratio using the equation below:

$$\frac{\ell}{z} = \frac{t_\ell}{t_x - t_f} \qquad (4.4)$$

Where z is the bed depth (cm), ℓ : the length or depth of the MTZ.

4.3.2. The effect of different parameters on the removal of metals onto fixed bed column

In this section, the removal of different metal ions by milled pine cone packed in a glass column (diameter 12 mm and 200 mm length) is described as well as the effect of different parameters such as the initial adsorbate concentration, bed height and flow rate that influence the metal removal.

4.3.2.1. Flow rate effect on the removal of Pb(II)

The flow rate is an important parameter that determines the contact time between the inlet effluent and the biosorbent. The effect of the flow rate on metal adsorption performance was studied at different values from 1.4 mL min^{-1} to 3 mL min^{-1} at an initial metal concentration of 50 $mg.L^{-1}$ and 0.7 cm corresponding to 0.2 g of adsorbent. As can be seen in Figure 4.18, when the flow rate increases, the time needed for the adsorption zone to reach the top of the column was shorter, causing a faster saturation level. The breakthrough parameters for Pb(II) adsorption were calculated (Table 4.6). The breakthrough and the exhaustion times (t_b and t_e) and breakthrough and exhaustion volumes (V_b and V_e) decrease when the flow rate increases. In the case of low flow rates, the efficiency of pine cone in removing Pb(II) increases and the adsorbent capacity was not exhausted. This fact is explained by an increase in the contact time between the adsorbate and the adsorbent, which allowed a higher adsorption capacity and a longer service time of the bed to be achieved. However, the bed was exhausted faster given that the rate of mass transfer

increased at higher flow rates, which could be explained by the lower residence time of the adsorbate inside the fixed-bed column leading to a shorter contact time between the metal and the adsorbent, resulting in a decrease in the breakthrough and exhaustion times. Figure 4.18 shows that in the case of a lower flow rate, the adsorption zone was greater and the contact time was longer, resulting in greater efficiency.

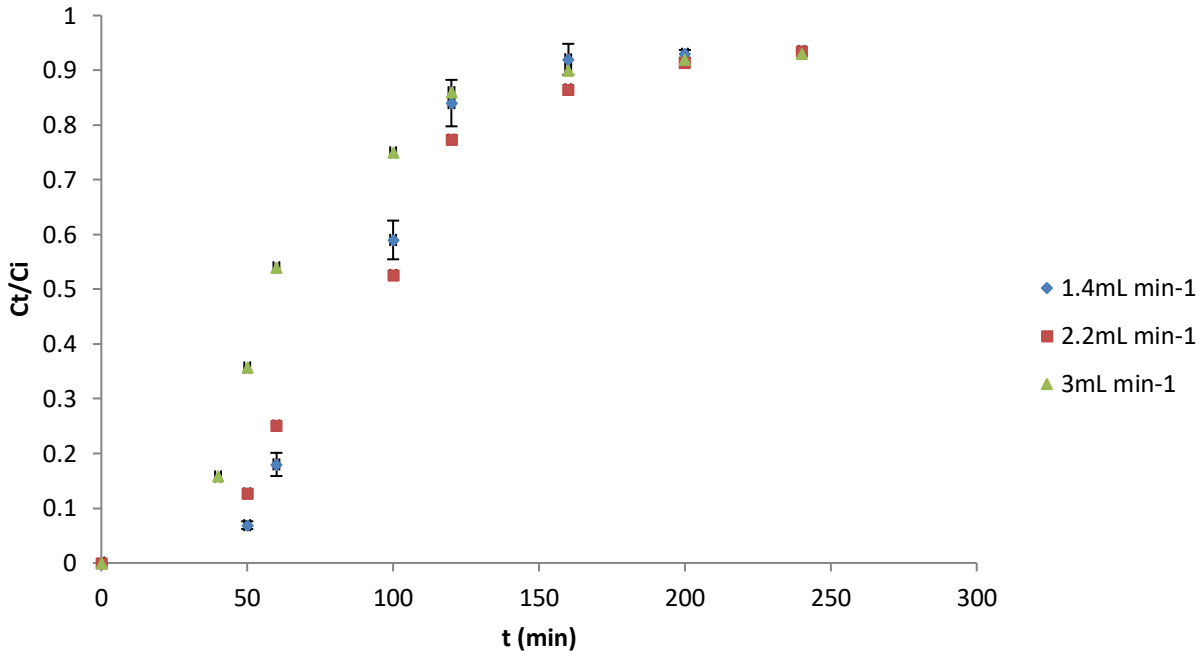

Figure 4.18. The effect of the flow rate on the adsorption of Pb(II) in a fixed bed column filled with pine cone: C_i=50 mg L^{-1}, bed height=0.7 cm, pH=5.6 (n=2).

Table 4.6. Column performance data at a constant bed height (0.7 cm) and an initial concentration of 50 mg L^{-1} of Pb(II).

Flow rate (mL min^{-1})	t_b (min)	t_s (min)	V_e (mL)	V_b (mL)	$t_ƨ$ (min)	t_f (min)
1.4	40	155	341	88	115	40
2.2	40	150	340	80	160	40
3	30	150	330	66	120	30

4.3.2.2. Bed height effect on the removal of Pb(II)

Bed height was varied from 0.5 cm to 1 cm to assess the impact of this parameter which corresponds to 0.15 g and 0.33 g of the biosorbent, respectively. As can be seen from Figure 4.19, the mass transfer zone MTZ increases with increased bed height, resulting in greater mass transfer at 1 cm of height and, hence, a longer exhaustion time. In contrast, the decrease in the amount of adsorbent resulted in a higher exhaust time. A lower amount of adsorbent results in an insufficient contact time between the solute and the adsorbent, reducing the diffusion of the solute inside the adsorbent and so the saturation of the bed is faster due to the greater movement of the MTZ. Table 4.7 shows the results of the breakthrough and exhaustion times obtained from different bed heights. At longer column lengths, exhaustion is difficult. Furthermore, breakthrough and exhaustion times (t_b and t_e) and breakthrough and exhaustion volumes (V_b and V_e) increased with increasing bed depth. Similar results were obtained on the removal of various contaminants from synthetic wastewater by a fixed-bed column (Patel, 2020). We can conclude that an earlier breakthrough point is attained due to the lower bed height and that there is a sharp increase after the breakthrough point due to the exit of MTZ. Hence, the removal efficiency of Pb (II) improved with increased bed height.

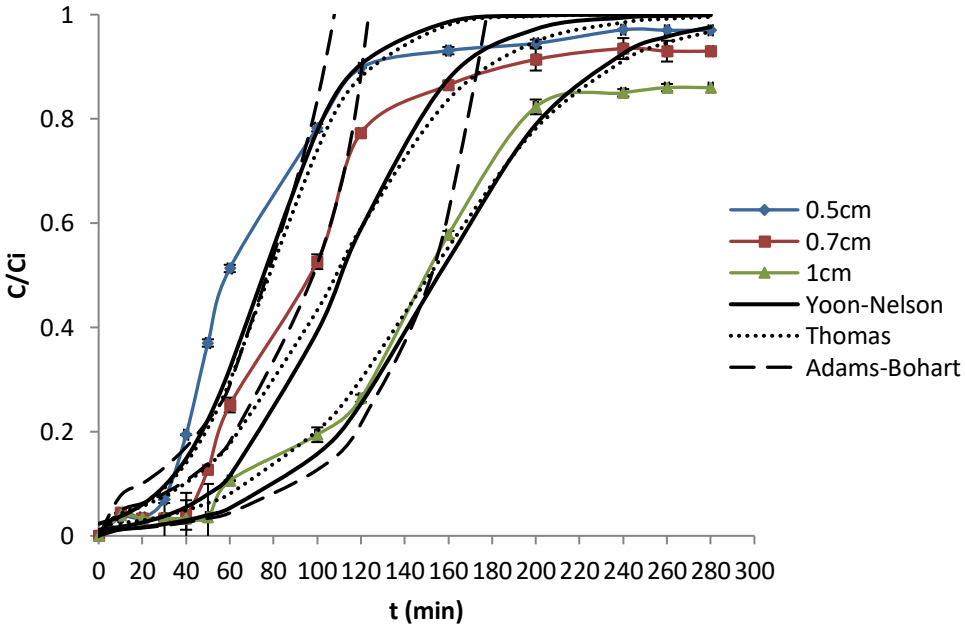

Figure 4.19. Effect of the bed height on Pb (II) adsorption in a fixed-bed column packed with pine cone: C_i=50 mg L^{-1}, flow rate=2.2 mL min^{-1}, pH=5.6 (n=2).

Table 4.7. Data of the performance of the fixed bed column system for Pb(II) adsorption at different bed heights, a constant flow rate of 2.2 mL min^{-1} and an initial Pb(II) concentration of 50 mg L^{-1}.

Bed height (cm)	Amount of adsorbent (g)	t_b (min)	t_s (min)	V_e (mL)	V_b (mL)	$t_ƨ$ (min)	t_f min)
0.5	0.15	25	160	352	55	135	25
0.7	0.23	40	200	440	88	160	40
1	0.33	50	230	506	110	180	50

4.3.2.3. The effect of the initial metal concentration on the Pb(II) adsorption

The effect of the initial metal concentration was studied at different values from 20 to 100 mg L^{-1}. The results are shown in Figure 4.20. As we can see from this figure, the increase in the initial metal concentration causes a decrease in the removal efficiency due to the fast saturation of the adsorbent as the available sites to bind metal ions become scarcer. In the case of lower concentrations the diffusion rate of metals takes a longer time to reach the saturation providing greater removal efficiency. Moreover, the breakthrough and exhaustion time and breakthrough and exhaustion volume decreased when the initial metal concentration increased which shows the saturation of the adsorbent in few time (Table 4.8). The adsorption capacity of pine cone for Pb (II) was higher with higher concentrations resulting in a greater driving force to overcome the mass transfer resistance of the metal ions in the solution leading to a greater contact between the metal ions and the available sites on the adsorbent surface.

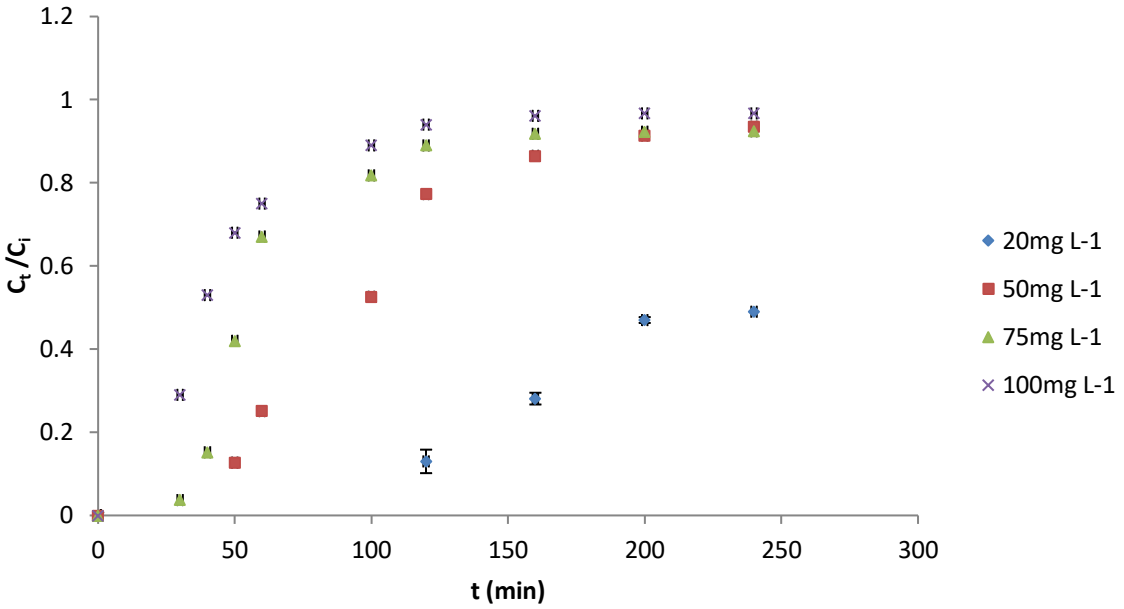

Figure 4.20. Effect of the initial Pb(II) concentration on the performance of the fixed bed column system: flow rate=2.2 mL min^{-1}, bed height=0.7 cm, pH=5.6 (n=2).

Table 4.8. Data of the performance of the fixed bed column system for Pb(II) adsorption at different initial metal concentrations, a flow rate of 2.2 mL min^{-1} and a bed height of 0.7 cm.

Initial Pb(II) concentration (mg L^{-1})	t_b (min)	t_s (min)	V_e (mL)	V_b (mL)	$t_ƨ$ (min)	t_f (min)
20	100	220	484	220	120	100
50	40	200	440	88	160	40
75	30	140	308	66	242	30
100	20	120	264	44	100	20

4.3.2.4. Modeling breakthrough curve

Different models such as the Adams and Bohart, Yoon-Nelson, and Thomas models have been applied to characterize the adsorbent–adsorbate system dynamic behaviour in fixed bed column and to calculate the related kinetic parameters. Mathematical models allow the determination of the sorbent capacity and operating life span as well as provide information about the process mechanism. Mathematical correlations for adsorption in fixed-bed columns are based on the

assumption of axial dispersion, external mass transfer, intraparticle diffusion and nonlinear isotherms (Patel, 2019).

4.3.2.4.1. Adams-Bohart model

The Adams-Bohart model also named as Bed Depth Service Time (BDST) is applied to check the dynamic behavior of the column and assumes that the adsorption rate is proportional to both the residual capacity of the adsorbent and the concentration of the adsorbing species. This model describes the relationship between the bed heights with the service time of the column as:

$$\ln(\frac{C_t}{C_i}) = K_{AB}C_i t - K_{AB}N_0\frac{Z}{F} \qquad (4.5)$$

C_i and C_t are the metal ion concentration of influent and effluent outlet respectively (mg L^{-1}), K_{AB} is the kinetic constant (L mg^{-1} min^{-1}), N_0 is the sorption capacity of the sorbent (mg L^{-1}), Z is the bed height of the sorbent in the column (cm), and F is the linear flow rate of the liquid phase (cm min^{-1}).

Table 4.9 shows the parameters obtained from Adams-Bohart model. The results indicate that with increasing metal concentration and flow rate, the kinetic constant K_{AB} decreases and the volumetric sorption capacity, N_0 increases. The competition between the metals towards the functional groups of the biosorbent increases at higher metal concentrations resulting in the saturation of the biosorbent. At higher bed heights N_0 decreases given that there are more amount of sorbent and , hence, more available sites to bind the metal ions.

4.3.2.4.2. Thomas model

This model is based on the assumption of Langmuir kinetics of reversible adsorption-desorption following second-order reversible reaction kinetics and no axial dispersion in the column. The model allows the calculation of the maximum adsorption capacity and of the rate constant from:

$$\ln(\frac{C_i}{C_t} - 1) = \frac{K_{Th}q_0 m}{Q} - K_{Th}C_i t \qquad (4.6)$$

In the K_{Th} Thomas model constant (mL min^{-1} mg^{-1}), q_0 is the adsorption capacity (mg g^{-1}), m is the amount of adsorbent (g), and Q indicates the flow rates (mL min^{-1})

The parameters K_{Th} and q_0 were calculated from the slope and intercept of the linear curve and are presented in Table 4.9. The good fitting of the Thomas model with the experimental breakthrough curve in all the tested conditions is shown by the determination coefficient (R^2) which is ranging from 0.73 to 0.96.

As can be seen in this table, the adsorption capacity, q_0 increases with increasing the initial metal concentration whereas q_0 decreases with the bed height. By increasing the flow rate, the adsorption capacity decreases as a result of a reduction of the contact time between the metal ions and the adsorbent at higher flow rates. The greatest adsorption capacity for Pb(II), 77.92 mg g^{-1}, was obtained when the bed height was 0.7 cm; the initial metal concentration, 75 mg L^{-1}; and the flow rate, 2.2 mL min^{-1}. The K_{Th} values decreased with decreased flow rate and increased with greater bed height. The decrease in K_{Th} as the concentration rises is as a result of the system being controlled by external mass transfer at the initial part of the column.

The Thomas model was applied to express the experimental data of Cd(II) and Pb(II) removal using grape stalk waste with adsorption capacities of 33.12 and 56.11 mg g^{-1}, respectively (Miralles et al., 2010). Another study shows that the Thomas model is the best one to fit the data for Cu(II) and Cr(VI) removal using almond shell with capacities of 2.39 and 21.92 mg g^{-1} in the following conditions 7 cm of bed height, a flow of 3 mL min^{-1} and initial concentration of 67.54 mg L^{-1} (Yahya et al., 2020). Moreover, sugarcane bagasse was used to remove Cd(II) and Pb(II) and the results obtained show good agreement with the Thomas model with adsorption capacities of 0.143 and 0.133 mg g^{-1} (Vera et al., 2019). Watermelon rind in a fixed bed column was able to remove Pb(II) with an adsorption capacity of 50.3 mg g^{-1} with 1 mL min^{-1}, 5 cm of bed height and an initial metal concentration of 500 mg L^{-1} (Lakshmipathy and Sarada, 2015).

4.3.2.4.3. Yoon-Nelson model

This model does not take into consideration the properties of adsorbate and adsorbent assuming that the decrease in the rate of metal adsorption is directly related to adsorbate adsorption and breakthrough of the adsorbent. This is due to describe practical industrial adsorption processes. The linear equation of this model was expressed below:

$$\ln\left(\frac{C_t}{C_i - C_t}\right) = K_{YN}t - \tau K_{YN} \qquad (4.7)$$

where t is the operating time (min), K_{YN} is the constant of proportionality of the Yoon-Nelson model (min^{-1}) and τ is the time (min) required to retain 50% of the initial adsorbate.

The Yoon-Nelson model parameters and the values of R^2 in the different operational tested conditions are set out in Table 4.9. The results show that K_{YN} decreased with increasing initial metal concentration, bed depth and flow rate. Whereas, the value of τ decreased with increasing metal concentration, this is due to the competition of the metal ions for the available sites of the adsorbent. It can be concluded that the time required for 50% metal breakthrough decreases at higher concentrations.

However, the time (τ) required to retain 50% of the initial metal concentration increased with the bed depth as a result of the presence of more available sites for the metal ions on the surface of the biosorbent. The good fitting of the Yoon-Nelson model with the experimental breakthrough curve in all the tested conditions is shown by the determination coefficient (R^2) which is ranging from 0.72 to 0.96, the same values obtained with the Thomas model.

In different studies on the removal of Pb(II) with agricultural wastes onto a fixed bed column, the results obtained followed both Thomas and Yoon-Nelson models (Miralles et al., 2010; Lakshmipathy and Sarada, 2015; Vera et al., 2019).

Table 4.9. Parameters of Adams-Bohart, Thomas and Yoon-Nelson models calculated from the data obtained from Pb(II) adsorption by pine cone in a fixed-bed column system .

Initial concentration (mg L^{-1})	**Flow rate (mL min^{-1})**	**Bed height (cm)**	**Adams-Bohart**			**Thomas**			**Yoon-Nelson**		
			K_{AB} (L mg^{-1} min^{-1})	**N_0 (mg L^{-1})**	**R^2**	**K_{Th} (mL min^{-1} mg^{-1})**	**q_0 (mg g^{-1})**	**R^2**	**K_{YN} (min^{-1})**	**τ (min)**	**R^2**
20	2.2	0.7	1.38	13.4	0.82	1.54	39.06	0.84	0.029	221.4	0.84
50	2.2	0.7	0.28	32.33	0.73	0.56	59	**0.91**	0.028	110.06	0.81
50	1.4	0.7	0.46	18.06	0.72	0.76	40.51	0.86	0.05	114	0.89
50	3	0.7	0.39	38.9	0.53	0.67	77.49	0.74	0.035	115	0.72
50	2.2	0.5	0.24	39.9	0.63	0.55	71.73	0.87	0.03	91	0.87
50	2.2	1	0.29	24.35	0.92	0.48	56.05	**0.96**	0.026	156.07	**0.96**
75	2.2	0.7	0.18	42.34	0.57	0.34	77.92	0.74	0.027	97.93	0.74
100	2.2	0.7	0.1	50.16	0.44	0.26	57.39	0.73	0.026	60.71	0.74

4.3.3. Competitive biosorption between Cd(II), Cu(II) and Pb(II)

The good performance of milled pine cone to remove toxic metals from aqueous effluents makes it a suitable biosorbent to be applied to separate these pollutants from industrial effluents. The competitive adsorption between Cu(II), Cd(II) and Pb(II) onto pine cone was studied at initial concentrations of 25 mg L^{-1}, 50 mg L^{-1}, and 100 mg L^{-1} of each metal (Fig. 4.21). As we can see from this figure, the breakthrough point and the exhaustion time decreased with increasing initial metal concentration, this is explained by the competition of the three metal ions for the functional groups on the adsorbent surface which resulted in its saturation. In the case of the initial concentration of 25 mg L^{-1}, Cd(II) has the lowest breakthrough and exhaustion times followed by Cu(II) and Pb(II), which indicates that Cd(II) was the first metal to occupy the available sites and to pass through the column due to its lower affinity for pine cone. These results agree with those of the batch experiments as the removal percentages were of 92.56% for Pb(II), 89.9% for Cu(II), and 82% for Cd(II). Moreover, the figures show a greater mass transfer at lower metal initial concentration resulting in a more quickly saturation of the fixed bed column whereas earlier breakthrough time and exhaustion time are achieved at higher concentration. When $C_t/C_i=1$, the column feed was completely in equilibrium with all metal ions adsorbed on the biosorbent. The same behavior and affinity order, Pb(II)>Cu(II)>Cd(II), was observed when aerobic granule sludge was used as adsorbent in a fixed bed column system for the removal of these three metal ions from a multi-metal aqueous solution (Trung and Ping, 2014).

At initial concentrations of 50 and 100 mg L^{-1} with a bed height of 1 cm, and a flow rate of 2.2 mL min^{-1}, breakthrough and exhaustion times of Cu(II) and Cd(II) are similar whereas they differ from those of Pb(II). The slow passage of lead through the column led us to conclude that this metal had the greatest affinity to pine cone and the presence of other metals, such as Cu(II) and Cd(II), does not affect the percentage of Pb(II) adsorbed, proving the absence of competition of Pb(II) with the other two metal ions in the tested conditions and indicating that pine cone is able to treat multi-metal effluents. The greater affinity of milled pine cone to Pb(II) can be explained by its lower degree of hydration and hydration radius as well as by its highest ionic radius and covalent index in comparison with Cu(II) and Cd(II).

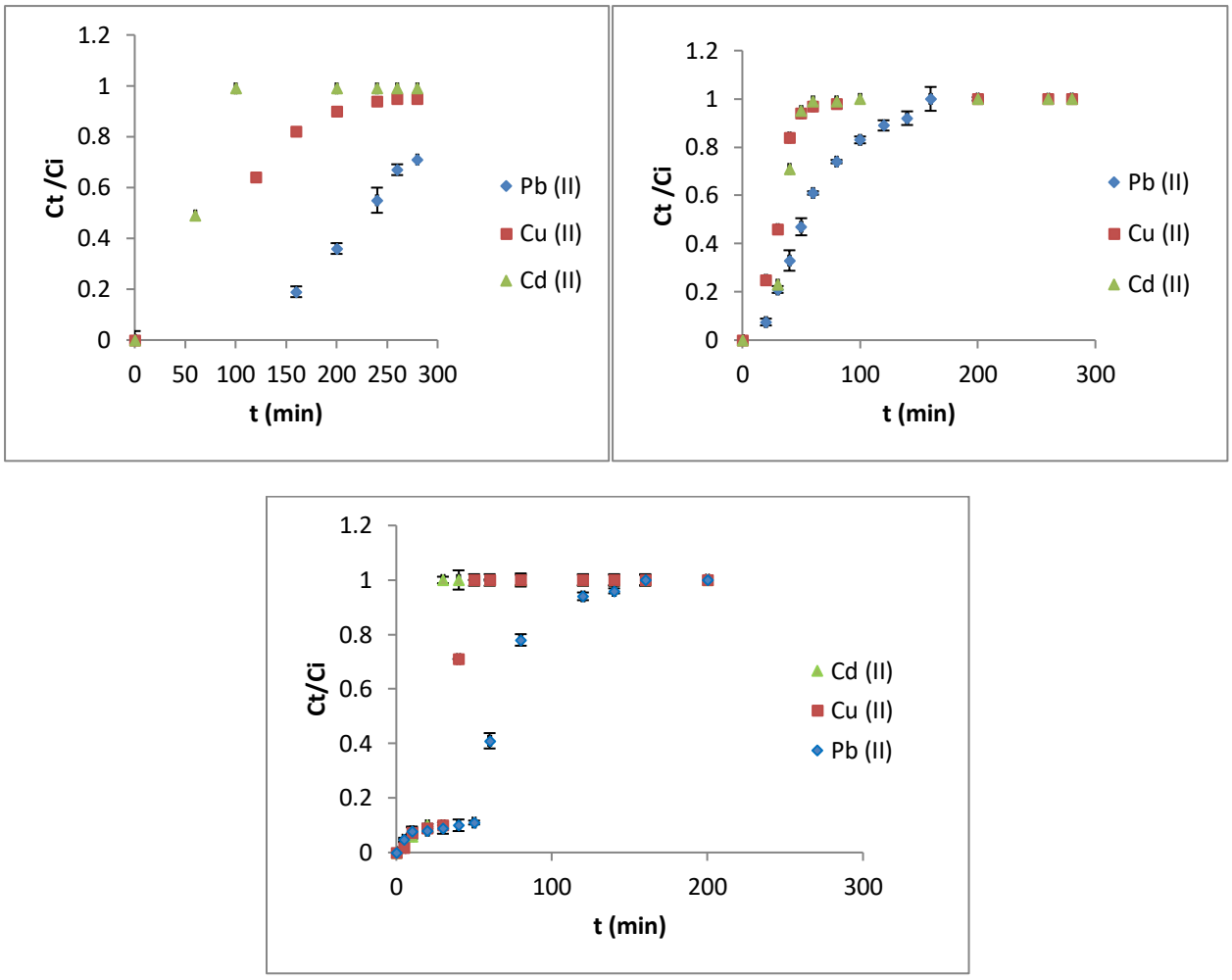

Figure 4.21. Adsorption of Cu(II), Cd(II) and Pb(II) by pine cone in a fixed-bed column system: C_i=25 mg L^{-1} (a), 50 mg L^{-1} (b), 100 mg L^{-1} (c), bed height=1 cm, pH=5.6, flow rate=2.2 mL min^{-1} (n=2).

4.3.4. Competitive adsorption of Cu(II), Pb(II), Cd(II), and Ca(II) by milled pine cone in a fixed bed column

The adsorption of the three heavy metal ions in the presence of soft divalent cations such as Ca (II) at pH 5.6 has been evaluated using a 1 cm bed height of pine cone and a flow rate of 2.2 mL min^{-1} (Figure 4.22). Equal initial metal concentrations for Cd(II), Cu(II), and Pb(II) were of 50 mg L^{-1} whereas for Ca(II) it was of 100 mg L^{-1}. From the results obtained, it is seen that Ca(II) is not adsorbed by milled pine cone when the other metal ions are present and that the adsorption of Cu(II), Cd(II) and Pb(II) is not affected by Ca(II). The adsorption of Pb(II), Cu(II) and Cd(II) ions seems to take place through surface complexation due to the presence of hydroxyl and

carboxylic functional groups that act as ligands rather than through electrostatic interactions between the metal ions and the negatively charged sites of pine cone due to the deprotonation of the functional groups (Amar et al., 2021).

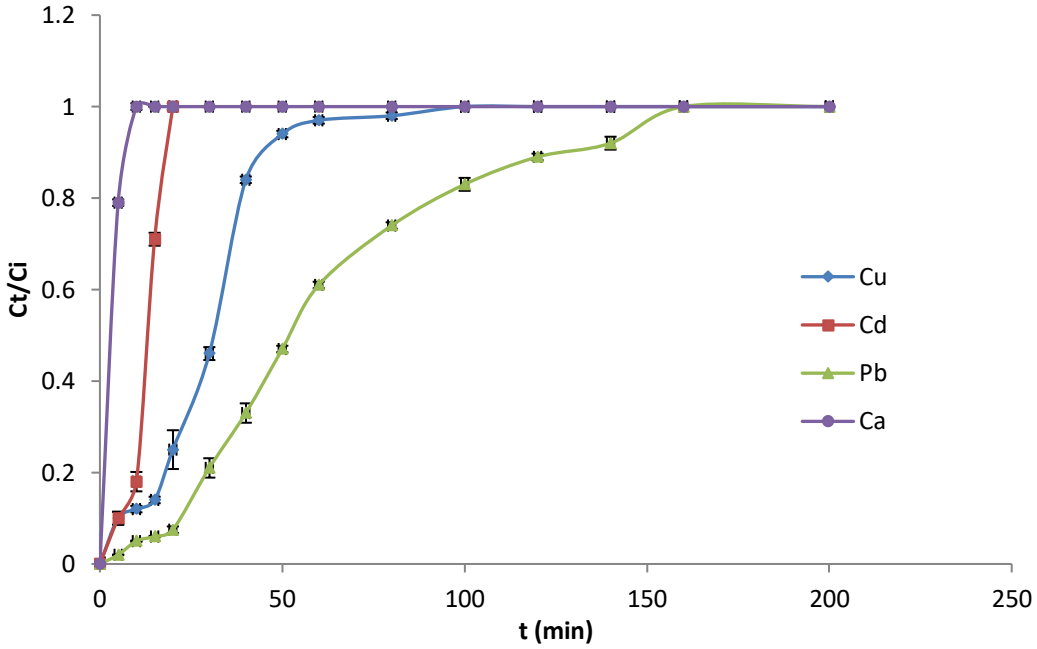

Figure 4.22. Competition of metal ions with calcium in a fixed bed column filled with pine cone: flow: 2.2 mL min^{-1}, bed height: 1 cm, C_i=50 mg L^{-1} for Cd(II), Cu(II), Pb(II) and C_i=100 mg L^{-1} for Ca^{2+}, pH=5.6 (n=2).

4.3.5. Adsorption of Cu(II), Cr(VI) and Ni(II) from simulated electroplating effluents

The efficiency of a biosorption process not only depends on the properties of the adsorbent but also on the composition of the wastewater. The type of metal ions found in effluents is highly dependent on the industrial processes that are treated by the plant. In the case of electroplating industries, the effluent is mainly composed of Cu(II), Ni(II) and Cr(VI) at pH=4.4. Agricultural residues such as *Syzygium cumini* and *Populus deltoids* leave powder that have been used for the biosorption of metal ions from electroplating industrial effluents (Kaur et al., 2013). Taking into account the affinity of milled pine cone for these metal ions, their separation in dynamic conditions at laboratory scale using a column with a fixed bed of 2 cm of pine cone and a flow rate of flow rate 2.2 mL min^{-1} has been evaluated. An aqueous solution simulating the composition of electroplating effluent containing 20 mg L^{-1} of Cu(II), 30 mg L^{-1} of Cr(VI), and

100 mg L^{-1} of Ni(II) at pH 4.4 was prepared (Singh and Ram, 2016). Figure 4.23 shows the breakthrough curves of the three metal ions obtained in the above mentioned experimental conditions. Cr(VI) due to their lower affinity for pine cone at pH >2 broke through the column faster than Cu(II) and Ni(II). Moreover, Ni(II) broke through the column faster than Cu(II) at 30 min. Cu(II) was the last metal to break through the column at 80 min, indicating its higher affinity for the biosorbent. At 20, 80 and 240 min the concentrations of Cr(VI), Ni(II), and Cu(II), at the column effluent reached the equilibrium point (C_t/C_i=1).

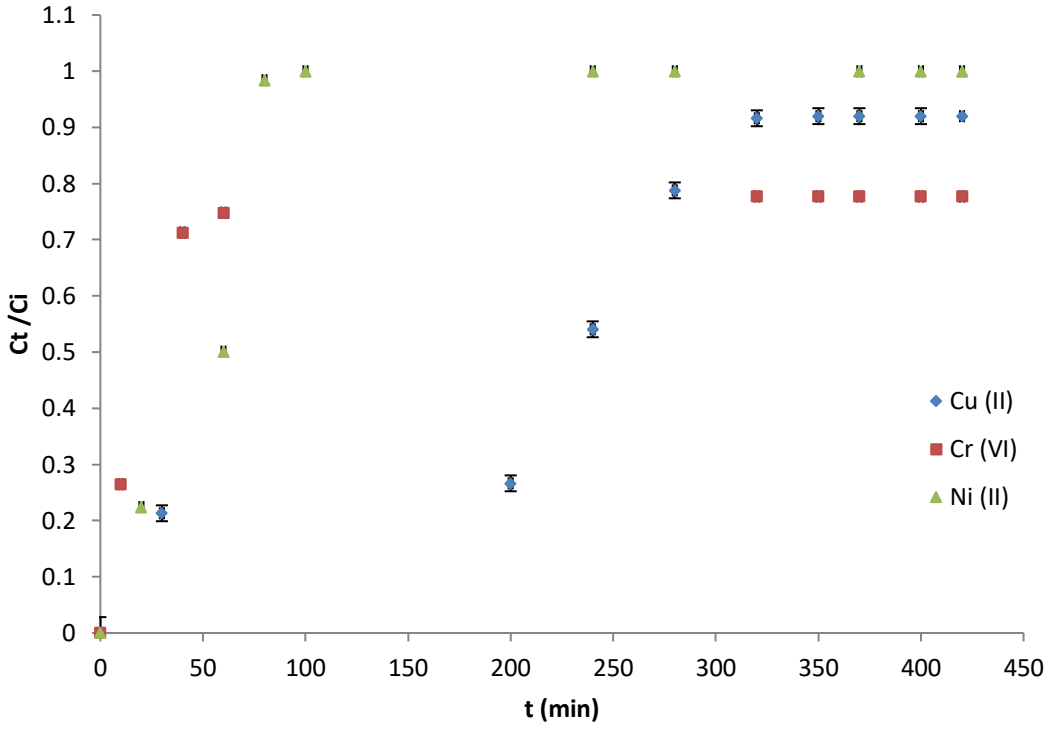

Figure 4.23. Breakthrough curves in a fixed bed column filled with pine cone (bed height= 2 cm, flow rate= 2.2 mL min^{-1}) for treating electroplating effluent composed of 20 mg L^{-1} of Cu(II), 30 mg L^{-1} of Cr(VI), and 100 mg L^{-1} of Ni(II) at pH 4.4 (n=2).

The mechanism of multi-metal ions biosorption in the competitive system depends on the electronegativity and the ionic radius of the metal ion. Furthermore, Ni(II) and Cu(II) have higher electronegativity in comparison with Cr(VI) which proved their higher strong electrostatic attraction and their higher affinity. However, the ionic radius of Cu(II), Ni(II) and Cr(VI) are 0.73 Å, 0.69 Å and 0.62 Å. In this case, larger ions are preferably accumulated at the interface and may fit into a binding sites and bind several functional groups. The pH is a parameter that can

play an important role in the separation of these metals. In the case of Cr(VI), since it is an anion its adsorption is favored at low acidic pHs when the functional groups of the adsorbent are protonated thus, it broke through the column faster. The removal percentage of Cu(II), Ni(II) and Cr(VI) are 99%, 98% and 73%. Encapsulated *moringa oleifera* in a fixed bed column (bed height 25 cm and 1 mL min^{-1}) showed removal percentages of 70.57% for Co, 99.69% for Cu, 98.92% for Ni, 98.59% for Mn and 84.21% for Zn when an electroplating waste containing initial concentrations of 9.08, 5.32, 6.7, 116.08 and 24.15 mg L^{-1} of these metal ions was treated (Radhakrishnan et al., 2016). Another study shows that xanthated chitosan packed onto a fixed bed column, 20 cm of bed height and a flow rate of 5 mL min^{-1}, was able to remove Cr(VI) from electroplating wastewater and synthetic electroplating water with adsorption capacities of with 129.2 mg g^{-1} and 202.25 mg g^{-1}, respectively (Chauhan and Sankararamakrishnan, 2011).

4.3.6. Desorption of Cu(II), Ni(II) and Cr(VI) from pine cone in a fixed-bed column

The desorption studies are an important part that can prove the practical applicability of the dynamic adsorption process in term of the ability to reuse the adsorbent and recover the metals. After the metal ions were adsorbed using milled pine cone (Figure 4.24), experiments were performed to recover these pollutants. Thus, HCl (0.5M) was used to desorb Cu(II), Cr(VI) and Ni(II) from the fixed bed column, 2 cm of bed height, after performing the adsorption of these metals ions by passing through the column at a flow rate of 1.2 mL min^{-1} a solution containing initial concentrations of 20 mg L^{-1} of Cu(II), 30 mg L^{-1} of Cr(VI), 100 mg L^{-1} of Ni(II) at pH 4.4. Figure 4.24 shows the percentage of adsorption-desorption of these pollutants and Figure 4.25 showed the breakthrough curves of adsorption-desorption. Cu(II) and Ni(II) are removed most efficiently, 97% and 95% respectively, due to their higher affinity to milled pine cone whereas for Cr(VI) the removal percentage was 93%. Moreover, the desorption percentage was higher in the case of Cu(II) and Ni(II) with 94% in comparison with Cr(VI) that was of 90%. This results show that probably a more concentrate HCl solution is needed to elute these metal ions from the adsorbent as well as a higher contact time (lower flow rate). However, it was proved that a complete desorption of these metal ions could not be obtained with 0.5 N HCl, which might be due to the metal ions being trapped in the intrapores and therefore difficult their release (Kaur et al., 2013). Coconut shell was treated with HNO_3 1 mol L^{-1} to permit its reuse in the removal of metals. The results show that after desorption, the removal capacities of the adsorbent were

reduced by more than 50% for Pb(II), 70% for Ni(II), 67% for Cd(II), 76% for Zn(II) and 75% for Cu(II) (Sousa et al., 2010).

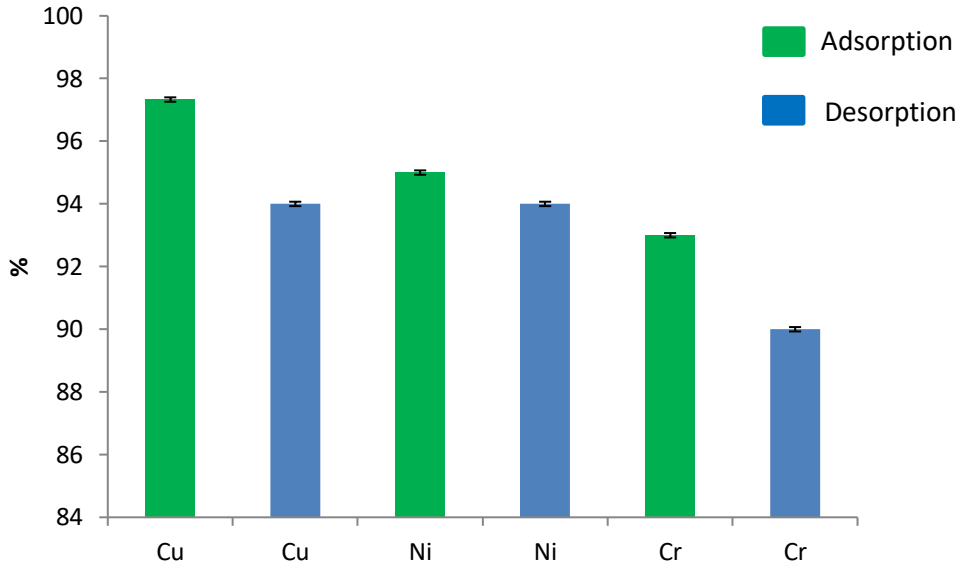

Figure 4.24. Adsorption-desorption percentages of Cu(II), Cr(VI) and Ni(II) in a fixed bed column filled with pine cone (2 cm of bed height). Aqueous solution composed of 20 mg L^{-1} Cu(II), 30 mg L^{-1} Cr(VI), and 100 mg L^{-1} Ni(II) at pH 4.4. Flow rate: 2.2 mL min^{-1} (n=2).

Hence, taking into account the low cost of pine cone and the difficulties in removing the metal ions from the adsorbent, it can be recommended to do not regenerate the adsorbent in the column and to replace it after exhaustion.

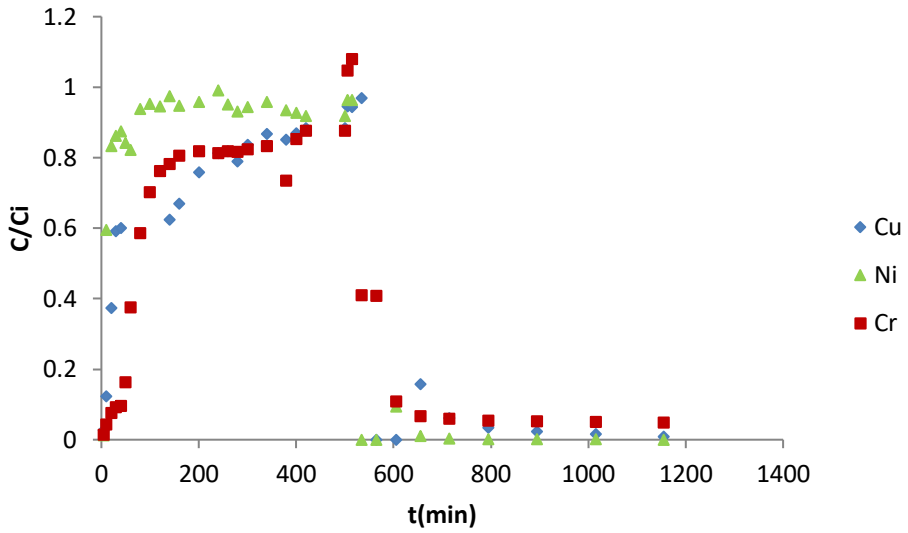

Figure 4.25. Breakthrough curves adsorption-desorption in a fixed bed column filled with pine cone (2 cm of bed height). Aqueous solution composed of 20 mg L^{-1} Cu(II), 30 mg L^{-1} Cr(VI), and 100 mg L^{-1} Ni(II) at pH 4.4. Flow rate: 2.2 mL min^{-1} (n=2). Desorption: 0.5M HCl, 1.2mL min^{-1}.

Dynamic adsorption in a fixed-bed column is an effective method for large scale treatment of water effluents due to cyclic adsorption/desorption. The effect of different parameters such as the initial adsorbate concentration, bed height and flow rate in the removal efficiency of Pb(II) by pine cone was evaluated resulting in an improvement with increased bed height and lower flow rates. The experimental data of Pb(II) removal agreed well with the Thomas model with an adsorption capacity of 77.92 mg g^{-1} at a flow rate of 2.2 mL min^{-1}, bed height 0.7 cm and an initial concentration of 50 mg L^{-1}.

For aqueous solutions containing equal concentrations (25 mg $L^{-1,}$ 50 mg L^{-1} and 100 mg L^{-1}) of Cu(II), Cd(II) and Pb(II), the highest exhaustion time was obtained for Pb(II), followed by Cu(II) and Cd(II), confirming the greater affinity of pine cone for this metal ion. The presence of other metals, such as Cu(II) and Cd(II), in the solution does not affect the percentage of Pb(II) adsorbed, proving the absence of competition in the tested conditions and indicating that pine cone is able to treat multi-metal effluents.

It was observed that the presence of soft meta ions such as Ca(II)does not affect the uptake of the Pb(II), Cu(II) and Cd(II) by pine cone, proving that surface complexation was the mechanism involved in the adsorption. Removal percentages of 97% for Cu(II), 95% for Ni(II) and 93% for Cr(VI) were obtained when a aqueous solution simulating the composition of an electroplating effluent was passed through a 2cm bed height fixed-bed column at a flow rate of 2.2 ml min^{-1}. Cr(VI) broke through the column faster than Cu(II) and Ni(II) as a result of its lower affinity for pine cone at pH >2. Ni(II) and Cu(II) broke through the column at 30 and 80 min, respectively. These results proved the capacity of pine cone to separate cations as Cu(II) (20 mg L^{-1}) and Ni(II) (100 mg L^{-1}) from anions as Cr(VI) (30 mg L^{-1}). After adsorption, a 0.5 M HCl solution was passed through the column to desorb the metal ions from milled pine cone. The higher desorption percentage was obtained for Cu(II) and Ni(II) with 94% comparison with Cr(VI) which was of 90%.

4.4. Removal of Cd(II), Cu(II) and Cr(VI) by Graphene Oxide

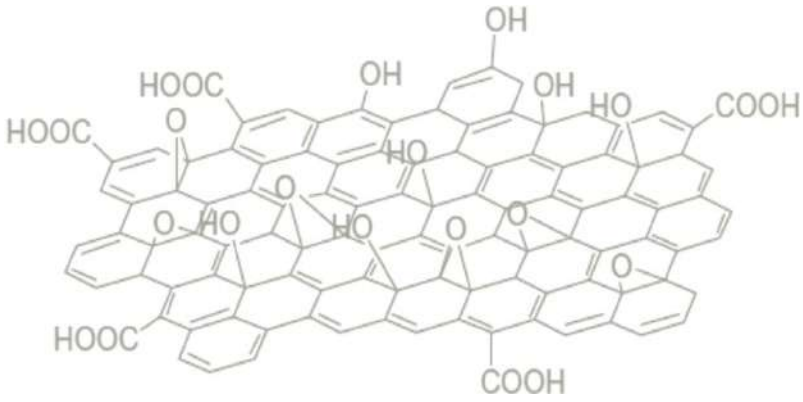

The presence of heavy metal ions in water is harmful to aquatic-life, the environment in general and to human health. Hence, the removal of the most toxic ions using efficient removal technologies such as adsorption is required. Graphene oxide, which is obtained by the oxidation of graphene, is considered to be a promising adsorbent for the removal of heavy metal ions such as Pb(II), Cu(II), Zn(II), Cd(II), and Co(II) (Peng et al., 2017). Several reviews have reported the affinity of GO and its composites for heavy metal ions, highlighting the characteristics of these materials and the adsorption mechanisms (Ahmad et al., 2020; Ali et al., 2019; Liu et al., 2019). The effect of the pH of the aqueous solution, contact time, temperature and the amount of adsorbent are the important parameters that finally affect the interaction mechanism of heavy metal ions with GO (Yu et al., 2015). This strong pH dependency has been shown in the case of Cd(II) and Co(II) sorption on GO nanosheets whereas a weak dependency has been found in the case of ionic strength (Zhao et al., 2011). Adsorption characterization of GO towards Cd(II), Pb(II), Cu(II) and Zn(II) have been investigated using powder X-ray diffraction (XRD), scanning electron microscopy (SEM), infrared spectroscopy (FT-IR) and X-ray photoelectron spectroscopy (XPS) (Sitko et al., 2013). The adsorption capacities of different GOs for metal ions are summarized in Table 1.4.

The commonly used method to synthesize GO is the Hummers and Offeman method (Hummers and Offeman, 1958), which uses concentrated sulfuric acid and potassium permanganate. Other researchers have used slightly changed methods but it is important to highlight that the prepared materials from these reactions exhibited strong differences, depending not only on the reaction conditions used, but also on the oxidants and graphite source. Despite these advances, the preparation of an efficient GO adsorbent by a low-cost, high quality and environmentally friendly manufacturing process is a challenging task. The researchers of the Chemistry Department of the Masaryk University (Brno, Czech Rep.) have investigated the preparation of graphenoids through a low-cost, green and fast synthetic route (Ševčík, 2020). These synthetic routes are not detailed here as they are under patent. Within the framework of our collaboration with this department, samples of four graphenoids, named GO-I, GO-II, 97 D and 227 A, are characterized and evaluated for the removal of divalent metal ions and chromate from aqueous solutions. Hence,

the aim of the present study is to investigate the capacity of these graphene oxides to remove cations such as Cu(II), Cd(II) and anions such as Cr(VI) from aqueous effluents and to characterize the adsorption isotherms and the adsorption mechanism and their relationship with the physical and chemical characteristics of the different GOs.

4.4.1. Graphene oxide characterization

The characterization of the graphene oxides was performed using different analytical techniques. Elemental analysis in volume, XPS and XRD analyses were performed at Masaryk University whereas FTIR, SEM, EDX and TGA/DTA were done at the University of Girona. The technical services of the University of La Laguna and University of Barcelona determined the surface area and porosimetry of 97D, 227 A and GO-I.

GO-I (Graphene Oxide – Type I (GO-I) **C_8O**) was prepared from graphite using an oxidizing system of type I, which resulted in a moderated oxidized GO (oxygen content ~ 13 %). It features large carbon layers with very low levels of damage as a consequence of being used in a mild oxidizing system and the oxygen-containing groups are mostly present on the edges of some of the carbon layers.

GO-II (Graphene Oxide – Type II (GO-II) **$C_{16}O$**) very moderately oxidized GO (oxygen content ~ 7.5 %) prepared from graphite using the type II oxidizing system.

In an attempt to introduce nitrogen-containing functional groups, GO-I and GO-II were treated with amines. The graphene oxide 97D was prepared from GO-I using polyamines and 227 A was prepared from GO-II by chemical treatment with an amine. However, after performing elemental analysis of both graphene oxides, nitrogen was not detected by elemental analysis and FTIR spectra did not show the corresponding bands. XPS results revealed that the percentage of C=O groups after this chemical treatment increased from 1.76 in GO-II to 3.06 in 227A, while the percentage of C=O slightly decreased from 2.62 in the case of GO-II to 2.40 in 97D (Table 4.10).

Table 4.10. Results of elemental and XPS analyses of graphene oxides. XPS results: particular peak area ratio corresponds to relative abundance (%) of the respective functional groups. * Total C≈O groups (%) (Ševčík, 2020).

GO	Elemental Analysis	XPS C=C(%)	XPS C-C(%)	XPS C-O(%)	XPS C=O(%)	XPS (C(O)-O(%)	XPS C≈O (%)*
GO-I	~86.5% C 13.0% O	61.96	23.66	6.69	2.62	2.69	12.00
GO-II	~92.0% C 7.5% O	63.72	24.10	5.38	1.76	4.71	11.85
97 D	~92%C 7% O	53.44	34.95	6.21	2.40	2.99	11.60
227 A	~93.6% C 5.3 % O	60.66	27.31	6.30	3.06	3.20	12.56

FT-IR spectroscopy allows the characterization of the different types of functional groups formed in the GO. The FT-IR spectra for GO-I are shown in Figure 4.26. FTIR spectrum a) was recorded in the 2500-500 range, although this suffered from noise and the intensities are low, the bands of C=O stretching modes (carbonyl and/or carboxyl groups) in the region of ca 1610-1750 cm^{-1} can be deduced. In FTIR spectrum b), the bands in this zone cannot be observed but in the 1900-2400 cm^{-1} region a band is clearly observed in both spectra and in all the spectra of the four graphene oxides. Moreover, the band at 3550 cm^{-1} in FTIR spectrum b can be associated to O-H bond stretching. More information about the different types of functional groups in the graphene oxides was obtained by XPS spectroscopy (Table 4.10).

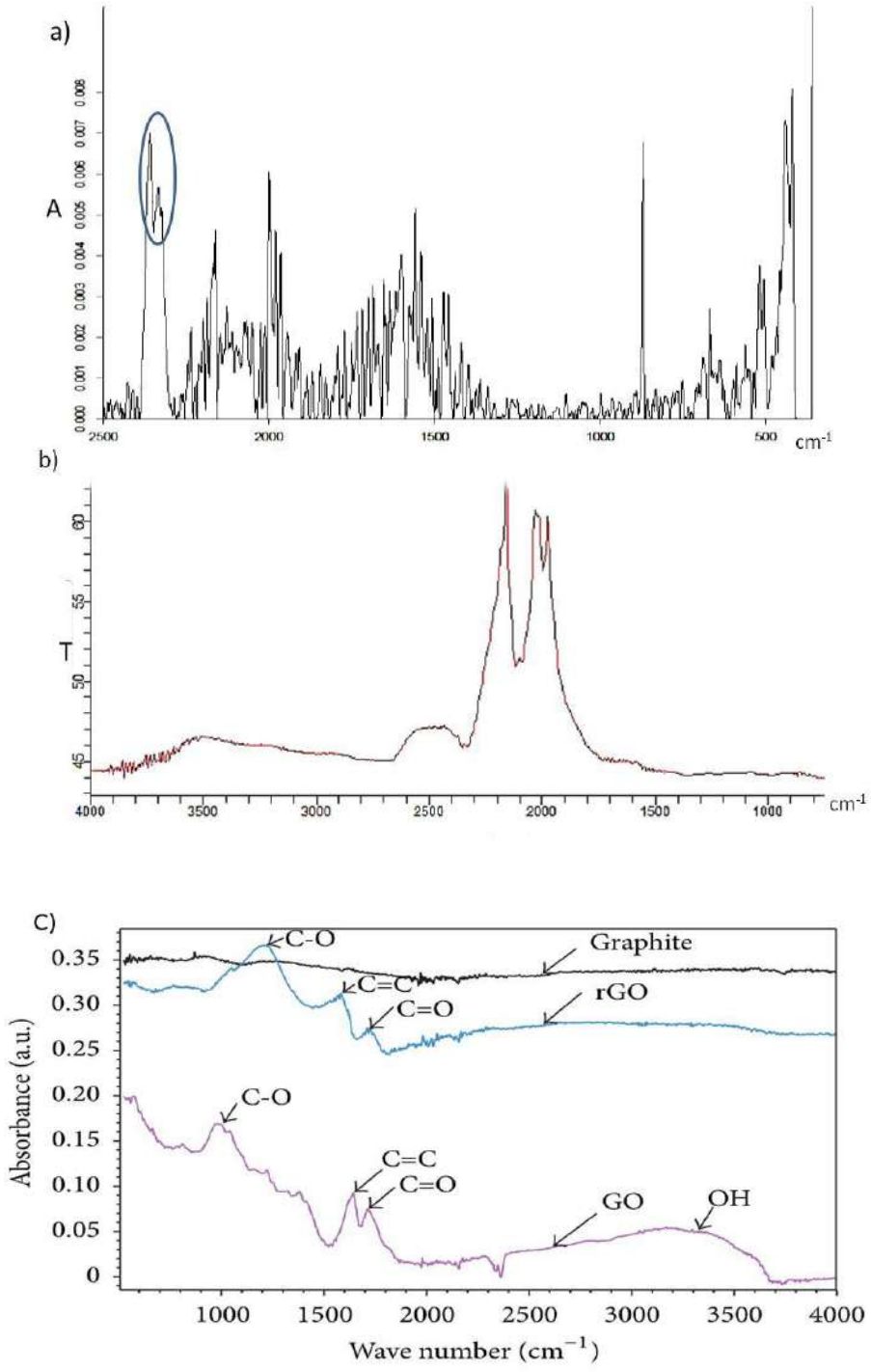

Figure 4.26. FTIR spectra of GO-I. a) FTIR spectrum recorded in the 500-2500 cm^1 range (Ševčík, 2020), b) FTIR spectrum recorded in the 1000-4000 cm^{-1}range, and c) FTIR spectra for graphene and graphene oxide with the most characteristic bands marked (Strankowski et al., 2016).

The XRD pattern of graphene oxide GO-I shows a diffraction peak at 2Φ = 26. 38º corresponding to an interlayer spacing of about ~ 0.34 nm. The intensity of this peak was reported to decrease when the oxidation levels of graphene increased (Krishnamoorthy et al., 2013). All the graphene oxides used in this study presented the same XRD pattern, showing that the oxidation levels were relatively low.

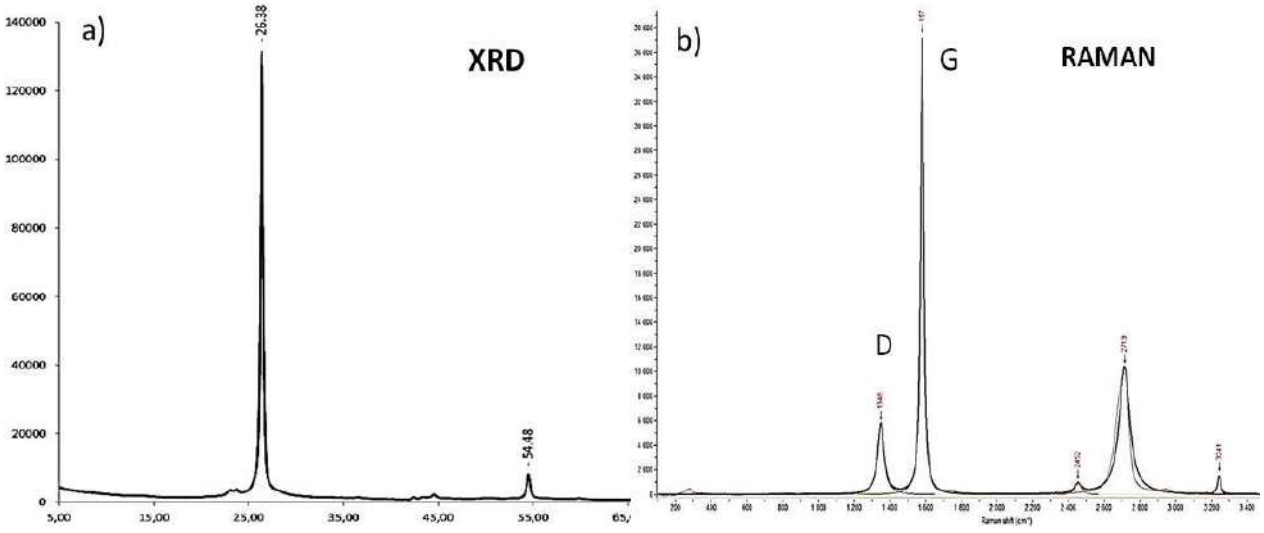

Figure 4.27. a) Diffractogram shows typical graphitic diffraction pattern with a prominent peak at ca 26.38° indicating no changes in interplanar distances caused by the presence of oxygen containing groups and defects in the graphene layers. b) Raman spectrum of GO-I: a low intensity band at ~ 1350 cm^{-1} (D band sp_3 carbon) indicates low damage of graphene layers. The band at ~ 1577 cm^{-1} (G band is assigned to sp_2 carbons) (Ševčík, 2020).

From the Raman spectrum, the possible defects presents in the graphene structure after performing the oxidation reaction for producing graphene oxides can be measured from the ratio of intensity of D/G bands. The G band is a result of in-plane vibrations of sp2 bonded carbon atoms whereas the D band is due to out of plane vibrations attributed to the presence of structural defects. When the spectra of graphene and graphene oxide are compared, GO will have a higher D band than graphene as GO has oxidative functional groups.

Figures 4.28, 4.29, and 4.30 show SEM images and surface composition determined by the EDX of each adsorbent. It can be seen that the composition of all the adsorbents is relatively similar, basically being composed of carbon, with percentages higher or around 88%, and oxygen, with percentages between 4 and 9%. These results are logical as the adsorbents are graphene oxides. The only exception is the adsorbent GO-I (Figure 4.30), where a remarkable percentage of tungsten (4.34%) was determined, which may have been a residue from the process of synthesis. The presence of tungsten explains the metallic appearance of this adsorbent in comparison with the other three adsorbents, which have a more carbonaceous appearance.

Table 4.11. Results of surface elemental analysis by EDX of the graphene oxides.

	C	O	Si	Al	Fe	S	Na	K	Mg	Ca
227 A	88.65	9.15	0.98	0.36	0.25	0.07	0.22	0.01	0.28	0.03
97 D	89.90	8.40	1.04	0.18	-	0.31	0.18	-	0.10	-
GO-I*	90.78	4.60	-	0.06	0.15	0.07	-	-	-	-
GO-II	94.23	4.27	0.52	0.21	0.31	0.15	0.10	-	0.18	0.04

*this adsorbent contained 4.34% of W (see Fig. 4.28).

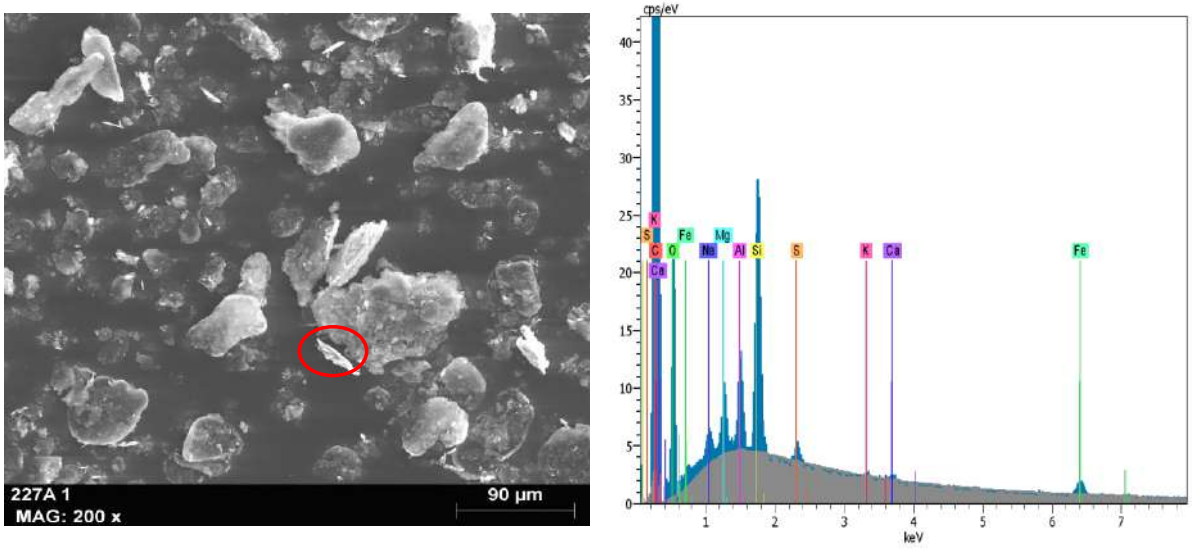

Figure 4.28. SEM image (227A sheet is marked in red) and EDX microanalysis of 227A.

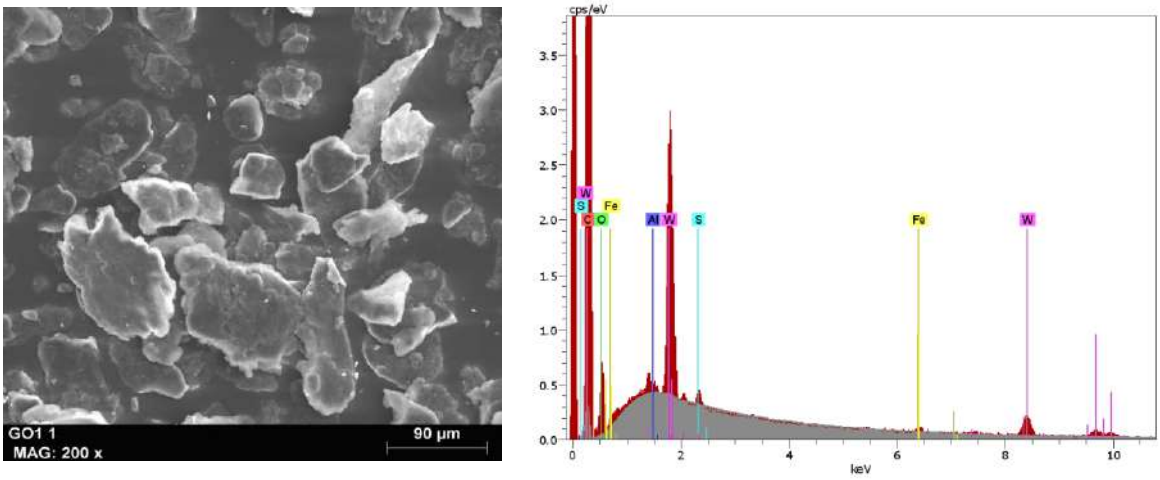

Figure 4.29. SEM image and EDX microanalysis of GO-I.

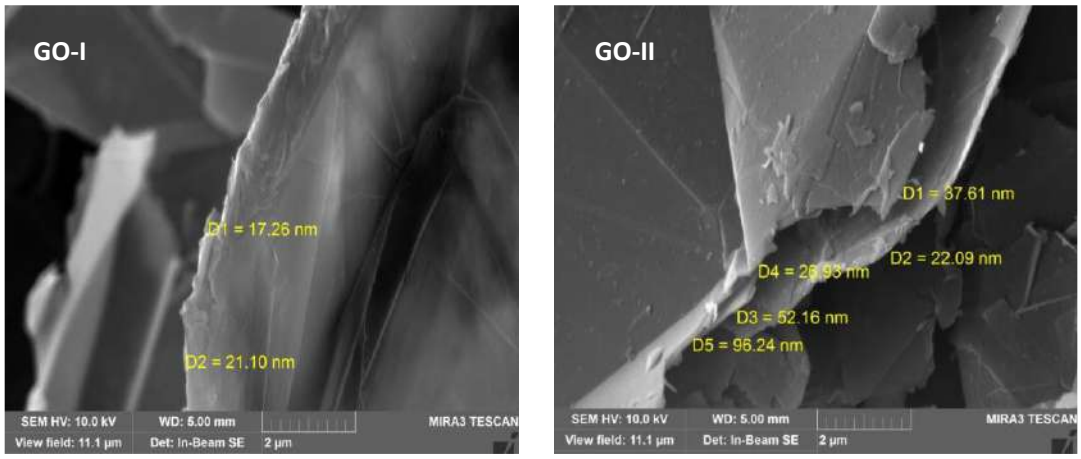

Figure 4.30. SEM image at 50.000 x showing the thickness and surface of graphitic oxides plates of GO-I and GO-II and plate size homogeneity (Ševčík, 2020).

Surface area and porosity are two properties of an adsorbent that can have an impact on their performance. These parameters for the graphene oxides: 97D, 227A and GO-I are presented in Table 4.12.

Table 4.12. Surface area and porosimetry of GOs.

Graphene	BET SA ($m^2 g^{-1}$)	Langmuir SA ($m^2 g^{-1}$)	BJH SA ($m^2 g^{-1}$)	Pore Volume ($cm^3 g^{-1}$)	Pore size (Å)
97 D	19.5917	26.9833	21.515	0.06347	129.5997
227 A	25.8041	35.5548	27.662	0.07389	114.5504
GO-I	14.2268	-	14.365	0.06996	196.7077

The surface areas are lower than those reported for different graphene oxides; however, the surface area values and the pore sizes depend on the synthesis method used and especially on the length of time spent in oxidizing the solution. Although the theoretical specific surface area of graphene is 2630 $m^2 g^{-1}$, the typical experimental values of the specific surface area for graphene oxides ranges from ~100 to ~1000 $m^2 g^{-1}$ (Dai et al., 2015).

Figure 4.31 shows the thermogravimetric analysis of 97D as a general representation of the other graphene oxides. In general, a loss of weight at low or moderate temperatures (up to 150ºC) corresponds to the loss of volatile components of the adsorbent, such as water, organic solvents of low molecular weight or absorbed gases. At temperatures between 150-250ºC the loss of components of low molecular weight, such as additives, water of crystallization or even first decomposition products at low temperatures, can be detected. Thermal degradation normally begins at temperatures above 225-250ºC and at temperatures above 500ºC, the carbonization of hydrocarbon compounds is produced. It can be seen that 97D is stable and does not suffer decomposition until temperatures of approximately 600ºC.

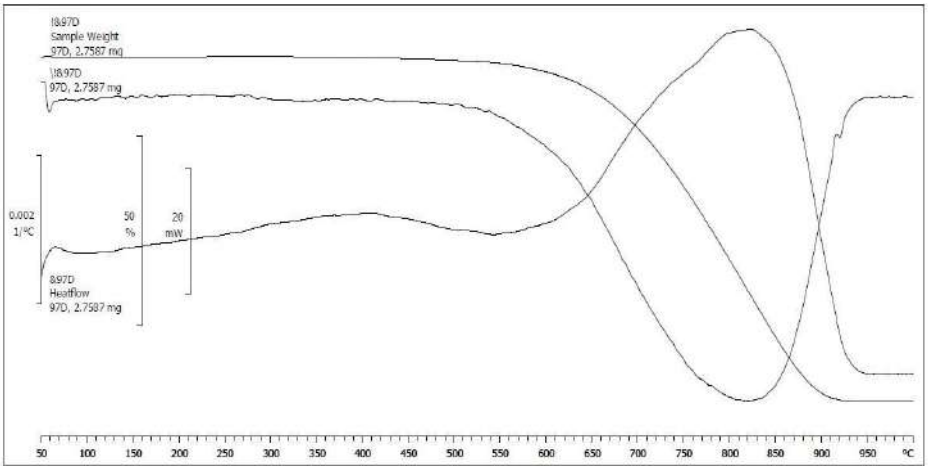

Figure 4.31. Thermogravimetric analysis of 97D.

4.4.2. Batch adsorption

Different experiments were performed in order to study the effect of adsorption parameters such as time, pH, amount of adsorbent, and initial metal concentration.

4.4.2.1. Effect of the contact time

The time needed for each metal and adsorbent to achieve equilibrium depends on the metal and adsorbent concentrations as well as on their chemical properties.

In the case of Cu(II) and Cd(II), it can be seen in Figure 4.32 that with an amount of sorbent (227A, 97D, GO-I, GO-II) of 2 g L^{-1} and an initial concentration of 5 mg L^{-1}, equilibrium is reached in 1 hour for three out of the four adsorbents. Only when adsorbent 97D was used, a time of 3 hours was needed to attain the equilibrium under the same conditions. In the case of Cr(VI) (Figure 4.33), an equilibrium time of 3 hours was required when an adsorbent concentration of 10 g L^{-1} (GO-I, GO-II) at pH=2 was used.

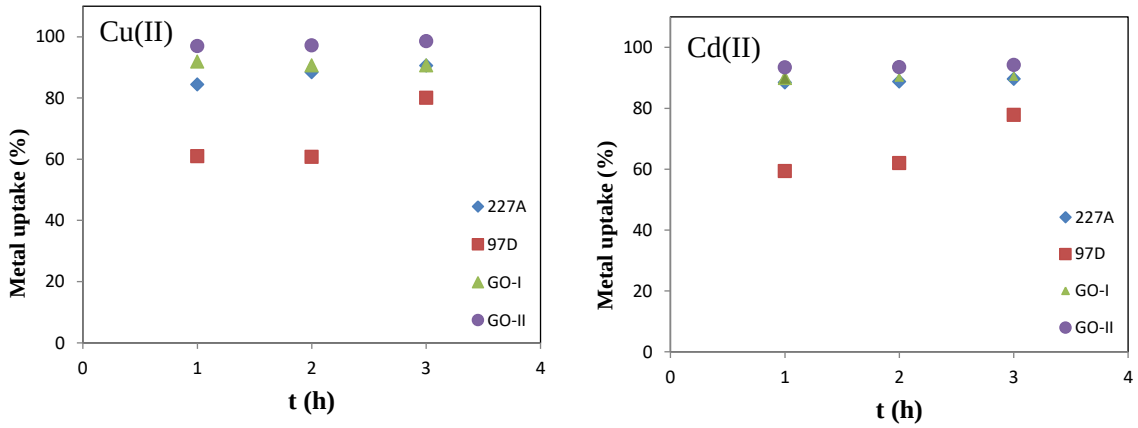

Figure 4.32. Effect of contact time on the adsorption of Cu (II) and Cd (II) for each graphene oxide. Adsorbent concentration= 2 g L^{-1}, initial concentration= 5 mg L^{-1}, pH=6. (n=3).

4.4.2.2. Effect of the adsorbent concentration

The amount of sorbent used in the batch experiments has an effect on the efficiency of the metal adsorption process. As can be seen in Figure 4.33, the adsorption percentage of Cu(II)and Cd(II)increased when the adsorbent concentration increased from 1 to 2 g L^{-1}. However, it showed a decrease when the amount was increased to 3 g L^{-1}. This result may be due to an aggregation of the sorbent that avoided the interaction of the functional groups of the adsorbent surface with the metal ions. The stability of GO sheets was reported to depend on the competition between repulsive electrostatic interaction and attractive, face-to-face Van der Waals interaction of overlapping sheets. As the zeta potential, which determines the value and sign of the effective surface charge density of GO, is pH-dependent, at pHs > pH_{PZC} electrostatic repulsion between GO sheets is reduced and they can form aggregates. The pH_{PZC} of graphene oxide was calculated from zeta potential analysis and reported to be of approximately 1.7 (Hu et al., 2015). For Cd(II), the results were assumed to be the same as for Cu(II) as they are both divalent ions.

In the case of CrO_4^{2-}, it was necessary to increase the amount of adsorbent to 10 g L^{-1} in order to obtain 68%, due to poor adsorption when working with low amounts. It is important to highlight that Cr (VI) adsorption was performed at pH 2 and although the concentration of adsorbent was increased the formation of GO sheet aggregates was not as significant as at pH 6. This fact

explains why Cu (II) adsorption percentage is reduced with a 3 g L^{-1} of adsorbent and for Cr (VI) there was not reduction when the concentration of adsorbent was increased until 10 g L^{-1}.

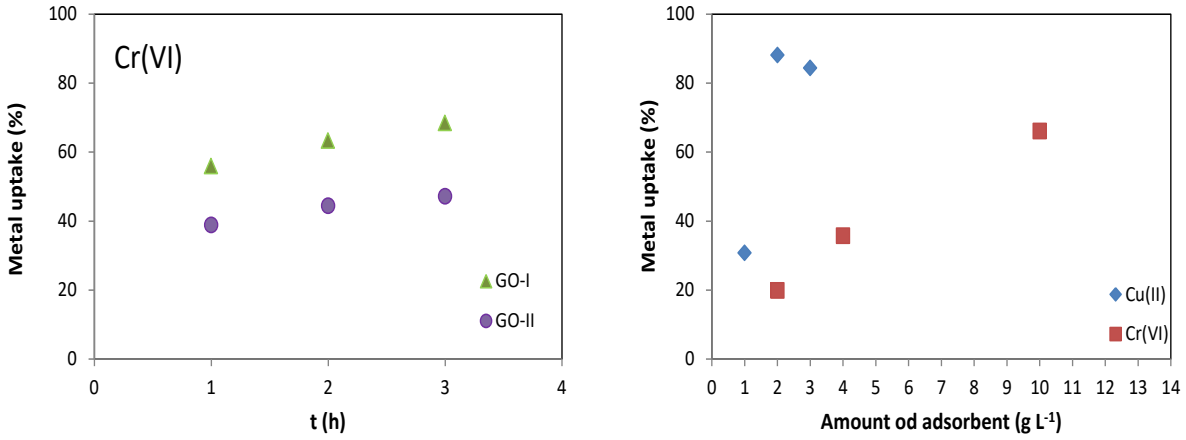

Figure 4.33. Effect of contact time on the adsorption of Cr (VI) for each graphene oxide, adsorbent concentration= 10 g L^{-1}, pH=2. (n=3) and effect of the adsorbent concentration on the adsorption of Cu^{2+} and CrO_4^{2-}. For Cu^{2+}, graphene 97D was used, 5 mg L^{-1} of Cu^{2+} at pH=6. For CrO_4^{2-}, sorbent GO-I was used, 5 mg L^{-1} of CrO_4^{2-} at pH=2. Equilibrium time: 3h. (n=3).

4.4.2.3. Effect of the pH of the aqueous solution

The pH of the metal ion solution has an important effect on the adsorption efficiency as the functional groups of the adsorbent can be protonated at low pH. The GOs used as adsorbents in this study consist of sheets with oxygen-containing functional groups on their basal planes and edges. These groups can be reversibly protonated under different pH values, rendering a pH-sensitive charge of GO. The isoelectric point (IEP or pI)/point-of-zero charge (pzc) provides a measure of the acid-base properties of these ionizable groups and, in turn, the surface charge behaviour as a function of the solution pH. At a pH above this value, the surface charge is mainly negative, while it is positive at and below it. Both processes, metal adsorption and charge transfer, are interfacial processes that are sensitive to the surface charge at the graphene-liquid interface (Hu et al., 2015).

Moreover, the metal ion can be hydrolysed at pHs > 6, depending on the metal ion. In the case of Cu(II), the formation of $Cu(OH)^+$ and the precipitation of $Cu(OH)_2$ start at pH= 6.5 (Figure 4.34) whereas in the case of Cd(II), the precipitation of $Cd(OH)_2$ occurs at pH>9. Thus, the effect of

the pH was studied at pHs, 2, 4 and 6. As can be seen in Figure 4.33, the percentage of Cu(II) adsorbed by graphene oxide 97 D increases when the pH increases. The adsorption of Cu(II) is pH dependent, and the removal efficiency increases when the pH increases. These results are explained by competition between Cu^{2+} and H_3O^+ for adsorption sites on the adsorbent. At low pH levels, an excess H_3O^+ competes with Cu^{2+}, resulting in a low level of adsorbed metal ion. When the pH increases, these functional groups are deprotonated and, hence, are available for this metal (Mi et al., 2012). In the case of Cd^{2+}, the same trend was expected to be observed, assuming that both divalent ions have the same behaviour.

On the other hand, in the case of Cr(VI) the adsorption percentage decreased as the pH was increased from 2 to 6 (Figure 4.34). At pH=2, the predominant form of Cr(VI) is its protonated form, $HCrO_4^-$ as can be observed in the fraction diagram for Cr(VI) (Fig. 4.34). This species can electrostatically interact with the protonated groups of the sorbent that are positively charged at low pHs (1-2) (Hu et al., 2015), leading to greater adsorption at low pHs. The decrease of the chromium adsorption percentage from pH 2 (67.75%) to pH 6 (19.16%) can be explained by the deprotonation of the functional groups of GO-I. Infrared spectroscopy of GO performed in another study indicates that in GO sheets, the ionization of the carboxylic groups is the main contributor to the charge on the graphene sheets; phenolic and hydroxyl groups are also present. The authors assigned a pK of 4 to carboxylic groups bearing a −OH group in an ortho position (Konkena and Vasudevan, 2012).

In the FTIR spectra of GO-I (Figure 4.29), the band corresponding to the −OH group has been identified, as well as the bands corresponding to the carbonyl group. However, it was not possible to fully characterize the bands in the 800−2000 cm^{-1} spectral range, which correspond to the fingerprint region for the different oxygen functional groups. Assuming that the carboxylic group of the GO-I has a pK of approximately 4, 50% of these groups were negatively charged at pH 4 avoiding the uptake that also negatively charged $HCrO_4^-$ while reducing the adsorption percentage to 38.7 % (half of 68.7% obtained at pH 2). At pH 6 this percentage was reduced to 19.2% as a result of higher deprotonation of the carboxylic groups and the increase in the fraction of CrO_4^{2-} in the aqueous solution.

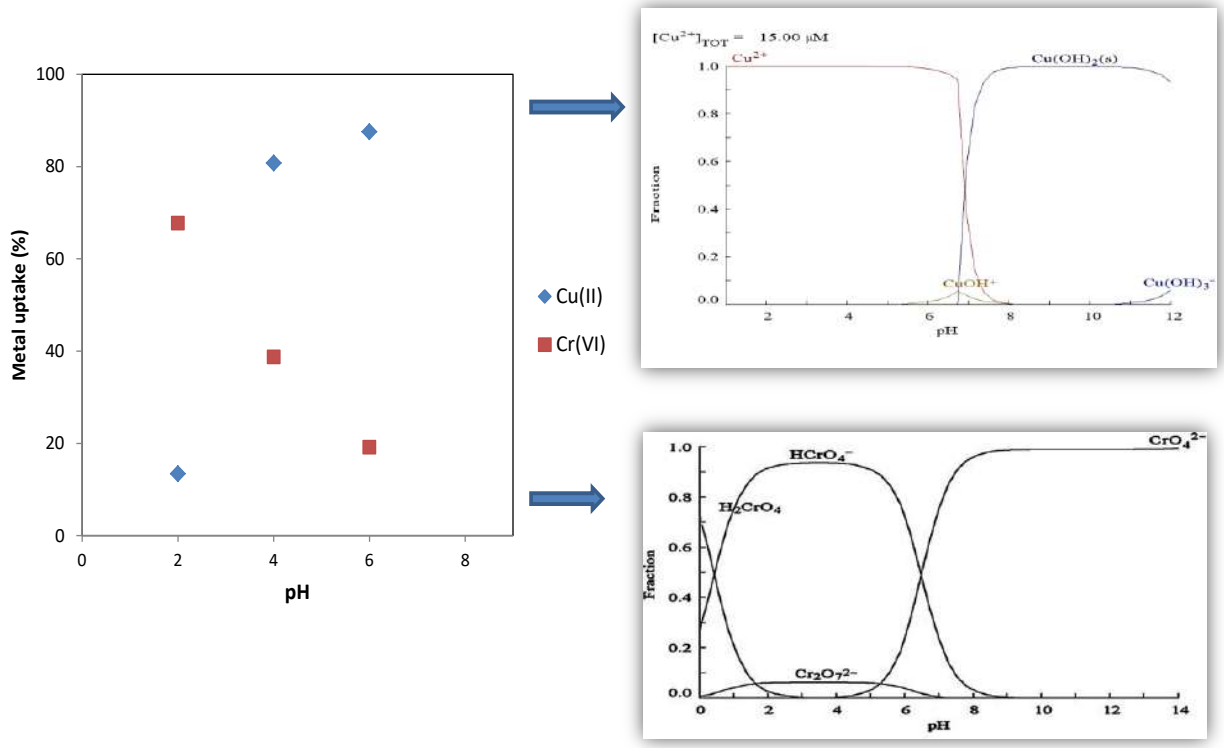

Figure 4.34. a) Effect of the pH of the aqueous solution on the adsorption of Cu(II) and Cr(VI). For Cu(II), graphene 97D was used (2 g L^{-1}), 5 mg L^{-1} of Cu(II) at pH=6. For Cr(VI), sorbent GO-I was used (10 g L^{-1}), 5 mg L^{-1} of Cr(VI) at pH=2. Equilibrium time: 3h. (n=3), b) Fraction diagrams of Cu(II) and Cr(VI) as a function of the pH at the initial metal concentrations.

4.4.2.4. Effect of the initial metal concentration

In the case of each metal, Cu^{2+}, Cd^{2+} and CrO_4^{2-}, and each adsorbent, we studied how the initial metal concentration affected the adsorption process.

The results presented in Figure 4.35 show that the percentage of adsorption decreased when the initial metal concentration increased. These results can be explained by the lack of free sites on the surface of the graphene when more metal ions were present in the solutions as a result of the low functionalization of 97D, 227 A, GO-I and GO-II adsorbents. As can be seen, the highest removal percentages were obtained at the lowest initial concentration (5 mg L^{-1}) tested for all the metals and adsorbents. Moreover, no significant differences were observed between graphene

oxides 227A, GO-I and GO-II with respect to Cu(II) and Cd(II) uptake percentages. However, in the case of 97D, the adsorption efficiency is lower in all the experiments although a longer period of time (t=3 h) was required to achieve equilibrium. There are no significant differences regarding the oxygen content percentage at the surface between 97D and 227A that can help to explain these differences. Moreover, GO-I and GO-II have lower oxygen content and the metal adsorption percentages for Cu(II) and Cd(II) are similar to those obtained with 227A. However, 97 D has the lowest content of C-O functional groups (Table 4.10 XPS results) and the lowest pore volume.

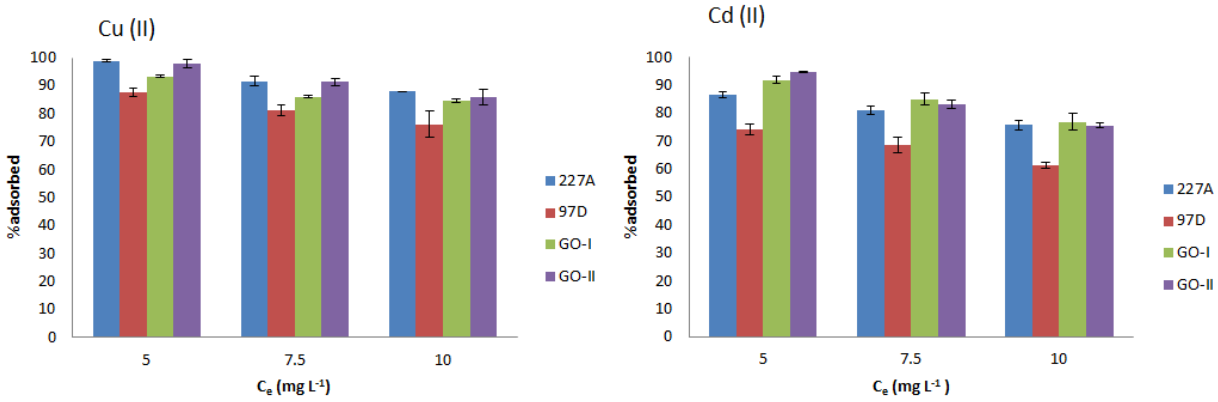

Figure 4.35. Effect of the initial concentration of Cu (II) and Cd (II) on the adsorption efficiency of each graphene. Adsorbent concentration= 2 g L^{-1} at pH=6, t=1h, except for 97D t=3h.

In the case of Cr(VI), the effect of the initial concentration on Cr(VI) adsorption was evaluated using GO-I and GO-II at pH 2 and 10 g L^{-1} of adsorbent. The increase in the metal concentration resulted in a decrease in the adsorption percentage indicating the lack of available sites on the adsorbent surface. Sorption percentages were higher for GO-I, which have 13% of O and 2.66% of C=O functional groups, than for GO-II, 7% of O and 1.76% of C=O (Table 4.11).

4.4.2.5. Competitive adsorption of Cu(II) and Cd(II)

The adsorption of a target metal ion by the graphene (97D) can be affected by the presence of another metal ion in the initial solution which can compete with it for the sorption sites at the adsorbent surface. As wastewater effluents generally contain a variety of metals, we performed some experiments with an aqueous solution containing the same initial concentrations (5 mg L^{-1}) of Cu(II) and Cd(II).

The results obtained are shown in Figure 4.36 and were compared with those obtained using a single metal ion solution in the same conditions. As can be seen in this figure, no significant differences in the adsorbed percentage were observed; showing that in the experimental conditions used there is no competition between Cu(II) and Cd(II) for the sorption sites of the graphene 97D surface.

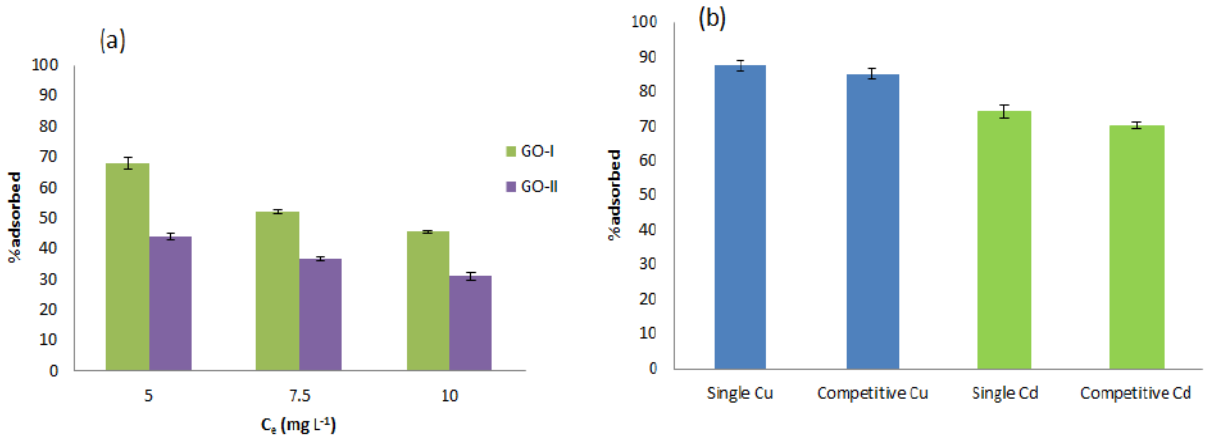

Figure 4.36. a) Effect of the initial concentration of Cr (VI) on the adsorption efficiency of graphene oxides GO-I and GO-II. Adsorbent concentration= 10 g L^{-1} at pH=2, t=1h. b) Comparison of the adsorption of Cu^{2+} and Cd^{2+} by 97D. Adsorbent concentration= 2 g L^{-1}, initial concentrations= 5 mg L^{-1} at pH=6. Equilibrium time: 3h (n=3).

4.4.2.6. Adsorption isotherm models

In general, an adsorption isotherm describes the phenomenon of adsorption of a substance from the aqueous media to a solid-phase at a constant temperature and pH. Here, three isotherm models (Langmuir, Freundlich, and Langmuir-Freundlich) were applied by using both non-linearized and linearized equations to analyze the equilibrium experimental data of the sorption of Cu(II), Cd(II) and Cr(VI) on different graphene-based sorbents. In the case of the non-linearized

equations, both the experimental points and the calculated models are depicted in Figures 4.37 and 4.38. As can be seen in these figures, there is good agreement between the experimental points in the case of Cd(II) and Cr(VI) and the curves corresponding to the three models in the case of Cd(II) for GO-I, 227A and 97D, Cr(VI) for GO-I and GO-II, and Cu(II) for 97D. In the case of Freundlich and Freundlich-Langmuir models, there is good agreement with Cd(II)-GO-II, Cu(II)-GO-I and Cu(II)-GO-II.

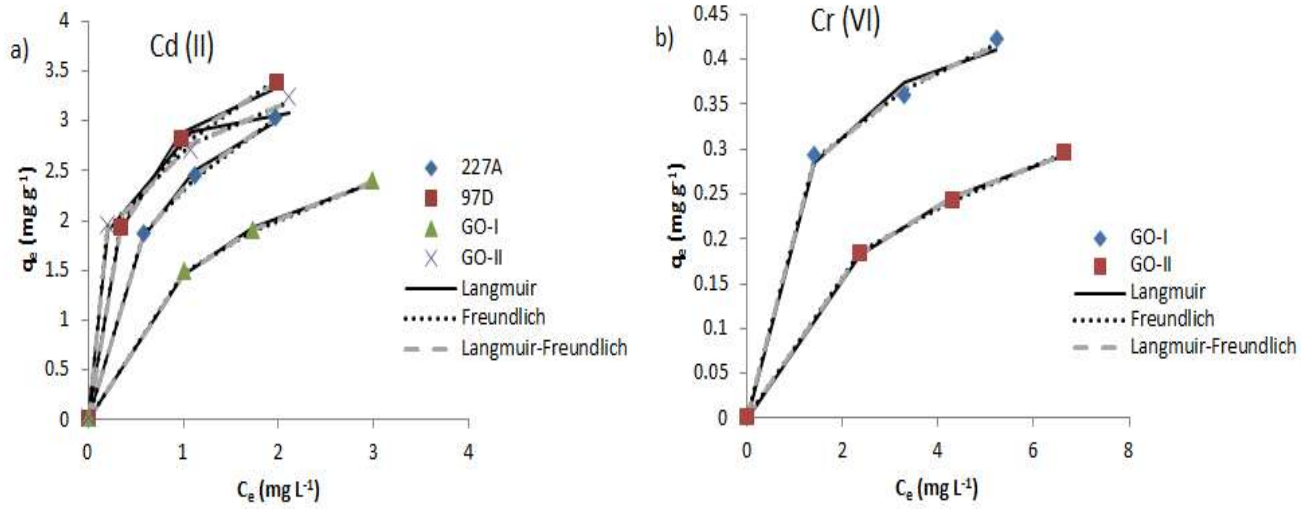

Figure 4.37. Adsorption isotherms for each graphene oxide for a) Cd(II) at pH=6, t=1h, except for 97D t=3h and b) CrO_4^{2-} at pH=2, t=3h (n=3).

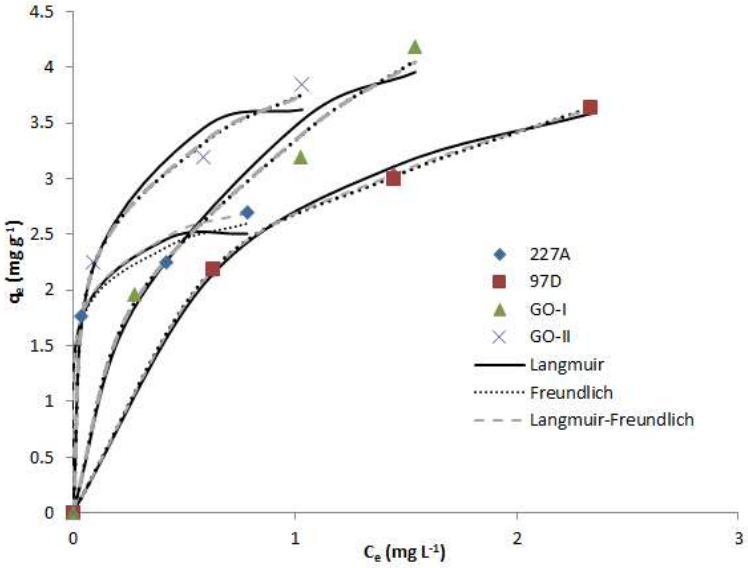

Figure 4.38. Adsorption isotherms of Cu(II) for each graphene oxide at pH=6, t=1h, except for 97D t=3h (n=3).

The results obtained by applying the linearized Langmuir, Freundlich, and Langmuir-Freundlich equations are recorded in Tables 4.13, 4.14 and 4.15. The slope and the intercept of each linear model that were used to calculate the parameters of Langmuir, Freundlich and Freundlich-Langmuir models and the determination coefficients for each metal and adsorbent. As the determination coefficient (R^2) of each model were very similar other statistical criteria such as Akaike's criterion and the F test were applied to select the best model (Akpa and Unuabonah, 2011). The model which has the lowest AIC corresponds to the best model and in the case of the F tests only models having different degrees of freedom such as Langmuir and Langmuir-Freundlich and the Freundlich and Langmuir-Freundlich can be compared. The results obtained by applying these statistical were also presented in the tables 4.13, 4.14, and 4.15.

The adsorption experimental data of Cu(II) and Cr(VI) fitted well with the Freundlich isotherm model according to the Akaike criterion, the determination coefficients (R^2) and the F test. The K_F values ranged from 2.61 (97D) to 3.72 (GO-II) and are similar, in the case of 97D and 227 A, to those obtained by Wu et al. (2012), who obtained a K_F of 2.844. Moreover, this study demonstrates that the adsorption of Cu(II) is due to its interaction with the functional groups (COO^-, or O^-) on the surface of GO to form a metal ion complex. In the case of Cr(VI), the K_F value is higher for GO-I than for GO-II in agreement with the high content of CO groups in GO-I (see Table 4.10). However, another study (Mondal and Chakraborty, 2020) showed that the best isotherm model to express the adsorption data of Cr(VI) onto graphene oxide was the Langmuir model with an adsorption capacity of 1.222 mg g^{-1}. In our study the maximum adsorption capacity for GO-I was similar (1.1 mg g^{-1}). The adsorption experimental data of Cd(II) fitted well with the Freundlich isotherm model in the case of 227A (K_F 2.32) and GO-II (K_F 2.71), whereas Langmuir-Freundlich was the best model for 97D and GO-I with adsorption capacities of 5.19 and 5.28 mg g^{-1}, respectively, proving that this metal ion was adsorbed onto both homogeneous and heterogeneous surfaces. In contrast, other researchers have found that the adsorption data of Cd(II) by GO fitted the Langmuir model well with adsorption capacities of 44.46 mg g^{-1} at pH 4 using 0.50 g L^{-1} of adsorbent dosage. It was found that ion-exchange, electrostatic attraction and physical adsorption were involved in the adsorption mechanisms of Cd(II) (Xue et al., 2016). The

result indicated that the adsorption of Cd(II) on GOs can be explained well by both ionic exchange and the surface complexation mechanisms (Huang et al., 2015).

Table 4.13. Results obtained by applying the adsorption isotherm models to the experimental data of Cu^{2+} for each adsorbent.

Cu^{2+}						
			227A	**97D**	**GO-I**	**GO-II**
Langmuir	q_{max} (mg g^{-1})		2.56	4.77	5.28	3.86
	K_L (L mg^{-1})		53.58	1.29	1.92	14.39
	R^2		0.89	0.95	0.95	0.85
	R_L	C_i=5mg L^{-1}	0.0069	0.12	0.099	0.021
		C_i=7.5mg L^{-1}	0.0046	0.087	0.069	0.014
		C_i=10mg L^{-1}	0.0035	0.066	0.052	0.010
Freundlich	1/n		0.13	0.38	0.44	0.22
	K_F		2.68	2.61	3.34	3.72
	R^2		**0.92**	**0.98**	**0.98**	**0.95**
Langmuir-Freundlich	q_{LF} (mg g^{-1})		9.82	12.02	47.46	16.46
	K_{LF}		0.006	0.083	0.004	0.01
	M_{LF}		0.18	0.51	0.47	0.26
	R^2		0.90	0.92	0.92	0.94
	Akaike (AIC)		-16.63(L-F)> -24.78(L)> **-33.81(F)**	-37.82(L)> -45.47(LF)> **-70.53(F)**	-14.19(L-F)> -17.47(L)> **-26.88(F)**	-20.89 (L)> -21.42(L-F)> **-35.04(F)**
	F test L, L-F		F=2.67 P=0.1634	F=39.39 P=0.0015	F=8.17 P=0.0355	F=15.12 P=0.0115

Table 4.14. Results obtained by applying the adsorption isotherm models to the experimental data of Cd^{2+} for each adsorbent.

Cd^{2+}						
			227A	**97D**	**GO-I**	**GO-II**
Langmuir	q_{max} (mg g^{-1})		4.05	3.96	3.49	3.31
	K_L (L mg^{-1})		1.43	2.71	0.71	6.35
	R^2		0.95	0.89	0.97	0.83
	R_L	C_0=5mg L^{-1}	0.12	0.22	0.067	0.038
		C_0=7.5mgL^{-1}	0.082	0.16	0.046	0.026
		C_0=10mgL^{-1}	0.063	0.12	0.035	0.020
Freundlich	1/n		0.38	0.31	0.43	0.22
	K_F		2.32	2.76	1.48	2.71
	R^2		**0.98**	0.92	0.95	**0.94**
Langmuir-Freundlich	q_{LF} (mg g^{-1})		6.26	5.19	5.28	11.61
	K_{LF}		0.45	1.31	0.25	0.015
	M_{LF}		0.63	0.64	0.69	0.28
	R^2		0.97	**0.97**	**0.98**	0.90
	Akaike (AICs)		-51.39(L)> -68.48(LF)> **-69.68(F)**	-45.70(L)> -46.05(F)**>** **-104.83(L-F)**	-60.68(L)> -74.63(F)> **-77.57(L-F)**	-27.09(L)> -34.20(L-F)> **-50.20(F)**
	F test L, L-F		F=121.73 P=0.0001	F=13523.8 P<0.0001	F=118.9 P=0.0001	F=36.77 P=0.0018
	F test F, L-F		F=11.60 P=0.0191	F=13013.33 P<0.0001	F=21.30 P=0.0058	-

Table 4.15. Results obtained by applying the adsorption isotherm models to the experimental data of CrO_4^{-2} for each adsorbent.

CrO_4^{2-}				
			GO-I	**GO-II**
Langmuir	q_{max} (mg g^{-1})		0.49	0.44
	K_L (L mg^{-1})		0.97	0.29
	R^2		0.93	0.97
	R_L	C_0=5mg L^{-1}	0.18	0.40
		C_0=7.5mg L^{-1}	0.13	0.31
		C_0=10mg L^{-1}	0.099	0.25
Freundlich	1/n		0.28	0.45
	K_F		0.26	0.12
	R^2		**0.98**	**0.99**
Langmuir-Freundlich	q_{LF} (L mg^{-1})		1.1	0.53
	K_{LF}		0.05	0.19
	M_{LF}		0.41	0.82
	R^2		0.97	0.98
	Akaike (AIC)		-70.57(L-F)> -71.93(L)> **-86.55(F)**	-91.62(L-F)> -95.77(L)> **-129.27(F)**
	F test L, L-F		F=11.3 P=0.0201	F=6.96 P=0.046
	Ftest F, L-F		-	-

The graphene oxides (227A, 97D, GO-I and GO-II), prepared in the Chemistry Dpt. of Masaryk University (Brno, Czech Rep.), presented the same XRD pattern and the Raman spectrum showed a lower degree of functionalization and a lower oxidation level given that the percentage of C≈O groups, measured by XPS, ranged from 11.6 to 12.56%. This low functionalization was confirmed by the surface composition determined by EDX, which showed C percentages ≥ 88%, and oxygen percentages between 4 and 9%. FTIR identifies the presence of carbonyl/carboxyl and OH bands on the surface of the adsorbents. BET surface areas ranged from 14.2268 to 25.8041 m^2 g^{-1}, which are lower than the areas reported for other graphene oxides (Alam et al., 2017). Pore volumes ranged from 0.063 to 0.070 cm^3 g^{-1}.

The maximum removal percentage of Cu(II) (>90%) and Cd(II) (>88%) using 227A, GO-I and GO-II were obtained at pH 6 in 5 mg L^{-1} and 2 g L^{-1}. Percentages of <80% for Cu(II) and <60% for Cd(II) were obtained when 97D was used as an adsorbent. In the case of Cr(VI), maximum percentage removal was obtained at pH 2 and 10 g L^{-1} with 68% and 45% for GO-I and GO-II, respectively.

The experimental data of the sorption systems studied fitted the Freundlich isotherm model well in the case of Cu(II) with 227A (K_F 2.68), 97D (K_F 2.61), GO-I (K_F 3.34) and GO-II (K_F 3.72). The Freundlich isotherm is also the best model to express the adsorption data of Cd(II) for 227A (K_F 2.32) and GO-II (K_F 2.71) whereas the Langmuir-Freundlich model provides the best fit for 97D and GO-I with adsorption capacities of 5.19 and 5.28 mg g^{-1}, respectively. The adsorption mechanism of Cu(II) and Cd(II) seems to take place due to their interaction with the functional groups (COO^-, or O^-) on the surface of GO to form a metal ion complex. For Cr(VI), Freundlich was considered the best model in the case of both GO-I (K_F 0.26) and GO-II (K_F 0.12). The adsorption mechanism of Cr (VI) occurred through an electrostatic interaction of $HCrO_4^-$ species with the protonated groups of the sorbent surface at low pHs (1-2).

The results obtained suggest that all the adsorbents tested can be effectively used to remove metallic cations, such as Cu^{2+} or Cd^{2+}, as well as anions, such as CrO_4^{2-} from aqueous solutions. This remains true independently of whether we are dealing with single metal or multi-metal compositions as there is no competition between Cu(II) and Cd(II) for the adsorbent in the experimental conditions tested.

In general, the adsorption capacities obtained for the target metal ions with these GOs were lower than those reported for other graphene oxides (Table 1.4) showing that the synthetic procedures led to a low degree of oxidation of the graphene also affecting the physical properties (surface area, porosity and pore size) of the resulting graphene oxides. Another alternative to improve the adsorption capacity of GOs is to prepare composite materials using lignocellulosic materials a good example is the composite graphene oxide/almond shell (GO@AS) which allowed maximum sorption capacities of 121.95 mg g^{-1} for Cd (II) and 69.93 mg g^{1} for Ni(II) to be reached (Moghaddam et al., 2019).

4.5. Removal of As(III) and As(V) by Basolite® F300 and synthetic Nano-{Fe-BTC} MOF

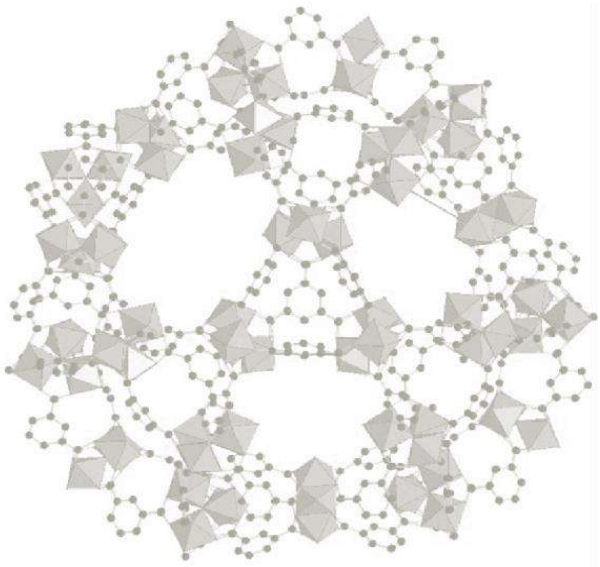

Metal organic frameworks (MOFs) a class of crystalline porous materials consisting of metal nodes (i.e. metal ions or clusters) and organic linkers connected via coordination bonds present a series of interesting features, including having a large surface area, controlled porosity, structural tailorability, and high crystallinity, that potentially make them efficient adsorbents for water treatment. Arsenic contamination is a global threat due to its acute toxicity and carcinogenicity. Arsenic pollution of drinking water supplies has been reported in over 70 countries, posing a serious health hazard to an estimated 150 million people worldwide, particularly in Bangladesh, India as well as in other countries of South and South-East Asia, and in other countries that occasionally have problems due to the presence of As in groundwater, such as the North-East of Catalonia (Spain). Moreover, arsenic toxicity is closely related to its oxidation state: the most common forms of arsenic in natural water are the inorganic forms of arsenate As(V) and arsenite As(III), with As (III) being more toxic than As(V) (Güell et al., 2010). Broad technology options of water purification have been established to deal with As contamination, such as adsorption, chemical coagulation–precipitation, ion-exchange and membrane separation (Güell et al., 2011). Among them, adsorption is one of the most frequently used water treatment techniques and a variety of adsorbents, including both conventional and engineered ones, have been employed for the removal of arsenic. A review of these functional sorbents for adsorptive removal of arsenic ions in aqueous systems has recently been published (Liu et al., 2020).

Advanced materials for arsenic removal include graphene oxides (GOs), carbon nanotubes (CNTs) and metal organic frameworks (MOFs) as well as many other porous materials. The most efficient materials in adsorbing arsenic species are those that have been modified as iron-based magnetic GO, zeolite-reduced GO (ZrGO), zirconium oxide-coated CNTs and iron-based CNTs. It has been reported that the oxygen-containing groups of CNTs form hydroxylated surface complexes due to the reaction between Fe-OH and As(V) (Chen et al., 2014). Hence, as the presence of metal ions favour the adsorption of arsenic species, MOFs can be promising adsorbents for the removal of arsenic. Several studies have analyzed the capability of MOFs for both As(V) and As(III) removal and their results have been collected in a review in which the adsorption of organoarsenicals is also revised (Wang et al., 2019). Iron and 1,3,5-benzenetricarboxylic (Fe−BTC) metal−organic coordination polymers have been synthesized via

a simple solvothermal method and applied to the adsorption of As(V) species from water solutions (Zhu et al., 2012).

Other MOFs, including those of the zeolitic imidazolate frameworks (ZIFs) and the Materials Institute Lavoisier (MILs) families, were also investigated for their capacity to remove Arsenic. Adsorption capacities for As(V) of 76.5 mg g^{-1} and 106 mg g^{-1} were reported for ZIF-8 and MIL-53(Al), respectively (Li et al., 2014a, b). ZIF-8 was able to adsorb As(III) at neutral pH with a capacity of 49 mg g^{-1}. This capacity was increased to values higher than 100 mg g^{-1} by changing the morphology of ZIF-8 or by preparing composite ZIF-8 with metal oxides (e.g. Fe_3O_4@ZIF-8 and MnO_2@ZIF-8) (Huo JB et al., 2018).

Iron-based MILs exhibited a great affinity for As(V) and their capacities and kinetics have been improved from 21 mg g^{-1} of MIL-53(Fe) (Vu et al., 2014), 110 mg g^{-1} of MIL-100(Fe) (Cai et al., 2016) to 156 mg $g^{-1}$of MIL-88B (Hou S et al., 2018). A MIL-100(Fe) based filter was proposed for the efficient removal of As (III) from synthetic groundwater through oxidation and the adsorption of the resulting As(V) (Wang et al., 2018), presenting a high uptake capacity of 120 mg g^{-1} for As(III) (Georgiou et al., 2018). MIL-101(Fe) has proved to adsorb As(V) and organoarsenicals with maximum adsorption capacities of 232.98 mg g^{-1} for As(V) and, 507.97, 379.65 and 158.94 mg g^{-1} for roxarsone, p-arsanilic acidand dimethyl arsenate, respectively (Li et al., 2019).

The aim of this study is to investigate As(V) and As(III) uptake by using two different iron-based porous MOFs, the commercial Basolite®F300 and the synthesised Nano-{Fe-BTC}MOF based on the coordination of Fe(III) ions with trimesate organic linkers (benzene tricarboxylic acid). Both MOFs have been characterized and applied to the removal of As(V) and As(III) varying parameters such as contact time, pH, the amount of adsorbent and the initial arsenic concentration. The experimental data of the adsorption of arsenic was expressed by the adsorption isotherm.

4.5.1. Characterization of the adsorbents

In this study two MOFs have been used: one is commercial Basolite F300 and the second is a synthesized Nano-{Fe-BTC}(Conde-González et al., 2021). The functional groups of both materials have been characterized by FTIR, elemental surface composition by EDX, morphology

by SEM, and thermal stability by TGA. The specific surface area, pore size distribution, and pore volume were measured by the Brunauer, Emmett and Teller method (BET).

The morphology of the materials was examined by scanning electron microscope (SEM). The SEM image of Basolite F300 shows that it is formed by homogenous and well dispersed nanoparticles (Fig. 4.39 (a)). In the case of Nano-{Fe-BTC}, a series of cracks and asymmetric pores with an open pores structure with particle size which generated a large internal surface area are observed in the SEM image (Fig. 4.39 (b)). The elemental analysis of the adsorbent surface was performed by EDX. Basolite F300 was found to be mainly composed of carbon (74.39%), oxygen (21.84%) and iron (2.97%) whereas Nano-{Fe-BTC} MOF was composed of a similar percentage of carbon (78.05%), slightly less oxygen (17.09%), a greater percentage of iron (3.68%), and chlorine (0.87%).

The surface area and pore volume of these nanocrystallines were measured by the BET method.

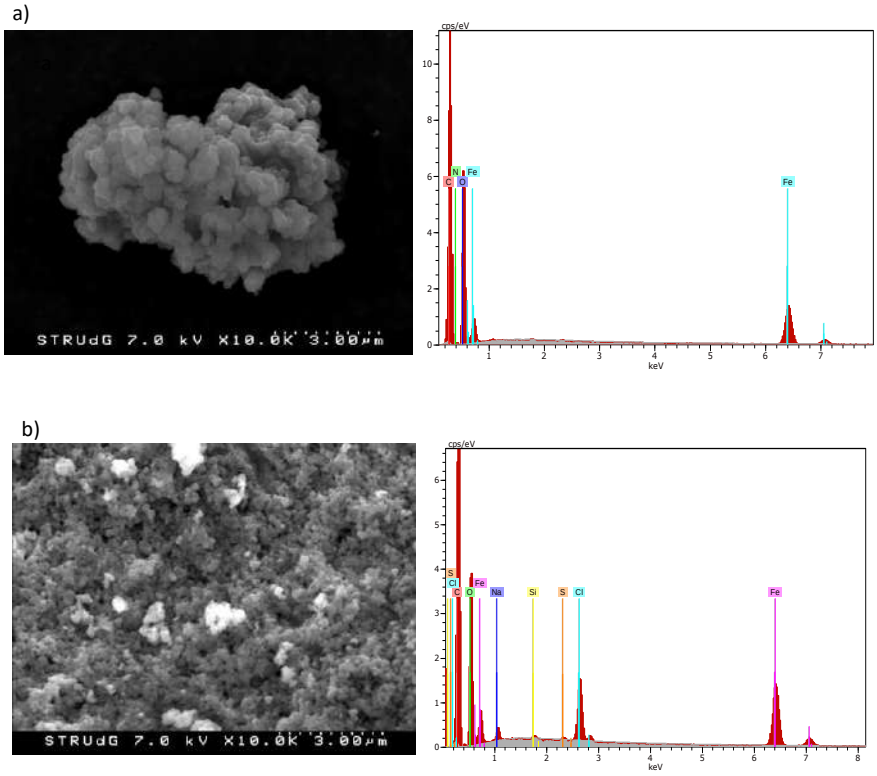

Figure 4.39. SEM images and EDX spectra of a) Basolite F300 and b) Nano-{Fe-BTC} MOF.

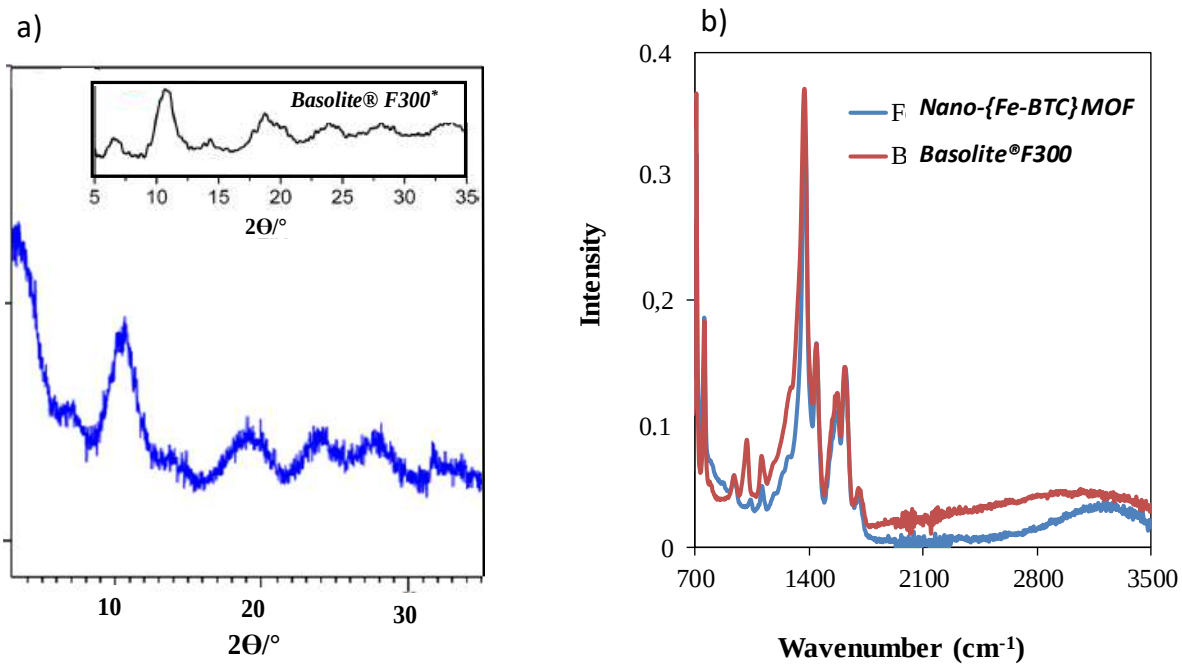

Figure 4.40. a) PXRD patterns of Nano-{Fe-BTC} MOF and Basolite F300 and b) FTIR spectra of both nanomaterials (Conde-González et al., 2021).

The PXRD patterns of the Nano-{Fe-BTC} MOF and commercial Basolite®F300 were compared in terms of relative and absolute intensities, and the position of the diffraction bands, showing a very good fit (Fig. 4.40 (a)). The diffraction peaks of the synthesized Nano-{Fe-BTC} MOF, which are characteristic of the crystalline order and similar to those of commercial Basolite F300, reveal that the basic building blocks and connectivity of the crystalline counterparts are maintained. The broad peak shapes seen in the diffractogram are presumably due to their small crystallite size. The infrared spectra of the commercial Basolite F300 and the synthesized Nano-{Fe-BTC} MOFs show similar bands, including in the 650-1800 cm^{-1} region, which is generally considered to be a fingerprint of MOFs. However, differences in intensity between the two materials are found in the 950-1300 cm^{-1} region (Fig. 4.40 (b)) (Conde-Gonzálezа et al., 2021).

The thermal stability of both materials was determined by TGA. Figure 4.41 (a) of the TGA analyses of commercial Basolite F300 and Nano-{Fe-BTC} MOF showed that they shared similar behavior in terms of their thermal stability as they decompose at the same temperature (275°C). The porosity of Nano-{Fe-BTC} MOF and commercial Basolite F300 was determined

by N_2 adsorption-desorption isotherms at 77 K (Fig. 4.41(b)). On comparing the results obtained, the slope in the $0.2< P/P_0 > 0.7$ range before a plateau is reached is more accentuated for Nano-{Fe-BTC} MOFs than for Basolite F300. In the $0.8<P/P_0<1$ region, there is a sharper amount of N_2 uptake for Nano-{Fe-BTC}, both facts indicating the presence of mesopores with a diameter in the upper size range (between 2 nm and 50 nm) in the case of Nano-{Fe-BTC} MOFs. The curves of Nano-{Fe-BTC} MOFs displayed an intermediate mode between the micropores and mesopores (Fig. 4.41 b). As can be seen in Table 4.16, the synthesized material has a larger volume of pores than Basolite F300 whereas this commercial MOF has a larger surface area.

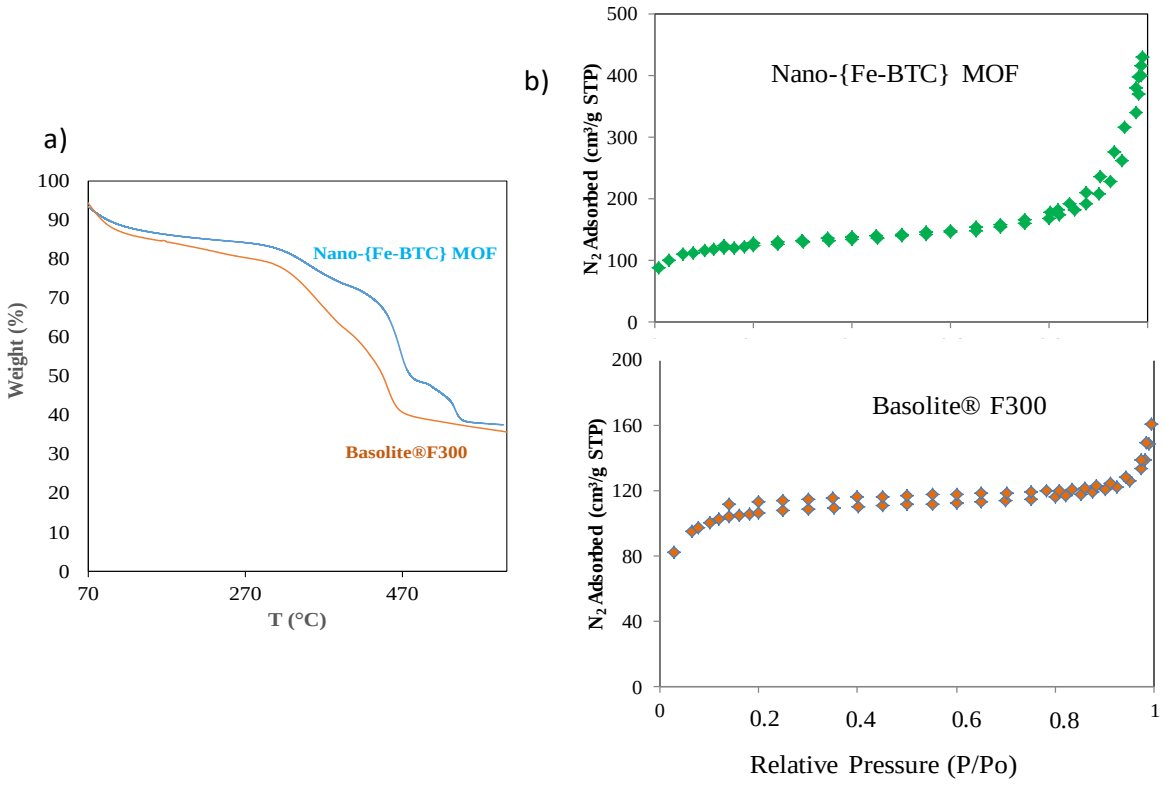

Figure 4.41. a) TGA of Basolite F300 and Nano-{Fe-BTC} MOF and b) N_2 adsorption-desorption isotherms for both nanomaterials (Conde-González et al., 2021).

Table 4.16. Porosity parameters of Basolite F300 and Nano-{Fe-BTC} MOF estimated from the N_2 adsorption-desorption isotherms, the pore size distribution and SEM images.

Parameter	Basolite F300	Nano-{Fe-BTC} MOF
BET surface area ($m^2\ g^{-1}$)	431.6	427.2
Pore volume ($cm^3\ g^{-1}$)	0.41	0.53
Porosity (%)	29.95%	10.12%
Pore size (Å)	25.29	21.7

4.5.2. Batch adsorption

The effect of different parameters such as time, pH, amount of adsorbent and initial concentration on the removal of arsenite and arsenate by BasoliteF300 and Nano-{Fe-BTC} MOF was investigated. First at all, the adsorption processes of As(V) and As(III) by Basolite F300 were characterized.

4.5.2.1. Kinetics of the adsorption process

The kinetics of the As(III) and As(V) adsorption were studied by varying the contact time from 2 min to 120 min using 0.1 g L^{-1} of Basolite F300 with an initial arsenic concentration of 10 mg L^{-1} at pH 7 for As(V) and the same concentration at pH 11 for As (III). The adsorption capacities (q_t) at the different times for both anions are represented in Figure 4.42. As can be seen in this figure, the equilibrium was reached approximately after 1 hour.

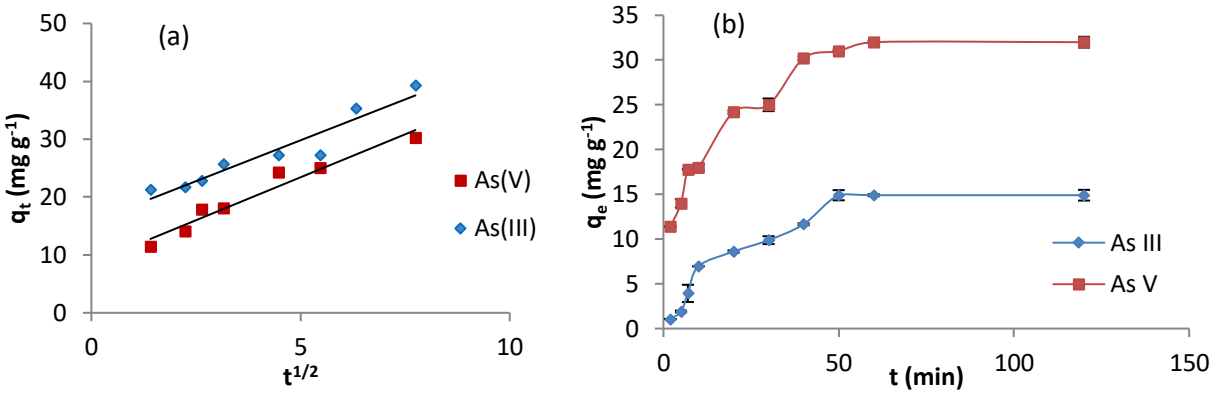

Figure 4.42. (a) Intraparticle diffusion kinetic model and experimental data (b) effect of contact time: C_i=10 mg L^{-1}, adsorbent concentration of 0.1 g L^{-1}, pH=5.6 (As(V)), pH=9.5 (As(III)) (n=3).

In order to describe the adsorption process of arsenite and arsenate, pseudo first order, pseudo second order and intraparticle diffusion kinetic models were applied (Table 4.18). The experimental data of both anions fitted the pseudo second-order model well with a determination coefficient of R^2>0.9. This model confirms that chemisorption is the dominant mechanism for the adsorption of As(III) and As(V). The adsorption process is assumed to take place via: 1) transference of the arsenic species through the external boundary layer of the adsorbent, 2) intraparticle diffusion in the pores of the adsorbent, and 3) adsorption at the sites on the adsorbent surface, and it is assumed that boundary layer diffusion or/and intraparticle diffusion control the kinetics of the adsorption process. As can be seen in Figure 4.42, the first step lasts about 10 minutes and the second slower step lasted 1 hour until equilibrium was achieved, resulting in an adsorption capacity of 11 mg g^{-1} for As(III) and 34 mg g^{-1} for As(V), respectively. The first step is associated to the direct binding of arsenic to the coordinatively unsaturated sites on the metal nodes (Liu et al., 2019).

Intraparticle diffusion model allows the rate controlling step (K_P) and diffusion mechanism to be investigated. The relatively linearity of the model for As(III) and As(V) indicates that intraparticle diffusion can be the rate controlling process. However, there is a little contribution of boundary layer diffusion, that is higher for As(V) than for As(III) (C values in Table 4.17).

Table 4.17. Kinetic parameters for the adsorption of As(III) and As(V) by Basolite F300.

	Pseudo first order $Log(q_e - q_t) = \log q_e - K_1/2.303\ t$			**Pseudo second order** $t/q_t = 1/K_2 . q_e^2 + 1/q_e\ t$			**Intraparticle diffusion** $q_t = K_p t^{0.5} + C$		
As(V)	**q_e (mg g^{-1})**	**K_1 (min^{-1})**	**R^2**	**q_e (mg g^{-1})**	**K_2 (g mg^{-1} min^{-1})**	**R^2**	**K_p (mg g^{-1} min^{-1})**	**C**	**R^2**
	16.81	0.022	0.89	32.67	0.0047	0.99	2.1	11.4	0.95
As(III)	15.05	0.012	0.82	11	0.67	0.98	1.59	0.34	0.91

4.5.2.2. Effect of the pH of the aqueous solution

The pH is an important parameter that affects the removal percentage of As (III) and As (V) as their speciation depends significantly on the pH and the redox potential (Figure 4.43). Moreover, the pH also affects the surface properties of adsorbents.

The effect of the pH was evaluated by varying the pH from 2 to 12 using initial concentrations of 5 mg As L^{-1} and 0.5 g L^{-1} of the adsorbent with a contact time of 1 h. Figure 4.44 shows the effect of pH on the removal of both As(III) and As(V) species. In the case of As(V), the adsorption capacity increases from pH 2 to pH 5.6 and then remains constant until pH=10.5. On the other hand, for As(III) the adsorption capacity is negligible between pH 2 and pH 8.5 and increases at pH 9.5-10.5. Based on the above results, 5.6 was chosen as the optimum pH for As (V) adsorption while in the case of As (III), pH 9.5 was the optimum.

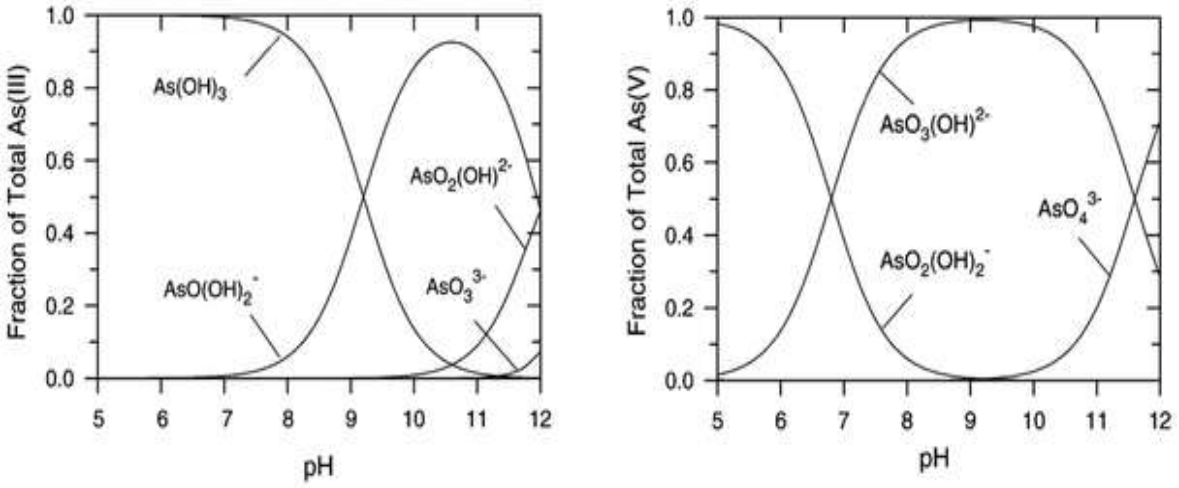

Figure 4.43. Speciation of As(III) and As(V).

At pH 3-8, the arsenate species present in solution was $H_2AsO_4^-$, an anionic ligand with an ability to donate a pair of electrons (Lewis base) that interacts strongly with centred Fe^{3+} cations (Lewis acid). The electrostatic interaction between arsenate and the positive charge of the centred Fe^{3+} also enhances As(V) adsorption. In the pH 8-11 range, the predominance of the $HAsO_4^{2-}$ species, which is also a Lewis base, with two negative charges favour the electrostatic interaction with the iron cations, resulting in a higher affinity of As(V) by the MOFs. Similar results were obtained with Zn-MOF-74 (Yu et al., 2019) as the As(V) adsorption capacity increased sharply at pH= 3–7, but a rapidly decrease was observed at pH 10-12 while in our study the adsorption capacity remained constant from pH 5.6-10.5. The effect of the pH on As(V) adsorption reported in other studies is different as it depended on the characteristics of the adsorbent used. For MIL-53(Fe), an adsorption percentage of 99% was obtained at pH 5 and decreased to 87% at pH 11 (Vu et al., 2014). The removal percentage of As(V) by the Fe−BTC polymer was above 96% in the range of pH 2−10 with a maximum removal efficiency of 98.2% at pH 4, whereas when the pH was increased to 12, it decreased to 35.8% as a result of Fe-BTC instability in strong base conditions (Zhu et al., 2012).

In the case of As(III), at pH=3-9, the arsenite species present in solution is the neutral H_3AsO_3 species, which explains the lower adsorption of As(III) in this pH range. At pHs > 9, the predominance of the negatively charged $H_2AsO_3^-$ species, which is considered to be a soft Lewis

base, allows its interaction with the centred iron cations. These results are similar to those obtained for As(III) by Li et al., 2014. However, the As(III) adsorption by MIL-100(Fe) was reported to reach the maximum adsorption (120 mg g^{-1}) at pH 7. To explain this result, Georgiou et al., (2018) modelled pH-edge data with a surface complexation method showing that As (III) binds in its neutral form (H_3AsO_3), with the Fe sites of the Fe-oxide layer.

Synthesized iron-trimesic MOFs present acid properties and the pH_{pzc} of Fe-BTC-based MOFs is around 4and the funcional groups at the adsorbent surface (BTC linkers) were negatively charged at pHs > 4 (Zhang et al., 2020). The fact that the adsorption of negatively charged arseniate species increases at pHs > 4 seems to confirm that arsenic uptake by Fe-BTC MOFs takes place through Fe(III) interaction. At acidic pHs < 4 it has been reported that iron-based MOFs suffered from deterioration and that iron is leached from the material (Zhang et al., 2020).

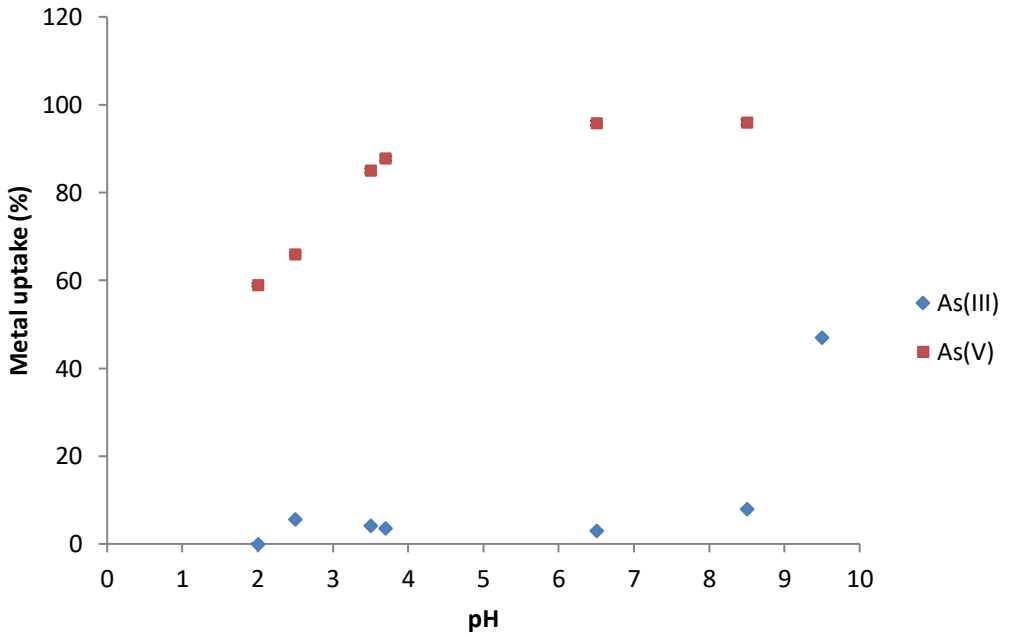

Figure 4.44. Effect of the pH on the adsorption of As(III) and As(V) by Basolite F300: C_i=5 mg L^{-1}, adsorbent concentration=0.5 g L^{-1}, t=1h (n=3).

4.5.2.3. The effect of the amount of adsorbent

The adsorbent concentration effect was studied by varying the quantity from 0.1 to 2 g L^{-1} and maintaining the other parameters constant (C_i=5 mg L^{-1}, t=1h, pH=5.6 for As (V) and pH=9.5 for As(III)). Figure 4.45 shows that the arsenic uptake percentage increases on increasing the amount of adsorbent until saturation. Maximum adsorption was achieved using 0.5 g L^{-1} for both As(III) and As(V). Generally, MOF concentrations in the 0.06 – 0.5 g L^{-1} range were used in other studies (Liu et al. 2014; Cai et al., 2016; Li et al., 2019).

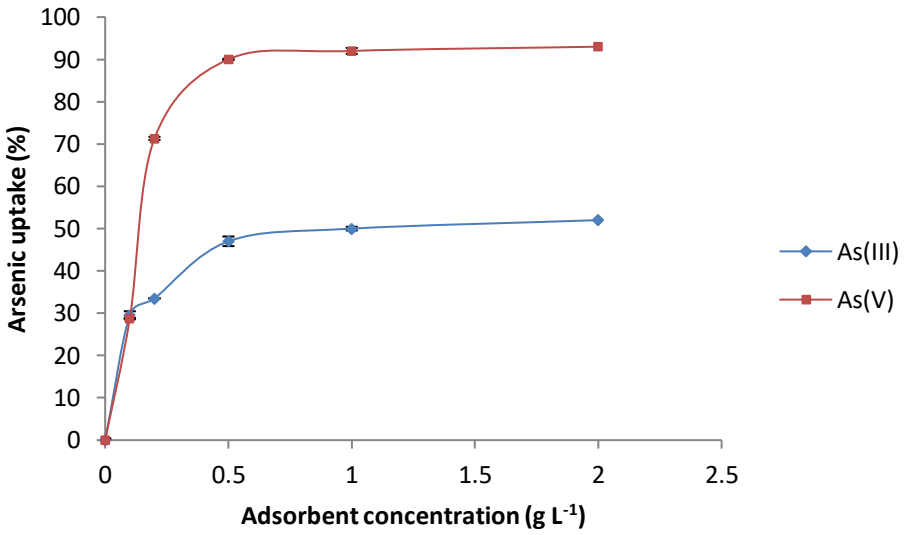

Figure 4.45. Effect of the amount of adsorbent on the adsorption of As(III) and As(V) by Basolite F300 : C_i=5 mg L^{-1}, t=1h, pH=5.6 (As (V)), pH=9.6 (As (III)) (n=3).

4.5.2.4. Initial concentration effect

The effect of the arsenic initial concentration on the removal of As(III) and As(V) was studied by varying the initial concentration from 0.5 mg L^{-1} to 10 mg L^{-1} (Figure 4.46). When the concentration was increased, the adsorption capacity increased indicating the high affinity of the arsenate and arsenite ions for Basolite F300, as in the experimental conditions, saturation was not reached it seems that Basolite F300 is able to adsorb greater amounts of As(V). In the case of As

(III) it can be observed the tendency to reach a plateau of the graph indicating the lower affinity of As(III) for Basolite F300 in comparison with As(V).

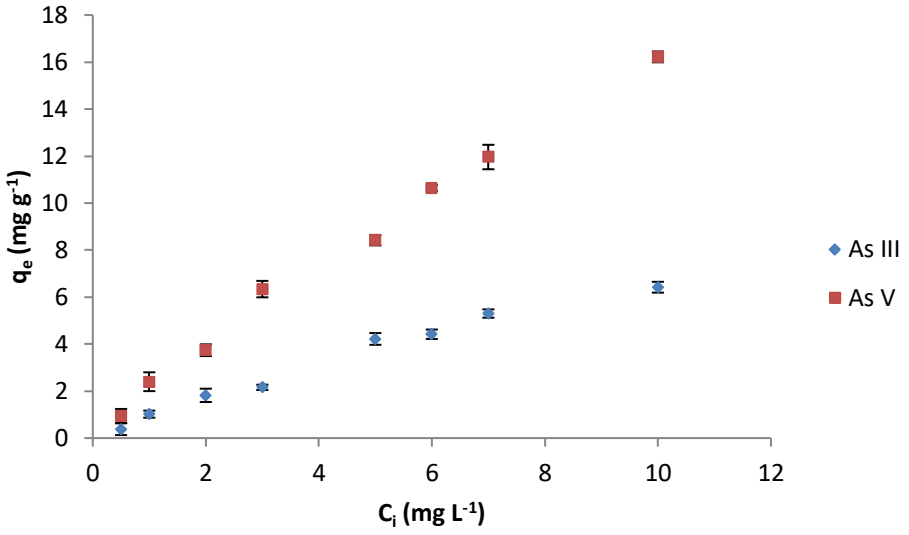

Figure 4.46. Effect of the initial arsenic concentration on the adsorption of As(III) and As(V) by Basolite F300: amount of adsorbent=0.1 g L^{-1}, t=1h, pH=9.6 for As(III), pH=5.6 for As(V) (n=3).

4.5.2.5. Isotherm adsorption

Experimental data of the adsorption of arsenate and arsenite by Basolite F300 has been analyzed using three isotherm models (Langmuir, Freundlich, and Langmuir-Freundlich) by using both non-linearized and linearized equations. In the case of the non-linearized equations, both the experimental points and the calculated models are depicted in Figure 4.47. As can be seen in this figure, there is good agreement between the experimental points in the case of As(III) with the Langmuir model whereas the Freundlich model has the best fit for As(V). The degree of agreement was assessed by comparing the determination coefficient (R^2) of each model and by applying Akaike's criterion (AIC) and the F test as R^2 is insufficient to perform the comparison of the models. The best model has the lowest AIC. As can be seen in Table 4.19, when the F test was used to compare Langmuir and Langmuir-Freundlich, Langmuir was the best model for As(III). In the case of As(V), after comparing the Freundlich and Langmuir-Freundlich models, the Freundlich model was selected for As(V).

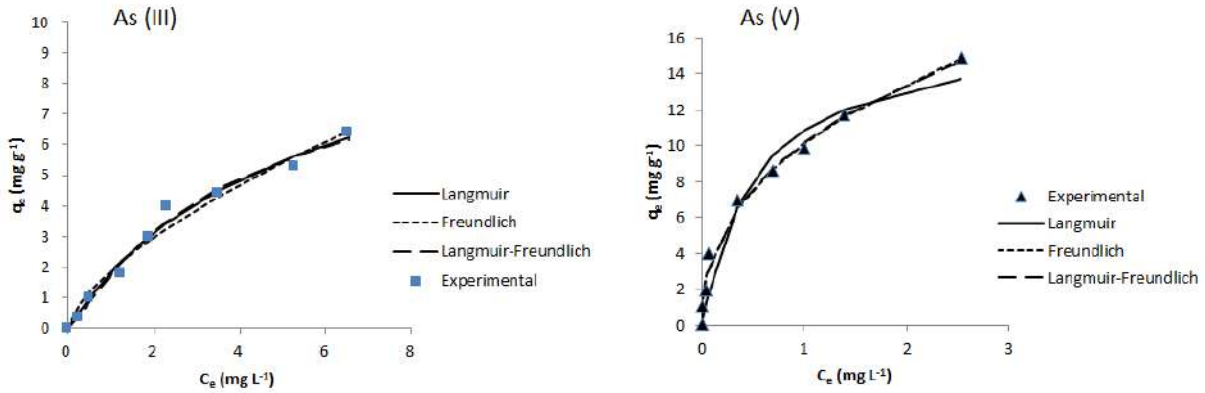

Figure 4.47. Adsorption isotherm of As(III) at pH 9.5 and As(V) at pH 5.6 using Basolite F300 as adsorbent.

Linearized equations were then applied to calculate the adsorption parameters for each model. Table 4.18 shows the parameters obtained from the Langmuir, Freundlich and Langmuir-Freundlich isotherm models. The results obtained demonstrate that the strength of adsorption 1/n is below 1 in the case of As(V), indicating the favorability of the adsorption. Moreover, As(V) presents the highest K_F (10 mg g^{-1}). However, the results of As(III) follow better to the Langmuir model with an adsorption constant K_L of 0.3 L mg^{-1} and a maximum adsorption capacity of 10 mg g^{-1}.

The results obtained from pseudo-second order show that As(III) presented the highest K_2 (0.67 g mg^{-1} min^{-1}) and that the maximum sorption capacity q_e was found for As(V), however, this later presented the lowest kinetic rate constant (0.0047 g mg^{-1} min^{-1}). These results proved a higher affinity of Basolite F300 for As(V) than for As (III)resulting in a higher adsorption capacity for As(V).

Table 4.18. Results of the application of the adsorption isotherm models to the adsorption of As(III) and As(V) by Basolite F300. Parameters obtained from isotherm adsorption models.

	Langmuir **Linearised form** $\frac{C_e}{q_e} = \frac{1}{q_{max}.b} + \frac{1}{q_{max}} C_e$ **Non-linearised form** $q_e = \frac{q_{max} b C_e}{1 + b C_e}$			**Freundlich** **Linearised form** $\ln q_e = \ln K_F + \frac{1}{n} \ln C_e$ **Non-linearised form** $q_e = K_F C_e^{1/n}$			**Langmuir-Freundlich** **Linearised form** $\frac{1}{q_e} = \frac{1}{q_{LF} K_{LF}} (\frac{1}{C_e})^{M_{LF}} + \frac{1}{q_{LF}}$ **Non-linearised form** $q_e = \frac{q_{LF}(K_{LF} C_e)^{M_{LF}}}{1 + (K_{LF} C_e)^{M_{LF}}}$						
	q_{max} **(mg g^{-1})**	**K_L** **(L mg^{-1})**	**R^2**	**K_F** **(mg g^{-1})**	**1/n**	**R^2**	**q_{LF}** **(mg g^{-1})**	**K_{LF}**	**M_{LF}**	**R^2**	Akaike (AICs)	F test (L, L-F)	F test (F, L-F)
As(V)	21	0.4	0.89	10	0.4	**0.96**	14	3	1	0.74	28.88(L-F >23.01(L) >**10.3(F)**	F=15.79 P=0.0165 (L-F)	F=0.04 P=0.8484 **(F)**
As(III)	10	0.3	**0.92**	2	0.6	0.90	7	0.5	1.2	0.94	18.97(L-F) >4.7(F) >**0.7(L)**	F=0.21 P=0.6728 **(L)**	F=2.93 P=0.1621 (F)

The adsorption capacities of Basolite F300 for As(V) and As(III) are compared with other MOF-based materials (Table 4.19). Among all the adsorbents, the highest adsorption capacity (232.98 mg g^{-1}) for arsenic was obtained with MIL-101(Fe) (Li et al., 2019) given that this MOF has a high surface area (1172.5 m^2 g^{-1}) MIL-88B(Fe) also presented a high adsorption capacity for As(V) of 156.7mg g^{-1} although it has a lower surface area (Huo et al., 2018). An adsorption capacity of 145 mg g^{-1} was reported for MIL-88A microrods,which is explained by its unique microstructure with abundant OH^- groups and its large swelling towards water (Wu et al., 2018).

Activated MIL100(Fe) has the highest surface area and presented a maximum adsorption capacity of 110 mg g^{-1} at 298 K according to the Langmuir adsorption model while at 278 K, the maximum adsorption capacity was found to be of 27 mg g^{-1}. Fe-BCT and 2D ZIF-L (have higher adsorption capacities for As(V) Cai et al., 2016) and As(III) (Nasir et al., 2018), respectively, than Basolite F300 although their surface areas are lower. However, higher amount of adsorbent and higher arsenic concentrations were used in both studies.

Therefore, the adsorption capacities for arsenite and arsenate depend on the experimental conditions used such as contact time, pH, dose, surface area and MOF based materials.

4.5.2.6. Comparison between Basolite and synthetic on the removal of As(III) and As(V)

In order to study the efficiency of Basolite F300 in comparison with Nano-{Fe-BTC} MOF, experiments on the adsorption of As(V) and As(III) with nano-{Fe-BTC} MOFs were performed at the best experimental conditions used with Basolite F300 (pH 5.6 for As(V) and pH 9.5 for As(III)) with an initial arsenic concentration of 5 mg L^{-1} and 0.5 g L^{-1} of adsorbent). As it can be seen in Figure 4.48, arsenic uptake percentages of 90 % for As(V) and 47% for As(V) were obtained with Basolite F300 whereas with nano-{Fe-BTC} MOF the percentages were of 47% and 36%, respectively. These differences in the case of As(V) adsorption are explained by the higher surface area and porosity of Basolite F300 (Table 4.16). In the case of As(III), the smaller percentages obtained for nano-{Fe-BTC} MOF together with the fact that with Basolite F300 the arsenic adsorption percentage is less than 50% is explained by the lower affinity of As(III) by the sorbent. However, another factor to be considered is the instability of Fe-BTC-based MOFs at pH 11, which was reported for Fe-BCT polymers (Zhu et al., 2012).

Table 4.19. Adsorption capacity of MOF based adsorbents for As(V) and As(III).

Arsenic species	**MOF-based materials**	**Surface area ($m^2 g^{-1}$)**	**Adsorption capacity ($mg g^{-1}$)**	**Time**	**pH**	**Dose ($g L^{-1}$)**	**References**
As(V)	MIL-88B(Fe)	214	156.7	12h	6	40	Hou et al., 2018
As(V)	MIL-88A microrods	-	145	20min	5	0.4	Wu et al., 2018
As(V)	MIL-53(Fe)	14	21.27	120min	5	10	Vu et al., 2014
As(V)	MIL-101 Fe	1172.5	232.98	4h	7	0.5	Li et al., 2019
As(V)	MIL-100 Fe	1369.6	110	-	7	0.1	Cai et al., 2016
As(V)	Fe-BTC	-	57.705	-	4	5	Zhu et al., 2012
As(III)	2D ZIF-L	67	43.7	10h	10	-	Nasir et al., 2018
As(V) **As(III)**	Basolite F300	431.6	32.67 10	120min	5.6 9.5	0.1	Present study

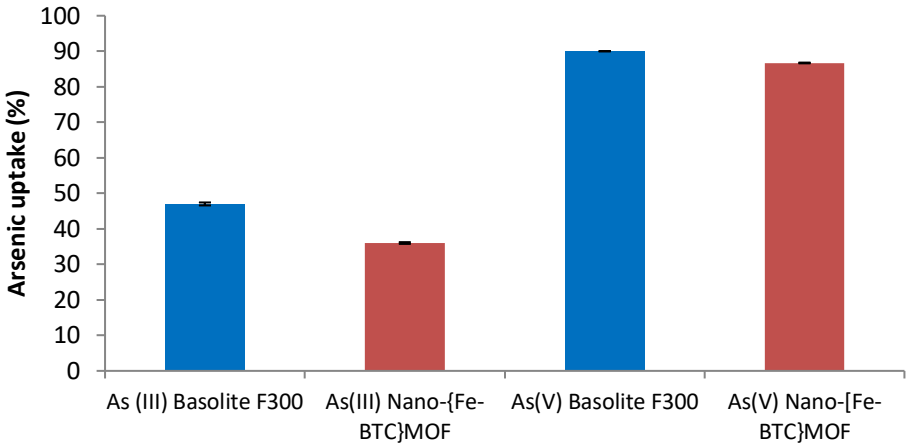

Figure 4.48. Comparison of the removal percentage of Basolite F300 and Nano-{Fe-BTC} MOFs. C_i=5 mg L^{-1}, amount of adsorbent=0.5 g L^{-1}, t=1h, pH=9.5 for As(III), pH=5.6 for As(V) (n=3).

4.5.2.7. Mechanism of As(V) and As(III) adsorption on Fe−BTC

FTIR analyses were performed before and after adsorption with the two Fe-BTC materials. The FTIR spectra of Basolite F300 and Nano-Fe-BTC MOFs have similar profiles (Figure 4.49) with bands in the 650-1800 cm^{-1} region, which is generally considered to be a fingerprint of MOFs. The peaks obtained at 1629 cm^{-1}, 1454 cm^{-1} and 1380 cm^{-1} are due to the presence of asymmetric and symmetric stretching vibration of carboxylate groups of the BTC ligand. The peak registered at 762 cm^{-1} suggests the presence of Fe-O indicating the coordination of BTC to the iron sites. Moreover, the synthetized Fe-BTC presents a broad band at 3197 cm^{-1} corresponding to water and OH^- of the material and the band at 2143 cm^{-1} to a stretching vibrations of –C=C-.

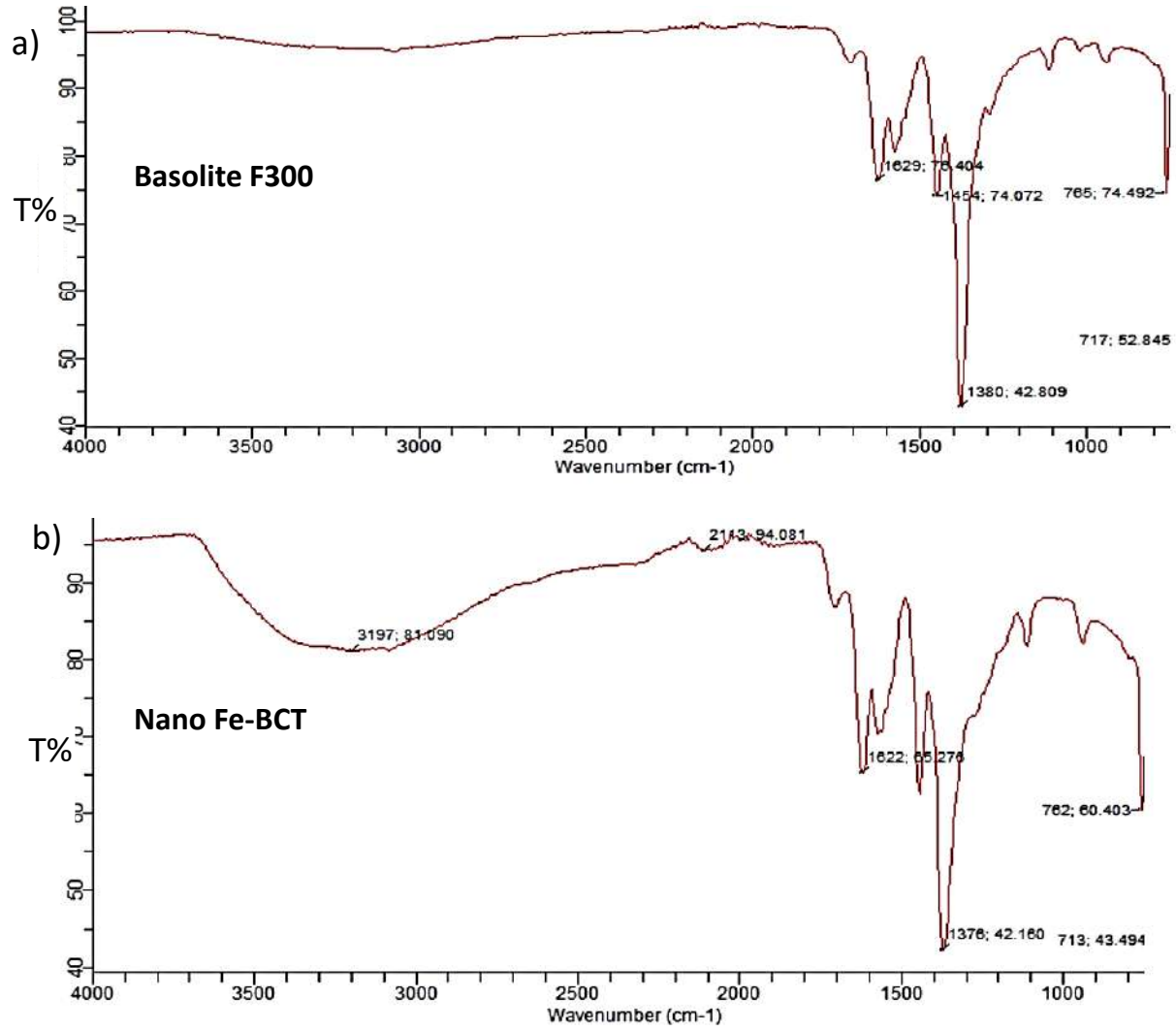

Figure 4.49. FTIR spectra of a) Basolite F300 and b) Nano-{Fe-BTC} MOF.

In Figure 4.50, the FTIR spectrum of Basolite F300 after the adsorption of As(V) is presented and compared with the spectra of MIL-100 before and after adsorption of As(V). As can be seen in the later, a new absorption band at 825 cm^{-1} attributed to Fe–O–As appears in the blue curve of FTIR spectra (Figure 4.50 (a)) confirming the interaction of As(V) with Fe (III) inside the MOFs (Cai et al., 2016). In the case of Fe−BTC polymer, the FTIR spectrum after adsorption of As(V) (Figure 4.50 (b)) show clearly a new peak at 824 cm^{-1} in comparison with the spectrum of the Fe−BTC polymer (Zhu et al., 2012). In the FTIR recorded in our laboratory, this peak cannot be clearly distinguished but it can be observed a band in this region.

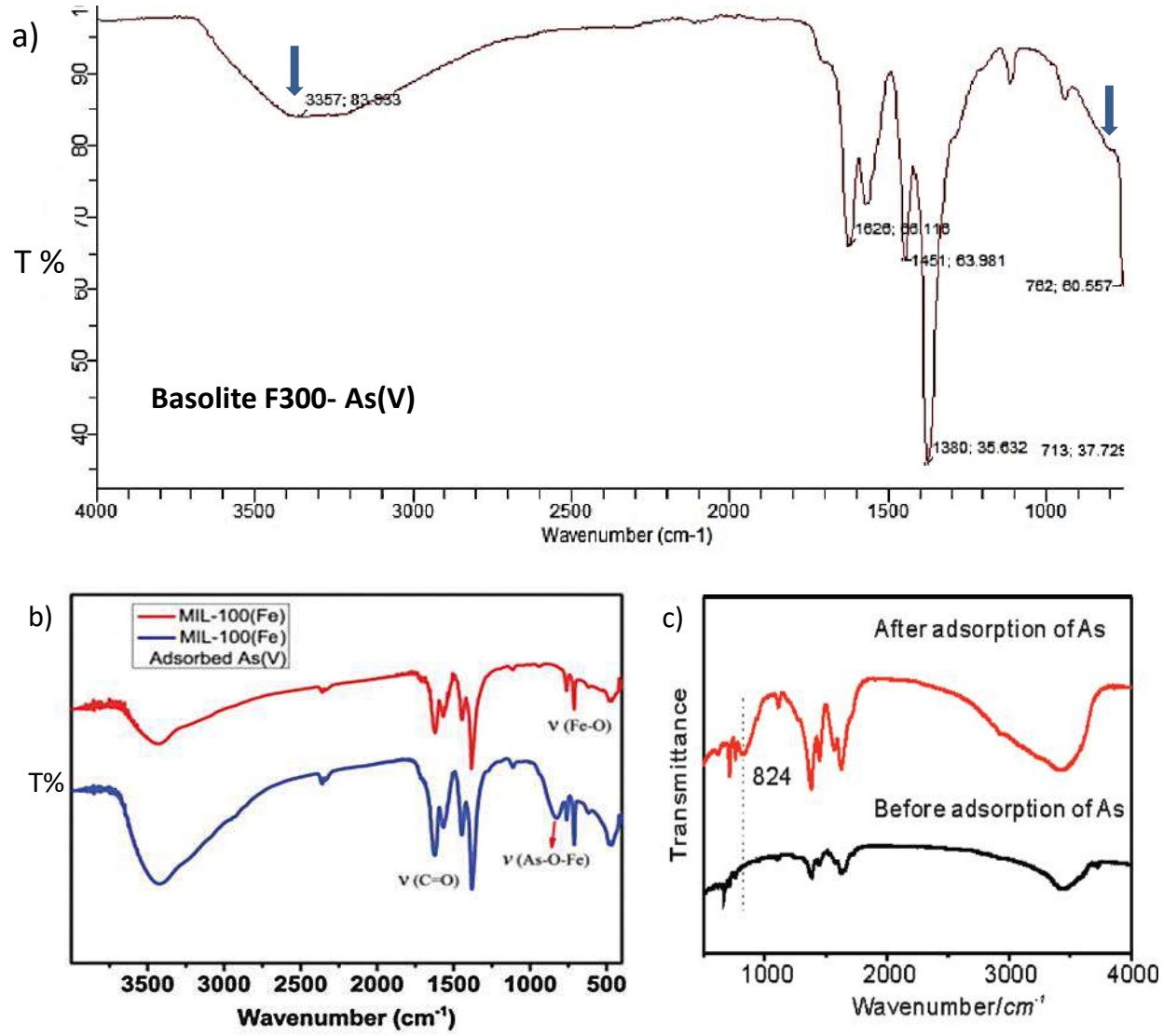

Figure 4.50. a) FTIR spectrum of Basolite after As (V) adsorption (the bands that differ from Basolite F300 spectrum are marked with a blue arrow), b)) FTIR spectra of MIL-100(Fe) before and after As(V) adsorption (Cai et al., 2016), and c) FTIR spectra of Fe−BTC polymer gel before and after adsorption of As(V) (Zhu et al.,2012).

The adsorption of arsenic species over Fe-based materials is explained by Fe-O-As coordination and the formation of bidentate binuclear, bidentate mononuclear and monodentate mononuclear complexes. The coordinative sites of arsenic species depend on the number of hydroxyl groups that is of three in the case of As(V), which can offer four possible edge sites to form monodentate mononuclear complex and six possible sites to form bidentate binuclear complex with Fe-BTC-based MOFs. Hence, the coordination between arsenate and the incomplete-coordinated cationic Fe in the cluster is the primary adsorption mechanism in iron-trimesate MOFs (Li et al, 2019).

Hence, arsenate is adsorbed not just through surface-occurring processes but also through structure-occurring processes. The possible adsorption mechanism in the case of MIL100(Fe) is illustrated in Fig. 4.51 based on the iron trimesate secondary building unit. Similar to MIL100(Fe), the unsaturated sites of Basolite F300 are occupied by H2O molècules that can be substitute for external molecules such as arsenate or arsenite to coordinate with Fe(III) (Cai et al., 2016).

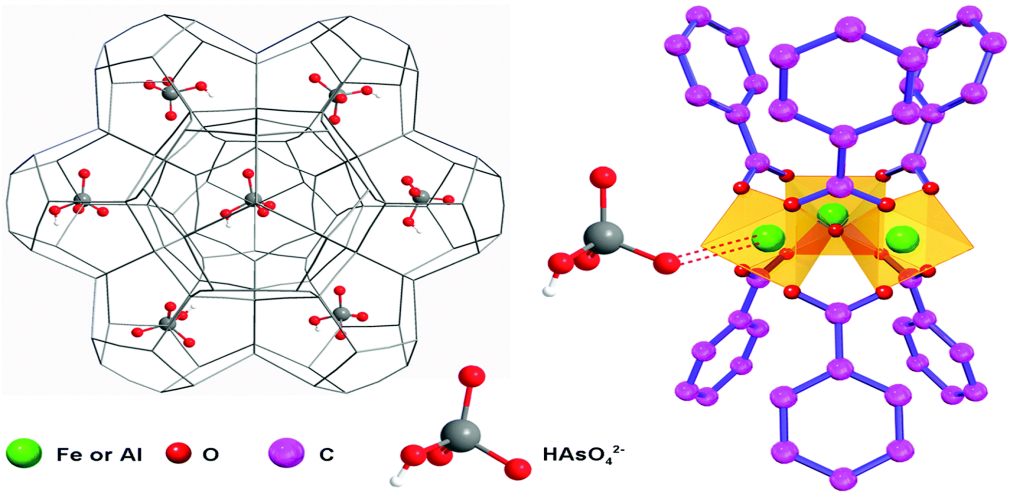

Figure 4.51. Schematic illustration of the adsorption mechanism of arsenate in MIL-100(Fe) (Cai et al., 2018).

4.5.2.8. Competition between As(III), As(V) and PO_4^{3-}

The study of the presence of other anions with arsenic in the same solution is an important factor that can affect the efficiency of the adsorbent and its potential for applications. Anions such as Cl^-, F^-, NO_3^-, SO_4^{2-} and PO_4^{3-}, which can be found in waters, may compete with arsenic during the adsorption process. Of these, only PO_4^{3-} has been reported as significantly affecting the adsorption capacity of nanomaterials to adsorb As(III) and As(V) (Li et al., 2014; Yu et al., 2019). Therefore, the effect of this anion on As(III) and As(V) removal was investigated by varying the initial concentration of PO_4^{3-} (10, 100 and 300 mg L^{-1}) while the As concentration was maintained constant at 10 mg L^{-1}. As can be seen in Figure 4.52, the presence of phosphate reduces the removal percentage of As(III) and As(V) by 18.5% and 6%, respectively. Due to the

competition between arsenite, arsenate and PO_4^{3-}, which may be due to their chemical similarity as these anions have similar electronegativity (2.18). The increase of PO_4^{3-} concentration led to a decrease in the removal percentage of As(V) and As(III).

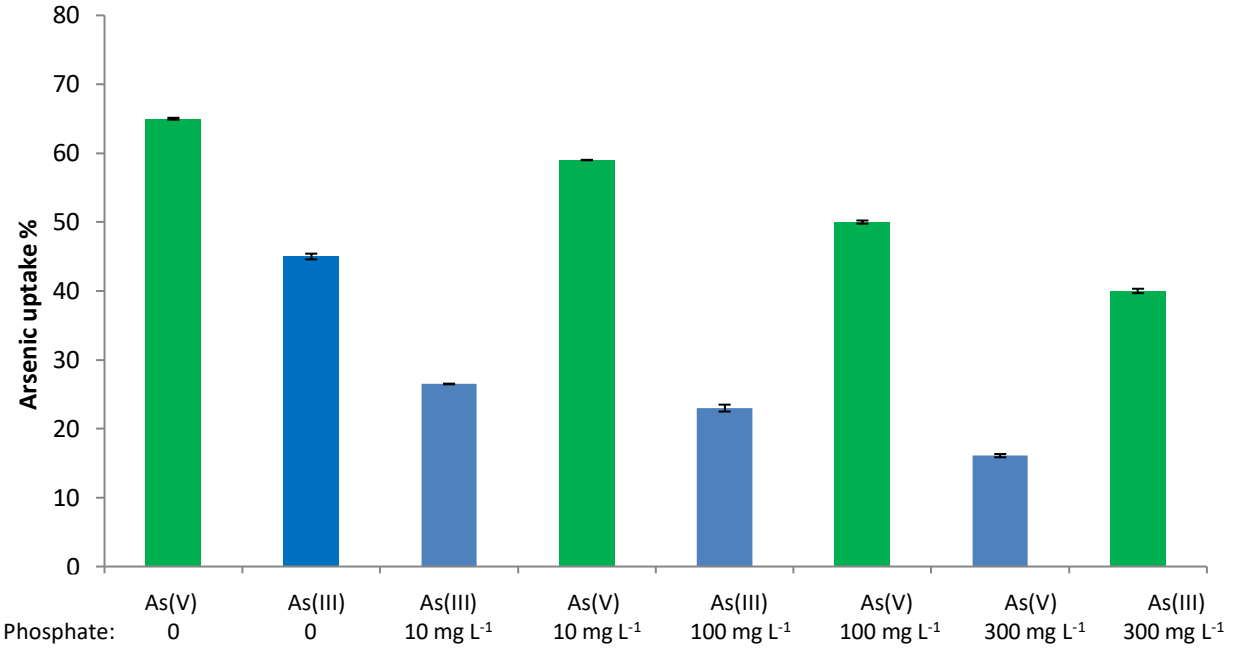

Figure 4.52. Competitive adsorption between As(V), As(III) and PO_4^{3-}: pH=5.6 for As(V), pH=9.5 for As(III), amount of adsorbent=0.1 g L^{-1} (n=3).

The presence of Arsenic in ground and/or drinking water is one of the most important environmental problems around the world. In this study, adsorption technology is considered a highly attractive option due to its simple design, low price, and easy operation. It is applied for the removal of arsenite and arsenate. Basolite F300 and nano-{Fe-BTC} are new porous crystalline materials used to remove arsenic from aqueous solutions. The results of characterization obtained by EDX show that Basolite F300 contain less percentage of iron (2.97%) than nano-{Fe-BTC} (3.68%). The BET results show the presence of mesopores with diameter in the upper size between 2 and 50 nm on the surface of Nano-{Fe-BTC}. This material has a higher pore volume (0.53 cm^3 g^{-1}) than Basolite F300 (0.41 cm^3 g^{-1}). However, this later

has a greater surface area with 431.6 m^2 g^{-1}. The TGA showed a similar behavior in terms of thermal stability for both materials.

The comparison between nano Fe-BTC MOFs and commercial Fe-BTC demonstrates that the commercial one has higher removal percentage for As(III) (47%) than synthetic material (36%) and for As(V) 90% and 86.7%, respectively.

The best removal efficiencies were obtained at pH 5.6 for As (V) and pH 9.5 for As (III) using 0.5 g L^{-1}. The good correlation found for arsenite and arsenate with the pseudo-second-order kinetic model which indicates a chemical sorption process. The adsorption of arsenic species over Fe-based materials is explained by Fe-O-As coordination and electrostacic interaction between arsenate or arsenite and the positive charge of the centred Fe^{3+} of the Fe-BTC based MOFs.The experimental data of the adsorption of As(V) fitted well the Freundlich model (K_F=10 mg g^{-1}), whereas, As(III) was described well by Langmuir isotherm with adsorption capacity 10 mg g^{-1}. Moreover, maximum adsorption capacity was found in the case of As(V) with 32.67 mg g^{-1} using Basolite F300. The results show that the presence of PO_4^{3-} in different concentrations (10, 100 and 300 mg L^{-1}) with arsenic 10 mg L^{-1} can influence on the removal of arsenic by Basolite due to their chemical similarity. The increase in the concentration of phosphate leads to a greater decrease in the arsenic removal.

5. CONCLUSIONS

In this thesis the efficiency of different adsorbents such as olive stone, pine cone and graphene oxides for the removal of Pb (II), Cu (II), Cd (II), and Cr (VI) from aqueous solutions has been evaluated as well as iron-trimesate MOFs for arsenite and arsenate uptake.

Even though the conclusions obtained from the different studies have been included in the Results and Discussion chapter, the main conclusions are summarized below:

1) Physico-chemical characterization of olive stone and pine cone showed that these agricultural wastes were mainly composed of carbon (~53%) and oxygen (~45.5%), and functional groups such as carboxylic and hydroxyl groups were present on their surfaces. Milled pine cone was found to have a greater surface area (0.2536 $m^2 g^{-1}$) than milled olive stone (0.1956 $m^2 g^{-1}$) whereas the latter had a smaller particle size (30.67 µm) than pine cone (50 µm). The pH at the point of the zero charge (pH_{pzc}) is 5.3 in the case of milled olive stone and 6.2 for pine cone.

2) Batch adsorption experiments were evaluated in order to remove Cu, Cd and Pb in single and multi-metal aqueous solutions using milled olive stone and milled pine cone. In the case of milled olive stone, the experimental data of Cu (II), Cd (II) and Pb (II) were described by the Langmuir isotherm model with adsorption capacities of 0.557, 0.3 and 0.581 mg g^{-1} for Cu (II), Cd (II) and Pb (II), respectively, at pH 6, whereas for Cr (VI), the Temkin model provided the best fit with a maximum capacity of 2.34 mg g^{-1} at pH 2. The pseudo-second-order kinetic model was found to have good agreement with all the metals, indicating a chemical sorption process. Moreover, Cd (II) has the highest kinetic constant, followed by Cu (II), Cr (VI) and Pb (II).

3) A decrease of 50% in the sorption capacity of Pb (II) by olive stone in the presence of Cu (II) and Cd (II) was found during the study of the competition between metals. In the case of these last two metals, the sorption capacities decreased by 30% and 15%, respectively, when the other metals were present. Since Cd had the highest rate constant, this metal was the first to saturate the available surface sites, followed by Cu and Pb.

4) The efficiency of milled pine cone in removing trace concentration levels of Pb (II), Cd (II), and Cu (II) has been demonstrated, resulting in maximum adsorption capacities of 100.01 mg g^{-1}, 78.73 mg g^{-1}, and 33.55 mg g^{-1} at pH 5.5, respectively. The experimental data of Pb (II) and Cd (II) followed the Langmuir-Freundlich model well whereas Cu (II) fitted the Langmuir model. In the case of Cr (VI), the adsorption data also fitted the Langmuir model with an adsorption capacity of 57.36 mg g^{-1} at pH 2 and 10 g L^{-1} of adsorbent.

5) In the case of the divalent ions (Pb (II), Cu (II), and Cd (II)), there was no competition between them towards the adsorbent sites of pine cone at low metal concentration levels (1-10 mg L^{-1}), given that the presence of other metal ions did not reduce the removal efficiencies.

6) The higher adsorption capacity of milled pine cone with respect to olive stone is explained by its greater surface area. The adsorption mechanism of Pb (II), Cu (II) and Cd (II) for both biosorbents occurred through surface complexation with the functional groups of the adsorbent surface. Pb (II) has the highest affinity for both biosorbents due to its greater electronegativity. In the case of Cr (VI) adsorption, maximum removal percentages of 46% for olive stone and 88 % for pine cone were obtained at pH 2, showing that this toxic anion can be removed via an ion-exchange mechanism coupled to a reduction reaction of Cr (VI) to Cr (III).

7) Dynamic adsorption in a fixed-bed column is an effective method for large scale treatment of water effluents due to cyclic adsorption/desorption. The results obtained in a lab-scale fixed-bed column filled with pine cone show that the experimental data of Pb (II) removal agreed well with the Thomas model with an adsorption capacity of 77.92 mg g^{-1} at a flow rate of 2.2 mL min^{-1}, bed height 0.7 cm and an initial concentration of 50 mg L^{-1}.

8) When solutions containing equal concentrations (25 mg $L^{-1,}$ 50 mg L^{-1} and 100 mg L^{-1}) of Cu (II), Cd (II) and Pb (II), were passed at a flow rate of 2.2 mL min^{-1} through a 1

cm bed height, the highest exhaustion time was obtained for Pb (II), followed by Cu (II) and Cd (II), confirming the greater affinity of pine cone for this metal ion.

9) The results obtained when 100 mg L^{-1} of Ca (II) were present in a multi-metal solution of Cu (II), Pb (II) and Cd (II) at equal initial concentrations of 50 mg L^{-1} at pH 5.6, showed that Ca (II) was not adsorbed and that its presence did not affect the adsorption of Pb (II), Cu (II) and Cd (II).

10) When a solution simulating an electroplating waste containing 20 mg L^{-1} of Cu (II), 100 mg L^{-1} of Ni (II) and 30 mg L^{-1} of Cr (VI) at pH 4.4 was passed through a 2cm bed height fixed-bed column at a flow rate of 2.2 mL min^{-1}, removal percentages of Cu (II), Ni (II) and Cr (VI) of 97%, 94% and 93%, respectively, were obtained. Cr (VI) broke through the column faster than Cu (II) and Ni (II) as a result of its lower affinity for pine cone at pH >2. Ni (II) and Cu (II) broke through the column at 30 and 80 min, respectively. These results proved the capacity of pine cone to separate cations as Cu (II) (20 mg L^{-1}) and Ni (II) (100 mg L^{-1}) from anions as Cr (VI) (30 mg L^{-1}).

11) The results of the desorption of Cu(II), Ni(II) and Cr(VI) from milled pine cone using a 1.0 M HCl solution demonstrate a higher desorption percentage in the case of all the metal ions, Cr(VI) with 90% and 94% for Cu(II) and Ni (II), which will allow the adsorbent to be reused.

12) All the graphene oxides (227A, 97D, GO-I and GO-II), prepared in the Chemistry Dpt. of Masayk University (Brno, Czech Rep.), presented the same XRD pattern and the Raman spectrum showed a lower degree of functionalization and a lower oxidation level given that the percentage of C≈O groups, measured by XPS, ranged from 11.6 to 12.56%. This low functionalization was confirmed by the surface composition determined by EDX, which showed C percentages ≥ 88%, and oxygen percentages between 4 and 9%. FTIR identifies the presence of carbonyl/carboxyl and OH bands on the surface of the adsorbents. BET surface areas ranged from 14.2268 to 25.8041 m^2 g^{-1}, which are lower than the areas reported for other graphene oxides. Pore volumes ranged from 0.063 to 0.070 cm^3 g^{-1}.

13) The maximum removal percentage of Cu (II) (>90%) and Cd (II) (>88%) using 227A, GO-I and GO-II were obtained at pH 6 in 5 mg L^{-1} and 2 g L^{-1}. Percentages of <80% for Cu (II) and <60% for Cd (II) were obtained when 97D was used as an adsorbent. In the case of Cr (VI), maximum percentage removal was obtained at pH 2 and 10 g L^{-1} with 68% and 45% for GO-I and GO-II, respectively. The experimental data of the sorption systems studied fitted the Freundlich isotherm model well in the case of Cu (II) with 227A (K_F 2.68), 97D (K_F 2.61), GO-I (K_F 3.34) and GO-II (K_F 3.72). The Freundlich isotherm is also the best model to express the adsorption data of Cd (II) for 227A (K_F 2.32) and GO-II (K_F 2.71) whereas the Langmuir-Freundlich model provides the best fit for 97D and GO-I with adsorption capacities of 5.19 and 5.28 mg g^{-1}, respectively.

14) The adsorption mechanism of Cu (II) and Cd (II) seems to take place due to their interaction with the functional groups (COO^-, or O^-) on the surface of GO to form a metal ion complex. For Cr (VI), Freundlich was considered the best model in the case of both GO-I (k_F 0.26) and GO-II (K_F 0.12). The adsorption mechanism of Cr (VI) occurred through an electrostatic interaction of $HCrO_4^-$ species with the protonated groups of the sorbent surface at low pHs (1-2).

15) Basolite F300 and Nano-{Fe-BTC} MOF, synthesized within collaboration with the Department of Chemistry of the University of La Laguna, were evaluated to remove As (V) and As (III). The elemental analysis of the adsorbent surface performed by EDX showed that Basolite F300 contains a lower percentage of iron (2.97%) than Nano-{Fe-BTC} MOF (3.68%). The results of TGA/DTA show that both materials have similar behaviour in terms of stability. The infrared spectra of the commercial Basolite F300 and the synthesized nano-{Fe-BTC} MOF show similar bands, including in the 650-1800 cm^{-1} region, which is generally considered to be a fingerprint of MOFs. Moreover, the presence of mesopores with diameters between 2 nm and 50 nm were found on the surface of Nano-{Fe-BTC}. A series of cracks and asymmetric pores with open pores structure with particle size which generated a large internal surface area were observed

in the SEM images of Nano-{Fe-BTC}. This nanomaterial has a higher pore volume (0.53 $cm^3\ g^{-1}$) than Basolite F300 (0.41 $cm^3\ g^{-1}$). However, Basolite F300 has a greater surface area (431.6 $m^2\ g^{-1}$) than Nano-{Fe-BTC} MOF (427.2 $m^2\ g^{-1}$).

16) The experimental adsorption data of As (V) and As (III) fitted the pseudo second-order model well, showing that chemisorption is the dominant mechanism for their adsorption. The experiments were performed at pH 5.6 for As (V) and at pH 9.5 for As (III) with an initial arsenic concentration of 10 mg L^{-1} and 0.1 g L^{-1} of Basolite F300. The equilibrium was reached approximately after 1 hour. Moreover, the relative linearity of the intraparticle diffusion kinetic model for As (III) and As (V) shows that intraparticle diffusion was the rate controlling process with little contribution of boundary layer diffusion.

17) Arsenic adsorption occurred through coordination and electrostatic interaction and depends on the pH. In the case of As(V), $H_2AsO_4^-$ is the predominant species in the 3-8 pH range and $HAsO_4^{2-}$ species is the predominant one in the 8-11 pH range, both anions are Lewis base that can strongly interact with centred Fe^{3+} cations (Lewis acid). Additionally, electrostatic interaction between arsenate and the positive charge of the centred Fe^{3+} enhanced As (V) adsorption. The maximum uptake percentage (90 %) was obtained at pH 5.6. In the case of As (III), pH 9.5 was the most appropriate for its removal with 47%, due to the presence at this pH of the $H_2AsO_3^-$ species which can interact with the centred Fe^{3+} cation. The results of FTIR after adsorption confirm that the adsorption of arsenic species over Fe-based materials occurred through Fe-O-As coordination.

18) The experimental data of the adsorption of As (V) was described with Freundlich (K_F=10 mg g^{-1}) whereas the best model was Langmuir for As (III) with an adsorption capacity of 10 mg g^{-1}. The maximum adsorption capacity of As (V), which was 32.67 mg $g^{-}1$, was obtained from the pseudo second order model. The presence of PO_4^{3-}, which has a similar chemical structure to arsenite and arsenate, in different concentrations (10, 100 and 300 mg L^{-1}) with arsenic (10 mg L^{-1}) shows a decrease in

the removal percentages of 18.5% and 6% for As (III) and As (V), respectively. The increase in the concentration of phosphate leads to a greater decrease in the arsenic removal.

19) Basolite F300 shows greater efficiency than Nano-{Fe-BTC} MOF in the removal of As (V) with removal rates of 90% and 86.7%, respectively, and in the case of As (III), of 47% and 36%, respectively.

6. BIBLIOGRAPHY

Abate, G., Masini, J.C. (2005). Adsorption of atrazine, hydroxyatrazine, deethylatrazine, and deisopropylatrazine onto Fe(III) polyhydroxy cations intercalated vermiculite and montmorillonite, Journal of Agricultural and Food Chemistry, 53: 1612–1619. https://doi.org/10.1021/jf048556j

Abbas, S., Kamar, F., Hossien, Y. (2018). Adsorption of methyl violet 2B dye from aqueous solutions onto waste of Banana peel using fixed-bed column, International Journal of Civil Engineering and Technology, 9: 2094–2109.

Abdel Salam, O.E., Reiad, N.A., ElShafei, M.M. (2011). A study of the removal characteristics of heavy metals from wastewater by low-cost adsorbents, Journal of Advanced Research, 2: 297–303. https://doi.org/10.1016/j.jare.2011.01.008

Abdel-Ghani, N.T., Elchaghaby, G.A. (2007). Influence of operating conditions on the removal of Cu, Zn, Cd and Pb ions from wastewater by adsorption, International Journal of Environmental Science and Technology, 4: 451–456. https://doi.org/10.1007/BF03325980

Abdelhafez, A.A., Li, J. (2016). Removal of Pb(II) from aqueous solution by using biochars derived from sugar cane bagasse and orange peel, Journal of the Taiwan Institute of Chemical Engineers, 61: 367–375. https://doi.org/10.1016/j.jtice.2016.01.005

Abdolali, A., Guo, W.S., Ngo, H.H., Chen, S.S., Nguyen, N.C., Tung, K.L. (2014). Typical lignocellulosic wastes and by-products for biosorption process in water and wastewater treatment: A critical review, Bioresource Technology, 160: 57–66. https://doi.org/10.1016/j.biortech.2013.12.037

Abudaia. A, J., O. Sulyman, M., Y. Elazaby, K., M. Ben-Ali, S. (2013). Adsorption of Pb(II) and Cu(II) from Aqueous Solution onto Activated Carbon Prepared from Dates Stones, International Journal of Environmental Science and Development, 4: 191–195. https://doi.org/10.7763/IJESD.2013.V4.333

Abdullah, N., Yusof, N., Lau, W.J., Jaafar, J., Ismail, A.F. (2019). Recent trends of heavy metal removal from water/wastewater by membrane technologies, Journal of Industrial and Engineering Chemistry, 76: 17–38. https://doi.org/10.1016/j.jiec.2019.03.029

Acharya, J., Kumar, U., Rafi, P. (2018). Removal of Heavy Metal Ions from Wastewater by Chemically Modified Agricultural Waste Material as Potential Adsorbent-A Review, International Journal of Current Engineering and Technology, 526-530.

https://doi.org/10.14741/ijcet/v.8.3.6

Adesola, B., Kemi, O., Kikelomo Tobi, S., Babatunde Damilare, A., Aanu, O., Elizabeth, H. (2016). Comparative study on the biosorption of Pb(II), Cd(II) and Zn(II) using Lemon grass (Cymbopogon citratus): Kinetics, isotherms and thermodynamics, International Journal of Chemistry, 2: 89–102. https://doi.org/10.31221/osf.io/3jb9u

Aeisyah, A., Ismail, M.H.S., Lias, K., Izhar, S. (2014). Adsorption process of heavy metals by low-cost adsorbent: A review, Research Journal of Chemistry and Environment, 18: 91–102. https://doi.org/10.5829/idosi.wasj.2013.28.11.1874

Afroze, S., Sen, T.K. (2018). A Review on Heavy Metal Ions and Dye Adsorption from Water by Agricultural Solid Waste Adsorbents, Water Air Soil Pollution, 229, 225. https://doi.org/10.1007/s11270-018-3869-z

Aguilar, K.M.M., Kose, Y., Amano, Y., Machida, M., Imazeki, F. (2016). Influence of Oxidation Conditions of Activated Carbon on Adsorption of Pb(II) from Aqueous Solution, Journal of Environmental Chemistry, 26: 109–114. https://doi.org/10.5985/jec.26.109

Ahmad, A., Ghazi, Z.A., Saeed, M., Ilyas, M., Ahmad, R., Khattak, A.M., Iqbal, A. (2017). A comparative study of the removal of Cr(VI) from synthetic solution using natural biosorbents, New Journal of Chemistry, 41: 10799–10807.
https://doi.org/10.1039/C7NJ02026K

Ahmad, S.Z.N., Wan Salleh, W.N., Ismail, A.F., Yusof, N., Mohd Yusop, M.Z., Aziz, F. (2020). Adsorptive removal of heavy metal ions using graphene-based nanomaterials: Toxicity, roles of functional groups and mechanisms, Chemosphere, 248, 126008.
https://doi.org/10.1016/j.chemosphere.2020.126008

Akpa, O., Unuabonah, E. (2011). Small-Sample Corrected Akaike Information Criterion: An appropriate statistical tool for ranking of adsorption isotherm models, Desalination, 272: 20–26. https://doi.org/10.1016/j.desal.2010.12.057

Al-Baidhani J.B and Al-Salihy S.T, (2016). Removal of heavy metals from aqueous solution by using low cost rice husk in batch and continuous fluidized experiments, International Journal of Chemical Engineering and Applications, 7 (1): 6-10.
https://doi.org/10.7763/IJCEA.2016.V7.532.

Alam, S. , Sharma, N., Kumar, L. (2017). Synthesis of Graphene Oxide (GO) by Modified Hummers Method and Its Thermal Reduction to Obtain Reduced Graphene Oxide (rGO)*. *Graphene*, **6**, 1-18. doi: 10.4236/graphene.2017.61001

Alkherraz AM, Ali AK, Elsherif, KM (2020). Removal of Pb(II), Zn(II), Cu(II) and Cd(II) from aqueous solutions by adsorption onto olive branches activated carbon: Equilibrium and thermodynamic studies, Chemistry International, 6: 11–20. https://doi.org/10.5281/zenodo.2579465

Aldawsari, A., Khan, M.A., Hameed, B.H., Alqadami, A.A., Siddiqui, M.R., Alothman, Z.A., Ahmed, A.Y.B.H. (2017). Mercerized mesoporous date pit activated carbon—A novel adsorbent to sequester potentially toxic divalent heavy metals from water, PLOS ONE, 12(9) e0184493. https://doi.org/10.1371/journal.pone.0184493

Ali, H., Khan, E., Sajad, M.A. (2013). Phytoremediation of heavy metals—Concepts and applications, Chemosphere, 91: 869–881. https://doi.org/10.1016/j.chemosphere.2013.01.075

Ali, I., Basheer, A.A., Mbianda, X.Y., Burakov, A., Galunin, E., Burakova, I., Mkrtchyan, E., Tkachev, A., Grachev, V. (2019). Graphene based adsorbents for remediation of noxious pollutants from wastewater, Environment International, 127: 160–180. https://doi.org/10.1016/j.envint.2019.03.029

Almendros, A.I., Martín-Lara, M.A., Ronda, A., Pérez, A., Blázquez, G., Calero, M. (2015). Physico-chemical characterization of pine cone shell and its use as biosorbent and fuel, Bioresource Technology, 196: 406–412. https://doi.org/10.1016/j.biortech.2015.07.109

Altundoğan, H.S., Topdemir, A., Çakmak, M., Bahar, N. (2016). Hardness removal from waters by using citric acid modified pine cone, Journal of Taiwan Institute of Chemical Engineers, 58: 219–225. https://doi.org/10.1016/j.jtice.2015.07.002

Amar, M.B., Walha, K., Salvadó, V. (2020). Evaluation of Olive Stones for Cd(II), Cu(II), Pb(II) and Cr(VI) Biosorption from Aqueous Solution: Equilibrium and Kinetics, International Journal of Environmental Research, 14: 193–204. https://doi.org/10.1007/s41742-020-00246-5

Amar, M.B., Walha, K., Salvadó, V. (2021). Valorisation of pine cone as an efficient biosorbent for the removal of Pb(II), Cd(II), Cu(II) and Cr(VI)m Adsorption Science and Technology. 2021: ID 6678530. https://doi.org/10.1155/2021/6678530

Aravind, C., Chanakya, K., Mahindra, K. (2017). Removal of heavy metals from industrial waste water using coconut coir, International Journal of Civil Engineering and Technology, 8: 1869–1871.

Atkovska, K., Lisichkov, K., Ruseska, G., Dimitrov, A.T., Grozdanov, A. (2018). Removal of heavy metal ions from wastewater using conventional and nanosorbents: A review, Journal of Chemical Technology and Metallurgy, 53: 202-219

Awad, F., Erkurt, H. (2014). Biosorption of lead(II) and copper(II) by Pinus resinosa: Modeling and mechanism, Fresenius Environmental Bulletin, 23: 540–549.

Awual, M.R., Ismael, M., Khaleque, M.A., Yaita, T. (2014). Ultra-trace copper(II) detection and removal from wastewater using novel meso-adsorbent. Journal of Industrial and Engineering Chemistry, 20: 2332–2340. https://doi.org/10.1016/j.jiec.2013.10.009

Azimi, A., Azari, A., Rezakazemi, M., Ansarpour, M. (2017). Removal of Heavy Metals from Industrial Wastewaters: A Review, ChemBioEng Reviews, 4: 37–59. https://doi.org/10.1002/cben.201600010

Bagherian, G., Nemati, E., Arab Chamjangali, M., Ashrafi, M. (2021). Removal of lead ions from aqueous solutions using functionalized pine cone powder, Journal of Iranian Chemical Society. https://doi.org/10.1007/s13738-021-02196-x

Barquilha, C.E.R., Cossich, E.S., Tavares, C.R.G., da Silva, E.A. (2019). Biosorption of nickel and copper ions from synthetic solution and electroplating effluent using fixed bed column of immobilized brown algae, Journal of Water Process Engineering, 32: 100904. https://doi.org/10.1016/j.jwpe.2019.100904

Belalia, M., Bendjelloul, M., Aziz, A., Elandaloussi, E.H. (2018). Surface Modification of Olive Stone Waste for Enhanced Sorption Properties of Cadmium and Lead Ions, Acta Chemica Iasi, 26(2):281-306

Bhatnagar, A., Kaczala, F., Hogland, W., Marques, M., Paraskeva, C.A., Papadakis, V.G., Sillanpää, M. (2014). Valorization of solid waste products from olive oil industry as potential adsorbents for water pollution control—a review, Environmental Science and Pollution Research, 21: 268–298. https://doi.org/10.1007/s11356-013-2135-6

Bhatnagar, A., Sillanpää, M., Witek-Krowiak, A. (2015). Agricultural waste peels as versatile biomass for water purification – A review, Chemical Engineering Journal, 270: 244–271. https://doi.org/10.1016/j.cej.2015.01.135

Biswas, S., Siddiqi, H., Meikap, B.C., Sen, T.K., Khiadani, M. (2019). Preparation and Characterization of Raw and Inorganic Acid-Activated Pine Cone Biochar and Its Application in the Removal of Aqueous-Phase Pb^{2+} Metal Ions by Adsorption, Water Air Soil Pollution, 231. https://doi.org/10.1007/s11270-019-4375-7

Blázquez, G., Hernáinz, F., Calero, M., Martín-Lara, M.A., Tenorio, G. (2009). The effect of pH on the biosorption of Cr (III) and Cr (VI) with olive stone, Chemical Engineering Journal, 148: 473–479. https://doi.org/10.1016/j.cej.2008.09.026

Blázquez, G., Calero, M., Hernáinz, F., Tenorio, G., Martín-Lara, M.A. (2010). Equilibrium biosorption of lead(II) from aqueous solutions by solid waste from olive-oil production, Chemical Engineering Journal, 160: 615–622. https://doi.org/10.1016/j.cej.2010.03.085

Blázquez, G., Martín-Lara, M.A., Dionisio-Ruiz, E., Tenorio, G., Calero, M. (2012). Copper biosorption by pine cone shell and thermal decomposition study of the exhausted biosorbent, Journal of Industrial and Engineering Chemistry, 18: 1741–1750. https://doi.org/10.1016/j.jiec.2012.03.018

Blázquez, G., Martín-Lara, M.A., Dionisio-Ruiz, E., Tenorio, G., Calero, M. (2011). Evaluation and comparison of the biosorption process of copper ions onto olive stone and pine bark, Journal of Industrial and Engineering Chemistry, 17: 824–833. https://doi.org/10.1016/j.jiec.2011.08.003

Bohli, T., Ouederni, A. (2016). Improvement of oxygen-containing functional groups on olive stones activated carbon by ozone and nitric acid for heavy metals removal from aqueous phase, Environmental Science and Pollution Research, 23: 15852–15861. https://doi.org/10.1007/s11356-015-4330-0

Bohli, T., Ouederni, A., Fiol, N., Villaescusa, I. (2015). Evaluation of an activated carbon from olive stones used as an adsorbent for heavy metal removal from aqueous phases, Comptes Rendus Chimie, 18: 88–99. https://doi.org/10.1016/j.crci.2014.05.009

Bohli, T., Ouederni, A., Villaescusa, I. (2017). Simultaneous adsorption behavior of heavy metals onto microporous olive stones activated carbon: analysis of metal interactions, Euro-Mediterranean Journal for Environmental Integration, 19. https://doi.org/10.1007/s41207-017-0030-0

Brahmaiah, T., Spurthi, L., Chandrika, K., Kausalya Chandra, L., Yashas, S., Ramanaiah, S., Sai Prasad, K.S. (2015). Removal of Heavy Metals from Waste Water Using Low Cost Adsorbent, International Journal of Trend in Research and Development, 3: 2394–9333.

Budinova, T., Petrov, N., Razvigorova, M., Parra, J., Galiatsatou, P. (2006). Removal of Arsenic(III) from Aqueous Solution by Activated Carbons Prepared from Solvent Extracted Olive Pulp and Olive Stones, Industrial and Engineering Chemistry Research, 45: 1896–1901. https://doi.org/10.1021/ie051217a

Cai, J., Mao, X., Song, W.-G. (2018). Adsorption behavior and structure transformation of mesoporous metal–organic frameworks towards arsenates and organic pollutants in aqueous solution, Materials Chemistry Frontiers, 2: 1389–1396. https://doi.org/10.1039/C8QM00002F

Cai, J., Wang, X., Zhou, Y., Jiang, L., Wang, C. (2016). Selective adsorption of arsenate and the reversible structure transformation of the mesoporous metal-organic framework MIL-100(Fe), Physical Chemistry Chemical Physics, 18: 10864–10867. https://doi.org/10.1039/c6cp00249h

Çakmak, M., Bahar, N., Topdemir, A., Altundoğan, H.S. (2016). Hardness removal from waters by using citric acid modified pine cone, Journal of the Taiwan Institute of Chemical Engineers, 58: 219-225. https://doi.org/10.1016/J.JTICE.2015.07.002

Calero, M., Hernáinz, F., Blázquez, G., Martín-Lara, M.A., Tenorio, G. (2009). Biosorption kinetics of Cd (II), Cr (III) and Pb (II) in aqueous solutions by olive stone, Brazilian Journal of Chemical Engineering, 26: 265–273. https://doi.org/10.1590/S0104-66322009000200004

Cao, D.-Q., Wang, X., Wang, Q.-H., Fang, X.-M., Jin, J.-Y., Hao, X.-D., Iritani, E., Katagiri, N. (2020). Removal of heavy metal ions by ultrafiltration with recovery of extracellular polymer substances from excess sludge, Journal of Membrane Science, 606, 118103. https://doi.org/10.1016/j.memsci.2020.118103

Carolin, C.F., Kumar, P.S., Saravanan, A., Joshiba, G.J., Naushad, M. (2017). Efficient techniques for the removal of toxic heavy metals from aquatic environment: A review, Journal of Environmental Chemical Engineering, 5: 2782–2799. https://doi.org/10.1016/j.jece.2017.05.029

Cataldo, S., Gianguzza, A., Milea, D., Muratore, N., Pettignano, A., Sammartano, S. (2018). A critical approach to the toxic metal ion removal by hazelnut and almond shells, Environmental Science and Pollution Research, 25:4238–4253. https://doi.org/10.1007/s11356-017-0779-3

Cechinel, M.A.P., Ulson de Souza, S.M.A.G., Ulson de Souza, A.A. (2014). Study of lead (II) adsorption onto activated carbon originating from cow bone, Journal of Cleaner Production, 65: 342–349. https://doi.org/10.1016/j.jclepro.2013.08.020

Chand, P., Pakade, Y.B. (2013). Removal of Pb from water by adsorption on apple pomace: Equilibrium, kinetics, and thermodynamics studies, Journal of Chemistry, 8: 164575. https://doi.org/10.1155/2013/164575

Chauhan, D., Sankararamakrishnan, N. (2011). Modeling and evaluation on removal of hexavalent chromium from aqueous systems using fixed bed column, Journal of Hazardous Materials, 185: 55–62. https://doi.org/10.1016/j.jhazmat.2010.08.120

Chawla, J., Kumar, R., Kaur, I. (2015). Carbon nanotubes and graphenes as adsorbents for adsorption of lead ions from water: a review. Journal of Water Supply: Research and Technology-Aqua, 64: 641–659. https://doi.org/10.2166/aqua.2015.102

Chen, Y., Bai, X., Ye, Z. (2020). Recent Progress in Heavy Metal Ion Decontamination Based on Metal–Organic Frameworks, Nanomaterials, 10(8) 1481. https://doi.org/10.3390/nano10081481

Chen, B., Zhu, Z., Ma, J., Yang, M., Hong, J., Hu, X., Qiu, Y., Chen, J. (2014). One-pot, solid-phase synthesis of magnetic multiwalled carbon nanotube/iron oxide composites and their application in arsenic removal, Journal of Colloid and Interface Science, 434: 9–17. https://doi.org/10.1016/j.jcis.2014.07.046

Cheraghi, M., Sobhanardakani, S., Zandipak, R., Lorestani, B., Merrikhpour, H. (2015). Removal of Pb (II) from aqueous solutions using waste tea leaves, Iranian Journal of Toxicology, 9: 1247–1253.

Chowdhury, Z., Abd Hamid, S.B., Zain, S. (2014). Evaluating Design Parameters for Breakthrough Curve Analysis and Kinetics of Fixed Bed Columns for Cu(II) Cations Using Lignocellulosic Wastes, BioResources, 10(1): 732-749. https://doi.org/10.15376/biores.10.1.732-749

Conde-González, J.E., Peña-Méndez, E.M., Melián-Fernández, A.M., Havel, J., Salvadó, V. (2021). Synthesis, performance and mechanism of nanoporous Fe-(1,3,5-tricarboxylic acid) metal-organic framework in the removal of anionic dyes from water, submitted to Environmental nanotechnology, monitoring and management (under revision).

Corral Bobadilla, M., Lostado Lorza, R., Somovilla Gómez, F., Escribano García, R. (2020). Adsorptive of Nickel in Wastewater by Olive Stone Waste: Optimization through Multi-Response Surface Methodology Using Desirability Functions, Water, 12(5) 1320. https://doi.org/10.3390/w12051320

Crini, G., Lichtfouse, E. (2019). Advantages and disadvantages of techniques used for wastewater treatment, Environmental Chemistry Letters, 17: 145–155. https://doi.org/10.1007/s10311-018-0785-9

Crini, G., Lichtfouse, E., Wilson, L., Morin-Crini, N. (2019). Conventional and non-conventional adsorbents for wastewater treatment, Environmental Chemistry Letters, 17: 195–213. https://doi.org/10.1007/s10311-018-0786-8

Dai, Y., Sun, Q., Wang, W., Lu, L., Liu, M., Li, J., Yang, S., Sun, Y., Zhang, K., Xu, J., Zheng, W., Hu, Z., Yang, Y., Gao, Y., Chen, Y., Zhang, X., Gao, F., Zhang, Y. (2018). Utilizations of agricultural waste as adsorbent for the removal of contaminants: A review, Chemosphere, 211: 235–253. https://doi.org/10.1016/j.chemosphere.2018.06.179

Dai, J.F., Wang, G.J., Ma, L., Wu, C.K. (2015). Surface properties of graphene: Relationship to graphene-polymer composites, Reviews on Advanced Materials Science, 40: 60–71.

Dastgheib, S.A., Rockstraw, D.A. (2002). A model for the adsorption of single metal ion solutes in aqueous solution onto activated carbon produced from pecan shells, Carbon, 40: 1843–1851. https://doi.org/10.1016/S0008-6223(02)00037-4

Davila-Guzman, N.E., Cerino-Córdova, F.J., Loredo-Cancino, M., Rangel-Mendez, J.R., Gómez-González, R., Soto-Regalado, E. (2016). Studies of Adsorption of Heavy Metals onto Spent Coffee Ground: Equilibrium, Regeneration, and Dynamic Performance in a Fixed-Bed Column, International Journal of Chemical Engineering, Article ID 9413879. https://doi.org/10.1155/2016/9413879

de Aguiar, T.R., Guimarães Neto, J.O.A., Şen, U., Pereira, H. (2019). Study of two cork species as natural biosorbents for five selected pesticides in water, Heliyon, 5, e01189. https://doi.org/10.1016/j.heliyon.2019.e01189

De Gisi, S., Lofrano, G., Grassi, M., Notarnicola, M. (2016). Characteristics and adsorption capacities of low-cost sorbents for wastewater treatment: A review, Sustainable Materials and Technologies, 9: 10–40. https://doi.org/10.1016/j.susmat.2016.06.002

Decret 130/2003, de 13 de maig , pel qual s'aprova el Reglament dels serveis públics de sanejament. Diari Oficial de la Generalitat de Catalunya Núm. 3894 – 29.5.2003 http://acaweb.gencat.cat/aca/documents/ca/legislacio/decrets/decret_130_2003.pdf

Değirmen, G., Kılıç, M., Cepelioğullar, O., Pütün, A.E. (2012). Removal of copper(II) and cadmium(II) ions from aqueous solutions by biosorption onto pine cone, Water Science and Technology, 66: 564–572. https://doi.org/10.2166/wst.2012.210

DeMessie, B., Sahle-Demessie, E., Sorial, G.A. (2015). Cleaning Water Contaminated with Heavy Metal Ions Using Pyrolyzed Biochar Adsorbents, Separation Science and Technology, 50: 2448–2457. https://doi.org/10.1080/01496395.2015.1064134

Deng, J.-H., Zhang, X.-R., Zeng, G.-M., Gong, J.-L., Niu, Q.-Y., Liang, J. (2013). Simultaneous removal of Cd(II) and ionic dyes from aqueous solution using magnetic graphene oxide nanocomposite as an adsorbent, Chemical Engineering Journal, 226: 189–200. https://doi.org/10.1016/j.cej.2013.04.045

Dhakshinamoorthy, A., Alvaro, M., Horcajada, P., Gibson, E., Vishnuvarthan, M., Vimont, A., Grenèche, J.-M., Serre, C., Daturi, M., Garcia, H. (2012). Comparison of Porous Iron Trimesates Basolite F300 and MIL-100(Fe) As Heterogeneous Catalysts for Lewis Acid and Oxidation Reactions: Roles of Structural Defects and Stability, ACS Catalysis, 2: 2060–2065. https://doi.org/10.1021/cs300345b

Ding, Y., Jing, D., Gong, H., Zhou, L., Yang, X. (2012). Biosorption of aquatic cadmium(II) by unmodified rice straw, Bioresource Technology, 114: 20–25. https://doi.org/10.1016/j.biortech.2012.01.110

Dialynas, E., Diamadopoulos, E. (2009). Integration of a membrane bioreactor coupled with reverse osmosis for advanced treatment of municipal wastewater, Desalination, 238: 302–311. https://doi.org/10.1016/j.desal.2008.01.046

Duru, C., Nnabuchi, M., Duru, I. (2019). Adsorption of Cu onto Maize Husk Lignocellulose in Single and Binary Cu-Zn Solution Systems: Equilibrium, Isotherm, Kinetic,

Thermodynamic and Mechanistic Studies, Egyptian Journal of Chemistry, 62: 1295-1305. https://doi.org/10.21608/ejchem.2019.6377.1539

Edelstein, M., Ben-Hur, M. (2018). Heavy metals and metalloids: Sources, risks and strategies to reduce their accumulation in horticultural crops, Scientia Horticulturae, 234: 431–444. https://doi.org/10.1016/j.scienta.2017.12.039

El-Sayed, G.O., Dessouki, H.A., Ibrahiem, S.S. (2011). Removal of Zn (II), Cd (II) and Mn (II) from aqueous solutions by adsorption on maize stalks, Malaysian Journal of Analytical Sciences, 15: 8–21.

El-Sikaily, A., Nemr, A.E., Khaled, A., Abdelwehab, O. (2007). Removal of toxic chromium from wastewater using green alga Ulva lactuca and its activated carbon, Journal of Hazardous Materials, 148: 216–228. https://doi.org/10.1016/j.jhazmat.2007.01.146

Etorki, A.M., El-Rais, M., Mahabbis, M.T., Moussa, N.M. (2014). Removal of Some Heavy Metals from Wastewater by Using of Fava Beans, American Journal of Analytical Chemistry, 5(4): 225-234. https://doi.org/10.4236/ajac.2014.54028

Feng, M., Zhang, P., Zhou, H.-C., Sharma, V.K. (2018). Water-stable metal-organic frameworks for aqueous removal of heavy metals and radionuclides: A review, Chemosphere, 209: 783–800. https://doi.org/10.1016/j.chemosphere.2018.06.114

Fomina, M., Gadd, G.M. (2014). Biosorption: current perspectives on concept, definition and application, Bioresource Technology, 160: 3–14. https://doi.org/10.1016/j.biortech.2013.12.102

Fu, W., Huang, Z. (2018). Magnetic dithiocarbamate functionalized reduced graphene oxide for the removal of Cu(II), Cd(II), Pb(II), and Hg(II) ions from aqueous solution: Synthesis, adsorption, and regeneration, Chemosphere, 209: 449–456. https://doi.org/10.1016/j.chemosphere.2018.06.087

Gadd, G.M. (2009). Biosorption: critical review of scientific rationale, environmental importance and significance for pollution treatment, Journal of Chemical Technology and Biotechnology, 84: 13–28. https://doi.org/10.1002/jctb.1999

Galvez, R., Lefrançois, P.J. (2016). Les sols contaminés par des métaux lourds: Distribution géochimique et techniques de restauration sols et eaux souterraines, Vecteur Environment, 38: 30–38.

Gao, Y., Aliques Tomas, M. del C., Garemark, J., Sheng, X., Berglund, L., Li, Y. (2021). Olive Stone Delignification Toward Efficient Adsorption of Metal Ions, Frontiers in Materials, 8:605931. https://doi.org/10.3389/fmats.2021.605931

Gao, H., Liu, Y., Zeng, G., Xu, W., Li, T., Xia, W. (2008). Characterization of Cr(VI) removal from aqueous solutions by a surplus agricultural waste--rice straw, Journal of Hazardous Materials, 150: 446–452. https://doi.org/10.1016/j.jhazmat.2007.04.126

Gauden, P., Terzyk, A.P., Kowalczyk, P., Aranovich, G.L., Ćwiertnia, M., Furmaniak, S., Rychlicki, G. (2008). Giles' classification of solute adsorption isotherms for binary non-electrolyte solutions via lattice DFT supported by experimental sorption data from aqueous solutions on carbonaceous materials. Carbon Materials - Theory and Practice. Editors: Artur P. Terzyk, Piotr A. Gauden, P. Kowalczyk, Published by Research Signpost, Kerala (india).

Georgiou, Y., Perman, J.A., Bourlinos, A.B., Deligiannakis, Y. (2018). Highly Efficient Arsenite [As(III)] Adsorption by an [MIL-100(Fe)] Metal–Organic Framework: Structural and Mechanistic Insights, Journal of Physical Chemistry C, 122: 4859–4869. https://doi.org/10.1021/acs.jpcc.7b11247

Ghaneian, M.T., Bhatnagar, A., Ehrampoush, M.H., Amrollahi, M., Jamshidi, B., Dehvari, M., Taghavi, M. (2017). Biosorption of hexavalent chromium from aqueous solution onto pomegranate seeds: kinetic modeling studies, International Journal of Environmental Science and Technology, 14: 331–340. https://doi.org/10.1007/s13762-016-1216-8

Ghrab, S., Benzina, M., Lambert, S.D. (2017). Copper Adsorption from Wasterwater Using Bone Charcoal, Advances in Materials Physics and Chemistry, 7(5): 139-147. https://doi.org/10.4236/ampc.2017.75012

Guezguez, B., Almakadi, M., Benoit, Y.D., Shapovalova, Z., Rahmig, S., Fiebig-Comyn, A., Casado, F.L., Tanasijevic, B., Bresolin, S., Masetti, R., Doble, B.W., Bhatia, M. (2016). GSK3 Deficiencies in Hematopoietic Stem Cells Initiate Pre-neoplastic State that Is Predictive of Clinical Outcomes of Human Acute Leukemia, Cancer Cell, 29: 61–74. https://doi.org/10.1016/j.ccell.2015.11.012

Gunatilake, S. (2015). Methods of Removing Heavy Metals from Industrial Wastewater, Journal of Multidiciplinary Engineering Science Studies, 1(1) JMESSP13420004.

Gupta, V.K., Nayak, A., Agarwal, S. (2015). Bioadsorbents for remediation of heavy metals: Current status and their future prospects, Environmental Engineering Research, 20: 1–18. https://doi.org/10.4491/eer.2015.018

Gurreri, L., Tamburini, A., Cipollina, A., Micale, G. (2020). Electrodialysis Applications in Wastewater Treatment for Environmental Protection and Resources Recovery: A Systematic Review on Progress and Perspectives, Membranes, 10: 146. https://doi.org/10.3390/membranes10070146

Güell, R., Fontàs, C., Anticó, E., Salvadó, V., Crespo, J.G., Velizarov, S. (2011). Transport and separation of arsenate and arsenite from aqueous media by supported liquid and anion-exchange membranes, Separation and Purification Technology, 80: 428–434. https://doi.org/10.1016/j.seppur.2011.05.015

Güell, R., Fontàs, C., Salvadó, V., Anticó, E. (2010). Modelling of liquid–liquid extraction and liquid membrane separation of arsenic species in environmental matrices, Separation and Purification Technology, 72: 319–325. https://doi.org/10.1016/j.seppur.2010.02.023

Haj Seyed Hadi, M., Darz, M., Ghandehari, Z., Riazi, G. (2011). Effects of vermicompost and amino acids on the flower yield and essential oil production from Matricaria chamomile L, Journal of Medicinal Plant Research, 5: 5611–5617.

Hamidpour, M., Hosseini, N., Mozafari, V., Rafsanjani, M.H. (2018). Removal of Cd(II) and Pb(II) from aqueous solutions by pistachio hull waste, Revista International Contaminacion Ambiental, 34: 307–316. https://doi.org/10.20937/RICA.2018.34.02.11

Hernáinz, F., Calero, M., Blázquez, G., Martín-Lara, M.A., Tenorio, G. (2008). Comparative study of the biosorption of cadmium(II), chromium(III), and lead(II) by olive stone, Environmental Progress, 27: 469–478. https://doi.org/10.1002/ep.10299

Ho, Y.-S. (2003). Removal of copper ions from aqueous solution by tree fern, Water Research, 37: 2323–2330. https://doi.org/10.1016/S0043-1354(03)00002-2

Hou, S., Wu, Y., Feng, L., Chen, W., Wang, Y., Morlay, C., Li, F. (2018). Green synthesis and evaluation of an iron-based metal–organic framework MIL-88B for efficient decontamination of arsenate from water, Dalton Transactions, 47: 2222–2231. https://doi.org/10.1039/C7DT03775A

Huo, J.-B., Xu, L., Yang, J.-C.E., Cui, H.-J., Yuan, B., Fu, M.-L., 2018. Magnetic responsive Fe3O4-ZIF-8 core-shell composites for efficient removal of As(III) from water. Colloids and Surfaces A: Physicochemical and Engineering Aspects 539, 59–68. https://doi.org/10.1016/j.colsurfa.2017.12.010

Hu, X., Yu, Y., Wang, Y., Zhou, J., Song, L. (2015). Separating nano graphene oxide from the residual strong-acid filtrate of the modified Hummers method with alkaline solution, Applied Surface Science, 329: 83–86. https://doi.org/10.1016/j.apsusc.2014.12.110

Huang, J., Wu, Z., Chen, L., Sun, Y. (2015). Surface complexation modeling of adsorption of Cd(II) on graphene oxides, Journal of Molecular Liquids, 209: 753–758. https://doi.org/10.1016/j.molliq.2015.06.047

Hummers, W.S., Offeman, R.E. (1958). Preparation of Graphitic Oxide, Journal of the American Chemical Society, 80: 1339–1339. https://doi.org/10.1021/ja01539a017

Huong, P.-T., Lee, B.-K., Kim, J., Lee, C.-H., Chong, M.N. (2016). Acid activation pine cone waste at differences temperature and selective removal of Pb^{2+} ions in water, Process Safety and Environmental Protection, 100: 80–90. https://doi.org/10.1016/j.psep.2015.12.002

Ibrahim, M.B., Mohammed, M.B. (2017). Dynamic adsorption studies for the removal of Cd (II) and Ni (II) from aqueous solutions using mahogany leaves, ChemSearch Journal, 8: 1-12. http://dx.doi.org/10.4314/csj.v8i1.1

Isaac, C.P.J., Sivakumar, A. (2013). Removal of lead and cadmium ions from water using Annona squamosa shell: kinetic and equilibrium studies, Desalination and Water Treatment, 51: 7700–7709. https://doi.org/10.1080/19443994.2013.778218

Isanloo, H., Nasseri; S. (2005) Cadmium removal from aqueous solutions by ground pine cone. Iranian Journal of Environmental Health Science and Engineering, 2:33-42.

Jain, C.K., Ali, I. (2000). Arsenic: occurrence, toxicity and speciation techniques, Water Research, 34: 4304–4312. https://doi.org/10.1016/S0043-1354(00)00182-2

Jian, M., Liu, B., Zhang, G., Liu, R., Zhang, X. (2015). Adsorptive removal of arsenic from aqueous solution by zeolitic imidazolate framework-8 (ZIF-8) nanoparticles, Colloids and Surfaces A: Physicochemical and Engineering Aspects, 465: 67–76. https://doi.org/10.1016/j.colsurfa.2014.10.023

Javaid, A., Bajwa, R., Shafique, U., Anwar, J. (2011). Removal of heavy metals by adsorption on Pleurotus ostreatus, Biomass and Bioenergy, 35: 1675–1682. https://doi.org/10.1016/j.biombioe.2010.12.035

Jibesh, D., Umesh, M. (2015). Performance of tea factory waste for sorption of chromium by batch study from aqueous environment, Journal of Environmental Research and Development, 9(3): 514-522.

Johnson, T.A., Jain, N., Joshi, H.C., Prasad, S. (2008). Agricultural and agro-processing wastes as low cost adsorbents for metal removal from wastewater: A review, Journal of Scientific and Industrial Research, 9: 647-658.

Joseph, L., Jun, B.-M., Flora, J.R.V., Park, C.M., Yoon, Y. (2019). Removal of heavy metals from water sources in the developing world using low-cost materials: A review, Chemosphere, 229: 142–159. https://doi.org/10.1016/j.chemosphere.2019.04.198

Karoui, S., Arfi, R.M., Fernández-Sanjurjo, M.J., Nuñez-Delgado, A., Ghorbal, A., Álvarez-Rodríguez., E. (2020), Optimization of synergistic biosorption of oxytetracycline and cadmium from binary mixtures on reed-based beads: modeling study using Brouers-Sotolongo models, Environmental Science and Pollution Research. https://doi.org/10.1007/s11356-020-09493-7

Kaur, R., Singh, J., Khare, R., Cameotra, S.S., Ali, A. (2013). Batch sorption dynamics, kinetics and equilibrium studies of Cr(VI), Ni(II) and Cu(II) from aqueous phase using agricultural residues, Applied Water Science, 3: 207–218. https://doi.org/10.1007/s13201-012-0073-y

Khalifa, M., Bidaisee, S. (2018). The Importance of Clean Water, Biomedical Journal of Scientific and Technical Research, 8 (5) MS.ID.001719. https://doi.org/10.26717/BJSTR.2018.08.001719

Khan, M. N., Sarwar, A. (2007). Determination of points of zero charge of natural and treated adsorbents, Surface Review and Letters, 14(3): 461–469. https://doi.org/10.1142/S0218625X07009517

Kharisov, B.I., Kharissova, O.V., Dimas, A.V., Fuente, I.G.D.L., Méndez, Y.P. (2016). Review: Graphene-supported coordination complexes and organometallics: properties and applications, Journal of Coordination Chemistry, 69: 1125–1151.

https://doi.org/10.1080/00958972.2016.1170817

Khouja, M.., Sghaiar, T., Khalidi, A., Nsibi, R. (1997). Estimation du rendement en cones et en graines du pin d'alep de la foret de ouercha (sakiet sidi youssef-Tunisie), Centre de Recherche Forestière, 84–89.

Kinuthia, G.K., Ngure, V., Beti, D., Lugalia, R., Wangila, A., Kamau, L. (2020). Levels of heavy metals in wastewater and soil samples from open drainage channels in Nairobi, Kenya: community health implication, Scientific Reports, 10 Article number: 8434. https://doi.org/10.1038/s41598-020-65359-5

Kobielska, P.A., Howarth, A.J., Farha, O.K., Nayak, S. (2018). Metal–organic frameworks for heavy metal removal from water, Coordination Chemistry Reviews, 358: 92–107. https://doi.org/10.1016/j.ccr.2017.12.010

Konkena, B., Vasudevan, S. (2012). Understanding Aqueous Dispersibility of Graphene Oxide and Reduced Graphene Oxide through pKa Measurements, Journal of Physical Chemistry Letters, 3: 867–872. https://doi.org/10.1021/jz300236w

Krishnamoorthy, K., Veerapandian, M., Yun, K., Kim, S.-J. (2013). The chemical and structural analysis of graphene oxide with different degrees of oxidation, Carbon 53: 38–49. https://doi.org/10.1016/j.carbon.2012.10.013

Kumar, P.S., Ramakrishnan, K., Kirupha, S.D., Sivanesan, S. (2010). Thermodynamic and kinetic studies of cadmium adsorption from aqueous solution onto rice husk, Brazilian Journal of Chemical Engineering, 27: 347–355. https://doi.org/10.1590/S0104-66322010000200013

Kumar, R., Chawla, J., Kaur, I. (2015). Removal of cadmium ion from wastewater by carbon-based nanosorbents: a review, Journal of Water and Health, 13: 18–33. https://doi.org/10.2166/wh.2014.024

Kumar, R., Obrai, S., Sharma, A. (2012). Biosorption of heavy metal ions by using modified waste tree bark material, International Journal on Environmental Sciences, 3(1): 720-726.

Kuroki, A., Hiroto, M., Urushihara, Y., Horikawa, T., Sotowa, K.-I., Alcantara-Avila, J. (2019). Adsorption mechanism of metal ions on activated carbon, Adsorption, 25: 1251–1258. https://doi.org/10.1007/s10450-019-00069-7

Kyzas, G.Z., Kostoglou, M., 2014. Green Adsorbents for Wastewaters: A Critical Review, Materials (Basel), 7: 333–364. https://doi.org/10.3390/ma7010333

Kyzas, G.Z., Bikiaris, D.N., Kostoglou, M., Lazaridis, N.K. (2013). Copper removal from aqueous systems with coffee wastes as low-cost materials. E3S Web of Conferences 1: article number 25004. https://doi.org/10.1051/e3sconf/20130125004

Labied, R., Benturki, O., Eddine Hamitouche, A.Y., Donnot, A. (2018). Adsorption of hexavalent chromium by activated carbon obtained from a waste lignocellulosic material (Ziziphus jujuba cores): Kinetic, equilibrium, and thermodynamic study, Adsorption Science and Technology, 36: 1066–1099. https://doi.org/10.1177/0263617417750739

Lakshmipathy, R., Sarada, N.C. (2015). A fixed bed column study for the removal of Pb^{2+} ions by watermelon rind, Environmental Science: Water Research and Technology, 1: 244–250. https://doi.org/10.1039/C4EW00027G

Lalmi, A., Bouhidel, K.-E., Sahraoui, B., Anfif, C. el H. (2018). Removal of lead from polluted waters using ion exchange resin with $Ca(NO_3)_2$ for elution, Hydrometallurgy, 178: 287–293. https://doi.org/10.1016/j.hydromet.2018.05.009

Lee, Y.-C., Yang, J.-W. (2012). Self-assembled flower-like TiO2 on exfoliated graphite oxide for heavy metal removal, Journal of Industrial and Engineering Chemistry, 18: 1178–1185. https://doi.org/10.1016/j.jiec.2012.01.005

Li, J., Wu, Y., Li, Z., Zhang, B., Zhu, M., Hu, X., Zhang, Y., Li, F. (2014a). Zeolitic Imidazolate Framework-8 with High Efficiency in Trace Arsenate Adsorption and Removal from Water, Journal of Physical Chemistry C, 118: 27382–27387. https://doi.org/10.1021/jp508381m

Li, J., Wu, Y., Li, Z., Zhu, M., Li, F. (2014). Characteristics of arsenate removal from water by metal-organic frameworks (MOFs), Water Science and Technology, 70: 1391–1397. https://doi.org/10.2166/wst.2014.390

Li, Z., Liu, X., Jin, W., Hu, Q., Zhao, Y. (2019). Adsorption behavior of arsenicals on MIL-101(Fe): The role of arsenic chemical structures, Journal of Colloid and Interface Science, 554: 692–704. https://doi.org/10.1016/j.jcis.2019.07.046

Liu, B., Jian, M., Liu, R., Yao, J., Zhang, X. (2015). Highly efficient removal of arsenic(III) from aqueous solution by zeolitic imidazolate frameworks with different morphology, Colloids and Surfaces A: Physicochemical and Engineering Aspects, 481: 358–366. https://doi.org/10.1016/j.colsurfa.2015.06.009

Liu, H., Liang, S., Gao, J., Ngo, H.H., Guo, W., Guo, Z., Wang, J., Li, Y. (2014). Enhancement of Cr(VI) removal by modifying activated carbon developed from Zizania caduciflora with tartaric acid during phosphoric acid activation, Chemical Engineering Journal, 246: 168–174. https://doi.org/10.1016/j.cej.2014.02.046

Liu, L., Li, W., Song, W., Guo, M. (2018). Remediation techniques for heavy metal-contaminated soils: Principles and applicability, Science of The Total Environment, 633: 206–219. https://doi.org/10.1016/j.scitotenv.2018.03.161

Liu, X., Ma, R., Wang, Xiangxue, Ma, Y., Yang, Y., Zhuang, L., Zhang, S., Jehan, R., Chen, J., Wang, Xiangke, (2019). Graphene oxide-based materials for efficient removal of heavy metal ions from aqueous solution: A review, Environmental Pollution, 252: 62–73. https://doi.org/10.1016/j.envpol.2019.05.050

Liu, B., Kim, K.-H., Kumar, V., Kim, S. (2020). A review of functional sorbents for adsorptive removal of arsenic ions in aqueous systems, Journal of Hazardous Materials, 388, 121815. https://doi.org/10.1016/j.jhazmat.2019.121815

López-Mesas, M., Navarrete, E.R., Carrillo, F., Palet, C. (2011). Bioseparation of Pb(II) and Cd(II) from aqueous solution using cork waste biomass. Modeling and optimization of the parameters of the biosorption step, Chemical Engineering Journal, 174: 9–17. https://doi.org/10.1016/j.cej.2011.07.026

Lu, F., Astruc, D. (2018). Nanomaterials for removal of toxic elements from water, Coordination Chemistry Reviews, 356: 147–164. https://doi.org/10.1016/j.ccr.2017.11.003

Luo, X., Wang, C., Luo, C., Dong, R., Tu, X., Zang, G. (2012), Adsorption of As (III) and As (V) from water using magnetite Fe_3O_4-reduced graphite oxide–MnO_2 nanocomposites, Chemical Engineering Journal, 187: 45-52, https://doi.org/10.1016/j.cej.2012.01.073

Maaloul, N., Oulego, P., Rendueles, M., Ghorbal, A., Díaz, M. (2017). Novel biosorbents from almond shells: Characterization and adsorption properties modeling for Cu(II) ions from aqueous solutions. Journal of Environmental Chemical Engineering, 5 (3): 2944-2954. https://doi.org/10.1016/j.jece.2017.05.037

Maaloul, N., Oulego, P., Rendueles, M., Ghorbal, A., Díaz, M.(2020). Enhanced Cu(II) adsorption using sodium trimetaphosphate–modified cellulose beads: equilibrium, kinetics,adsorption mechanisms, and reusability. Environmental Science and Pollution Research, https://doi.org/10.1007/s11356-020-10158-8

Maaloul, N., Oulego, P., Rendueles, M., Ghorbal, A., Díaz, M.(2021). Biopolymer composite from cellulose nanocrystals of almond (Prunus dulcis) shell as effective adsorbents for Cu^{2+} ions from aqueous solutions, Journal of Environmental Chemical Engineering, 9(2). https://doi.org/10.1016/j.jece.2021.105139

Madadrang, C.J., Kim, H.Y., Gao, G., Wang, N., Zhu, J., Feng, H., Gorring, M., Kasner, M.L., Hou, S. (2012). Adsorption Behavior of EDTA-Graphene Oxide for Pb (II) Removal, ACS Applied Materials and Interfaces, 4: 1186–1193. https://doi.org/10.1021/am201645g

Mahamadi, C. (2019). On the dominance of Pb during competitive biosorption from multi-metal systems: A review, Cogent Environmental Science, 5, 1635335. https://doi.org/10.1080/23311843.2019.1635335

Mahmoodi, N.M., Hayati, B., Arami, M., Lan, C. (2011). Adsorption of textile dyes on Pine Cone from colored wastewater: Kinetic, equilibrium and thermodynamic studies, Desalination, 268: 117–125. https://doi.org/10.1016/j.desal.2010.10.007

Mahmoud, D., Salleh, M., Karim, W. (2012). Langmuir model application on solid-liquid adsorption using agricultural wastes: Environmental application review, Journal of Purity, Utility Reaction and Environment, 1: 170-199.

Majumder, S., Gupta, V., Raghuvanshi, S., Gupta, S. (2016). Simultaneous sequestration of ternary metal ions (Cr^{6+}, Cu^{2+} and Zn^{2+}) from aqueous solution by an indigenous bacterial consortium, Process Safety and Environmental Protection, 102: 786–798. https://doi.org/10.1016/j.psep.2016.06.003

Malamis, S., Katsou, E. (2013). A review on zinc and nickel adsorption on natural and modified zeolite, bentonite and vermiculite: Examination of process parameters, kinetics and isotherms, Journal of Hazardous Materials, 252–253:428–461. https://doi.org/10.1016/j.jhazmat.2013.03.024

Malik, D., Jain, C., Yadav, A. (2016). Removal of heavy metals from emerging cellulosic low-cost adsorbents: a review, Applied Water Science, 7: 2113-2136. https://doi.org/10.1007/s13201-016-0401-8

Mallek, M., Chtourou, M., Portillo, M., Monclús, H., Walha, K., Salah, A. ben, Salvadó, V. (2018). Granulated cork as biosorbent for the removal of phenol derivatives and emerging contaminants, Journal of Environmental Management, 223: 576–585. https://doi.org/10.1016/j.jenvman.2018.06.069

Manousi, N., Giannakoudakis, D.A., Rosenberg, E., Zachariadis, G.A. (2019). Extraction of Metal Ions with Metal-Organic Frameworks, Molecules, 24(24): 4605. https://doi.org/10.3390/molecules24244605

Martínez, F., Leo, P., Orcajo, G., Díaz-García, M., Sanchez-Sanchez, M., Calleja, G. (2018). Sustainable Fe-BTC catalyst for efficient removal of mehylene blue by advanced fenton oxidation, Catalysis Today, 5th European Conference on Environmental Applications of Advanced Oxidation Processes, 313: 6–11. https://doi.org/10.1016/j.cattod.2017.10.002

Martín-Lara, M.A., Blázquez, G., Ronda, A., Pérez, A., Calero, M. (2013). Development and Characterization of Biosorbents to Remove Heavy Metals from Aqueous Solutions by Chemical Treatment of Olive Stone, Industrial and Engineering Chemistry Research, 52: 10809–10819. https://doi.org/10.1021/ie401246c

Martín-Lara, M.A., Blázquez, G., Calero, M., Almendros, A.I., Ronda, A. (2016). Binary biosorption of copper and lead onto pine cone shell in batch reactors and in fixed bed columns, International Journal of Mineral Processing, 148: 72–82. https://doi.org/10.1016/j.minpro.2016.01.017

Martín-Lara, M.A., Blázquez, G., Trujillo, M.C., Pérez, A., Calero, M. (2014). New treatment of real electroplating wastewater containing heavy metal ions by adsorption onto olive stone, Journal of Cleaner Production, 81: 120–129. https://doi.org/10.1016/j.jclepro.2014.06.036

Martín-Lara, M.Á., Calero de Hoces, M., Ronda Gálvez, A., Pérez Muñoz, A., Trujillo Miranda, M.C. (2016). Assessment of the removal mechanism of hexavalent chromium from aqueous solutions by olive stone, Water Science and Technology, 73: 2680–2688. https://doi.org/10.2166/wst.2016.081

Martín-Lara, M.Á., Trujillo Miranda, M.C., Ronda Gálvez, A., Pérez Muñoz, A., Calero de Hoces, M. (2017). Valorization of olive stone as adsorbent of chromium(VI): comparison between laboratory- and pilot-scale fixed-bed columns, International Journal of Environmental Science and Technology, 14: 2661–2674. https://doi.org/10.1007/s13762-017-1345-8

Masindi, V., Muedi, K.L. (2018). Environmental Contamination by Heavy Metals, Heavy Metals: 116-133 from Heavy Metals edited by Hosam El-Din M.Saleh and Refaat F. Aglan. https://doi.org/10.5772/intechopen.76082

Mathew, B.B., Jaishankar, M., Biju, V.G., Krishnamurthy Nideghatta Beeregowda (2016). Role of Bioadsorbents in Reducing Toxic Metals, Journal of Toxicology, 13 Article ID 4369604. https://doi.org/10.1155/2016/4369604

Mi, X., Huang, G., Xie, W., Wang, W., Liu, Y., Gao, J. (2012). Preparation of graphene oxide aerogel and its adsorption for Cu^{2+} ions, Carbon, 50: 4856–4864. https://doi.org/10.1016/j.carbon.2012.06.013

Miralles, N., Valderrama, C., Casas, I., Martínez, M., Florido, A. (2010). Cadmium and Lead Removal from Aqueous Solution by Grape Stalk Wastes: Modeling of a Fixed-Bed Column, Journal of Chemical and Engineering Data, 55: 3548–3554. https://doi.org/10.1021/je100200w

Miretzky, P., Cirelli, A.F. (2010). Cr(VI) and Cr(III) removal from aqueous solution by raw and modified lignocellulosic materials: a review, Journal of Hazardous Materials, 180: 1–19. https://doi.org/10.1016/j.jhazmat.2010.04.060

Mishra, A., Dubey, A., Shinghal, S. (2015). Biosorption of chromium(VI) from aqueous solutions using waste plant biomass, International Journal of Environmental Science and Technology, 12: 1415–1426. https://doi.org/10.1007/s13762-014-0516-0

Moghaddam, N.K., Lorestani, B., Cheraghi, M., Jamehbozorgi, S. (2019). Adsorption of Cd and Ni from water by graphene oxide and graphene oxide–almond shell composite, Water Environment Research, 91: 475–482. https:// doi.org/ 10.1002/wer.1045

Momčilović, M., Purenović, M., Bojić, A., Zarubica, A., Ranđelović, M. (2011). Removal of lead(II) ions from aqueous solutions by adsorption onto pine cone activated carbon, Desalination, 276: 53–59. https://doi.org/10.1016/j.desal.2011.03.013

Mondal, N.K., Chakraborty, S. (2020). Adsorption of Cr(VI) from aqueous solution on graphene oxide (GO) prepared from graphite: equilibrium, kinetic and thermodynamic studies, Applied Water Science, 10, 16. https://doi.org/10.1007/s13201-020-1142-2

Moubarik, A., Grimi, N. (2015). Valorization of olive stone and sugar cane bagasse by-products as biosorbents for the removal of cadmium from aqueous solution, Food Research International, 73: 169–175. https://doi.org/10.1016/j.foodres.2014.07.050

Muhammad Yaqub, null, Lee, W. (2019). Zero-liquid discharge (ZLD) technology for resource recovery from wastewater: A review, Science of the Total Environment, 681: 551–563. https://doi.org/10.1016/j.scitotenv.2019.05.062

Musico, Y.L.F., Santos, C.M., Dalida, M.L.P., Rodrigues, D.F. (2013). Improved removal of lead(II) from water using a polymer-based graphene oxide nanocomposite, Journal of Material Chemistry A, 1: 3789–3796. https://doi.org/10.1039/C3TA01616A

Muslim, A. (2017). Australian pine cones-based activated carbon for adsorption of copper in aqueous solution, Journal of Engineering Science and Technology, 12: 280–295.

Najim, T.S., Yasin, S.A.A.R. (2013). Adsorption of Cr(VI) from Aqueous Solution Using Low Cost Adsorbent: Equilibrium Study, Science Journal of University of Zakho, 1: 758–767.

Nakano, Y., Takeshita, K., Tsutsumi, T. (2001). Adsorption mechanism of hexavalent chromium by redox within condensed-tannin gel, Water Research, 35: 496–500. https://doi.org/10.1016/S0043-1354(00)00279-7

Nana, S., Xinjian, L. (2017). Application of Mathematical Statistics Analysis Algorithm for Chemical Data, International Journal of Materials Science and Applications, 6: 297. https://doi.org/10.11648/j.ijmsa.20170606.15

Nasir, A.M., Md Nordin, N.A.H., Goh, P.S., Ismail, A.F. (2018). Application of two-dimensional leaf-shaped zeolitic imidazolate framework (2D ZIF-L) as arsenite adsorbent: Kinetic, isotherm and mechanism, Journal of Molecular Liquids, 250: 269–277. https://doi.org/10.1016/j.molliq.2017.12.005

Nasri, N., Khaldi, A., Triki, S. (2004). Variabilité morphologique des cônes et graines de Pin d'Alep et de Pin pignon en Tunisie, Revue Forestière Française. https://doi.org/10.4267/2042/507

Nassar, M.M., Awida, K.T., Ebrahiem, E.E., Magdy, Y.H., Mehaedi, M.H. (2003). Fixed-Bed Adsorption for the Removal of Iron and Manganese onto Palm Fruit Bunch and Maize Cob, Adsorption Science and Technology, 21: 161–175. https://doi.org/10.1260/026361703769013899

Nasseh, N., Taghavi, L., Barikbin, B., Harifi-Mood, A.R. (2017). The removal of Cr(VI) from aqueous solution by almond green hull waste material: kinetic and equilibrium studies, Journal of Water Reuse and Desalination, 7: 449–460. https://doi.org/10.2166/wrd.2016.047

Negrea, A., Mihailescu, M., Mosoarca, G., Ciopec, M., Duteanu, N., Negrea, P., Minzatu, V. (2020). Estimation on Fixed-Bed Column Parameters of Breakthrough Behaviors for Gold Recovery by Adsorption onto Modified/Functionalized Amberlite XAD7,

International Journal of Environmental Research and Public Health, 17: 6868. https://doi.org/10.3390/ijerph17186868

Neis, F.A., de Costa, F., de Araújo, A.T., Fett, J.P., Fett-Neto, A.G. (2019). Multiple industrial uses of non-wood pine products, Industrial Crops and Products, 130: 248–258. https://doi.org/10.1016/j.indcrop.2018.12.088

Neris, J.B., Luzardo, F.H.M., da Silva, E.G.P., Velasco, F.G. (2019). Evaluation of adsorption processes of metal ions in multi-element aqueous systems by lignocellulosic adsorbents applying different isotherms: A critical review, Chemical Engineering Journal, 357: 404–420. https://doi.org/10.1016/j.cej.2018.09.125

Nicomel, N.R., Leus, K., Folens, K., Van Der Voort, P., Du Laing, G. (2015). Technologies for Arsenic Removal from Water: Current Status and Future Perspectives, International Journal of Environmental Research and Public Health, 13(1): 62. https://doi.org/10.3390/ijerph13010062

Nieto, L.M., Alami, S.B.D., Hodaifa, G., Faur, C., Rodríguez, S., Giménez, J.A., Ochando, J. (2010). Adsorption of iron on crude olive stones, Industrial Crops and Products, 32: 467–471. https://doi.org/10.1016/j.indcrop.2010.06.017

Nkechi, E.I., Chizaram, A.A. (2018). Use of agro-waste (Musa paradisiaca peels) as a sustainable biosorbent for toxic metal ions removal from contaminated water, Chemistry International, 4: 52–59. https://doi.org/10.31221/osf.io/yrpvn

Novoseltseva, V., Yankovych, H., Kovalenko, O., Václavíková, M., Melnyk, I. (2020). Production of high-performance lead(II) ions adsorbents from pea peels waste as a sustainable resource, Waste Management and Research, 39(4): 584-593. https://doi.org/10.1177/0734242X20943272

Nurchi, V.M., Floris, C., Pinna, R., Fiol Santaló, N., Villaescusa Gil, I. (2007). Metal ion uptake from aqueous solution by olive stones: A carbon-13 solid-state nuclear magnetic resonance and potentiometric study, Water Environment Research, 79: 2363-2367. https://doi.org/10.2175/106143007X183880

Ofomaja, A.E., Naidoo, E.B. (2010). Biosorption of lead(II) onto pine cone powder: Studies on biosorption performance and process design to minimize biosorbent mass, Carbohydrate Polymers, 82: 1031–1042. https://doi.org/10.1016/j.carbpol.2010.05.024

Ofomaja, A.E., Naidoo, E.B., Modise, S.J. (2010). Biosorption of copper(II) and lead(II) onto potassium hydroxide treated pine cone powder, Journal of Environmental Management, 91: 1674–1685. https://doi.org/10.1016/j.jenvman.2010.03.005

Okafor, P.C., Okon, P.., Daniel, E.., Ebenso, E.. (2012). Adsorption Capacity of Coconut (Cocosnucifera L.) Shell for Lead, Copper, Cadmium and Arsenic from Aqueous Solutions, International Journal of Electrochemical Science, 7: 12354–12369. https://doi.org/doi=10.1.1.658.6468

Ouazzane, H., Laajine, F., El Yamani, M., El Hilaly, J., Rharrabti, Y., Amarouch, M.-Y., Mazouzi, D. (2017). Olive mill solid waste characterization and recycling opportunities: A review, Journal of Materials and Environmental Science, 8: 2632–2650.

Oyewole, O., Adamu, B., Oladoja, E., Balogun, A., Okunlola, M., Odiniya, E. (2018). A review on heavy metals biosorption in the environment, Brazilian Journal of Biological Sciences, 5: 225–236. https://doi.org/10.21472/bjbs.051003

Ozaki, H., Sharma, K., Saktaywin, W. (2002). Performance of an ultra-low-pressure reverse osmosis membrane (ULPROM) for separating heavy metal: effects of interference parameters, Desalination, 144: 287–294. https://doi.org/10.1016/S0011-9164(02)00329-6

Özsin, G., Kılıç, M., Apaydın-Varol, E., Pütün, A.E. (2019). Chemically activated carbon production from agricultural waste of chickpea and its application for heavy metal adsorption: equilibrium, kinetic, and thermodynamic studies, Applied Water Science, 9: 56. https://doi.org/10.1007/s13201-019-0942-8

Pakulski, D., Czepa, W., Witomska, S., Aliprandi, A., Pawluć, P., Patroniak, V., Ciesielski, A., Samorì, P. (2018). Graphene oxide-branched polyethylenimine foams for efficient removal of toxic cations from water. Journal of Materials Chemistry A, 6: 9384–9390. https://doi.org/10.1039/C8TA01622D

Pang, F.M., Kumar, P., Teng, T.T., Mohd Omar, A.K., Wasewar, K.L. (2011). Removal of lead, zinc and iron by coagulation–flocculation, Journal of the Taiwan Institute of Chemical Engineers, 42: 809–815. https://doi.org/10.1016/j.jtice.2011.01.009

Paranavithana, G.N., Kawamoto, K., Inoue, Y., Saito, T., Vithanage, M., Kalpage, C.S., Herath, G.B.B. (2016). Adsorption of Cd^{2+} and Pb^{2+} onto coconut shell biochar and biochar-mixed soil, Environ Earth Sciences, 75: 484. https://doi.org/10.1007/s12665-015-5167-z

Park, D., Lim, S.-R., Yun, Y.-S., Park, J.M. (2007). Reliable evidences that the removal mechanism of hexavalent chromium by natural biomaterials is adsorption-coupled reduction, Chemosphere, 70: 298–305.
https://doi.org/10.1016/j.chemosphere.2007.06.007

Patel, H. (2019). Fixed-bed column adsorption study: a comprehensive review, Applied Water Science, 9: 45. https://doi.org/10.1007/s13201-019-0927-7

Patel, H. (2020). Batch and continuous fixed bed adsorption of heavy metals removal using activated charcoal from neem (Azadirachta indica) leaf powder, Scientific Reports, 10, 16895. https://doi.org/10.1038/s41598-020-72583-6

Peng, W., Li, H., Liu, Y., Song, S. (2017). A review on heavy metal ions adsorption from water by graphene oxide and its composites, Journal of Molecular Liquids, 230: 496–504. https://doi.org/10.1016/J.MOLLIQ.2017.01.064

Pereira, H. (2015). The Rationale behind Cork Properties: A Review of Structure and Chemistry, BioResources, 10(3): 6207–6229.

Pholosi, A., Naidoo, E.B., Ofomaja, A.E. (2020). Batch and continuous flow studies of Cr(VI) adsorption from synthetic and real wastewater by magnetic pine cone composite, Chemical Engineering Research and Design, 153: 806–818.
https://doi.org/10.1016/j.cherd.2019.11.004

Pholosi, A., Ofomaja, A., Naidoo, E. (2013). Effect of chemical extractants on the biosorptive properties of pine cone powder: Influence on lead(II) removal mechanism, Journal of Saudi Chemical Society, 17: 77-86. https://doi.org/10.1016/J.JSCS.2011.10.017

Pholosi, A., Naidoo, E.B., Ofomaja, A.E. (2019). Enhanced Arsenic (III) adsorption from aqueous solution by magnetic pine cone biomass, Materials Chemistry and Physics, 222: 20–30. https://doi.org/10.1016/j.matchemphys.2018.09.067

Pintor, A.M.A., Ferreira, C.I.A., Pereira, J.C., Correia, P., Silva, S.P., Vilar, V.J.P., Botelho, C.M.S., Boaventura, R.A.R. (2012). Use of cork powder and granules for the adsorption of pollutants: a review, Water Research, 46: 3152–3166.
https://doi.org/10.1016/j.watres.2012.03.048

Pooja D, T. (2016). Removal of copper from waste water by using potato and banana peels as bio-adsorbent, International journal of science engineering and technology, 5: 3038–3040.

Puigdomenech, I (2016), KTH Royal Institute of Technology, Sweden, Medusa software. available at https://www.kth.se/che/medusa/downloads-1.386254

Radhakrishnan, K., Sethuraman, L., Panjanathan, R., Natarajan, A., Solaiappan, V., Thilagaraj, W.R. (2016). Biosorption of heavy metals from actual electroplating wastewater using encapsulated Moringa oleifera beads in fixed bed column, Desalination and Water Treatment, 57: 3572–3587. https://doi.org/10.1080/19443994.2014.985725

Rahimi, E., Mohaghegh, N. (2016). Removal of Toxic Metal Ions from Sungun Acid Rock Drainage Using Mordenite Zeolite, Graphene Nanosheets, and a Novel Metal–Organic Framework, Mine Water and the Environment, 35: 18–28. https://doi.org/10.1007/s10230-015-0327-7

Rani, L., Kaushal, J., Srivastav, A.L., Mahajan, P. (2020). A critical review on recent developments in MOF adsorbents for the elimination of toxic heavy metals from aqueous solutions. Environmental Science and Pollution Research, 27: 44771–44796. https://doi.org/10.1007/s11356-020-10738-8

Ravat, C., Monteil-Rivera, F., Dumonceau, J. (2000). Metal Ions Binding to Natural Organic Matter Extracted from Wheat Bran: Application of the Surface Complexation Model, Journal of Colloid and Interface Science, 225: 329–339. https://doi.org/10.1006/jcis.2000.6782

Reina, G., González-Domínguez, J.M., Criado, A., Vázquez, E., Bianco, A., Prato, M. (2017). Promises, facts and challenges for graphene in biomedical applications, Chemical Society Reviews, 46: 4400–4416. https://doi.org/10.1039/C7CS00363C

Rizvi, A., Zaidi, A., Ameen, F., Ahmed, B., AlKahtani, M.D.F., Khan, M.S. (2020). Heavy metal induced stress on wheat: phytotoxicity and microbiological management, RSC Advances, 10: 38379–38403. https://doi.org/10.1039/D0RA05610C

Rodríguez, C., Leiva, E. (2020). Enhanced Heavy Metal Removal from Acid Mine Drainage Wastewater Using Double-Oxidized Multiwalled Carbon Nanotubes, Molecules, 25: 111. https://doi.org/10.3390/molecules25010111

Ronda, A., Martín-Lara, M.Á., Blázquez, G., Bachs, N.M., Calero, M. (2014). Copper biosorption in the presence of lead onto olive stone and pine bark in batch and continuous systems, Environmental Progress and Sustainable Energy, 33: 192–204. https://doi.org/10.1002/ep.11780

Sadegh, H., Ali, G.A.M., Gupta, V.K., Makhlouf, A.S.H., Shahryari-ghoshekandi, R., Nadagouda, M.N., Sillanpää, M., Megiel, E. (2017). The role of nanomaterials as effective adsorbents and their applications in wastewater treatment, Journal of Nanostructure in Chemistry, 7: 1–14. https://doi.org/10.1007/s40097-017-0219-4

Saif, M.J., Zia, K.M., Fazal-ur-Rehman, null, Usman, M., Hussain, A.I., Chatha, S.A.S. (2015). Removal of Heavy Metals by Adsorption onto Activated Carbon Derived from Pine Cones of Pinus roxburghii, Water Environment Research, 87: 291–297. https://doi.org/10.2175/106143015X14212658613433

Saka, C., Şahin, Ö., Küçük, M.M. (2012). Applications on agricultural and forest waste adsorbents for the removal of lead (II) from contaminated waters, International Journal of Environmental Science and Technology, 9: 379–394. https://doi.org/10.1007/s13762-012-0041-y

Saleem, J., Shahid, U.B., Hijab, M., Mackey, H., McKay, G. (2019). Production and applications of activated carbons as adsorbents from olive stones, Biomass Conversion and Biorefinery, 9: 775–802. https://doi.org/10.1007/s13399-019-00473-7

Sanchooli Moghaddam, M., Rahdar, S., Taghavi, M. (2016). Cadmium Removal from Aqueous Solutions Using Saxaul Tree Ash, Iranian Journal of Chemistry and Chemical Engineering, 35: 45–52.

Sanni, S.O., Viljoen, E.L., Ofomaja, A.E. (2020). Three-dimensional hierarchical porous carbon structure derived from pinecone as a potential catalyst support in catalytic remediation of antibiotics, RSC Advances, 10: 8717–8728. https://doi.org/10.1039/C9RA10638C

Sarin, V., Pant, K.K. (2006). Removal of chromium from industrial waste by using eucalyptus bark, Bioresource Technology, 97: 15–20. https://doi.org/10.1016/j.biortech.2005.02.010

Sarma, G.K., Sen Gupta, S., Bhattacharyya, K.G. (2019). Nanomaterials as versatile adsorbents for heavy metal ions in water: a review. Environmental Science and Pollution Research, 26: 6245–6278. https://doi.org/10.1007/s11356-018-04093-y

Scarazzato, T., Panossian, Z., Tenório, J.A.S., Pérez-Herranz, V., Espinosa, D.C.R. (2017). A review of cleaner production in electroplating industries using electrodialysis, Journal of Cleaner Production, 168: 1590–1602. https://doi.org/10.1016/j.jclepro.2017.03.152

Schwantes, D., Gonçalves, A.C., Campagnolo, M.A., Tarley, C.R.T., Dragunski, D.C., de Varennes, A., dos Santos Silva, A.K., Conradi, E. (2018). Chemical modifications on

pinus bark for adsorption of toxic metals, Journal of Environmental Chemical Engineering, 6: 1271–1278. https://doi.org/10.1016/j.jece.2018.01.044

Selatile, M.K., Ray, S.S., Ojijo, V., Sadiku, R. (2018). Recent developments in polymeric electrospun nanofibrous membranes for seawater desalination, RSC Advances, 8: 37915–37938. https://doi.org/10.1039/C8RA07489E

Semerjian L (2018) Removal of heavy metals (Cu, Pb) from aqueous solutions using pine (Pinus halepensis) sawdust: Equilibrium, kinetic, and thermodynamic studies, Environmental Technology and Innovation, 12:91–103. https://doi.org/10.1016/j.eti.2018.08.005

Şen, A., Pereira, H., Olivella, M.A., Villaescusa, I. (2015). Heavy metals removal in aqueous environments using bark as a biosorbent, International Journal of Environmental Science and Technology, 12: 391–404. https://doi.org/10.1007/s13762-014-0525-z

Ševčík, R. (2020). Personal Communication, Dpt. of Chemistry, Masaryk University (Brno, Czech Rep.).

Sfaksi, Z., Azzouz, N., Abdelwahab, A. (2014). Removal of Cr(VI) from water by cork waste, Arabian Journal of Chemistry, Special Issue: Environmental Chemistry, 7: 37–42. https://doi.org/10.1016/j.arabjc.2013.05.031

Shafique, U., Ijaz, A., Salman, M., Zaman, W. uz, Jamil, N., Rehman, R., Javaid, A. (2012). Removal of arsenic from water using pine leaves, Journal of the Taiwan Institute of Chemical Engineers, 43: 256–263. https://doi.org/10.1016/j.jtice.2011.10.006

Shafiq, M., Alazba, A.A., Amin, M.T. (2018). Removal of heavy metals from wastewater using date palm as a biosorbent: a comparative review, Sains Malaysia, 47: 35–49. http://dx.doi.org/10.17576/jsm-2018-4701-05

Shaheen, S., Derbalah, A., Moghanm, F. (2012). Removal of Heavy Metals from Aqueous Solution by Zeolite in Competitive Sorption System, International Journal of Environmental Sciences and Development, 3(4): 362-367. https://doi.org/10.7763/IJESD.2012.V3.248

Shayegan, H., Ali, G.A.M., Safarifard, V. (2020). Recent Progress in the Removal of Heavy Metal Ions from Water Using Metal-Organic Frameworks, ChemistrySelect, 5: 124–146. https://doi.org/10.1002/slct.201904107

Shen, L.-C., Nguyen, X.-T., Hankins, N.P. (2015). Removal of heavy metal ions from dilute aqueous solutions by polymer–surfactant aggregates: A novel effluent treatment process, Separation and Purification Technology, 152: 101–107. https://doi.org/10.1016/j.seppur.2015.07.065

Singh, S., Kumar, V., Datta, S., Dhanjal, D., Sharma, K., Samuel, J., Singh, J. (2019). Current advancement and future prospect of biosorbents for bioremediation, Science of the Total Environment, 709: 135895–135895. https://doi.org/10.1016/j.scitotenv.2019.135895

Singh, V., Ram, C., Kumar, A. (2016). Physico-Chemical Characterization of Electroplating Industrial Effluents of Chandigarh and Haryana Region, Journal of Civil and Environmental Engineering, 6: 1–6. https://doi.org/10.4172/2165-784X.1000237

Singha, B., Das, S.K. (2013). Adsorptive removal of Cu(II) from aqueous solution and industrial effluent using natural/agricultural wastes, Colloids and Surfaces B: Biointerfaces, 107: 97–106. https://doi.org/10.1016/j.colsurfb.2013.01.060

Sitko, R., Turek, E., Zawisza, B., Malicka, E., Talik, E., Heimann, J., Gagor, A., Feist, B., Wrzalik, R. (2013). Adsorption of divalent metal ions from aqueous solutions using graphene oxide, Dalton Transactions, 42: 5682–5689. https://doi.org/10.1039/C3DT33097D

Sousa, F.W., Oliveira, A.G., Ribeiro, J.P., Rosa, M.F., Keukeleire, D., Nascimento, R.F. (2010). Green coconut shells applied as adsorbent for removal of toxic metal ions using fixed-bed column technology, Journal of Environmental Management, 91: 1634–1640. https://doi.org/10.1016/j.jenvman.2010.02.011

Strankowski, M., Włodarczyk, D., Piszczyk, Ł., Strankowska, J. (2016). Polyurethane Nanocomposites Containing Reduced Graphene Oxide, FTIR, Raman, and XRD Studies, Journal of Spectroscopy, 752074. https://doi.org/10.1155/2016/7520741

Tan, P., Sun, J., Hu, Y., Fang, Z., Bi, Q., Chen, Y., Cheng, J. (2015). Adsorption of Cu^{2+}, Cd^{2+} and Ni^{2+} from aqueous single metal solutions on graphene oxide membranes, Journal of Hazardous Materials, 297: 251–260. https://doi.org/10.1016/j.jhazmat.2015.04.068

Taşar, Ş., Kaya, F., Özer, A. (2014). Biosorption of lead(II) ions from aqueous solution by peanut shells: Equilibrium, thermodynamic and kinetic studies, Journal of Environmental Chemical Engineering, 2: 1018–1026. https://doi.org/10.1016/j.jece.2014.03.015

Thommes, M., Kaneko, K., Neimark, A.V., Olivier, J.P., Rodriguez-Reinoso, F., Rouquerol, J., Sing, K.S.W. (2015). Physisorption of gases, with special reference to the evaluation of surface area and pore size distribution (IUPAC Technical Report), Pure and Applied Chemistry, 87: 1051–1069. https://doi.org/10.1515/pac-2014-1117

Thuong, N.T., Nhi, N.T.T., Nhung, V.T.C., Bich, H.N., Quynh, B.T.P., Bach, L.G., Trinh, N.D. (2019). A Fixed-Bed Column Study for Removal of Organic Dyes from Aqueous Solution by Pre-Treated Durian Peel Waste, Indonesian Journal of Chemistry, 19: 486–494. https://doi.org/10.22146/ijc.39712

Tofighy, M.A., Mohammadi, T. (2011). Adsorption of divalent heavy metal ions from water using carbon nanotube sheets, Journal of Hazardous Materials, 185: 140–147. https://doi.org/10.1016/j.jhazmat.2010.09.008

Torab-Mostaedi, M., Asadollahzadeh, M., Hemmati, A., Khosravi, A. (2013). Equilibrium, kinetic, and thermodynamic studies for biosorption of cadmium and nickel on grapefruit peel, Journal of the Taiwan Institute of Chemical Engineers, 44: 295–302. https://doi.org/10.1016/j.jtice.2012.11.001

Tóth (2000). Calculation of the BET-compatible surface area from any type I isotherms measured above the critical Temperature, Journal of Colloid and Interface Science,225 (2): 378-383. https://doi.org/10.1006/jcis.2000.6723.

Tran, H.N., Chao, H.-P. (2018). Adsorption and desorption of potentially toxic metals on modified biosorbents through new green grafting process, Environmental Science and Pollution Research, 25: 12808–12820. https://doi.org/10.1007/s11356-018-1295-9

Trung, N.Đ., Ping, N. (2014). Biosorption of Lead(II), Copper(II) and Cadmium(II) in Singe -and Multi-metal Systems by Aerobic Granule Sludge by Fixed-Bed Column and Batch Sorption, Journal of Science: Natural Sciences and Technology, 30: 643-656.

Tsai, W.-C., de Luna, M.D.G., Bermillo-Arriesgado, H.L.P., Futalan, C.M., Colades, J.I., Wan, M.-W. (2016). Competitive Fixed-Bed Adsorption of Pb(II), Cu(II), and Ni(II) from Aqueous Solution Using Chitosan-Coated Bentonite, International Journal of Polymer Science, 11, 1608939. https://doi.org/10.1155/2016/1608939

Ucun, H., Aksakal, O., Yildiz, E. (2009). Copper(II) and zinc(II) biosorption on Pinus sylvestris L, Journal of Hazardous Materials, 161: 1040–1045. https://doi.org/10.1016/j.jhazmat.2008.04.050

Ucun, H., Bayhana, Y.K., Kaya, Y., Cakici, A., Algur, O.F. (2003). Biosorption of lead (II) from aqueous solution by cone biomass of Pinus sylvestris, Desalination, 154: 233–238. https://doi.org/10.1016/S0011-9164(03)80038-3

United Nations (2015). Transforming our world: the 2030 Agenda for Sustainable Development. United Nations Sustainable knowledge platform, Sustainable Development Goals, 1–40. https://sustainabledevelopment.un.org/post2015/transformingourworld (consulted on November, 10th, 2020).

Vera, L.M., Bermejo, D., Uguña, M.F., Garcia, N., Flores, M., González, E. (2019). Fixed bed column modeling of lead(II) and cadmium(II) ions biosorption on sugarcane bagasse, Environmental Engineering Research, 24: 31–37. https://doi.org/10.4491/eer.2018.042

Vilardi, G., Ochando-Pulido, J.M., Verdone, N., Stoller, M., Di Palma, L. (2018). On the removal of hexavalent chromium by olive stones coated by iron-based nanoparticles: Equilibrium study and chromium recovery, Journal of Cleaner Production, 190: 200–210. https://doi.org/10.1016/j.jclepro.2018.04.151

Villen-Guzman, M., Gutierrez-Pinilla, D., Gomez-Lahoz, C., Vereda-Alonso, C., Rodriguez-Maroto, J.M., Arhoun, B. (2019). Optimization of Ni (II) biosorption from aqueous solution on modified lemon peel, Environmental Research, 179, part B, 108849. https://doi.org/10.1016/j.envres.2019.108849

Vu, T.A., Le, G.H., Dao, C.D., Dang, L.Q., Nguyen, K.T., Nguyen, Q.K., Dang, P.T., Tran, H.T.K., Duong, Q.T., Nguyen, T.V., Lee, G.D. (2014). Arsenic removal from aqueous solutions by adsorption using novel MIL-53(Fe) as a highly efficient adsorbent, RSC Advances, 5: 5261–5268. https://doi.org/10.1039/C4RA12326C

Wadhawan, S., Jain, A., Nayyar, J., Mehta, S.K. (2020). Role of nanomaterials as adsorbents in heavy metal ion removal from waste water: A review, Journal of Water Process Engineering, 33, 101038. https://doi.org/10.1016/j.jwpe.2019.101038

Wang, C., Liu, X., Chen, J.P., Li, K. (2015). Superior removal of arsenic from water with zirconium metal-organic framework UiO-66, Scientific Reports, 5, 16613. https://doi.org/10.1038/srep16613

Wang, C., Luan, J., Wu, C. (2019). Metal-organic frameworks for aquatic arsenic removal, Water Research, 158: 370–382. https://doi.org/10.1016/j.watres.2019.04.043

Wang, H., Yuan, X., Wu, Y., Huang, H., Zeng, G., Liu, Y., Wang, X., Lin, N., Qi, Y. (2013). Adsorption characteristics and behaviors of graphene oxide for Zn(II) removal from aqueous solution, Applied Surface Science, 279: 432–440. https://doi.org/10.1016/j.apsusc.2013.04.133

Wang, J. (2018). Reuse of Heavy Metal from Industrial Effluent Water. IOP Conference Series: Earth and Environmental Science, 199, 042002. https://doi.org/10.1088/1755-1315/199/4/042002

Wang, J., Chen, B. (2015). Adsorption and coadsorption of organic pollutants and a heavy metal by graphene oxide and reduced graphene materials, Chemical Engineering Journal, 281: 379–388. https://doi.org/10.1016/j.cej.2015.06.102

Wang, J., Guo, X. (2020). Adsorption isotherm models: Classification, physical meaning, application and solving method, Chemosphere, 258, 127279. https://doi.org/10.1016/j.chemosphere.2020.127279

Wang, K., Gu, J., Yin, N. (2017). Efficient Removal of Pb(II) and Cd(II) Using NH2-Functionalized Zr-MOFs via Rapid Microwave-Promoted Synthesis, Industrial and Engineering Chemistry Research, 56: 1880–1887. https://doi.org/10.1021/acs.iecr.6b04997

Wang, X., Chen, Z., Yang, S. (2015). Application of graphene oxides for the removal of Pb(II) ions from aqueous solutions: Experimental and DFT calculation, Journal of Molecular Liquids, 211: 957–964. https://doi.org/10.1016/j.molliq.2015.08.020

Wang, Xiangxue, Liu, Y., Pang, H., Yu, S., Ai, Y., Ma, X., Song, G., Hayat, T., Alsaedi, A., Wang, Xiangke (2018). Effect of graphene oxide surface modification on the elimination of Co(II) from aqueous solutions, Chemical Engineering Journal, 344: 380–390. https://doi.org/10.1016/j.cej.2018.03.107

Wang, Y., Pan, C., Chu, W., Vipin, A.K., Sun, L. (2019). Environmental Remediation Applications of Carbon Nanotubes and Graphene Oxide: Adsorption and Catalysis, Nanomaterials (Basel), 9(3): 439. https://doi.org/10.3390/nano9030439

Wang, D., Gilliland, S.E., Yi, X., Logan, K., Heitger, D.R., Lucas, H.R., Wang, W.-N. (2018). Iron Mesh-Based Metal Organic Framework Filter for Efficient Arsenic Removal, Environmental Science and Technology, 52: 4275–4284. https://doi.org/10.1021/acs.est.7b06212

Wang, J., Guo, X. (2020). Adsorption isotherm models: Classification, physical meaning, application and solving method, Chemosphere, 258: 127279. https://doi.org/10.1016/j.chemosphere.2020.127279

Wen, J., Fang, Y., Zeng, G. (2018). Progress and prospect of adsorptive removal of heavy metal ions from aqueous solution using metal–organic frameworks: A review of studies from the last decade, Chemosphere, 201: 627–643. https://doi.org/10.1016/j.chemosphere.2018.03.047

WHO, UN-Water (2014). Investing in Water and Sanitation: Increasing access, reducing inequalities.https://sustainabledevelopment.un.org/index.php?page=view&type=400&nr=1749&menu=1515 (consulted on November, 10th, 2020)

WHO (2017). Guidelines for drinking-water quality: fourth edition incorporating first addendum, World Health Organization. https://www.who.int/publications/i/item/9789241549950

Wu, H., Md, M., Wz, G., H, Y., Jg, Z., Z, C., P, X., Zy, D. (2018). Arsenic removal from water by metal-organic framework MIL-88A microrods, Environmental Science and Pollution Research, 25: 27196–27202. https://doi.org/10.1007/s11356-018-2751-2

Wu, W., Yang, Y., Zhou, H., Ye, T., Huang, Z., Liu, R., Kuang, Y. (2012). Highly Efficient Removal of Cu(II) from Aqueous Solution by Using Graphene Oxide. Water Air Soil Pollution, 224: 1372. https://doi.org/10.1007/s11270-012-1372-5

Xia, Q., Wang, H., Huang, B., Yuan, X., Zhang, Jingjing, Zhang, Jin, Jiang, L., Xiong, T., Zeng, G. (2019). State-of-the-Art Advances and Challenges of Iron-Based Metal Organic Frameworks from Attractive Features, Synthesis to Multifunctional Applications, Nano.Micro Small, 15(2) 1803088. https://doi.org/10.1002/smll.201803088

Xue, X., Xu, J., Baig, S.A., Xu, X. (2016). Synthesis of graphene oxide nanosheets for the removal of Cd(II) ions from acidic aqueous solutions, Journal of the Taiwan Institute of Chemical Engineers, 59: 365–372. https://doi.org/10.1016/j.jtice.2015.08.019

Yagub, M.T., Sen, T.K., Afroze, S., Ang, H.M. (2015). Fixed-bed dynamic column adsorption study of methylene blue (MB) onto pine cone, Desalination and Water Treatment, 55: 1026–1039. https://doi.org/10.1080/19443994.2014.924034

Yahya, M.D., Abubakar, H., Obayomi, K.S., Iyaka, Y.A., Suleiman, B. (2020). Simultaneous and continuous biosorption of Cr and Cu (II) ions from industrial tannery effluent using almond shell in a fixed bed column, Results in Engineering, 6, 100113.

https://doi.org/10.1016/j.rineng.2020.100113

Yin, N., Wang, K., Li, Z. (2016). Rapid Microwave-promoted Synthesis of Zr-MOFs: An Efficient Adsorbent for Pb(II) Removal, Chemistry Letters, 45: 625–627. https://doi.org/10.1246/cl.160148

Yu, S., Liu, J., Zhu, W., Hu, Z.-T., Lim, T.-T., Yan, X. (2015). Facile room-temperature synthesis of carboxylated graphene oxide-copper sulfide nanocomposite with high photodegradation and disinfection activities under solar light irradiation, Scientific Reports, 5, 16369. https://doi.org/10.1038/srep16369

Yu, W., Luo, M., Yang, Y., Wu, H., Huang, W., Zeng, K., Luo, F. (2019). Metal-organic framework (MOF) showing both ultrahigh As(V) and As(III) removal from aqueous solution, Journal of Solid State Chemistry, 269: 264–270. https://doi.org/10.1016/j.jssc.2018.09.042

Yunus, Z.M., Al-Gheethi, A., Othman, N., Hamdan, R., Ruslan, N.N. (2020). Removal of heavy metals from mining effluents in tile and electroplating industries using honeydew peel activated carbon: A microstructure and techno-economic analysis, Journal of Cleaner Production, 251 119738. https://doi.org/10.1016/j.jclepro.2019.119738

Yurekli, Y. (2016). Removal of heavy metals in wastewater by using zeolite nano-particles impregnated polysulfone membranes, Journal of Hazardous Materials, 309: 53–64. https://doi.org/10.1016/j.jhazmat.2016.01.064

Zhang, Q., Yu, J., Cai, J., Zhang, L., Cui, Y., Yang, Y., Chen, B., Qian, G. (2015). A porous Zr-cluster-based cationic metal–organic framework for highly efficient $Cr_2O_7^{2-}$ removal from water, Chemical Communication, 51: 14732–14734. https://doi.org/10.1039/C5CC05927E

Zhang, Y., Duan, X. (2020). Chemical precipitation of heavy metals from wastewater by using the synthetical magnesium hydroxy carbonate, Water Science and Technology, 81: 1130–1136. https://doi.org/10.2166/wst.2020.208

Zhang, Y., Ma, H.-L., Peng, J., Zhai, M., Yu, Z.-Z. (2013). Cr(VI) removal from aqueous solution using chemically reduced and functionalized graphene oxide, Journal of Materials Science, 48: 1883–1889. https://doi.org/10.1007/s10853-012-6951-8

Zhang, B.-L., Qiu, W., Wang, P.-P., Liu, Y.-L., Zou, J., Wang, L., Ma, J. (2020). Mechanism study about the adsorption of Pb(II) and Cd(II) with iron-trimesic metal-organic frameworks, Chemical Engineering Journal, 385, 123507. https://doi.org/10.1016/j.cej.2019.123507

Zhao, G., Li, J., Ren, X., Chen, C., Wang, X. (2011). Few-Layered Graphene Oxide Nanosheets As Superior Sorbents for Heavy Metal Ion Pollution Management, Environmental Science and Technology. 45: 10454–10462. https://doi.org/10.1021/es203439v

Zhou, Y.-T., Nie, H.-L., Branford-White, C., He, Z.-Y., Zhu, L.-M. (2009). Removal of Cu^{2+} from aqueous solution by chitosan-coated magnetic nanoparticles modified with α-ketoglutaric acid, Journal of Colloid and Interface Science, 330: 29–37. https://doi.org/10.1016/j.jcis.2008.10.026

Zhu, B.-J., Yu, X., Jia, Y., Peng, F., Sun, B., Zhang, M., Luo, T., Liu, J., Huang, X.-J. (2012). Iron and 1,3,5-Benzenetricarboxylic Metal–Organic Coordination Polymers Prepared by Solvothermal Method and Their Application in Efficient As(V) Removal from Aqueous Solutions, The Journal of Pysical Chemistry, 116(15): 8601-8607. https://doi.org/10.1021/JP212514A

Zhu, W.-P., Gao, J., Sun, S.-P., Zhang, S., Chung, T.-S. (2015). Poly(amidoamine) dendrimer (PAMAM) grafted on thin film composite (TFC) nanofiltration (NF) hollow fiber membranes for heavy metal removal, Journal of Membrane Science, 487: 117–126. https://doi.org/10.1016/j.memsci.2015.03.033

Zhu, W.-P., Sun, S.-P., Gao, J., Fu, F.-J., Chung, T.-S. (2014). Dual-layer polybenzimidazole/polyethersulfone (PBI/PES) nanofiltration (NF) hollow fiber membranes for heavy metals removal from wastewater, Journal of Membrane Science, 456: 117–127. https://doi.org/10.1016/j.memsci.2014.01.001

ANNEX

Published articles derived to the thesis

International Journal of Environmental Research
https://doi.org/10.1007/s41742-020-00246-5

RESEARCH PAPER

Evaluation of Olive Stones for Cd(II), Cu(II), Pb(II) and Cr(VI) Biosorption from Aqueous Solution: Equilibrium and Kinetics

Marwa Ben Amar[1,2] · Khaled Walha[1] · Victoria Salvadó[2]

Received: 2 August 2019 / Revised: 23 January 2020 / Accepted: 3 February 2020

Abstract

Milled olive stones are evaluated as a biosorbent for the removal of heavy metals such as Cd (II), Cu (II), Pb(II) and Cr(VI) from aqueous effluents. To this end, thermodynamic and kinetic studies for single and multimetal systems are performed through batch equilibrium isotherms. The biosorbent was characterized by elemental and FTIR analysis and scanning electron microscopy. The effect of the different parameters, such as contact time, pH, amount of adsorbent and initial metal concentration, on the sorption process is also investigated. The maximum removal percentage for 1 mg L^{-1} of cadmium, copper, and lead was 77.4%, 80.5%, and 94.5%, respectively, at pH 6 with 5 g L^{-1} of sorbent. In the case of Cr(VI), a removal percentage of 46% was obtained in 2 h at pH 2 using a larger amount of sorbent (10 g L^{-1}) and an initial concentration of 2 mg L^{-1}. Equilibrium data were analyzed by applying different adsorption isotherm models, resulting in—a good agreement with—the Langmuir model with maximum capacities of 0.557, 0.3 and 0.581 mg g^{-1} for Cu(II), Cd(II) and Pb(II), respectively, whereas for Cr(VI), the Temkin model provided the best fit with a maximum capacity of 2.34 mg g^{-1}. The kinetic data fitted well into the pseudo-second-order model which allowed the adsorption rate constants to be calculated. Cd(II) resulted to have the highest kinetic constant, followed by Cu(II), Cr(VI) and Pb(II). The results showed that milled olive stones can be used as a biosorbent for the removal of these metals from aqueous solutions.

Article Highlights

- **Trace concentrations of Cu(II), Cd(II), Pb(II), and Cr(VI) were adsorbed by olive stones.**
- **Removals of 77.4%, 80.5 and 94.5% were obtained for Cu(II), Cd(II), or Pb(II) at pH 6.**
- **For Cr(VI), a removal percentage of 46% was obtained at pH 2 with 10 g L^{-1} of sorbent.**
- **Langmuir isotherm model was fitted to Cu(II), Cd(II), and Pb(II) adsorption isotherm data.**
- **Cd(II) has the highest pseudo-second-order kinetic constant, followed by Cu(II), Cr(VI) and Pb(II).**
- **Milled olive stone is an effective and cheaper biosorbent to remove toxic metals.**

Keywords Biosorption · Heavy metal · Olive stones · Kinetics · Sorption isotherms

Introduction

The high toxicity and non-biodegradability of heavy metals make them a serious environmental concern, resulting in a health risk to living organisms due to their indiscriminate disposal into surface waters (Johnson et al. 2008). The discharge of metal-containing aqueous effluents from metal plating, pigment mining, electroplating, tanning, textile and other industries is the main contributor to metal pollution even where the legally required pretreatment of these effluents has been performed (Abdel Salam et al. 2011). Conventional treatments to remove heavy metals from aqueous

✉ Victoria Salvadó
victoria.salvado@udg.edu

[1] Laboratory of Material Sciences and Environment, Faculty of Sciences of Sfax, University of Sfax, Sfax, Tunisia

[2] Department of Chemistry, University of Girona, M. Aurèlia Capmany, 69, 17003 Girona, Spain

Published online: 14 February 2020

effluents include precipitation, ion exchange, and membrane processing, reverse osmosis and electrodialysis (Fu and Wang 2011). However, these methods do not completely remove these metals and require expensive equipment (Johnson et al. 2008).

Adsorption is an alternative technique that is exploited to decrease the amount of heavy metal and to purify the aqueous solution (Blázquez et al. 2005). Sorption processes are based on physical adsorption, chemical adsorption and ion-exchange mechanisms. Among the different sorbent materials, both powdered and granular activated carbon are the most widely used for the adsorption of heavy metal due to their large surface area, high adsorption capacity, porous structure (Bohli et al. 2012) and high internal surface area (Deliyanni et al. 2015). The main drawbacks are their high initial and regeneration costs (Alslaibi et al. 2014). Biosorption is a biological method based on the use of dead biomass to accumulate target pollutants through different mechanisms, such as complexation, chelation, ion exchange, inorganic micro precipitation, and hydrolysis of metal ions (Abbas et al. 2014; Pintor et al. 2012). In the search for highly efficient, eco-friendly and economic adsorbents, agricultural residues such as fava beans (Etorki et al. 2014), bark (Şen et al. 2015), maize stalk (El-Sayed et al. 2011), date stones (Abudaia et al. 2013), bone charcoal (Ghrab et al. 2017), rice straw (Gao et al. 2008), cork (Sfaksi et al. 2014), olive stones (Martín-Lara et al. 2016), pomegranate seeds (Ghaneiam et al. 2017), coffee waste (Kyzas 2012), and saxaul tree ash (Sanchooli Moghaddam et al. 2016) have been evaluated as biosorbents.

Several studies have reported the use of different biosorbents to efficiently eliminate heavy metals. Agricultural and forest waste adsorbents were used to remove Pb(II) ions in wastewater treatments (Saka et al. 2012): 98% removal of lead was achieved using apple pomace with a maximum uptake of 16.14 mg g^{-1} (Chand and Pakade 2013), and 99% removal of chromium (VI) at pH = 2 and an initial concentration of 250 mg L^{-1} was obtained with eucalyptus bark (max. uptake of 45 mg g^{-1}) (Sarin and Pant 2006). Coconut shell was able to remove 4.72 mg g^{-1} of Pb, 2.92 mg $g^{-1}$of Cu, 4.57 mg g^{-1} of Cd, and 2.02 mg g^{-1} of As from 5 mg L^{-1} aqueous solution (Okafor et al. 2012). Furthermore, other researchers have studied the removal of some heavy metals by milled olive stone. The maximum uptake of Pb(II) by milled olive stone was 6.57 mg g^{-1} at pH 6 and 10 mg L^{-1} (Hernáinz et al. 2008) and 43.46% of Cu(II) of an initial concentration of 10 mg L^{-1} at pH 5 was eliminated by the same sorbent (max. uptake of 1.96 mg g^{-1}) (Blázquez et al. 2011). Olive stone in packed bed columns has been successfully applied in the removal of heavy metals from electroplating wastewaters containing Cr(VI), Cu(II) and Ni(II) (Martín-Lara et al. 2014). In the case of Cr(VI), the biosorption process is greatly pH-dependent and in the sorption process two phenomena (biosorption and reduction) should be considered (Martín-Lara et al. 2016, Vinodhini and Das 2010).

In this study, milled olive stones, which can be easily produced from abundant and inexpensive agricultural waste in many Mediterranean countries, are evaluated as potential biosorbents due to their high adsorption capacity, which is related to the different functional groups on their surface, including carboxylate, hydroxyl, amine, amide and phosphate (Budinova et al. 2006).

The aim of this study is to investigate the capacity of milled olive stones to remove heavy metal from aqueous solution, to study the kinetics of the adsorption processes for Cd(II), Pb(II), Cu(II) and Cr(VI) and to characterize these processes by applying isotherm adsorption models. Moreover, the effect of the pH, the competition between metals, and the amount of adsorbent on the removal process is also studied.

Materials and Methods

Olive Stone Preparation

The residue obtained after olive oil extraction is composed of skin (epicardium), pulp (mesocarp) and stone (endocarp). After the initial separation of olive oil from the solid residue by the application of pressure, further extraction of oil is performed using hexane. Screening ventilation is then applied to dry and separate the remaining residue into shell and stone. The hard material, which is separated from the soft skin, is ground into fine flour using an industrial grinding mill machine. The stone, called the woody endocarp, represents about 18–25% of the full weight of the olive and is mainly composed of lignin, hemicellulose and cellulose. The biomass used in this study consisted of olive stone crushed and sieved to obtain particles of < 1 mm.

Reagents and Instruments

The working metal solutions were prepared by dilution of a 1000 mg L^{-1} stock solution prepared by adding appropriate amounts of $Cu(NO_3)_2{\cdot}3H_2O$, $Cd(NO_3)_2{\cdot}4H_2O$, $Pb(NO_3)_2$ and K_2CrO_4 (Panreac, Barcelona, Spain) in ultra-pure water. Calibration solutions of different concentrations were obtained by dilution of a 1000 mg L^{-1} standard solution (Merck, Mollet del Vallès, Spain) of each individual metal. The pH was adjusted by adding HNO_3 0.1 M (Panreac, Barcelona, Spain). Metal determination was performed by inductively coupled plasma emission spectrometry (ICP-AES) with an ICP-AES instrument (Varian, Liberty series, Australia).

Characterization of the Adsorbent

FTIR analysis was performed to identify the chemical functional groups present in the biosorbent using a Perkin-Elmer Paragon 2000 FTIR spectrometer in the range of 575 cm^{-1} to 3838 cm^{-1}. The morphology of the olive stone was observed by a scanning electron microscope (Model ZEISS DSM-960A) operating at 30 kV. Samples were examined at a magnification range of 100× to 1000×. The SEM was equipped with an energy-dispersive X-ray spectrometer Bruker Nano XFlash Detector 5010 to determine the surface composition of the material.

The specific surface area and pore size of olive stone were measured using the Brunauer–Emmett–Teller (BET) method with an ASAP 2020 (Micromeritics France S.A., Mérignac, France) instrument.

The pH at the point of zero charge (pzc) of an adsorbent surface is the pH at which this surface has a net neutral charge. This value was calculated by adding 1 g of milled olive stones to 100 mL of distilled water and varying the pH from 3 to 11, stirring for 2 h. The initial pH was adjusted by adding either HCl (0.1 M) or NaOH (0.1 M). The final pH of the solution was measured and the $\Delta pH = pH_f - pH_i$ was plotted against the pH of the initial solution.

Batch Experiments

The equilibrium time was studied with a 5 g L^{-1} adsorbent solution obtained by adding 100 mg of milled olive stone to 20 mL of metal solution with an initial concentration of 5 mg L^{-1} at pH 6. To determine the optimum pH of metal solution, the same experimental conditions (5 g L^{-1} adsorbent solution and 5 mg L^{-1} metal solution) at different pHs (2, 3 and 6) were used.

Different adsorbent concentrations (2, 4, 5, 6, 7.5, 10, 12.5 and 15 g L^{-1}) were tested by adding the corresponding amount to 20 mL of a 5 mg L^{-1} metal solution at pH 6 and shaking them for 1 h in the case of Cd(II), Cu(II) and Pb(II), and for 2 h in the case of a 10 mg L^{-1} solution of Cr(VI) at pH 2. Moreover, the pH of the solutions was measured before and after adsorption.

Separate tests with initial Cd (II), Cu(II) and Pb(II) concentrations of 1, 2, 5 and 10 mg L^{-1} were performed for 1 h with a sorbent concentration of 4 g L^{-1}, whereas in the case of Cr(VI), a 10 g L^{-1} adsorbent solution was used and the period of time was 2 h.

Competition experiments were then performed for 1 h using a metal solution containing 5 mg L^{-1} of each metal (Cu, Cd and Pb) at pH 6 and a 5 g L^{-1} adsorbent solution concentration.

All experiments were performed in triplicate at room temperature (20 ± 1 °C).

Results and Discussion

Sorbent Characterization

The characterization of the biosorbent is important to understand explain its behavior during the sorption process and the mechanism of the metal removal. Fourier transform infrared spectroscopy (FTIR) spectra were recorded in the range of 600 cm^{-1} to 4000 cm^{-1} to identify the chemical groups present in the milled olive stone. Moreover, FTIR spectra were also recorded after performing metal biosorption. As can be seen in Fig. 1, the broad band that appeared at 3364 cm^{-1} is characteristic of the stretching vibration of the hydroxyl group, which is due to hydrogen bonding O–H to a carboxyl, phenol or alcohol group. The peak observed at 1727 cm^{-1} may correspond to the stretching vibration of the carbonyl C–O or the aromatic C–C. The peaks around 1239 cm^{-1} and 1031 cm^{-1} show stretching vibrations of the C–O group in

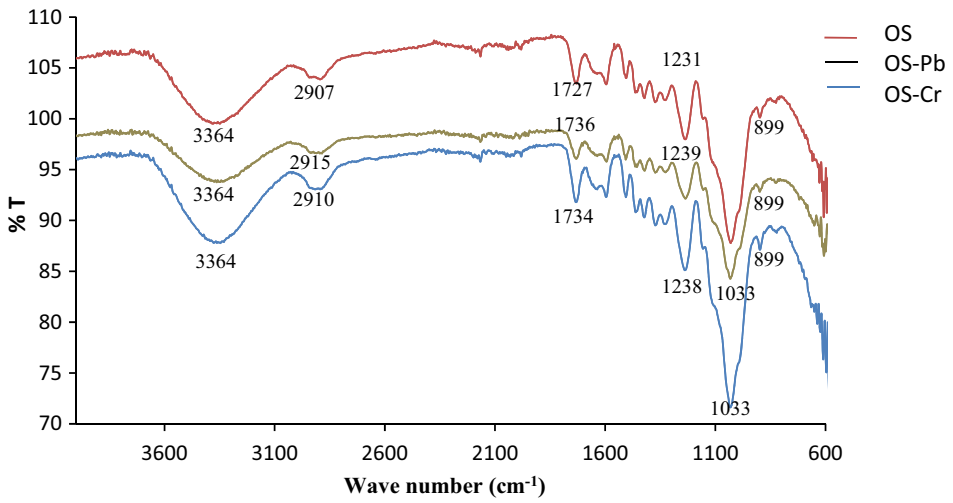

Fig. 1 FTIR spectra of milled olive stone (OS), OS after lead biosorption (OS–Pb) and OS after chromium biosorption (OS–Cr)

the carboxylic and alcoholic groups. Other bands observed at 899 cm^{-1} are attributed to inorganic groups or stretching vibrations of C–C. These peaks and bands proved the presence of the hydroxyl group and the carboxylic groups of the lignin, cellulose and hemicellulose in the biosorbent, which are responsible for the metal adsorption. The results are similar to those obtained by other researchers (Ronda et al. 2014). The results of the adsorbent before and after biosorption were compared: as can be seen there are significant changes in some bands, 3364 cm^{-1}, 2907 cm^{-1} and 1727 cm^{-1} and 1031 cm^{-1}. These band shifts indicated that the hydroxyl group and carboxyl group are involved in the adsorption of the metals.

The SEM images (Fig. 2) show irregularly shaped milled olive stone particles with an average diameter of 30.67 µm (Fig. 2 1000×), which favor the biosorption of heavy metals ions. The BET surface area, which is related to the adsorption capacity of adsorbent, is 0.1956 $m^2\ g^{-1}$, whereas the Langmuir surface area is 0.2341 $m^2\ g^{-1}$. These values are similar than those reported by other authors (Martín-Lara et al. 2016). The pH at the point of the zero charge (pH_{pzc}) of milled olive stone is 5.3. Above this pH, the surface charge becomes negative facilitating the interaction with the metal cations.

Equilibrium Time

The percentage of copper, cadmium, lead and chromium adsorbed over time is shown in Fig. 3. Maximum removal percentages for Cd(II), Cu(II), and Pb(II) of 22.6%, 40%, and 75.2%, respectively, are achieved in just 1 h in the experimental conditions tested ($C_i = 5$ mg L^{-1}) at pH 6 and 5 g L^{-1} of adsorbent. This good performance is explained by the high number of sites that are initially available to receive metal ions. In the case of Cr(VI), equilibrium is reached after 2 h and the maximum sorption percentage is 39% at pH 2. This percentage was calculated by:

$$\% = \frac{C_i - C_f}{C_i} * 100 \quad (1)$$

where C_i is the initial metal concentration (mg L^{-1}) and C_f is the final metal concentration (mg L^{-1}).

Effect of pH

The pH is an important parameter that influences the removal of heavy metal by milled olive stone since it affects metal speciation and the charge of the adsorbent surface, given that the functional groups can be protonated depending on the pH of the solution. As can be seen in Fig. 4, the percentages of sorption increased for the three divalent metals when the pH increased from 2 to 6. These results can be explained by the decrease in the number of H^+ in the media, which resulted in less competition with the metal ions for the available sites on the sorbent surface. Hence, at $pH < pH_{pzc} = 5.3$ the competition of H^+ for the sorbent sites is high. However, at $pH > pH_{pzc}$ metal sorption is more favorable given that the surface becomes negatively charged and the metals ions are retained better.

In the case of chromium, the sorption percentage decreases from 37 to 18% as the pH is increased from 2 to 6. These results can be explained by the fact that at low pH, $HCrO_4^-$ is the predominant species and the sorbent surface is protonated. The increase in the pH led to a reduction in the surface protonation and, at $pH > 5.3$, the surface is negatively charged, causing a decrease in the interaction between negatively charged species as CrO_4^{2-} and the adsorbent (Blázquez et al. 2009). Several authors (Mishra et al. 2015; Martín-Lara et al. 2016) have reported a reduction of

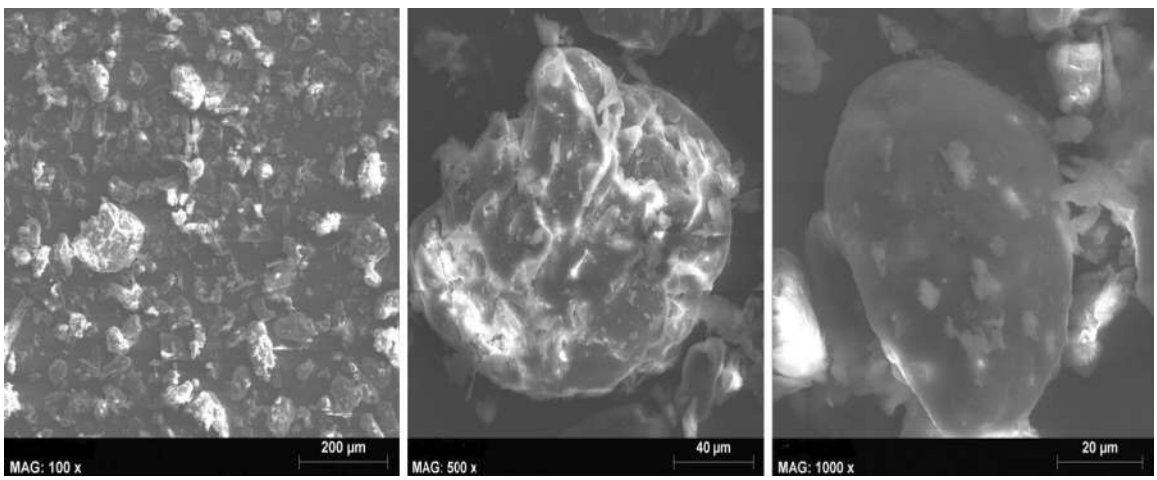

Fig. 2 SEM images of milled olive stone

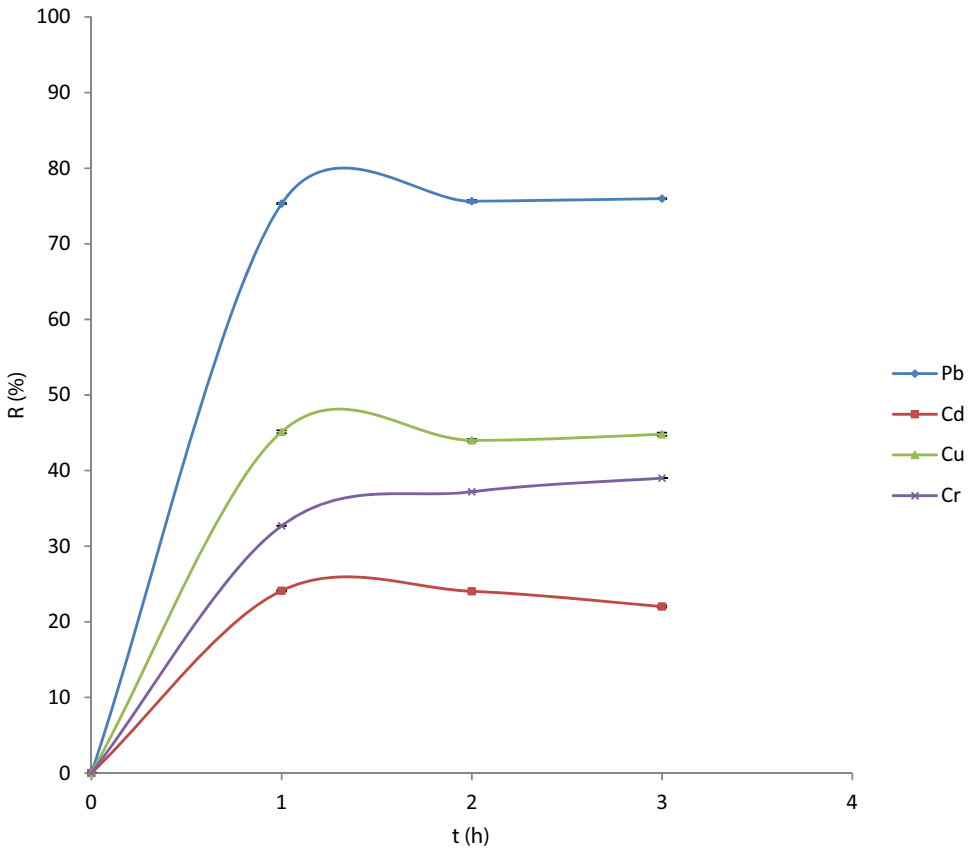

Fig. 3 Effect of the contact time on the removal (R %) ($n = 3$) of Pb(II), Cd(II), Cu(II) and Cr(VI). $[C]_i = 5$ mg L^{-1} at pH = 6, except for Cr(VI) (pH 2), adsorbent concentration of 5 g L^{-1}

Cr(VI) to Cr(III) at acidic pHs when biosorbents such as milled olive stone and rice straw were used at acidic conditions. According to Nakano et al. (2001), a large amount of protons are consumed in the reduction of Cr(VI) by the carbon present in the biosorbent, resulting in an increase of the pH of the metal solution. To verify this fact, the pH of 5 mg L^{-1} Cr(VI) solution, that was in contact with 10 g L^{-1} milled olive stone, was measured after 2 h (equilibrium time) resulting in a decrease of 0.23 units of the pH after metal adsorption showing that in our experimental conditions Cr(VI) was not reduced to Cr(III). In the case of the other metal ions, Pb(II), Cd(II) and Cu(II), the pH variation before and after biosorption was of 0.1 units when initial metal concentrations of 5 mg L^{-1} at pH 6 were used. At this pH > 5.3, we assumed that most of the functional groups of the biosorbent are negatively charged and that biosorption is taking place through electrostatic interactions rather than by the exchange of the H^+ of the functional groups by the metal ions.

The Effect of the Adsorbent Concentration

The percentage of metal ions adsorbed by milled olive stone depends on the amount of sorbent as well as the initial metal concentration and the pH of the solution. The removal percentages of cadmium, copper and lead increased to 22.4%, 45.8% and 74.5%, respectively, as the amount of adsorbent was raised from 2 to 6 g L^{-1}, before rapidly falling off on further increasing the amount of sorbent (Fig. 5). This fact is explained by the aggregation of the biosorbent particles, avoiding the interaction of the metals with the surface sites, when more than 6 g L^{-1} of adsorbent solution was used. As can be seen in Fig. 5, the sorption percentage for the three metals was the same with 7.5 g L^{-1} at pH 6, showing that at these conditions, there are fewer available sites and that metal sorption at these conditions occurred through unspecific interactions. However, in the case of Cr(VI), the removal percentage increased significantly up to 4 g L^{-1} before continuing with a much slower but constant rise up to 15 g L^{-1}, finally reaching 46.84%. Martín-Lara et al. (2016) obtained higher removal rates of 96.38% for Cr(VI) using 10 g L^{-1} of adsorbent and an initial concentration of 10 mg L^{-1} of Cr(VI) at pH 2. Moreover, they found that Cr(VI) was reduced to Cr(III) by the adsorbent at low pHs and the removal process of Cr(VI) was reported to involve two processes: biosorption and reduction. Taking into account that in this study the sorption of Cr(VI) decreased until 18% when the pH increased from 2 to 6, we consider that Cr(VI) biosorption occurred only through an ion-exchange mechanism.

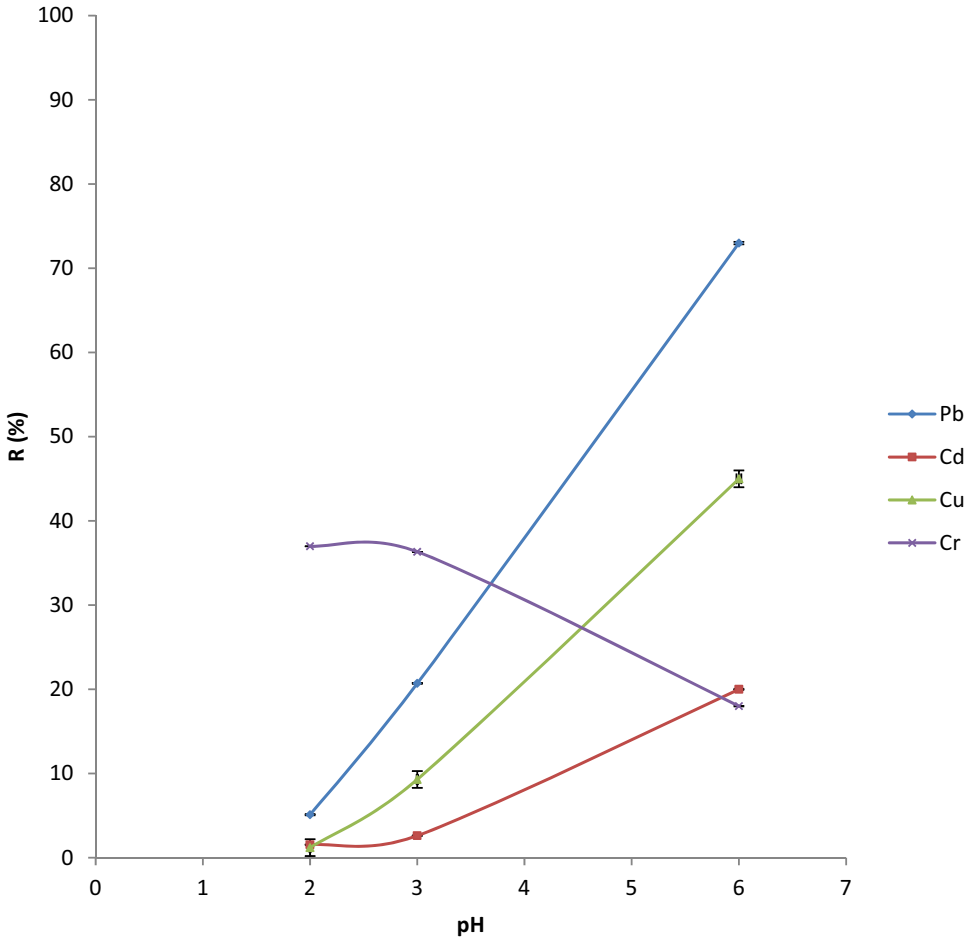

Fig. 4 Effect of the pH on the removal (R %) ($n=3$) of Pb(II), Cd(II), Cu(II) and Cr(VI). $[C]_i=5$ mg L^{-1}, adsorbent concentration of 5 g L^{-1}, 1 h of contact time, except for Cr(VI) (2 h)

The Effect of the Initial Metal Concentration

The results given in Fig. 6 show that the percentage of biosorption decreased as the initial concentration increased in the case of Cu(II), Pb(II) and Cd(II), due to the lack of availability of sites on the surface of the sorbent at a sorbent concentration of 5 g L^{-1}. As can be seen in this figure, at an initial metal concentration of 2 mg L^{-1} the highest removal percentage was achieved with Pb(II) (84.4%), followed by Cu(II) (60.9%), and Cd(II) (47.9%). When the initial metal concentration was increased to 5 mg L^{-1}, the removal efficiency decreased to 60%, 37%, and 18.29% for Pb(II), Cu(II) and Cd(II), respectively. In the case of Cr(VI), the removal rate decreased from 46 to 35% when the initial concentration increased from 2 to 5 mg L^{-1} at pH 2 and a solution containing 10 g L^{-1} of biosorbent was used.

Adsorption Isotherms

Different models (Langmuir, Freundlich and Temkin) of sorption isotherms (Fig. 7) were studied to describe the adsorption equilibrium and to express the relation between the metal concentration at equilibrium and the adsorbed quantity at a constant temperature.

The amount of metal ions adsorbed at equilibrium per mass unit of adsorbent was determined by applying Eq. 2:

$$q_e = \frac{(C_i - C_e) \cdot v}{m} \tag{2}$$

where C_i is the initial concentration (mg L^{-1}), C_e is the equilibrium concentration (mg L^{-1}), V is the volume of the solution (l) and m is the mass of the adsorbent (g)

The Langmuir adsorption isotherm assumes the formation of a monolayer of adsorbate on the outer surface of the adsorbent and after that no further adsorption takes place. The Langmuir isotherm is valid for monolayer adsorption onto a surface containing a finite number of identical sites. The linear Langmuir model is presented by Eq. 3:

$$\frac{C_e}{q_e} = \frac{1}{q_{max} \cdot b} + \frac{1}{q_{max}} C_e \tag{3}$$

where q_{max} is the maximum adsorption capacity (mg g^{-1}) and b is the Langmuir constant (L mg^{-1})

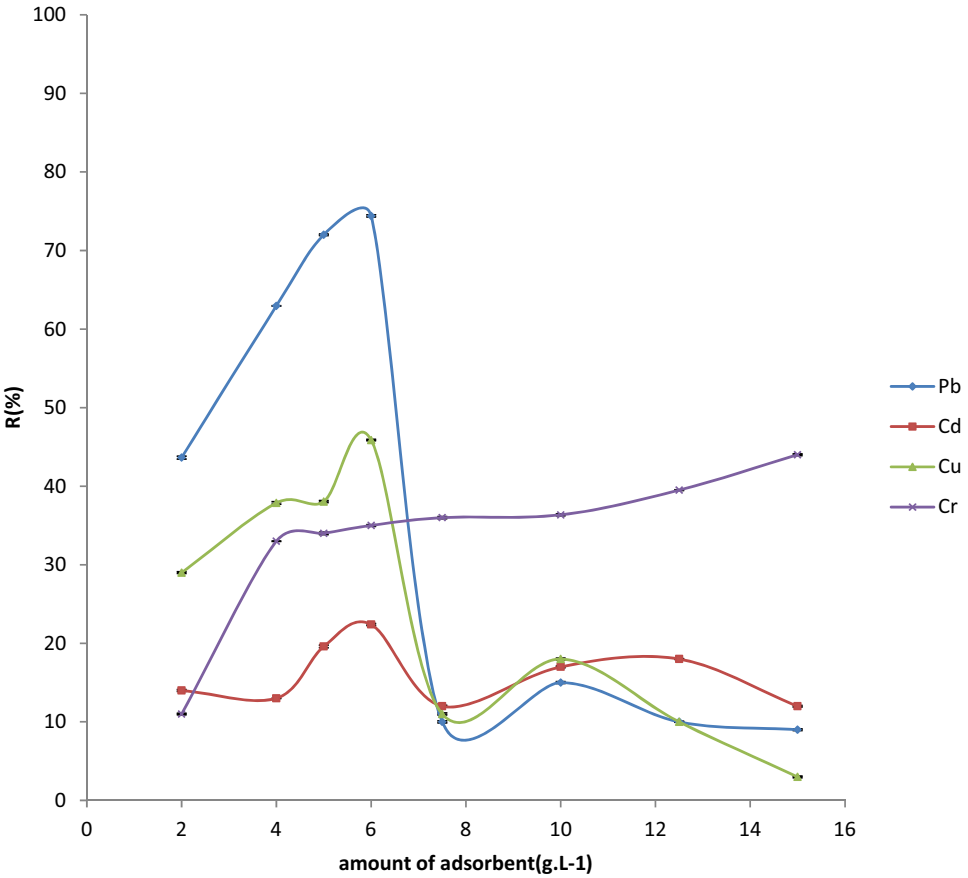

Fig. 5 Effect of the adsorbent concentration on the removal (R %) ($n=3$) of Pb(II), Cd(II), Cu(II), and Cr(VI). $[C]_i=5$ mg L^{-1} at pH 6, 1 h of contact time, except for Cr(VI) (pH 2, 2 h)

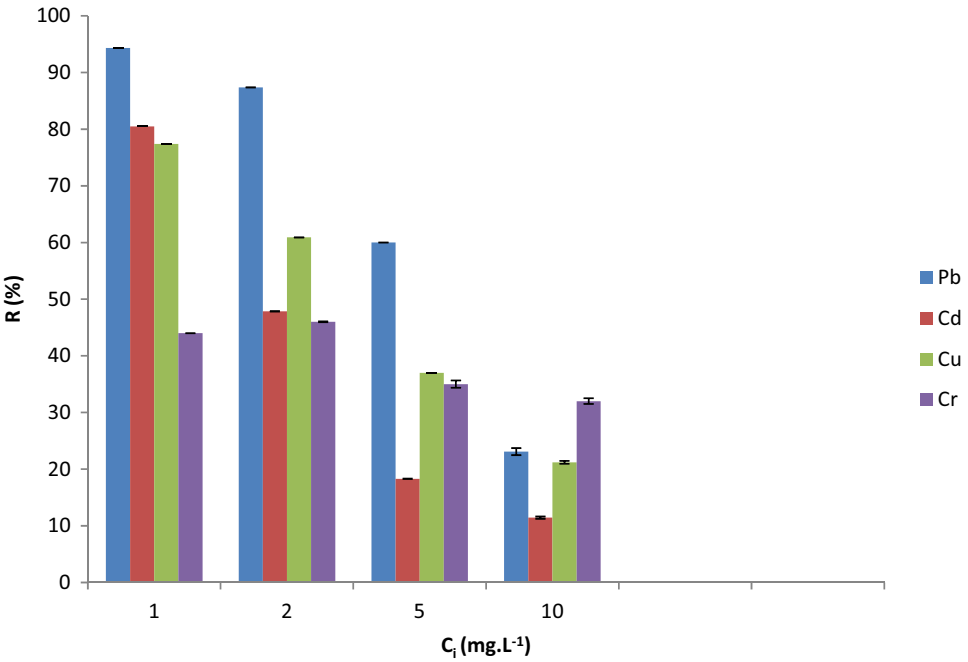

Fig. 6 Effect of initial concentration on the removal (R %) ($n=3$) of Pb(II), Cd(II), Cu(II), and Cr(VI). Adsorbent concentration of 4 g L^{-1} at pH 6, 1 h of contact time except for Cr(VI) (10 g L^{-1} at pH 2, contact time of 2 h)

The essential characteristic of the Langmuir isotherm can be explained by the equilibrium separation factor (R_L) defined as follows:

$$R_L = \frac{1}{1 + C_0 b}. \quad (4)$$

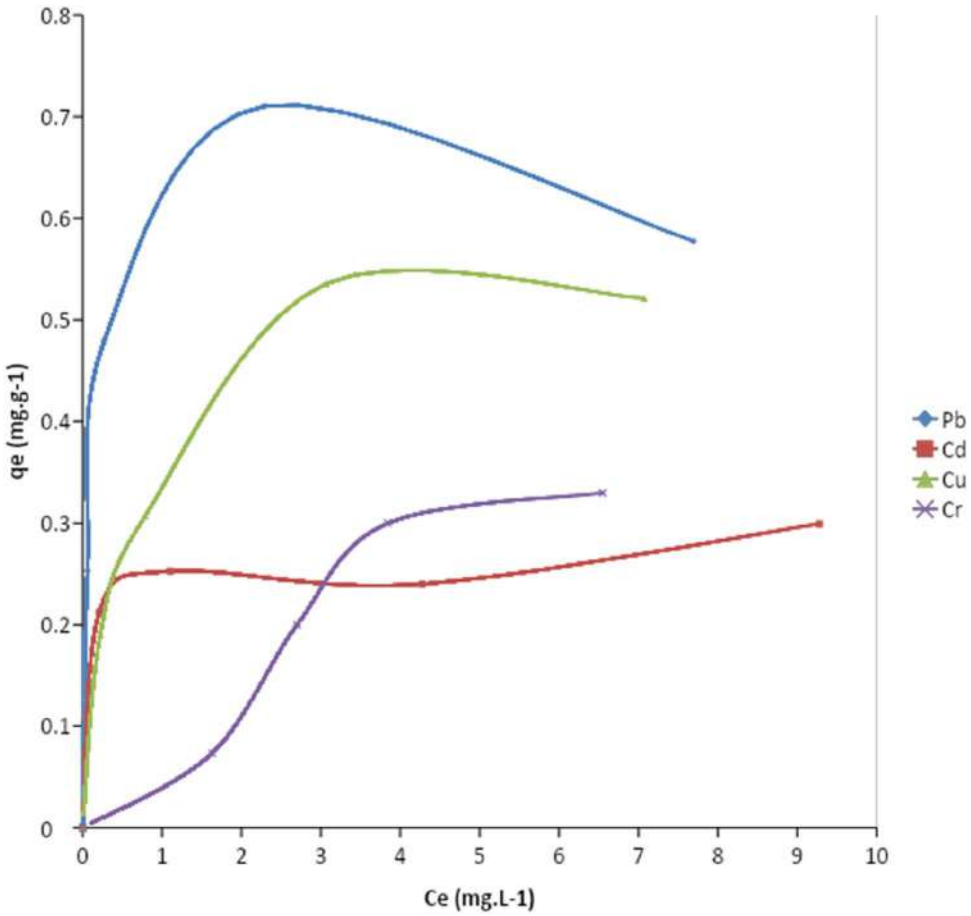

Fig. 7 Adsorption isotherms on milled olive stone of Pb(II), Cd(II), Cu(II) at pH 6, and Cr(VI) at pH 2

Table 1 Values of the separation factor (R_L) obtained for the adsorption of Cu (II), Cd (II), Pb(II) and Cr(VI) by milled olive stone

Metal	C_i (mg L^{-1})	R_L
Cu	1	0.301
	2	0.177
	5	0.079
	10	0.043
Cd	1	0.263
	2	0.151
	5	0.066
	10	0.034
Pb	1	0.012
	2	0.0061
	5	0.0024
	10	0.0012
Cr	1	0.97
	2	0.94
	5	0.88
	10	0.79

$R_L = 0$: irreversible adsorption, $0 < R_L < 1$: favorable adsorption and $R_L = 1$: linear adsorption, as can be seen in Table 1, so the R_L at all the concentrations was between 0 and 1, showing that the adsorption is favorable for all the metals. R_L decreases with increasing initial metal concentration which indicates that in higher concentration the sites available decrease indicating its saturation. In the case of Cr(VI), R_L values are close to 1 (linear adsorption) for the lowest concentrations (1 and 2 mg L^{-1}) in agreement with the results obtained in Fig. 7.

The Freundlich isotherm model assumes that the metal ion adsorption takes place on a heterogeneous surface with multilayer adsorption. The linear Freundlich model is expressed by Eq. 5:

$$\ln q_e = \ln k_F + \frac{1}{n} \ln C_e \quad (5)$$

where q_e is the amount of metal adsorbed at equilibrium (mg g^{-1}), C_e is the equilibrium concentration (mg L^{-1}) and K_F is the Freundlich constant.

The constant K_F is an indicator of adsorption capacity, while $1/n$ is the strength of adsorption in the adsorption process. When $1/n$ is below 1, as it is the case for Cu(II), Cd(II) and Pb(II), it indicates a normal adsorption and when $1/n$ is

Table 2 Results obtained by applying the Langmuir, Freundlich and Temkin models to the experimental data

Isotherm model	Isotherm parameters	Cu (II)	Cd(II)	Pb(II)	Cr(VI)
Langmuir	q_m (mg g^{-1})	0.557	0.3	0.581	2.345
	K_L (L mg^{-1})	2.318	2.801	80.64	0.026
	R^2	**0.995**	**0.985**	**0.999**	0.030
Freundlich	n	3.285	1.375	5.649	0.889
	K_F (mg g^{-1})	0.61	0.537	0.739	0.299
	R^2	0.926	0.718	0.735	0.847
Temkin	A (L mg^{-1})	4.125	102.51	20.65	1.005
	B (J mol^{-1})	0.245	0.0531	0.174	0.437
	R^2	0.928	0.9704	0.714	**0.920**

Bold value indicates the best correlation coefficient for each metal and isotherm model

above one, as in the case of Cr(VI), it indicates a cooperative adsorption (Table 2).

Temkin isotherm model takes into account the effects of indirect adsorbate–adsorbate interactions on the adsorption process; it is also assumed that the heat of adsorption of all molecules in the layer decreases linearly as a result of increase surface coverage. It is expressed by the following equation:

$$q_e = B \ln A + B \ln C_e \tag{6}$$

where A is the Temkin constant (L mg^{-1}) and B is the Temkin constant related to heat adsorption (J mol^{-1}).

The Langmuir, Freundlich and Temkin isotherm constants and their determination coefficients (r^2) are listed in Table 2. As can be observed, the Cu data fitted well with the Langmuir, Freundlich and Temkin models with a determination coefficient > 0.92 and a maximum adsorption capacity of 0.557 mg g^{-1}. In the case of Pb, the adsorption isotherm followed the Langmuir model and the corresponding adsorption constant is higher (80 L mg^{-1}) than those obtained for copper and cadmium, 2.32 and 2.80, respectively, showing the great affinity of this metal for milled olive stone. Cd correlated with both the Langmuir and Temkin models with a maximum adsorption capacity of 0.3 mg g^{-1}. Similar results were obtained by other authors (Blázquez et al. 2011) and (Hernáinz et al. 2008). They showed that Cu(II), Cd(II) and Pb(II) adsorbed by milled olive stone fitted the Langmuir model with maximum adsorption capacities of 1.97 mg g^{-1}, 4.897 mg g^{-1} and 6.57 mg g^{-1} at pH 5. As can be seen in Table 2, the q_m values obtained in this study are lower given that the BET surface area is approximately the half than those reported by these researchers (Blázquez et al. 2011).

In the case of the Cr(VI), the best fit of the data was with the Temkin isotherm, with a correlation of 0.92 and a Temkin constant of 1.005 L mg^{-1}. However, it is important to remark that the Temkin isotherm is valid only for an intermediate range concentration. In comparison, the experimental data for the adsorption of Cr(VI) by rice straw at pH 2 fitted well with the Langmuir model with a q_m of 3.15 mg g^{-1} (Gao et al. 2008).

Kinetics of the Adsorption

The kinetics of the adsorption process is the main characteristic defining the sorption efficiency. Two kinetic models, the first-order and the pseudo-second-order, were tested in this study. The first model assumes that the rate of occupation of sorption sites is proportional to the number of unoccupied sites, expressed by Eq. 7:

$$\frac{dq_t}{dt} = K_1(q_e - q_t) \tag{7}$$

where q_e and q_t are the adsorption capacity at equilibrium and at time t, respectively (mg g^{-1}) and k_1 is the rate constant of pseudo-first-order adsorption (min^{-1})

The pseudo-second-order kinetic model is based on the assumption that the rate-limiting step is related to chemical sorption and is expressed by Eq. 8:

$$\frac{dq_t}{dt} = K_2(q_e - q_t) \tag{8}$$

where K_2 (g mg^{-1} min^{-1}) is a second-order kinetic rate.

The parameters calculated for both kinetic models are collected in Table 3. Good correlation ($r^2 > 0.99$) is obtained between the experimental data and the pseudo-second-order model indicating that the adsorption of Cu(II), Cd(II), Pb(II), and Cr(VI) was controlled by a chemical process. The results obtained show that Cd(II) presented the highest K_2 and that the maximum sorption capacity q_e was found for

Table 3 Kinetic parameters of metal ion adsorption by milled olive stones

	Pseudo-first-order			Pseudo-second-order		
	q_e (mg g^{-1})	K_1 (min^{-1})	R^2	q_e (mg g^{-1})	K_2 (g mg^{-1} min^{-1})	R^2
Cd	0.021	0.0088	0.436	0.252	1.086	0.999
Cu	0.240	0.0038	0.207	0.474	0.251	0.998
Pb	0.444	0.0031	0.635	0.856	0.124	0.993
Cr	0.383	0.0035	0.800	0.392	0.188	0.998

Pb(II), however, this metal ion presented the lowest kinetic rate constant.

Competitive Adsorption of Cd, Cu and Pb

We then investigated the effect on the sorption capacity of milled olive stones when a mixture of Cu, Cd, and Pb was employed. Figure 8 shows a decrease in the percentage of the metals removed when there was competition. In single metal experiments with milled olive stone, for 1 h at pH 6, lead was the most adsorbed metal (75%). This value decreased to 37.8% (50% of reduction) in the case of multiple metal experiments, when Cu and Cd were also present at the same concentration. In the case of Cu and Cd, the sorption capacities decreased to 6.8% (30% reduction), and 9.8% (15% reduction), respectively. Since Cd has the highest rate constant, this metal was the first to saturate the available surface sites, followed by Cu and Pb. The highest reduction on the sorption capacity in multiple metal experiments was obtained for Pb(II), which has the lowest kinetic rate constant although this metal ion showed the maximum sorption capacity (Table 3). These results demonstrated that the kinetic parameters can significantly affect the sorption process in the case of multimetal biosorption. Ronda et al. 2014 reported that the greater affinity of the functional groups of the biosorbent to one metal ion is related to the ionic characteristics of this metal, which are measured by parameters including the ionic radius (r), the electronegativity (X_m) or covalent index: $CI = X_m^2 (r + 0.85)$. The sorption capacity is higher for metals with a higher covalent index than the other metals: lead has a covalent index of 11.1 whereas copper and cadmium have covalent indexes of 5.56 and 5.14, respectively.

Conclusions

This study into the efficiency of milled olive stones, an agricultural waste product containing carboxylic groups, to remove heavy metals suggests that they effectively eliminate cations, such as copper, cadmium and lead, and anions, such as chromium. Here we have identified the best conditions for the removal of the metals (pH, contact time, amount of adsorbent and initial metal concentration). We have also found that Pb(II), which has the greatest electronegativity and ionic radius, presented the highest sorption rates by milled olive stone, followed by Cu(II) and Cd(II). In the case of Cr(VI), the need of an acidic pH seems to indicate that the sorption process may take place through an ion-exchange mechanism. The Langmuir isotherm correlated well with the experimental data in single-ion solutions, resulting in maximum adsorption capacities at pH 6 of 0.581, 0.557 and 0.3 mg g^{-1}, for lead, copper and cadmium, respectively, whereas chromium data correlated well with the Temkin isotherm model, with a maximum capacity of 2.345 mg g^{-1} at pH 2. The good correlation found for all the metals with the pseudo-second-order kinetic model indicates a chemical sorption process. The results obtained in this study show that milled olive stones are an efficient

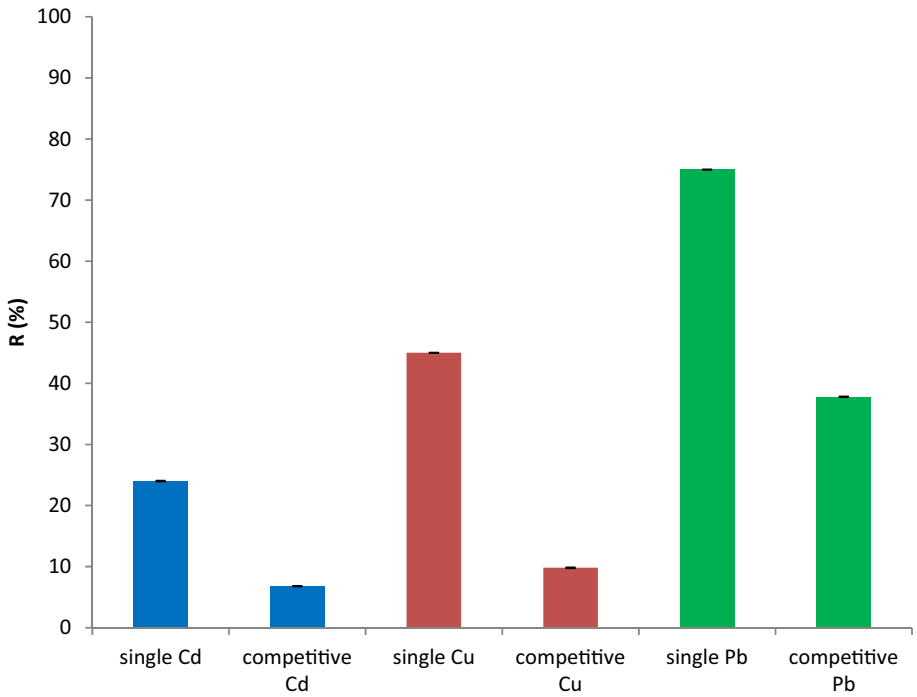

Fig. 8 Comparison of the removal (R %) ($n = 3$) in multimetal competitive (Cu(II), Cd(II) and Pb(II)) adsorption by milled olive stone with the removal of a single metal solution. $[C]_i = 5$ mg L^{-1}, adsorbent concentration of 5 g L^{-1} and 1 h of contact time

biosorbent to remove most of the heavy metals from industrial effluents and wastewaters.

Acknowledgements M. Ben Amar acknowledges the financial support of the Faculty of Science (University of Sfax, Tunisia) and of The Environmental and Analytical Chemistry Research Group of the Department of Chemistry (University of Girona, Spain).

References

Abbas SH, Ismail IM, Mostafa TM, Sulaymon AH (2014) Biosorption of heavy metals: a review. J Chem Sci Tech 3(4):74–102

Abdel Salam OE, Reiad NA, ElShafei MM (2011) A study of the removal characteristics of heavy metals from wastewater by low-cost adsorbents. J Adv Res 2:297–303. https://doi.org/10.1016/j.jare.2011.01.008

Abudaia JA, Sulyman MO, Elazaby KY, Ben-Ali SM (2013) Adsorption of Pb(II) and Cu (II) from aqueous solution onto activated carbon prepared from dates stones. Int J Environ Sci Dev 4:191–195. https://doi.org/10.7763/IJESD.2013.V4.333

Alslaibi TM, Abustan I, Ahmad MA, Foul AA (2014) Preparation of activated carbon from olive stone waste: optimization study on the removal of Cu^{2+}, Cd^{2+}, Ni^{2+}, Pb^{2+}, Fe^{2+}, and Zn^{2+} from aqueous solution using response surface methodology. J Dispers Sci Technol 35:913–925. https://doi.org/10.1080/01932691.2013.809506

Blázquez G, Hernáinz F, Calero M, Ruiz-Núñez LF (2005) Removal of cadmium ions with olive stones: the effect of some parameters. Proc Biol 40:2649–2654. https://doi.org/10.1016/j.procbio.2004.11.007

Blázquez G, Hernáinz F, Calero M, Martin-Lara MA, Tenorio G (2009) The effect of pH on the biosorption of Cr(III) and Cr(VI) with olive stone. Chem Eng J 148:473–479. https://doi.org/10.1016/j.cej.2008.09.026

Blázquez G, Martín-Lara MA, Dionisio-Ruiz E, Tenorio G, Calero M (2011) Evaluation and comparison of the biosorption process of copper ions onto olive stone and pine bark. J Ind Eng Chem 17:824–833. https://doi.org/10.1016/j.jiec.2011.08.003

Bohli T, Ouederni A, Fiol N, Villaescusa I (2012) Uptake of Cd^{2+} and Ni^{2+} metal ions from aqueous solutions by activated carbons derived from waste olive stones. Int J Chem Eng Appl 3:232–236. https://doi.org/10.7763/IJCEA.2012.V3.192

Budinova T, Petrov N, Razvigorova M, Parra J, Galiatsatou P (2006) Removal of arsenic(III) from aqueous solution by activated carbons prepared from solvent extracted olive pulp and olive stones. Ind Eng Chem Res 45:1896–1901. https://doi.org/10.1021/ie051217a

Chand P, Pakade YB (2013) Removal of Pb from water by adsorption on apple pomace: equilibrium, kinetics, and thermodynamics studies. J Chem (Hindawi, Online) Article ID 164575. https://doi.org/10.1155/2013/164575

Deliyanni EA, Kyzas GZ, Triantafyllidis KS, Matis KA (2015) Activated carbons for the removal of heavy metal ions: A systematic review of recent literature focused on lead and arsenic ions. Open Chem 13:699–708

El-Sayed GO, Dessouki HA, Ibrahiem SS (2011) Removal of Zn (II), Cd (II) and Mn(II) from aqueous solutions by adsorption on maize stalks. MJAS 15:8–21

Etorki AM, El-Rais M, Mahabbis MT, Moussa NM (2014) Removal of some heavy metals from wastewater by using of fava beans. Am J Anal Chem 05:225. https://doi.org/10.4236/ajac.2014.54028

Fu F, Wang Q (2011) Removal of heavy metal ions from wastewaters: a review. J Environ Manag 92:407–418. https://doi.org/10.1016/j.jenvman.2010.11.011

Gao H, Liu Y, Zeng G, Xu W, Li T, Xia W (2008) Characterization of Cr(VI) removal from aqueous solutions by a surplus agricultural waste—rice straw. J Hazard Mater 150:446–452. https://doi.org/10.1016/j.jhazmat.2007.04.126

Ghaneiam MT, Bhatnagar A, Ehrampoush MH, Amrollahi M, Jamsihi B, Dehvari M, Taghavi M (2017) Biosorption of hexavalent chromium from aqueous solution onto pomegranate seeds: kinetic modeling studies. Int J Environ Sci Technol 14:331–340. https://doi.org/10.1007/s13762-016-1216-8

Ghrab S, Benzina M, Lambert SD (2017) Copper adsorption from wastewater using bone charcoal. Adv Mat Phys Chem 07:139. https://doi.org/10.4236/ampc.2017.75012

Hernáinz F, Calero M, Blázquez G, Martin-Lara MA, Tenorio G (2008) Comparative study of the biosorption of cadmium(II), chromium(III), and lead(II) by olive stone. Environ Prog 27:469–478. https://doi.org/10.1002/ep.10299

Johnson TA, Jain N, Joshi HC, Prasad S (2008) Agricultural and agro-processing wastes as low cost adsorbents for metal removal from wastewater: a review. J Sci Ind Res (India) 67:647–658

Kyzas GZ (2012) Commercial coffee wastes as materials for adsorption of heavy metals from aqueous solutions. Materials 5(10):1826–1840. https://doi.org/10.3390/ma5101826

Martín-Lara MA, Blázquez G, Trujillo MC, Pérez A, Calero M (2014) New treatment of real electroplating wastewater containing heavy metal ions by adsorption onto olive stone. J Clean Prod 81:120–129. https://doi.org/10.1016/j.jclepro.2014.06.036

Martín-Lara MA, Calero de Hoces M, Ronda Gálvez A, Pérez Muñoz A, Trujillo Miranda MC (2016) Assessment of the removal mechanism of hexavalent chromium from aqueous solutions by olive stone. Water Sci Technol 73:2680–2688. https://doi.org/10.2166/wst.2016.081

Mishra A, Dubey A, Shinghal S (2015) Biosorption of chromium(VI) from aqueous solutions using waste plant biomass. Int J Environ Sci Technol 12:1415–1426. https://doi.org/10.1007/s13762-014-0516-0

Nakano Y, Takeshita K, Tsutsumi T (2001) Adsorption mechanism of hexavalent chromium by redox within condensed-tannin gel. Water Res 35:496–500. https://doi.org/10.1016/S0043-1354(00)00279-7

Okafor PC, Okon P, Daniel E, Ebenso E (2012) Adsorption capacity of coconut (*Cocos nucifera* L.) shell for lead, copper, cadmium and arsenic from aqueous solutions. Int J Electrochem Sci 7:12354–12369. http://www.electrochemsci.org/papers/vol7/71212354.pdf

Pintor AMA, Ferreira CIA, Pereira JC, Correia P, Silva SP, Vilar VP, Botelho CM, Boaventura RA (2012) Use of cork powder and granules for the adsorption of pollutants: a review. Water Res 46:3152–3166. https://doi.org/10.1016/j.watres.2012.03.048

Ronda A, Martín-Lara MÁ, Blázquez G, Moreno N, Calero M (2014) Copper biosorption in the presence of lead onto olive stone and pine bark in batch and continuous systems. Environ Prog Sustain Energy 33:192–204. https://doi.org/10.1002/ep.11780

Saka C, Sahin O, Küçük MM (2012) Applications on agricultural and forest waste adsorbents for the removal of lead (II) from contaminated waters. Int J Environ Sci Technol 9:379–394. https://doi.org/10.1007/s13762-012-0041-y

Sanchooli Moghaddam M, Rahdar S, Taghavi M (2016) Cadmium removal from aqueous solutions using saxaul tree ash. Iran J Chem Chem Eng 35:45–52

Sarin V, Pant KK (2006) Removal of chromium from industrial waste by using eucalyptus bark. Bioresour Technol 97:15–20. https://doi.org/10.1016/j.biortech.2005.02.010

Şen A, Pereira H, Olivella MA, Villaescusa I (2015) Heavy metals removal in aqueous environments using bark as a biosorbent. Int J Environ Sci Tech 12:391–404. https://doi.org/10.1007/s13762-014-0525-z

Sfaksi Z, Azzouz N, Abdelwahab A (2014) Removal of Cr(VI) from water by cork waste. Arab J Chem 7:37–42. https://doi.org/10.1016/j.arabjc.2013.05.031

Vinodhini V, Das N (2010) Relevant approach to assess the performance of sawdust as adsorbent of chromium (VI) ions from aqueous solutions. Int J Environ Sci Technol 7(1):85–92. https://doi.org/10.1007/bf03326120

Hindawi
Adsorption Science & Technology
Volume 2021, Article ID 6678530, 12 pages
https://doi.org/10.1155/2021/6678530

Research Article

Valorisation of Pine Cone as an Efficient Biosorbent for the Removal of Pb(II), Cd(II), Cu(II), and Cr(VI)

Marwa Ben Amar,[1,2] Khaled Walha,[1] and Victoria Salvadó[2]

[1]*Laboratory of Material Sciences and Environment, Faculty of Science, University of Sfax, Tunisia*
[2]*Department of Chemistry, Faculty of Science, University of Girona, M. Aurèlia Capmany, 69, 17003 Girona, Spain*

Correspondence should be addressed to Victoria Salvadó; victoria.salvado@udg.edu

Received 2 January 2021; Revised 30 March 2021; Accepted 13 April 2021; Published 27 April 2021

Academic Editor: Stefano Salvestrini

Valorisation of pine cone as an efficient, low-cost, and eco-friendly biosorbent for the removal of heavy metals from aqueous solutions is evaluated. The morphology and surface chemistry of the biosorbent are characterized by scanning electron microscopy, energy-dispersive elemental analysis, and Fourier transform infrared spectroscopy, revealing the presence of carboxylic and alcoholic functional groups that interact with metal ions. The effect of the contact time, pH, amount of adsorbent, and initial metal concentration in the adsorption is studied, resulting in removal percentages for Cd(II), Cu(II), Pb(II), and Cr(VI) (metal concentration of 5 mg L^{-1}) of 82.24%, 93.71%, 94.67%, and 88.8%, respectively (pH = 5.4, 2 g L^{-1} of adsorbent), except for Cr(VI) (pH = 2, 10 g L^{-1}). The equilibrium data of Pb(II) and Cd(II) were found to follow the Langmuir-Freundlich model, with maximum adsorption capacities of 100.01 and 78.73 mg g^{-1}, respectively, whereas Cu(II) followed the Langmuir model with 33.55 mg g^{-1}. Cr(VI) adsorption data also fitted the Langmuir model, and the maximum adsorption capacity was 57.36 mg g^{-1}. Adsorption data was obtained at pH 5.4 for divalent metal ions and at pH 2 for Cr(VI) and in a range of metal concentrations ranging from 1 to 500 mg L^{-1} at 298.2 K. The presence of the three metal ions in the solution does not affect the percentage of the target metal ion adsorbed, proving the absence of competition between them and showing the pine cone to be an efficient adsorbent to treat multimetal effluents allowing water reuse.

1. Introduction

It is increasingly difficult to obtain access to clean water due to the highly contaminating effect of certain industries compounded by ever more frequent conditions of drought, and so the removal of heavy metals such as Cd(II), Cu(II), Cr(VI), and Pb(II) from industrial wastewater is a major concern for society, given that their lack of biodegradability and toxicity are especially damaging to both ecosystems and human health [1].

Different technologies, such as ion exchange, solvent extraction, chemical precipitation, electrolysis, reverse osmosis, and adsorption on activated carbon, have been applied to remove heavy metals from wastewaters. However, the applicability of all these techniques has several disadvantages, including incomplete metal removal, high investment and operational costs, energy and reagent requirements, and generation of toxic sludge and other waste products [2]. Activated carbon is the most widely used adsorbent given its large surface area and porous structure; however, the poor functionalization of its surface is a drawback for the adsorption of metal ions [3]. The large amount of functional groups on the surface and high specific surface areas of nanomaterials, such as graphene oxides, carbon nanotubes, carbon nitride (C_3N_4), chitosan materials, and covalent organic frameworks (COFs), makes them excellent adsorbents for the elimination of metal ions [4]. The preparation of magnetic COF with high adsorption capacities allows the removal of pollutants such as Cr(VI) at the same time facilitating easier separation of the adsorbent [5]. The high price of these nanomaterials, which is due to the synthesis process, together with their tendency to aggregate, which results in a reduction in the available active sites, currently restricts their real applications [6]. Biochar and biochar-supported composites

showed high sorption capacities for heavy metal ions allowing the simultaneous elimination of both organic and inorganic pollutants [7]. However, biochar preparation and modification process are costly due to the consumption of chemical reagents and energy.

Biosorption, which uses low cost and readily available dead and live biomass, is an effective treatment to eliminate heavy metals from industrial effluents through many different metal binding mechanisms, such as ion exchange, chelation/coordination, precipitation, and sorption by other physical and chemical forces [8, 9]. A wide variety of agricultural residues has been evaluated as biosorbents taking advantage of the local availability of different vegetable matter around the world and their low cost as most of them are considered waste products. These include, among others, potato and banana peels [8], waste tea leaves [10], plantain peels [11], rice husk [12], and sweetsop [13], pistachio shells [14], date palm leaves [15], mahogany leaves [16], lemon grass [17], coconut shell [18], and almond green hull [19]. One drawback of using biosorbents is their low sorption capacity in comparison with other sorbents. Although this limitation can be overcome by modifying their surface through physical and chemical treatments that improve their capacity to bind to metal ions, these treatments require the use of energy and chemical reagents, which increase the cost. Two examples are the chemical treatment applied to modify lemon peel, resulting in an improved capacity to remove Ni(II) [20], and the thermal treatment of pea peels at 600°C to adsorb Pb(II) [21]. Besides the use of lignocellulose-rich biomass for bioethanol production, this biomass has been shown to be more efficient than other biosorbents to remove metal ions. The different types of plant parts such as stems, stalks, leaves, husk, shells, roots, and barks as raw material or as agricultural residues can be used to reduce environmental pollution.

Pine cones are produced in large quantities annually all over the world. In the Western Mediterranean, Spain has a pine-cultivated area of 460,000 hectares [22], whereas in the Southern Mediterranean, 320,000 hectares of forest cover in Tunisia is made up of Pinus halepensis and Pinus pinea [23]. After the separation of the pine nuts, the remaining material is typically released into the environment as waste [24]. Pine cones are mainly composed of cellulose, hemicellulose, and lignin, which have functional groups such as carbonyl (ketone), carboxyl, sulfhydryl (thiol), sulfonate, thioether, amine, alcohols, and esters that can bind heavy metals. Moreover, the cones have excellent physicochemical properties, including water retention, swelling capacity, and mechanical strength, that make them particularly suitable for use as an adsorbent [25]. Pine cones have been used in previous studies to adsorb different metal ions including Cr(VI) [25], Cu(II) and Cd(II) [26], Cu(II) [27], Pb(II) [28], and binary solutions of Cu(II) and Pb(II) [29].

Moreover, pine cones have also been applied to the removal of textile dyes from coloured wastewater [30]. A chemical treatment using KOH was successfully applied to improve the surface properties of pine cones to adsorb Pb(II) and Cu(II) [31]. Pine cone was also used as a precursor of organic carbon and then directly applied to the removal of Pb(II), Cu(II), Ni(II), and Cr(VI) [32] and to produce a porous carbon low-cost photocatalyst support for environmental remediation [33].

However, milled pine cone is used in this study without performing any previous biosorbent treatment to reduce the costs and complexity of the biosorbent process. Hence, the aims of the present study are to characterize the milled pine cone and to valorise it as a biosorbent for the removal of heavy metals such as Pb(II), Cd(II), Cu(II), and Cr(VI) from water solutions.

2. Materials and Methods

Pine cones were collected from a forest in Tunisia and were washed several times with distilled water and sun-dried for two days. The dried samples were then crushed to a powder and sieved to obtain particle size < 1 mm.

The morphology of the milled pine cones was analysed by scanning electron microscopy (SEM) (Model ZEISS DSM-960A) operated at 30 kV. Samples were examined at magnification ranges of 50x, 500x, and 1000x. The SEM was equipped with an energy-dispersive X-ray spectrometer Bruker Nano XFlash Detector 5010 to determine the surface composition of the material. The particle size distribution was determined by the analysis of SEM images.

The adsorbent material was analysed by Fourier transformed infrared spectroscopy (Perkin-Elmer Paragon 2000 FTIR spectrometer) from 600 cm^{-1} to 3600 cm^{-1} to identify the functional groups present on the adsorbent.

The surface area of the adsorbent was determined using Brunauer-Emmett-Teller (BET) measurements. This analysis was carried out by the N_2 adsorption at 22°C using BET micromeritics ASAP 2020.

The pH at the point of zero charge (pH_{PZC}) of an adsorbent surface is the pH at which this surface has a net neutral charge. This value was calculated by adding 1 g of milled pine cones to 100 mL of distilled water and varying the pH from 2 to 11, stirring for 2 hours. The initial pH was adjusted by adding either HCl (0.1 M) or NaOH (0.1 M). The final pH of the solution was measured and the $\Delta pH = pH_f - pH_i$ was plotted against the pH of the initial solution.

Stock solutions of metals of 1000 mg L^{-1} were prepared by dissolving appropriate quantities of $Cd(NO_3)_2{\cdot}4H_2O$, K_2CrO_4, $Cu(NO_3)_2{\cdot}3H_2O$, and $Pb(NO_3)_2$ (Panreac, Barcelona, Spain) in ultrapure water and diluted to obtain different concentrations.

2.1. Batch Experiments. The equilibrium time was studied by adding 0.04 g of milled pine cone to 20 mL of a metal solution with an initial metal concentration of 5 mg L^{-1} at pH 5.4. After equilibrium was reached, the solutions were filtered to eliminate the adsorbent and analysed by inductively coupled plasma emission spectrometry (Varian, Liberty series ICP-AES). Calibration solutions of different concentrations were prepared by dilution of a 1000 mg L^{-1} standard solution (Merck, Mollet del Vallès, Spain) of each individual metal. The effect of the amount of adsorbent was studied by using different concentrations ranging from 1 g L^{-1} to 10 g L^{-1} with an initial metal concentration of 5 mg L^{-1} at pH = 5.5 for

Pb(II), Cu(II), and Cd(II), except for Cr(VI), which was at pH = 2.

Separate tests with initial Cd(II), Cu(II), Cr(VI), and Pb(II) concentrations ranging from 1 to 500 mg L^{-1} were performed by adding 0.04 g of adsorbent to 20 mL of each solution for 2 hours.

The effect of pH on the metal adsorption was evaluated by adding 0.04 g of adsorbent to 20 mL of a 5 mg L^{-1} solution at different pHs (2, 5.5, and 9), adjusted by adding HNO_3 0.1 M and NaOH 0.1 M (Panreac, Barcelona, Spain). The pH of the solution was measured before and after adsorption.

Competition experiments between Cd(II), Cu(II), and Pb(II) were then performed using 0.04 g of adsorbent and 20 mL of metal solution containing (1, 5, and 10 mg L^{-1}) of each metal at pH 5.5 for 2 hours. All experiments were performed in triplicate at room temperature.

3. Results and Discussion

3.1. Milled Pine Cone Characterization before and after Adsorption. The FTIR spectrum of milled pine cone is presented in Figure 1(a). Five bands corresponding to the different functional groups can be seen in this figure. The broad band at 3379 cm^{-1} proved the presence of hydroxyl groups (O-H stretching vibration), indicating strong hydrogen bonding. The peak at 2935 cm^{-1} indicates the presence of aliphatic C-H group stretching vibrations of the $–CH_3$ and $–CH_2$ groups. The peak observed at 1635 cm^{-1} denotes the stretching vibration of C=O of carboxylic groups, the peaks at 1386 cm^{-1} and 1268 cm^{-1} can be associated to carboxylic/aromatic hydroxyl (–OH) stretching of phenol group, and the peak at 1033 cm^{-1} shows the stretching vibration of C-O of the primary alcohol group. As can be seen in Figure 1(a), there are changes in the bands at 3352 cm^{-1}, 2929 cm^{-1}, 1610 cm^{-1}, 1378 cm^{-1}, 1275 cm^{-1}, and 1027 cm^{-1} after metal biosorption. These band shifts indicate that the hydroxyl and carboxylic groups are involved in the adsorption of the metals as have been reported for lignocellulosic substrates in which two acid sites—a low-pH (carboxylic) site and a high-pH (phenolic) site—are present [34]. Moreover, there is a decrease in the intensity after metal biosorption indicating an ion exchange or surface complexation process as the interaction with the metal ions prevents, in most of the cases, the vibration of the bonds [35]. Martín-Lara et al. [29] also reported that the carboxylic group is the main active site of pine cone, and this finding is supported by the slightly acidic value of pH_{PZC} = 5.62. However, in our study, we found a pH_{PZC} of 6.2.

The SEM images before and after adsorption show some modifications, an accumulation of metals on the cracks of the adsorbent surface (Figures 1(b) and 1(c)). The study of the chemical composition of the biosorbent is important to explain its behaviour during the sorption process. Pine cone is a lignocellulosic material with hemicellulose, lignin, cellulose, and extractive materials [36]. The surface elemental analysis of milled pine cones performed by EDX analysis (Figure 1(b)) showed a composition of 53.48% of C, 44.77% of O, and 0.17% of S which is similar to the findings of other studies [22, 29]. The characterization by EDX after adsorption (Figure 1(c)), which was performed by putting the milled pine cones into contact with a solution containing three divalent metal ions, confirms the presence of Cd, Cu, and Pb in the material with weight percentages of 0.3, 4.61, and 12.41%, respectively. Lead has the highest percentage, indicating the greater affinity of the biosorbent for this metal ion, followed by copper and cadmium. This result is in agreement with the strength of binding by the carboxylic and hydroxyl functional groups that follow the sequence Pb (II) > Cu(II) > Cd(II) [34].

The BET surface area, which is related to the capacity of the adsorbent, is 0.2536 m^2g^{-1}, whereas the Langmuir surface area is 0.3108 m^2g^{-1}. These values are smaller than those reported for pine cones and other agricultural wastes ($0.5 > S_{BET} > 5\ m^2/g$) [29]. The results obtained for the particle size distribution show that 88% of the particles of the 6376 particles analysed have a diameter of 50 μm, 8% of 100 μm, 3% of 150 μm, and 1% of 200 μm.

3.2. Batch Adsorption

3.2.1. Effect of Contact Time on Biosorption. The effect of contact time on the adsorption of metals onto the pine cones was studied. All four metals achieved equilibrium in 2 hours with removal percentages of 82.24% for Cd(II), 93.71% for Cu(II), 94.67% for Pb(II), and 75.43% for Cr(VI) (Figure 2(a)). The high adsorption percentage of Cu(II) and Pb(II) is explained by their greater affinity to the carboxylic, ketonic, and aldehyde functional groups [37].

3.2.2. Effect of pH. The influence of the pH solution is an important parameter as it affects both the protonation of the functional groups on the adsorbent surface and the metal speciation. Figure 2(b) shows the percentage removal of Cd(II), Cu(II), Pb(II), and Cr(VI) at different pHs.

At pH 2, low percentages of metals were removed. This percentage was higher when the pH was increased, reaching a maximum at pH 5.5 with percentages of 82.24%, 93.17%, and 94.67% for Cd(II), Cu(II), and Pb(II), respectively. This result is explained by the competition between protons and metal ions for the available sites of the functional groups on the adsorbent surface. At acidic pH, the presence of protons H^+ increased in the solution, protonating the functional groups present on the adsorbent surface. At higher pHs, the percentage of H^+ decreased in the solution resulting in the binding of a greater number of metal ions to the functional groups. This tendency continued until pH 8.8 only in the case of Cd(II) as precipitation of Cu(II) and Pb(II) hydroxides starts at pH > 6.7 in accordance with the fraction diagrams calculated with Medusa software [38]. The fraction diagrams were calculated at 5 mg L^{-1} showing that Cu^{2+} and Pb^{2+} ions are the predominant species until pH 6 while Cd^{2+} is predominant until pH 9. Moreover, the adsorbent surface becomes deprotonated at $pH > pH_{PZC}$, facilitating the electrostatic interaction between Cd(II) and the negatively charged groups (OH– and COO–) of the adsorbent, explaining the increase in the percentage of metal removal from 82.24% at pH 5.5 to 94.12% at pH 8.8.

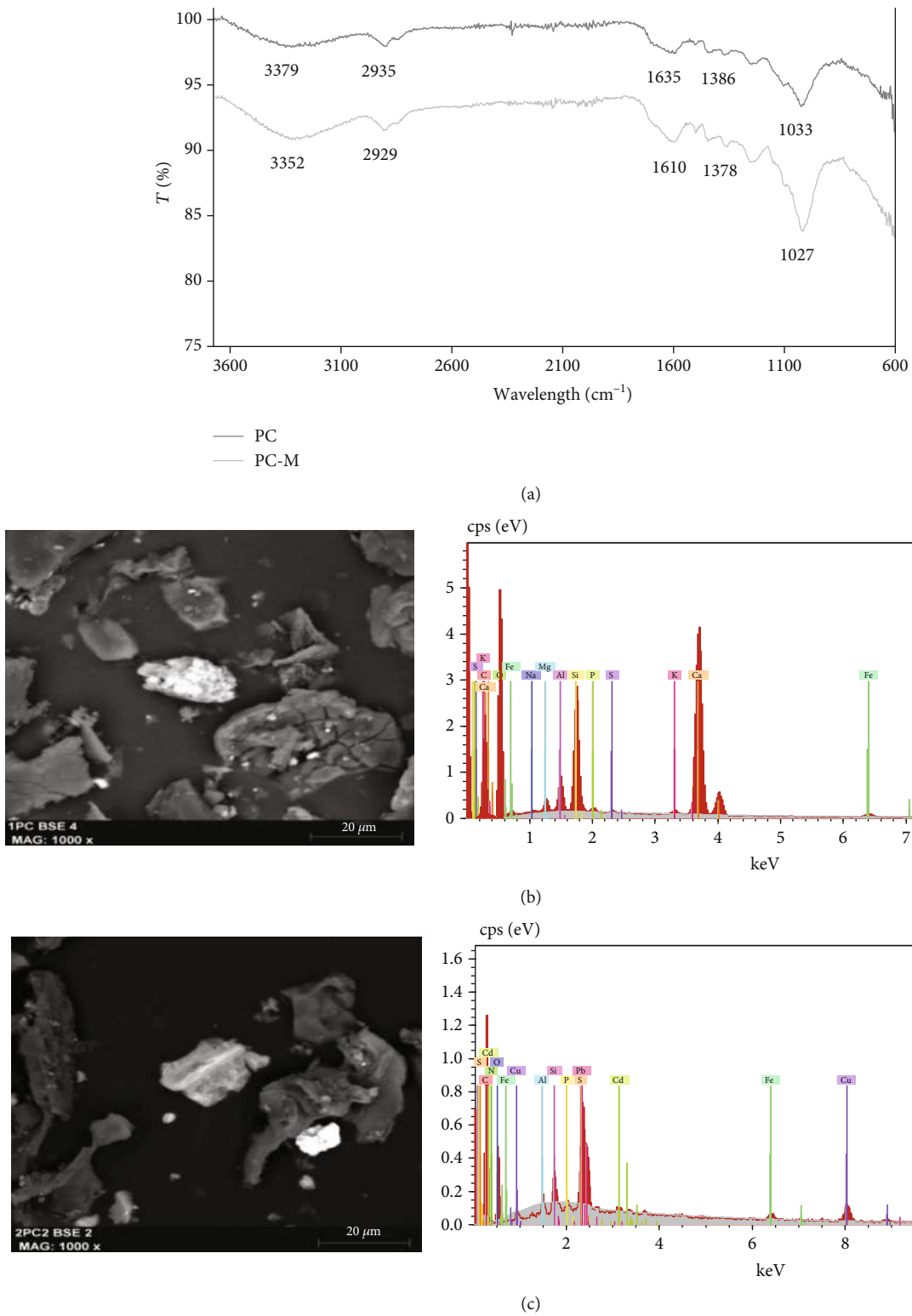

Figure 1: (a) FTIR spectra of pine cone (PC) and pine cone after metal adsorption (PC-M), (b) SEM micrograph and EDX spectra of pine cone, and (c) SEM micrograph and EDX spectra of pine cone after adsorbing Cu(II), Cd(II), and Pb(II).

In the case of chromium, the lower the pH, the greater the adsorption percentage, with values of 76% at pH = 2, 70% at pH = 5.5, and 5.8% at pH = 9. The pH of the aqueous solution influences chromium speciation and the acid-based properties of active functional groups (–OH, –COOH) of the lignocellulosic material, which are protonated at low pHs. Negatively charged $HCrO_4^-$ and CrO_4^{2-} species predominate in the aqueous solution at pH values between 2.0

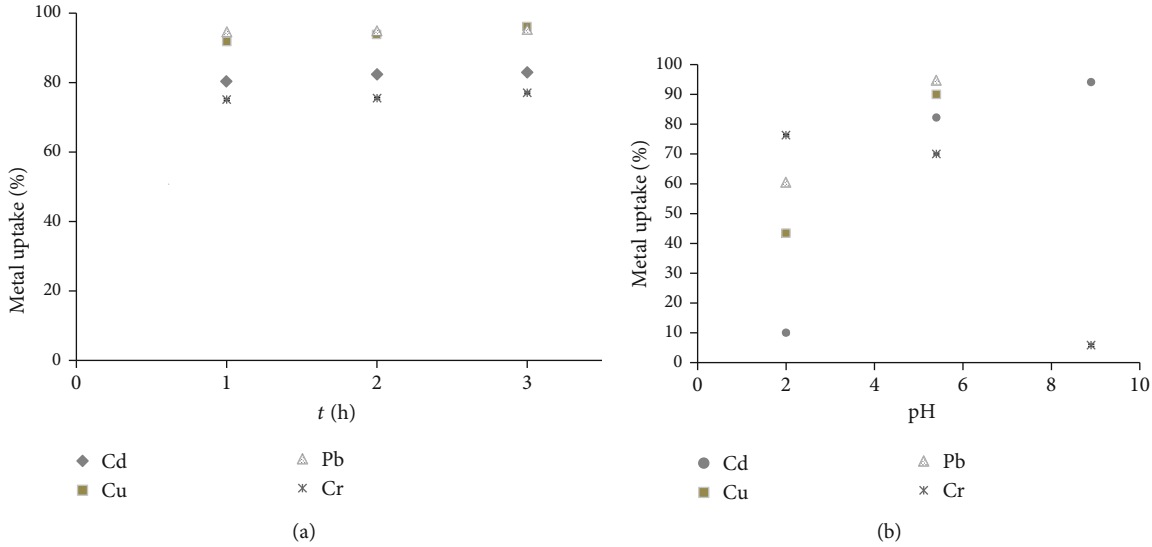

Figure 2: (a) Effect of the time on the metal uptake percentage of Cd(II), Cu(II), Pb(II), and Cr(VI) (pH = 2), $C_i = 5\,\text{mg L}^{-1}$, pH = 5.4, and adsorbent concentration = $2\,\text{g L}^{-1}$ ($n = 3$). (b) Effect of the pH on the metal uptake percentage of Cd(II), Cu(II), Pb(II), and Cr(VI), $C_i = 5\,\text{mg L}^{-1}$, adsorbent concentration = $2\,\text{g L}^{-1}$, and $t = 2\,\text{h}$ ($n = 3$).

and 6.0 for concentrations less than $500\,\text{mg L}^{-1}$. These negatively charged species can interact with the protonated functional groups at the adsorbent surface. At pH > 6, the competition of the anionic CrO_4^{2-} with the OH^- for the active sites of the adsorbent and the fact that at pHs > pH_{PZC} most of these active sites are negatively charged led to a dramatic reduction of the Cr(VI) adsorption [28]. Similar results were reported in other studies [39, 40, 37], which found the maximum Cr(VI) removal at low pH. Nowadays, the adsorption-coupled reduction reaction is the most accepted mechanism to explain Cr(VI) biosorption by natural materials [29, 41, 42]. In this mechanism, the removal of Cr(VI) involved two processes: biosorption and reduction to Cr(III) [43]. Different biomaterials, including pine cone, were used to demonstrate this coupled mechanism by verifying the oxidation state of chromium by X-ray photoelectron spectroscopy and measuring the pH variation during the adsorption process at low pHs. Protons and electrons, supplied by electron-donor groups of the biomaterial such as carboxylic groups, are required for the reduction of Cr(VI) to Cr(III), resulting in an increase in the pH of the metal solution [41]. In our study, an increase of 0.3 units of pH of the solution after the adsorption of chromium proved the reduction of one part of Cr(VI) to Cr (III), showing that adsorption of Cr(VI) may take place through this coupled mechanism.

In the case of the divalent metals, Pb(II), Cu(II), and Cd(II), the removal was through surface complexation by their association with carboxylic or OH groups as is indicated by the band shifts of these functional groups in the FTIR spectra after the adsorption of the metal ions (Figure 1(a)). As the pH of the solution is increased, the presence of ligands and the deprotonation of functional groups such as hydroxyl (-OH) and carboxyl (-COOH) on the surface of the biosorbent facilitate the formation of complexes with the metal ions, leading to further adsorption.

3.2.3. Effect of the Adsorbent Concentration. Figure 3(a) shows that higher removal percentages of Cd(II) and Cr(VI) were obtained by increasing the amount of biosorbent, while for Pb(II) and Cu(II), the removal percentages did not change when the amount was increased. As can be deduced from this figure, $2\,\text{g L}^{-1}$ is the optimum dosage of milled pine cone at pH 5.5 to remove Cu(II) and Pb(II) with percentages of 93.71% and 94.97%, respectively. In the case of Cd(II), the best results (89%) were obtained with a dose of $5\,\text{g L}^{-1}$ at pH 5.5, whereas for Cr(VI), this percentage was achieved with a dose of $10\,\text{g L}^{-1}$ at pH 2.

3.2.4. Effect of the Initial Metal Concentration. The initial metal concentration is an important parameter that affects the efficiency of biosorption. It was studied at different values ranging from 1 to $500\,\text{mg L}^{-1}$. Figure 3(b) shows the removal percentage of metals as a function of the initial metal concentration. As can be seen, the removal efficiency of milled pine cone decreases as the initial metal concentration increases. This effect is higher for Cu(II), Cd(II), and Cr(VI) than for Pb(II), more than 60% of which is removed at an initial concentration of $300\,\text{mg L}^{-1}$. This decrease is explained by the fact that at higher concentrations, the saturation of the adsorbent surface is faster given the competition for the available binding sites resulting in more ions without there being more sites to attach to. However, in the case of Pb(II), the adsorption capacity increases when the initial concentration was increased from 1 to $20\,\text{mg L}^{-1}$ indicating that the presence of more metal ions generates a driving force that overcomes the mass transfer resistance between the aqueous and the solid phases. The biosorption capacity for Pb(II) remains practically constant from 20 to $100\,\text{mg L}^{-1}$, showing that there were available binding sites on the pine cone surface. The greater affinity of pine cone to Pb(II) can be explained by its longer ionic radius (119 pm) in comparison with Cd(II)

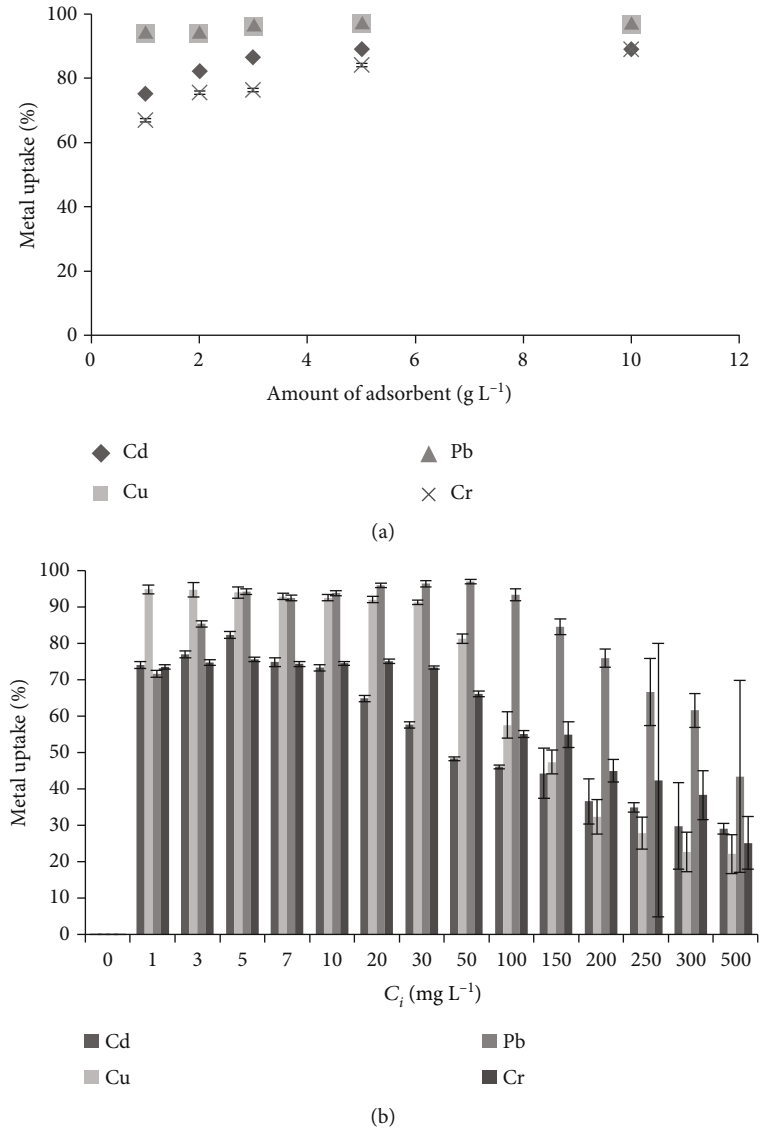

Figure 3: (a) Effect of the adsorbent concentration on the metal uptake percentage of Pb(II), Cu(II), Cd(II), and Cr(VI) (pH = 2), C_i = 5 mg L^{-1}, pH 5.4, and t = 2 h (n = 3). (b) Effect of the initial metal concentration on the metal uptake percentage of Cd(II), Cu(II), Pb(II), and Cr(VI) (pH = 2), adsorbent concentration = 2 g L^{-1}, t = 2 h, and pH = 5.4 (n = 3).

(95 pm) and Cu(II) (73 pm) as well as by the fact that it has the lowest hydration ion radius and the highest covalent index [29]. The covalent index is a function of the ionic radius (r) and the electronegativity (X_m) and is defined by the following: $\mathrm{CI} = {X_m}^2(r + 0.85)$. The greater the covalent index of the metal ion, the greater the potential of this metal ion to form covalent bonds with the functional groups of the biosorbent. Lead has a covalent index of 11.1 whereas copper and cadmium have covalent indexes of 5.56 and 5.14, respectively [44].

Moreover, the metal removal efficiencies at low concentrations such as 1 and 3 mg L^{-1} are greater for Cu(II) than for the other metals, whereas at concentrations ranging from 5 to 30 mg L^{-1}, removal rates of more than 90% were obtained for Cu(II) and Pb(II). At higher concentrations, the removal percentages of Cu(II), Cd(II), and Cr(VI) fell. The removal efficiencies for the divalent metals follow the order Pb(II) > Cu(II) > Cd(II), which corresponds to the order of their affinity towards OH from phenolic groups [34].

3.3. Adsorption Isotherm. In the adsorption isotherm graph, the amount of adsorbate per mass unit of adsorbent is represented as a function of the equilibrium concentration in the solution at a constant temperature. The shape of the line depends on the adsorbent and adsorbate characteristics and on the type of interaction between them. This shape is used to classify the adsorption isotherms in different types following the Giles classification [45]. As can be seen in Figure 4, the sorption isotherms for Pb(II), Cu(II), and Cr(VI) are type I (convex shape), corresponding to an L-type isotherm where the slopes remain constant at a maximum sorption value. The L type is associated to a monolayer adsorption of

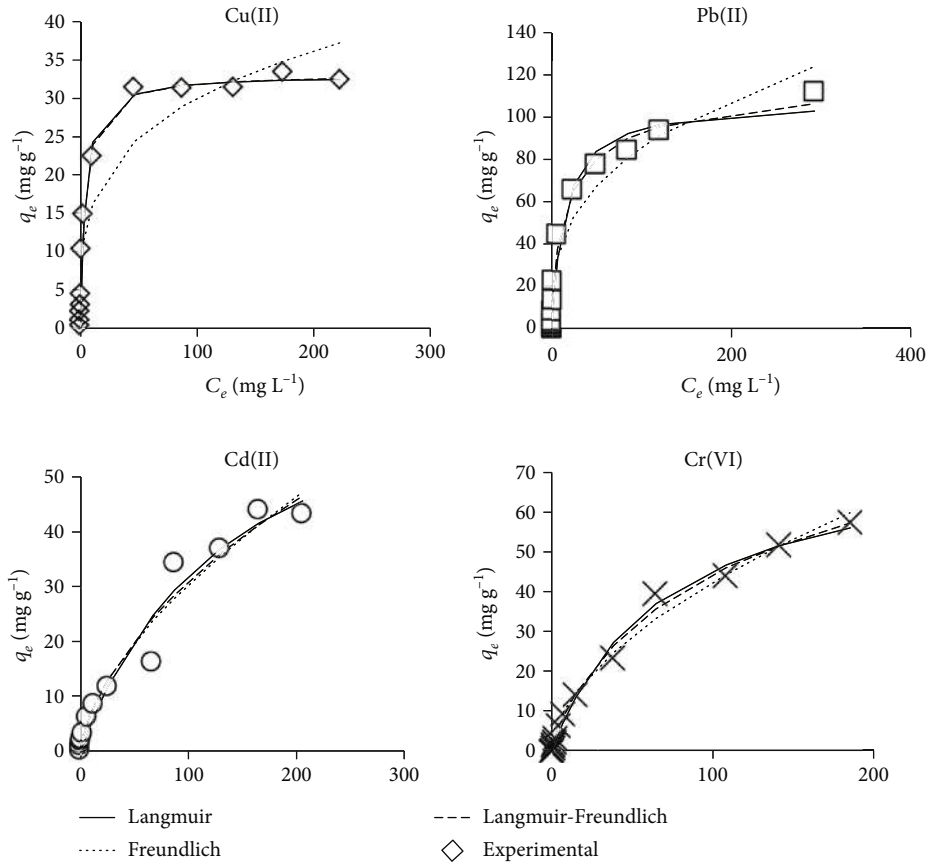

Figure 4: Adsorption isotherms of Cd(II), Cu(II), and Pb(II) at pH = 5.4 and Cr(VI) (pH = 2).

nonporous or microporous adsorbent, which is the type of adsorption isotherm most typically found in the case of agricultural wastes. The sorption isotherm of Cd(II) is type IV, which is characterized by the presence of two plateaus separated by an inflection due to the change from the first plateau to a concave shape until the second plateau is reached.

The Langmuir, Freundlich, and Langmuir-Freundlich models (Table 1) can be used to characterize the experimental data of the metal adsorption isotherm.

The Langmuir isotherm is characterized by the separation factor R_L, which can measure the facility for adsorption. The expression of R_L is defined as follows:

$$R_L = \frac{1}{1 + C_i b}, \quad (1)$$

where b is the Langmuir constant (L mg^{-1}) and $R_L = 0$ means that an irreversible adsorption process is taking place, whereas if $R_L = 1$, the adsorption is linear, and if $0 < R_L < 1$, it is considered that the adsorption is favoured.

The R_L values obtained, which varied between 0 and 1, indicate that biosorption onto the milled pine cones was favoured. When the initial metal concentration was increased, the separation factor R_L decreased at a constant rate for all metals, indicating the high affinity of these metals to the biosorbent even with high metal concentrations. In the case of the lowest initial metal concentration of 1 mg L^{-1}, the R_L values were close to 1 (linear adsorption) for Cd(II), Pb(II), Cu(II), and Cr(VI), whereas in the case of the highest initial concentration of 300 mg L^{-1}, R_L values were lower and varied between 0.02 and 0.13. Moreover, Cu(II) and Pb(II) had the lowest separation factor R_L values at an initial concentration of 20 mg L^{-1} (0.25 and 0.56, respectively) indicating the greater affinity of both metal ions to the biosorbent.

The fit of the experimental data to Langmuir, Freundlich, and Langmuir-Freundlich isotherm models was determined by using both nonlinearized and linearized equations. In the case of the nonlinearized equations, both the experimental points and the calculated models are depicted in Figure 4. As can be seen in this figure, there is good agreement between the experimental points in the case of Cu(II) and Pb(II) and the curves corresponding to the Langmuir and Langmuir-Freundlich isotherm models, while in the case of Cd(II) and Cr(VI), the curves of the three models agree with the experimental points. In order to find out the best adsorption isotherm model, we employed linearized equations, as have most published papers [46], despite the inherent bias created by linearization. The results obtained by applying the linearized Langmuir, Freundlich, and Langmuir-Freundlich equations are recorded in Table 1. The degree of agreement was assessed by comparing the determination coefficient (R^2) of each model and by applying the Akaike criterion (AIC), and the F test as R^2 is insufficient to perform the comparison of the models.

Table 1: Results obtained from the linearized Langmuir, Freundlich, and Langmuir-Freundlich isotherms.

	Langmuir (L) $q_e = q_{max} bC_e/(1 + bC_e)$			Freundlich (F) $q_e = K_F C_e^{1/n}$			Langmuir-Freundlich (L-F) $q_e = q_{L\text{-}F}(K_{L\text{-}F}C_e)^{M_{L\text{-}F}}/\left(1 + (K_{L\text{-}F}C_e)^{M_{L\text{-}F}}\right)$				Akaike criterion*	F test* L and L-F	F test* F and L-F
Metal	q_{max} (mg g^{-1})	b (L mg^{-1})	R^2	K_F	$\frac{1}{n}$	R^2	$q_{L\text{-}F}$ (mg g^{-1})	$K_{L\text{-}F}$	$M_{L\text{-}F}$	R^2	AICc	$P < 0.05$	$P < 0.05$
Cu(II)	33.04 ± 0.75	0.26 ± 0.01	0.99	8.67 ± 0.05	0.27 ± 0.15	0.86	33.21 ± 0.08	0.25 ± 0.03	0.97 ± 0.04	0.90	50.69(F) > 16.34 (L-F) > 10.92(L)	$F = 0.12$ $P = 0.735$ L	$F = 186.32$ $P < 0.0001$ L-F
Cd(II)	77.12 ± 0.41	0.007 ± 0.01	0.90	1.81 ± 0.75	0.61 ± 0.007	0.98	78.73 ± 0.06	0.009 ± 0.005	0.72 ± 0.07	0.94	48.27(F) > 44.02(L) > 14.98(L-F)	$F = 104.22$ $P < 0.0001$ L-F	$F = 144.72$ $P < 0.0001$ L-F
Cr(VI)	57.36 ± 0.70	0.014 ± 0.004	0.96	3.21 ± 0.90	0.55 ± 0.10	0.80	56.31 ± 0.05	0.018 ± 0.007	0.79 ± 0.10	0.90	32.86(F) > 29.14 (L-F) > 28.53(L)	$F = 4.19$ $P = 0.0709$ L	$F = 133.19$ $P < 0.0001$ L-F
Pb(II)	108.05 ± 0.77	0.07 ± 0.02	0.8	17.75 ± 0.02	0.34 ± 0.09	0.75	100.01 ± 0.04	0.05 ± 0.03	0.71 ± 0.02	0.90	72.04(F) > 63.58 (L) > 58.31(L-F)	$F = 10.92$ $P = 0.008$ L-F	$F = 104.48$ $P < 0.0001$ L-F

*AICc: the lowest value corresponds to the best model. *F test: the null hypothesis is that the simpler model (Langmuir or Freundlich) is correct and alternative model L-F is better than L or F when $P < 0.05$.

Table 2: Comparison of the adsorption capacity of milled pine cone for Pb(II), Cu(II), Cd(II), and Cr(VI) with the other biosorbents.

Biosorbents	Metals	Particle size	pH	Concentration ($mg\,L^{-1}$)	Dose ($g\,L^{-1}$)	q_m ($mg\,g^{-1}$)	References
Custard apple	Cd(II)	—	5	50-200	1.5	71	Isaac and Sivakumar [13]
	Pb(II)		5	5-200	1.5	90.93	
Ulva lactuca	Cr(VI)	≤0.063 mm	1	5-50	2	10.61	El-Sikaily et al. [48]
Olive stone	Cu(II)	<0.250-1 mm	5	10-300	10	1.97	Blázquez et al. [40]
Pine bark	Cu(II)	—	5	10-300	10	11.94	
Maize husk	Cu(II)	1.8 mm	6	—	—	1.21	Duru et al. [9]
Pine sawdust	Pb(II)	0.6-1.2 mm	5	1-50	10	13.48	Semerjian [49]
	Cu(II)		7	1-50	10	9.59	
Rice husk	Cd(II)	<0.125 mm	—	—	—	5.54	Jabbar et al. [12]
Pine cone	Cd(II)	—	7	20-200	2	14.7	Izanloo and Nasseri [50]
Pine cone	Cr(VI)	—	1	10-120	2	65.36	Najim and Yasin [37]
Pine cone	Cu(II)	—	5	50-250	3	18.69	Değirmen et al. [46]
	Pb(II)		7	50-250	3	23.2	
Pine cone	Cu(II)	4-8 mm	5	5-100	10	6.52	Martín-Lara et al. [29]
	Pb(II)		5	5-100	10	17.41	
Pine cone (*P. resinosa*)	Cu(II)	<0.15 mm	5	10-300	10	9.68	Awad and Erkurt [51]
	Pb(II)		5	10-300	10	17.24	
Olive stone	Pb(II)	—	6	1-10	5	0.581	Amar et al. [44]
	Cu(II)		6	1-10	5	0.557	
	Cd(II)		6	1-10	5	0.3	
	Cr(VI)		2	1-10	10	2.345	
Pine cone	Pb(II)		5.4	1-500	2	95	Present study
	Cu(II)		5.4	1-500	2	33.55	
	Cd(II)		5.4	1-500	2	50	
	Cr(VI)		2	1-500	2	68.03	

In the case of the Akaike criterion, the model for which corrected AIC (AICc) has the lowest value is selected as the best model [47]. The F test, based on traditional statistical hypothesis testing, compares the least-square regression fits of the linearized Langmuir or Freundlich equations with those of the linearized Langmuir-Freundlich model. As can be seen in Table 1, when the F test was used to compare Freundlich and Langmuir-Freundlich, the latter was the best model for all the metal ions; however, in comparing the Langmuir and Langmuir-Freundlich models, Langmuir was the selected model for Cr(VI) and Cu(II) and the Langmuir-Freundlich model for Pb(II) and Cd(II). These results are in agreement with those obtained by applying the Akaike criterion (Table 1).

The experimental data of Cu(II) fitted the Langmuir model with a maximum adsorption capacity of $33.04\,mg\,g^{-1}$. Consequently, this metal ion was adsorbed onto the surface of the pine cone, forming a monolayer, which provides a single site to attach each metal ion. A similar result was obtained by Blázquez et al. [27], who proposed a surface complexation model for the adsorption of Cu(II) by pine cone shell. The Langmuir model was also the best suited to describe the experimental data for Cr(VI) adsorption with a maximum adsorption capacity of $57.36\,mg\,g^{-1}$. In the case of Pb(II) and Cd(II), the best model is the Langmuir-Freundlich isotherm with maximum adsorption capacities of 100.01 and $78.73\,mg\,g^{-1}$, respectively. This model is suitable for predicting adsorption on heterogeneous surfaces, thereby avoiding the limitation of increased adsorbate concentrations associated with the Freundlich model, but at a high concentration of adsorbate, it predicts the Langmuir model (monolayer adsorption); hence, the Langmuir-Freundlich isotherm is a concentration-dependent model.

The differences between the adsorption isotherm models for Cu(II) and Pb(II) can explain the differences in the metal removal percentages when the initial metal concentration was varied from 1 to $5\,mg\,L^{-1}$. As has been discussed earlier in the case of Cu(II), at these low initial concentrations, the metal uptake percentage remained constant (~94%), whereas for Pb(II), it increased from 73.5 to 94%.

As can be in Table 1, the values of the maximum adsorption capacities calculated from the Langmuir and Langmuir-Freundlich models are similar in the case of Cd(II) and Pb(II) and the same, considering the standard deviation, in the case of Cr(VI) and Cu(II). With regard to R^2, the highest values correspond to the Langmuir model for Cu(II) and Cr(VI) and to the Langmuir-Freundlich model for Cd(II) and Pb(II). This statistic is in agreement with the results of the application of the Akaike criterion and F test to compare the Langmuir and Langmuir-Freundlich models for each metal ion.

Table 2 summarizes the comparison of the adsorption capacity of milled pine cones for Cu(II), Cd(II), Pb(II), and Cr(VI) with other nontreated biosorbents. It is seen in these results that the milled pine cone has the highest adsorption capacity for all metals. Pine cone was a more effective

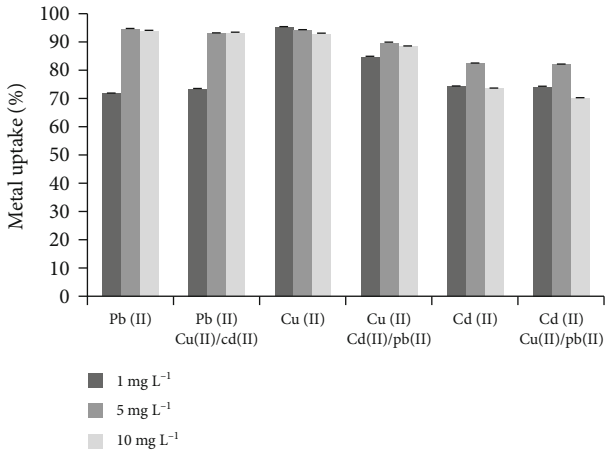

FIGURE 5: Comparison of the removal percentage of Pb(II), Cu(II), and Cd(II) between single metal and multimetal solutions at different initial concentrations: pH = 5.4, adsorbent concentration = 2 g L^{-1}, and t = 2 h (n = 3).

biosorbent for Pb(II) than custard apple [13], Ulva lactuca [45], and olive stones [41]. Moreover, milled pine cone presents a higher adsorption capacity for Cd(II) and Cr(VI) than that obtained by rice husk [12, 36] and olive stones [44]. In the case of Cu(II), pine cone is also more efficient than maize husk [9] and olive stones [40]. Therefore, milled pine cone has been demonstrated to be more efficient than milled olive stone in the removal of Pb(II), Cu(II), Cd(II), and Cr(VI). However, the maximum adsorption capacities for these ions differ depending on the experimental conditions used (initial metal concentrations, particle size, dosage of adsorbent, and pH and the type of pine biomass: pine bark or pine cone, Pinus halepensis, or Pinus resinosa).

3.4. Competition between Cu(II), Pb(II), and Cd(II). The competition of different metals to occupy the binding sites of the adsorbent was investigated using three multimetal solutions containing Pb(II), Cd(II), and Cu(II) at different initial concentrations of 1 mg L^{-1}, 5 mg L^{-1}, and 10 mg L^{-1} at pH 5.4 using 2 g L^{-1} of adsorbent for 2 h. Figure 5 compares the adsorption efficiency of milled pine cones towards a solution containing a single metal ion and three metal ions. In the case of Pb(II), the removal percentage increased from 71.6% to 94% when the initial concentration was increased from 1 to 5 mg L^{-1}, and the same results were obtained when Cu(II) and Cd(II) were present at the same concentration levels, showing that the presence of these metal ions did not affect Pb(II) removal. A similar trend was observed in the case of Cd(II), whose removal percentages were the same for both the single and multimetal solutions, except in the case of the highest concentration (10 mg L^{-1}). Cu(II) was the only metal ion affected by the competition with the other ones, and its removal percentage decreased by around 10% in the presence of Pb(II) and Cd(II) at all the concentrations tested, confirming the higher affinity of pine cone by Pb(II). The biosorption of the binary Cu(II)–Pb(II) system by pine cone was investigated in a batch reactor and in a fixed-bed column. The results obtained in both operational modes confirmed a slight suppression of copper biosorption due to the presence of lead when both metal ions are present in the solution [29]. Recently, a review on the dominance of Pb during competitive biosorption from multimetal systems has concluded that most biosorbents can effectively remove Pb(II) even in the presence of other heavy metals, but the adsorption of Cu(II), Cd(II), Zn(II), Ni(II), and Cr(III) decreases significantly due to the presence of Pb(II) [52].

4. Conclusions

In this study, milled pine cone was used to remove metal ions such as Pb(II), Cu(II), Cd(II), and Cr(VI). The effect of different parameters such as the contact time, pH, amount of adsorbent, and initial metal concentration on the removal efficiency was studied. Milled pine cone is seen to be an effective biosorbent for the removal of divalent metal ions due to the high affinity of these ions for the carboxylic and hydroxyl groups, which are present on the adsorbent surface, as well as for its availability and low cost. The efficiency of milled pine cone to remove trace concentration levels of Pb(II), Cd(II), and Cu(II) has been demonstrated, resulting in capacities of 100.01 mg g^{-1}, 78.73 mg g^{-1}, and 33.04 mg g^{-1} at pH 5.5, respectively. These capacities are higher than those reported for other biosorbents with similar characteristics. Moreover, an adsorption capacity of 57.36 mg g^{-1} was obtained for Cr(VI) at pH 2, and its maximum removal percentage (88.8%) was obtained at pH 2 with 10 g L^{-1}, showing that this toxic anion can be removed via an ion-exchange mechanism. The experimental adsorption data correlated well with the Langmuir model for Cu(II) and Cr(VI), whereas for Pb(II) and Cd(II), the best correlations were obtained with the Langmuir-Freundlich model. In the case of the divalent ions (Pb(II), Cu(II), and Cd(II)), there is no competition between them towards the adsorbent sites at low metal concentration levels (1-10 mg L^{-1}), given that the presence of other metal ions did not reduce the removal efficiencies.

The prolific production of pine cones around the Mediterranean rim results in the abundant availability of waste residue that can be successfully valorised for the creation of the environmentally valuable process developed in this study to remove heavy metals from industrial effluents such as the highly toxic multimetal-containing wastewaters released by electroplating industries.

Data Availability

The data that support the findings of this study are available from the corresponding author (VS) upon reasonable request.

Conflicts of Interest

The authors do not declare any conflict of interest.

Acknowledgments

This study was financed by the research project PID2019-107033GB-(AEI/FEDER/UE) of the "Agencia Española de

Investigación." Marwa Ben Amar acknowledges the financial support of the Faculty of Science (University of Sfax, Tunisia) and of the Environmental and Analytical Chemistry Research Group of the Department of Chemistry (University of Girona, Spain).

References

[1] A. E. Ofomaja, E. B. Naidoo, and S. J. Modise, "Biosorption of copper(II) and lead(II) onto potassium hydroxide treated pine cone powder," *Journal of Environmental Management*, vol. 91, no. 8, pp. 1674–1685, 2010.

[2] F. Fu and Q. Wang, "Removal of heavy metal ions from wastewaters: a review," *Journal of Environmental Management*, vol. 92, no. 3, pp. 407–418, 2011.

[3] A. Aldawsari, M. A. Khan, B. H. Hameed et al., "Mercerized mesoporous date pit activated carbon—a novel adsorbent to sequester potentially toxic divalent heavy metals from water," *PLoS One*, vol. 12, no. 9, article e0184493, 2017.

[4] N. S. Alharbi, B. Hu, T. Hayat et al., "Efficient elimination of environmental pollutants through sorption-reduction and photocatalytic degradation using nanomaterials," *Frontiers of Chemical Science and Engineering*, vol. 14, no. 6, pp. 1124–1135, 2020.

[5] X. Zhong, Z. Lu, W. Liang, and B. Hu, "The magnetic covalent organic framework as a platform for high-performance extraction of Cr(VI) and bisphenol a from aqueous solution," *Journal of Hazardous Materials*, vol. 393, p. 122353, 2020.

[6] X. Liu, H. Pang, X. Liu et al., "Orderly porous covalent organic frameworks-based materials: superior adsorbents for pollutants removal from aqueous solutions," *The Innovation*, vol. 2, no. 1, p. 100076, 2021.

[7] B. Hu, Y. Ai, J. Jin et al., "Efficient elimination of organic and inorganic pollutants by biochar and biochar-based materials," *Biochar*, vol. 2, no. 1, pp. 47–64, 2020.

[8] C. Duru, M. Nnabuchi, and I. Duru, "Adsorption of Cu onto maize husk lignocellulose in single and binary Cu-Zn solution systems: equilibrium, isotherm, kinetic, thermodynamic and mechanistic studies," *Egyptian Journal of Chemistry*, vol. 62, pp. 1295–1305, 2019.

[9] D. T. Pooja, "Removal of copper from waste water by using potato and banana peels as bio-adsorbent," *International journal of science, Engineering and Technology Research (IJSETR)*, vol. 5, pp. 3038–3040, 2016.

[10] M. Cheraghi, S. Sobhanardakani, R. Zandipak, B. Lorestani, and H. Merrikhpour, "Removal of Pb (II) from aqueous solutions using waste tea leaves," *Iranian Journal of Toxicology*, vol. 9, pp. 1247–1253, 2015.

[11] E. I. Nkechi and A. A. Chizaram, "Use of agro-waste (Musa paradisiaca peels) as a sustainable biosorbent for toxic metal ions removal from contaminated water," *Chemistry International*, vol. 4, pp. 52–59, 2018.

[12] H. Jabbar, B. Al, and T. A.-S. Simaa, "Removal of heavy metals from aqueous solution by using low cost rice husk in batch and continuous fluidized experiments," *International Journal of Chemical Engineering and Applications*, vol. 7, no. 1, pp. 6–10, 2016.

[13] C. P. J. Isaac and A. Sivakumar, "Removal of lead and cadmium ions from water using Annona squamosa shell: kinetic and equilibrium studies," *Desalination and Water Treatment*, vol. 51, no. 40-42, pp. 7700–7709, 2013.

[14] M. Hamidpour, N. Hosseini, V. Mozafari, and M. H. Rafsanjani, "Removal of Cd(II) and Pb(II) from aqueous solutions by pistachio hull waste," *Revista Internacional de Contaminación Ambiental*, vol. 34, no. 2, pp. 307–316, 2018.

[15] M. Shafiq, A. A. Alazba, and M. T. Amin, "Removal of heavy metals from wastewater using date palm as a biosorbent: a comparative review," *Sains Malaysiana*, vol. 47, no. 1, pp. 35–49, 2018.

[16] M. B. Ibrahim and M. B. Mohammed, "Dynamic adsorption studies for the removal of Cd (II) and Ni (II) from aqueous solutions using mahogany leaves," *ChemSearch Journal*, vol. 8, no. 1, pp. 1-2, 2017.

[17] B. Adesola, K. Ogundipe, K. T. Sangosanya, B. D. Akintola, and A. O. Hassan, "Comparative study on the biosorption of Pb(II), Cd(II) and Zn(II) using Lemon grass (Cymbopogon citratus): Kinetics, isotherms and thermodynamics," *International Journal of Chemistry*, vol. 2, pp. 89–102, 2016.

[18] C. Aravind, K. Chanakya, and K. Mahindra, "Removal of heavy metals from industrial waste water using coconut coir," *International Journal of Civil Engineering and Technology*, vol. 8, pp. 1869–1871, 2017.

[19] N. Nasseh, L. Taghavi, B. Barikbin, and A. R. Harifi-Mood, "The removal of Cr(VI) from aqueous solution by almond green hull waste material: kinetic and equilibrium studies," *Journal of Water Reuse and Desalination*, vol. 7, no. 4, pp. 449–460, 2017.

[20] M. Villen-Guzman, D. Gutierrez-Pinilla, C. Gomez-Lahoz, C. Vereda-Alonso, J. M. Rodriguez-Maroto, and B. Arhoun, "Optimization of Ni (II) biosorption from aqueous solution on modified lemon peel," *Environmental Research*, vol. 179, p. 108849, 2019.

[21] V. Novoseltseva, H. Yankovych, O. Kovalenko, M. Václavíková, and I. Melnyk, "Production of high-performance lead(II) ions adsorbents from pea peels waste as a sustainable resource," *Waste Management & Research*, vol. 39, no. 4, pp. 584–593, 2020.

[22] A. I. Almendros, M. A. Martín-Lara, A. Ronda, A. Pérez, G. Blázquez, and M. Calero, "Physico-chemical characterization of pine cone shell and its use as biosorbent and fuel," *Bioresource Technology*, vol. 196, pp. 406–412, 2015.

[23] N. Nasri, A. Khaldi, and S. Triki, "Variabilité morphologique des cônes et graines de Pin d'Alep et de Pin pignon en Tunisie," *Revue Forestière Française*, vol. 56, no. 1, p. 22, 2004.

[24] M. Khouja, T. Sghaiar, A. Khalidi, and R. Nsibi, "Estimation du rendement en cones et en graines du pin d'alep de la foret de ouercha (sakiet sidi youssef-Tunisie)," *Centre de Recherche Forestière*, vol. 30, pp. 84–89, 1997.

[25] H. S. Altundoğan, A. Topdemir, M. Çakmak, and N. Bahar, "Hardness removal from waters by using citric acid modified pine cone," *Journal of the Taiwan Institute of Chemical Engineers*, vol. 58, pp. 219–225, 2016.

[26] G. Değirmen, M. Kılıç, O. Cepelioğullar, and A. E. Pütün, "Removal of copper (II) and cadmium (II) ions from aqueous solutions by biosorption onto pine cone," *Water Science and Technology*, vol. 66, no. 3, pp. 564–572, 2012.

[27] G. Blázquez, M. A. Martín-Lara, E. Dionisio-Ruiz, G. Tenorio, and M. Calero, "Copper biosorption by pine cone shell and thermal decomposition study of the exhausted biosorbent," *Journal of Industrial and Engineering Chemistry*, vol. 18, no. 5, pp. 1741–1750, 2012.

[28] H. Ucun, Y. K. Bayhana, Y. Kaya, A. Cakici, and O. F. Algur, "Biosorption of lead (II) from aqueous solution by cone

biomass of Pinus sylvestris," *Desalination*, vol. 154, no. 3, pp. 233–238, 2003.

[29] M. A. Martín-Lara, G. Blázquez, M. Calero, A. I. Almendros, and A. Ronda, "Binary biosorption of copper and lead onto pine cone shell in batch reactors and in fixed bed columns," *International Journal of Mineral Processing*, vol. 148, pp. 72–82, 2016.

[30] N. M. Mahmoodi, B. Hayati, M. Arami, and C. Lan, "Adsorption of textile dyes on pine cone from colored wastewater: kinetic, equilibrium and thermodynamic studies," *Desalination*, vol. 268, no. 1-3, pp. 117–125, 2011.

[31] A. E. Ofomaja and E. B. Naidoo, "Biosorption of lead(II) onto pine cone powder: studies on biosorption performance and process design to minimize biosorbent mass," *Carbohydrate Polymers*, vol. 82, no. 4, pp. 1031–1042, 2010.

[32] M. Momčilović, M. Purenović, A. Bojić, A. Zarubica, and M. Ranđelović, "Removal of lead(II) ions from aqueous solutions by adsorption onto pine cone activated carbon," *Desalination*, vol. 276, no. 1-3, pp. 53–59, 2011.

[33] S. O. Sanni, E. L. Viljoen, and A. E. Ofomaja, "Three-dimensional hierarchical porous carbon structure derived from pinecone as a potential catalyst support in catalytic remediation of antibiotics," *RSC Advances*, vol. 10, pp. 8717–8728, 2020.

[34] C. Ravat, F. Monteil-Rivera, and J. Dumonceau, "Metal ions binding to natural organic matter extracted from wheat bran: application of the surface complexation model," *Journal of colloid and interface science*, vol. 225, no. 2, pp. 329–339, 2000.

[35] H. Yuh-Shan, "Removal of copper ions from aqueous solution by tree fern," *Water Research*, vol. 37, no. 10, pp. 2323–2330, 2003.

[36] A. Pholosi, A. E. Ofomaja, and E. B. Naidoo, "Effect of chemical extractants on the biosorptive properties of pine cone powder: influence on lead(II) removal mechanism," *Journal of Saudi Chemical Society*, vol. 17, no. 1, pp. 77–86, 2013.

[37] T. S. Najim and S. A. Yasin, "Adsorption of Cr(VI) from aqueous solution using low cost adsorbent: equilibrium study," *Science Journal of University of Zakho*, vol. 1, pp. 758–767, 2013.

[38] I. Puigdomenech, *KTH Royal Institute of Technology*, Medusa Software, Sweden, 2016, https://www.kth.se/che/medusa/downloads-1.386254.

[39] A. Javaid, R. Bajwa, U. Shafique, and J. Anwar, "Removal of heavy metals by adsorption on Pleurotus ostreatus," *Biomass and Bioenergy*, vol. 35, no. 5, pp. 1675–1682, 2011.

[40] G. Blázquez, M. A. Martín-Lara, E. Dionisio-Ruiz, G. Tenorio, and M. Calero, "Evaluation and comparison of the biosorption process of copper ions onto olive stone and pine bark," *Journal of Industrial and Engineering Chemistry*, vol. 17, no. 5-6, pp. 824–833, 2011.

[41] D. Park, S. R. Lim, Y. S. Yun, and J. M. Park, "Reliable evidences that the removal mechanism of hexavalent chromium by natural biomaterials is adsorption-coupled reduction," *Chemosphere*, vol. 70, no. 2, pp. 298–305, 2007.

[42] P. Miretzky and A. F. Cirelli, "Cr(VI) and Cr(III) removal from aqueous solution by raw and modified lignocellulosic materials: a review," *Journal of hazardous materials*, vol. 180, no. 1-3, pp. 1–19, 2010.

[43] G. Blázquez, F. Hernáinz, M. Calero, M. A. Martín-Lara, and G. Tenorio, "The effect of pH on the biosorption of Cr (III) and Cr (VI) with olive stone," *Chemical Engineering Journal*, vol. 148, no. 2-3, pp. 473–479, 2009.

[44] M. B. Amar, K. Walha, and V. Salvadó, "Evaluation of olive stones for Cd(II), Cu(II), Pb(II) and Cr(VI) biosorption from aqueous solution: equilibrium and kinetics," *International Journal of Environmental Research*, vol. 14, no. 2, pp. 193–204, 2020.

[45] P. A. Gauden, A. P. Terzyk, P. Kowalczyk et al., "Giles' classification of solute adsorption isotherms for binary non-electrolyte solutions via lattice DFT supported by experimental sorption data from aqueous solutions on carbonaceous materials," *Carbon Materials-Theory and Practice*, 2008.

[46] J. Wang and X. Guo, "Adsorption isotherm models: classification, physical meaning, application and solving method," *Chemosphere*, vol. 258, p. 127279, 2020.

[47] O. M. Akpa and E. I. Unuabonah, "Small-sample corrected Akaike information criterion: an appropriate statistical tool for ranking of adsorption isotherm models," *Desalination*, vol. 272, no. 1-3, pp. 20–26, 2011.

[48] A. El-Sikaily, A. El Nemr, A. Khaled, and O. Abdelwehab, "Removal of toxic chromium from wastewater using green alga Ulva lactuca and its activated carbon," *Journal of Hazardous Materials*, vol. 148, no. 1-2, pp. 216–228, 2007.

[49] L. Semerjian, "Removal of heavy metals (Cu, Pb) from aqueous solutions using pine (Pinus halepensis) sawdust: equilibrium, kinetic, and thermodynamic studies," *Environmental Technology and Innovation*, vol. 12, pp. 91–103, 2018.

[50] H. Izanloo and S. Nasseri, "Cadmium removal from aqueous solutions by ground pine cone," *Iranian Journal of Environmental Health Science & Engineering*, vol. 2, no. 1, pp. 33–42, 2005.

[51] F. Awad and H. A. Erkurt, "Biosorption of lead (II) and copper (II) by Pinus resinosa: modeling and mechanism," *Fresenius Environmental Bulletin*, vol. 23, no. 2, pp. 540–549, 2014.

[52] C. Mahamadi, "On the dominance of Pb during competitive biosorption from multi-metal systems: a review," *Cogent Environmental Science*, vol. 5, no. 1, article 1635335, 2019.